Foraging Behaviour of the Particle Phenomenologist

A Broad Exploration of Physics Beyond the Standard Model

A Dissertation

Presented to the Faculty of the Graduate School

of Cornell University

in Partial Fulfillment of the Requirements for the Degree of

Doctor of Philosophy

by

Wee Hao Ng

December 2018

Foraging Behaviour of the Particle Phenomenologist

A Broad Exploration of Physics Beyond the Standard Model

Wee Hao Ng, Ph.D.

Cornell University 2018

Despite its numerous successes, the Standard Model (SM) of particle physics is known to be incomplete. In this thesis, we explore a variety of topics regarding physics beyond the SM (BSM).

In the minimal supersymmetric Standard Model (MSSM), the leptons and Higgs have separate superpartners; however, it is possible to construct a model where the Higgs is the superpartner of one generation of left-handed leptons. In Chapter 2, we explore various implications of this Higgs-as-slepton model, in particular on electroweak precision and neutrino experiments. In Chapter 3, we use the model to explain various excesses reported in leptoquark and W' searches by the CMS experiment in 2014. These excesses were observed in electron but not muon channels, hence suggesting the violation of lepton universality, a hallmark of the model.

In Chapter 4, we propose a supersymmetric left-right symmetric (SUSY LRS) model that can explain various excesses reported in W' searches by the CMS and ATLAS experiments around 2014–2015, but at the same time generate a large tree-level Higgs mass, hence resolving the usual issue of the Higgs mass being too small in the MSSM. In the most basic SUSY LRS model, a large Higgs mass also requires a large $\tan\beta$ (the ratio of the two Higgs vacuum expectation values in the model), whereas the excesses seem to favour a smaller value. We resolve this tension by introducing heavy down-type vector-like quarks that mix with the light

quarks; a large $\tan\beta$ can now still remain consistent with the excesses.

Lepton flavour models based on A_4 symmetry are popular because they predict a tri-bimaximal mixing pattern for the Pontecorvo-Maki-Nakagawa-Sakata (PMNS) matrix, often regarded to be in good agreement with experimental measurements. However, recent results from the Daya Bay and RENO experiments have shown that the θ_{13} angle of the matrix is rather large, contrary to the predicted mixing pattern. We investigate in Chapter 5 whether a model based on the $SO(3) \to A_4$ symmetry-breaking pattern can accommodate these recent results. The enlargement to $SO(3)$ is intended to motivate the A_4 from a UV completion standpoint. We find that contrary to typical A_4 models, the $SO(3) \to A_4$ model does generally predict a large θ_{13} due to mixing in the charged-lepton sector.

In Chapter 6, we present a new mechanism for freeze-out dark matter which we call co-annihilation. This differs from most freeze-out mechanisms in that depletion is driven not by Boltzmann suppression, but by out-of-equilibrium decay that eventually "switches off". Such a model is hard to probe using direct detection and collider production experiments, but should present enhanced indirect detection signatures.

Hydrogen-antihydrogen (H-$\bar{\text{H}}$) oscillations are forbidden in the SM and hence represent signs of new physics. In the interstellar medium (ISM), any H atom that oscillates into $\bar{\text{H}}$ may subsequently undergo annihilation with other atoms, producing γ-rays that can be detected in astronomical surveys. While a bound on these oscillations was originally derived by Feinberg *et al.*, we re-evaluate the bound in Chapter 7 using a more comprehensive theoretical framework, a multiphase description of the ISM, as well as recent γ-ray data from the *Fermi* Large Area Telescope.

Biographical Sketch

Wee Hao Ng grew up in Singapore, and read physics at Oxford University in the early 2000s. After a short stint in military service, he spent a few year working in an applied physics laboratory, before coming over to Cornell in the early 2010s. He enjoys spending long hours out in nature by himself, except for the company of wildlife, and cares deeply about conservation issues. Since this thesis will eventually become public domain, due to concerns over privacy and identity theft, he would rather avoid overly-specific details in this biographical sketch. Actually he did write a more detailed version, but subsequently found it too self-aggrandising to his liking.

To my family.

Acknowledgements

Acknowledgements are hard to write, since there will always be someone whom I sincerely want to thank but had happened to slip my mind at the moment of writing.

First and foremost, I owe much to my advisor, Prof. Yuval Grossman. His unflappable sense of humour, as well as continued support despite being aware of my decision to cross over to conservation, made what would otherwise have been a difficult journey much lighter. Along with Yuval, I would like to thank LEPP theory and experiment faculty Prof. Jim Alexander, Csaba Csaki, Lawrence Gibbons, Thomas Hartman, Liam McAllister, Maxim Perelstein and Peter Wittich, as well as LEPP theory postdocs Marco Farina, Eric Kuflik and Paul McGuirk, from whom I learnt much about particle physics and quantum field theory. Extra shout out to Csaba and Maxim for providing the bedrock of my knowledge, and to Jim for always being there as a listening ear.

Among my fellow LEPP theory graduate students, a special mention to my number one collaborator Jeff Dror. Our partnership, in which you would throw out wild ideas to which I would then play Devil's advocate, had borne surprising fruit, and would probably have continued to do so had I not made the cross-over decision. I am also grateful to Nima Afkhami-Jeddi, Thomas Bachlechner, Mathieu Cliche, Jack Collins, Mehmet Demirtas, Gowri Kurup, Salvator Lombardo, Cody Long, Mario Martone, Mitrajyoti Ghosh, Nicholas Rey-Le Lorier, Mike Saelim, Mike Savastio, John Stout, Amirhossein Tajdini, Ofri Telem and Yu-dai Tsai for being great colleagues whom I can have engaging discussions with.

On the teaching side, I am extremely grateful for the fact that my interactions as a TA with the professors have been consistently positive. Besides Yuval, Jim and Peter, I also like to acknowledge LEPP faculty Prof. Ivan Bazarov and Andre

LeClair, LASSP faculty Prof. Kin Fai Mak and Eric Mueller, and Math department faculty Prof. Alex Townsend.

For administrative support, I can always count on Kacey Acquilano, Debra Hatfield and Katerina Malysheva to make sure that I don't mess things up. Also, it would be remiss of me not to mention the cheerfulness and leadership the administrative director Craig Wiggers has brought to the department.

Last but certainly not least, I would like to thank my friends here at Cornell: Robin Bjorkquist, Jennifer Chu, Azar Eyvazov, Jun Wei Lam, Jordan Moxon and Shao Min Tan, as well as my family and friends back home in Singapore, for your unwavering emotional support. Life would have been very different without you.

Table of Contents

Chapter 1
Introduction

1.1 Why high-energy physics?

Gently treading along the leaf-littered trail of Sapsucker Woods, the foliage gradually falling away to reveal the quiescent water of Sapsucker Pond reflecting the orange-hued sky of a clear autumn dawn, one often encounters a myriad of avian life: perpetually-optimistic chickadees foraging in the pines; a pair of stunningly-plumaged wood ducks swimming among the reeds; from afar a downy woodpecker whinnying and drumming on a hollow log. Yet any bird, from the smallest hummingbird to the largest ostrich, begins with the humble egg: a relatively simple package comprising the shell, the albumen (or egg white), the yolk suspended in the middle by gelatinous strips called the chalaze, various membranes, and a collection of cells called the germinal disc [1]. Remarkably, only minimal external influence, in the form of gas exchange and heat transfer, is required for the spontaneous development of a much more complex structure within this package: an intelligent hatchling, with the capability to grow, communicate and learn.

It is hard to see how advances in high-energy physics could in any way facilitate our understanding of this miraculous transition. Even if we know all the elementary laws and have the computational ability to perform any required simulations, as Steven Weinberg puts it [2]: "... all you have would be a mountain of computer tape. How in that mountain of computer tape would you ever recognise the properties that interest you ...?". The ability to reproduce phenomenon through computer simulations does not imply the ability to understand the physics behind the phenomenon. Rather, entirely new concepts have to be developed as we delve

into systems of increasing size and complexity, the notion of emergent phenomena [3]. Furthermore, the energy scales involved in these phenomena are typically low enough that using a low-energy effective theory in place of the Standard Model (SM) as the elementary description is often more than adequate.

With this in mind, what makes it still worthwhile to pursue research in high-energy physics, when it seems that so much more can be learnt from developments in the field of emergent phenomena?

1. *Incomplete description of elementary laws.* Despite the tremendous successes of the SM and general relativity (GR), there still remain many phenomena that can only be explained by modifications at the level of the elementary laws. Examples include rotation curves of spiral galaxies [4], neutrino oscillations [5–7], as well as anomalous results from various low-energy experiments [8, 9]. The same is also often true for observations that contain imprints of the early universe, for instance the cosmic microwave background (CMB) [10–12], and the observed matter-antimatter asymmetry [13]. The types of modifications required are generally well agreed-upon: neutrino masses [14, 15], dark matter [16], baryogenesis [17] and the inflaton [18–21]; however, none of the proposed implementations have been experimentally tested to the point of widespread acceptance. Therefore, from the explanatory perspective, meaningful progress can still be made by advancements in high-energy physics.

2. *Unsatisfactory theoretical status.* Efforts to address theoretical concerns in established theories have at times led to unexpected developments. Perhaps the most famous example is the unification of electromagnetism and optics by James Clerk Maxwell [22], after he introduced the displacement current

to restore mathematical consistency between Ampere's law and the charge continuity equations[1]. At present, various theoretical aspects of the SM remain unsatisfactory, in particular the fine-tuning required for the Higgs mass-squared [23,24], the strong CP angle [25], and the cosmological constant [26]. The resolution of these issues may well bring forth a significant leap in our understanding of the elementary laws.

3. *Unexpected spin-offs.* The specific needs of high-energy physics have at times given rise to ideas and innovations that eventually found widespread use outside the field itself. For instance, the challenges of information management in large-scale high-energy physics experiments involving collaborators worldwide ultimately led to the development of the World Wide Web by Tim Berners-Lee in CERN [27]. Another potential example currently unfolding before us is the AdS-CFT correspondence [28]. The sheer difficulty of coming up with a consistent ultraviolet (UV) completion of quantum gravity have played a major role in string theory [29, 30] entering the mainstream, after the Green-Schwarz mechanism [31] kickstarted the first superstring revolution by demonstrating that string theory could be one such UV completion. Rapid developments since then have culminated in the discovery of the AdS-CFT correspondence by Juan Maldacena, which is now beginning to find applications in other disciplines such as nuclear [32] and condensed matter physics [33].

4. *Objective reductionism.* Imagine an impossibly powerful computer capable of simulating macroscopic number of low-energy particles interacting via all the known elementary forces, to any desired level of numerical precision.

[1] Although some have argued that Maxwell's original motivation was to establish electromagnetic duality between Ampere's law and Faraday's law, and not because of the said consistency issue.

> Then in principle, practically any low-energy experiment can be replaced by a numerical simulation on such a computer; progress in entire disciplines can continue uninterrupted without any new physical experiments as long as such a computer is at their disposal. Again, it is important to point out that these simulations do not lead to an improved understanding of the phenomena observed, and are simply proxies for physical experiments. As explained by Philip Warren Anderson [3], fundamentally new concepts independent of the elementary laws may have to be discovered in order to understand the phenomena. However, it is also clear that such a computer can never replace a high-energy physics experiment trying to discover physics beyond the SM. Therefore, the elementary laws are also fundamental in a different sense of the word, in that they are always specified at the "input level", and can never be discovered even in principle without a physical experiment. This argument is closely related to what Weinberg[2] referred to as objective reductionism [2].

This thesis is a compilation of the author's work over the past six years in the field of high-energy phenomenology. The work covers an extremely wide range of topics: from supersymmetry to left-right symmetric models, from flavour to neutrino physics, from dark matter to astrophysical bounds on SM-forbidden processes. This reflects the highly diverse nature of the field, and also perhaps (more negatively) the lack of focus on the author's part, not unlike a foraging chickadee: at times gleaning for insects in pine needles, de-fluffing cattails by the water, and grabbing sunflower seeds from garden feeders.

Given the range of topics involved, this thesis is structured as a thesis-by-

[2]Contrary to folklore within certain circles, Weinberg did not disagree with Anderson's viewpoints about emergence [2], nor did he promulgate the phrase "a theory of everything" which in fact he disliked [34]. The Anderson-Weinberg debate was ultimately about whether objective reductionism justified a higher funding status for high-energy physics.

publication rather than a single coherent monograph. Each subsequent chapter corresponds to a single publication and is intended to be self-contained. In the next section, we provide a brief synopsis of the motivations behind and the main results of each chapter.

1.2 Chapter synopsis

1.2.1 The Higgs as the slepton (Chapters 2 and 3)

Supersymmetry

The gauge hierarchy problem refers to the observation that radiative corrections to the Higgs mass are typically much larger than the measured value, implying that there must be almost complete cancellation between the bare Higgs mass and the radiative corrections, hence leaving a much smaller value. A well-known approach to avoid this fine-tuning is to enlarge the space-time Poincare symmetry of the SM into what is commonly known as supersymmetry (SUSY) [35]. Exact SUSY ensures that all bosons must come with degenerate fermionic superpartners, and vice versa. Since fermionic masses are protected from power-law divergences in the radiative corrections by chiral symmetry [24], this degeneracy implies that all scalar masses are similarly protected. Indeed, one can show that exact SUSY implies the presence of additional interactions required to make the existing Lagrangian supersymmetric, and these interactions lead to new radiative corrections to scalar masses that cancel the original quadratic divergences.

Even if SUSY exists in nature, it cannot be exact since no superpartners have

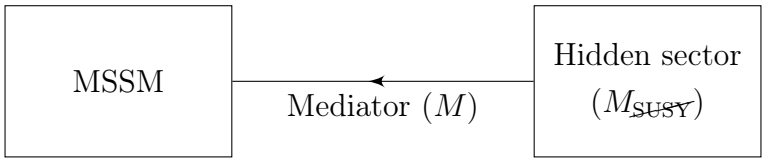

Figure 1.1: Standard picture of SUSY breaking.

been observed so far, despite their supposed degeneracy with the SM counterparts. Breaking exact SUSY allows the superpartners to become more massive and hence out of present experimental reach, but it must be done in a way that does not re-introduce large radiative corrections to the Higgs mass. At the level of an effective theory, this involves adding only a restricted set of non-supersymmetric "soft" terms, typically characterised by a mass scale m_{soft}, to the original supersymmetric Lagrangian. In doing so, the superpartners gain additional mass contributions of order m_{soft}, which we can then set to be much larger than the electroweak scale v_H to push them out of present experimental reach. On the other hand, some fine-tuning is required to prevent v_H from being raised to the same scale as m_{soft}, so m_{soft} is usually assumed to lie just within one or two orders of magnitudes of v_H to limit the severity of this "little hierarchy problem".

While the restriction to "soft" terms might seem rather arbitrary, it is actually supported by the standard UV picture of SUSY breaking (see Figure 1.1): One first defines the minimal supersymmetric Standard Model (MSSM) containing the SM particles and their superpartners. Next, spontaneous SUSY breaking occurs in a hidden sector at a scale $M_{\not{\text{SUSY}}}$, the effects of which are then communicated to the MSSM via some mechanism characterised by a very high mediation scale M. One can then show that in this picture, the low-energy effective theory only contains the supersymmetric MSSM Lagrangian, "soft" terms with $m_{\text{soft}} \sim M^2_{\not{\text{SUSY}}}/M$, as well as highly-suppressed "hard" terms that are usually ignored.

The MSSM

At the level of an effective theory, the MSSM is often regarded as the minimal supersymmetric extension of the SM. We describe some of its features below.

- All particles are assumed to come with a superpartner. The fields of a particle and its superpartner together form a superfield.
- Since the Higgs superfield H_d contains a chiral fermion (the Higgsino), a second Higgs superfield H_u with opposite hypercharge is required to ensure the cancellation of gauge anomalies. In other words, the MSSM is really a supersymmetric version of the two-Higgs-doublet model (2HDM).

  Introducing H_u also resolves a problem with up-type quark masses. Up-type Yukawa terms in the SM cannot be incorporated into the supersymmetric Lagrangian with just H_d alone, due to what is known as the holomorphicity requirement. At the same time, they are also "hard" terms and hence expected to be highly suppressed if added directly as a non-supersymmetric term. This suppression makes it hard to explain, for example, the size of the top mass.
- An additional discrete symmetry called the R-parity is often imposed to forbid terms in the full Lagrangian that violate the conservation of baryon and lepton numbers B and L. All SM particles have R-parity $+1$ and their superpartners -1.

The Higgs as a slepton

Since it has the same gauge quantum numbers as a left-handed (LH) lepton, could the Higgs actually be a slepton? In that case, we no longer need to introduce the

superfield H_d, since the Higgs can now be embedded within one of the LH lepton superfields. We present the usual objections and how one might be able to get around them. For simplicity, we assume the lepton generation whose superfield contains the Higgs to be the electron unless otherwise specified.

- In this setup, the supersymmetric Lagrangian contains Dirac mass terms of the form

$$-\frac{gv_H}{\sqrt{2}}e^-\tilde{W}^+ - \frac{gv_H}{2}\nu_e\tilde{W}^0 + \frac{g'v_H}{2}\nu_e\tilde{B} + \text{h.c.}, \tag{1.1}$$

  where e^- is the electron, ν_e the electron neutrino, $\tilde{W}^{+,0}$ and $\tilde{B}$ the Winos and Binos, and g and g' the electroweak gauge couplings. If $\tilde{W}^0$ and $\tilde{B}$ also acquire Majorana masses from the "soft" terms, diagonalising the resultant mass matrix then shows that the physical neutrino has a Majorana mass of order $\frac{v_H^2}{m_{\text{soft}}}$, which is way too large.

  To get around this, one can impose an $U(1)_R$ symmetry that forbids Majorana masses, and at the same time introduce new adjoint superfields Φ_W and Φ_B, as well as "soft" Dirac mass terms

$$-M_{\tilde{W}}\psi^0_{\tilde{W}}\tilde{W}^0 - M_{\tilde{B}}\psi_{\tilde{B}}\tilde{B} + \text{h.c.}, \tag{1.2}$$

  where $\psi_{\tilde{W}}$ and $\psi_{\tilde{B}}$ are the fermion components of Φ_W and Φ_B, and $M_{\tilde{W}}$ and $M_{\tilde{B}}$ mass parameters of order m_{soft}. Doing so now allows the physical neutrino to remain massless, while the physical gauginos become Dirac particles with masses approximately $M_{\tilde{W}}$ and $M_{\tilde{B}}$. These gauginos are called Dirac gauginos to contrast them with the usual Majorana gauginos in the MSSM. Also note that R-parity is no longer required since the $U(1)_R$ symmetry already forbids terms that violate B and L conservation, even though some of the terms allowed by $U(1)_R$ symmetry actually violate R-parity.

- By removing the superfield H_d, one is also forced to remove H_u to avoid gauge anomalies[3], hence causing the issue of up-type quark masses to return. In other words, one can only introduce SM up-type Yukawa terms as "hard" terms, which as mentioned before are typically highly suppressed and hence cannot explain the top mass.

  One solution is to assume that new physics beyond this supersymmetric effective theory occurs at a scale Λ not far above m_{soft}, and that the new physics allows the usual suppression factor $\frac{m_{\text{soft}}}{M}$ in these hard terms to be replaced by a less severe factor of $\frac{m_{\text{soft}}}{\Lambda}$. (There is still a factor of $\frac{1}{M}$ implicit in m_{soft}, which cannot be removed given the way SUSY breaking is communicated to the low-energy sector, but it is irrelevant to the discussion here.) As long as Λ remains sufficiently small, the "hard" terms can now generate the top mass without much difficulty.

- In this setup, the down-type Yukawa term for the electron cannot be incorporated into the supersymmetric Lagrangian, due to mathematical results involving the contraction of two identical $SU(2)$ doublets. (The muon and tau Yukawa terms are unaffected.) Nonetheless, just as above, we can still introduce this as a "hard" term, and invoke the new Λ scale to ensure that it is not overly suppressed.

To conclude, while there are numerous challenges in constructing a Higgs-as-slepton model, these challenges are not insurmountable. Such a model has indeed been proposed in [36]. Strictly speaking, this model is not more minimal than the MSSM despite the absence of the superfields H_u and H_d, since new adjoint superfields Φ_W

[3]Of course one can introduce yet another superfield to cancel the anomalies induced by H_u, but this defeats the point of trying to find a more minimal supersymmetric extension than the MSSM.

and Φ_B (and also Φ_G for the gluinos) have to be introduced to provide Dirac partners for the gauginos, not to mention the low UV cutoff Λ of the model.

Chapter 2, based on published work with C. Biggio, J. A. Dror and Y. Grossman [37], examines various phenomenological consequences of the Higgs-as-slepton model.

- Due to Eq. (1.1), the massless physical neutrino is not purely the electron neutrino ν_e, but instead contains a small mixture of the new adjoint fermions $\psi^0_{\tilde{W}}$ and $\psi_{\tilde{B}}$. The same can actually be said of the physical electron, which is not purely e^- but contains a small mixture of $\psi^-_{\tilde{W}}$. On the other hand, this mixing is absent for the muon and tau generation, hence implying a violation of lepton universality. This allows us to probe the model using precision electroweak and neutrino experiments.
- Since neutrino masses are small but nonzero, the $U(1)_R$ symmetry must ultimately be broken to allow Majorana masses. Presumably, this might occur through gravity mediation to account for the smallness of the breaking. By examining how this breaking is communicated to the neutrinos (which the mixing discussed above has a direct impact on), one can impose constraints on the model using measurements of the Pontecorvo-Maki-Nakagawa-Sakata (PMNS) matrix [15, 38].
- The $U(1)_R$ breaking discussed above implies that terms that violate B and L conservation are now allowed. Results from proton decay experiments can hence impose additional constraints on the model, in particular the size of the $U(1)_R$ breaking.

Chapter 3, based on published work with B. Josh and J. A. Dror [39], uses the Higgs-as-sneutrino model to explain the excesses seen in three separate searches during Run I of the CMS experiment. Two of them were leptoquark searches (coloured bosons that can decay to a single lepton and quark), based on pair-produced leptoquarks decaying to $eejj$ and $e\nu jj$ final states [40, 41], while the third was a search for the W_R gauge bosons (predicted in left-right symmetric models), based on decays to $eejj$ [42]. An intriguing fact is that no excesses were seen in the corresponding muon channels [42, 43]. Therefore, had these excesses been genuine and not just statistical anomalies, this would imply a violation of lepton universality in the new physics being discovered. This makes the Higgs-as-slepton model particularly attractive since the non-universality is a hallmark of the model, and not just an ad-hoc model input. We find that the model can indeed simultaneously explain the excesses seen in all three searches, with a first-generation squark playing the role of the leptoquark, and the W_R excess mimicked by gluino-squark production.

1.2.2 Supersymmetric left-right symmetric models and the 2 TeV diboson excess (Chapter 4)

Just as the electromagnetic gauge group $U(1)_Q$ is the unbroken subgroup of the larger electroweak gauge group $SU(2)_L \times U(1)_Y$, it is certainly plausible that the SM group (before further symmetry breaking) is itself the unbroken subgroup of a larger group. For example, in grand unified theories, the larger group is a simple Lie group like $SU(5)$ [44] or $SO(10)$ [45, 46]. Another example is the left-right symmetric (LRS) model [47, 48], which we briefly review below.

In the minimal LRS model, we begin with the gauge group $SU(3)_C \times SU(2)_L \times SU(2)_R \times U(1)_X$, which undergoes the breaking pattern $SU(2)_R \times U(1)_X \to U(1)_Y$ at an energy scale $v_R \gg v_H$. Just as the SM left-handed (LH) fermions form doublets under $SU(2)_L$, the right-handed (RH) fermions form doublets under $SU(2)_R$ (which necessitates the introduction of the RH neutrino to pair with the RH charged leptons). The SM Higgs has to be embedded within a $SU(2)_L \times SU(2)_R$ scalar bidoublet Φ, so that one can form Yukawa terms involving both LH and RH fermions. The bidoublet also implies that this is effectively a 2HDM. However, different scalar fields are required to achieve the required breaking to $U(1)_Y$ at the higher scale v_R. This is usually a complex $SU(2)_R$ triplet Δ_R, although a doublet H_R can also be used. The advantage of using Δ_R is that it can generate v_R-scale Majorana masses for the RH neutrinos, which through the seesaw mechanism implies small but nonzero masses for the light neutrinos. Finally, the breaking generates heavy gauge bosons W' and Z' with masses of order v_R. W' comprises mostly the $SU(2)_R$ gauge bosons W_R but also contains a small component of the $SU(2)_L$ bosons W_L due to the Φ vacuum expectation values (VEV). The W_L component is responsible for the diboson decay channel $W' \to WZ$.

Around 2014–2015, a number of searches by the CMS and ATLAS experiments reported excesses that hinted at the possibility of a W' with a mass near 2 TeV. Among the most significant are [49] based on the diboson decay (with the two bosons decaying hadronically), [42] based on decays to $eejj$, and [50] based on dijet decay. Chapter 4, based on published work with J. Collins [51], was motivated by trying to understand the implications of a LRS model consistent with these excesses on SUSY. In the MSSM, after the fine-tuning (associated with the little hierarchy problem) required to generate the right electroweak scale v_H, it turns out that the physical Higgs boson often ends up becoming too *light*. This issue is potentially

resolved in a SUSY LRS model since the new gauge bosons in the LRS provide additional contributions to the Higgs boson mass. However, the combined gauge boson contributions scale as $\cos^2(2\beta)$, where $\tan\beta$ is defined as the ratio of the two Higgs VEV in the bidoublet Φ, so we require a relatively large $\tan\beta$ near 10 to ensure that the combined contributions stay large. On the other hand, the ratio of the diboson to dijet partial widths scales as $\sin^2(2\beta)$, so a large $\tan\beta$ implies a small ratio of partial widths, which was inconsistent with the relatively large ratio observed in these excesses.

We found that the contradictory requirements on the size of $\tan\beta$ (Higgs mass versus partial width ratio) can be resolved by introducing heavy (TeV-scale) down-type vector-like quarks, and allowing them to mix with the usual light quarks. Since the vector-like quarks are singlets under $SU(2)_R$, this mixing will reduce the couplings between W' and the physical light quarks, hence boosting the ratio of partial widths so a large $\tan\beta$ can now be accommodated. Doing so also resolves an issue with quark mass ratios: Due to the holomorphicity requirements from SUSY discussed in the previous section, there is only one way to couple Φ to the quarks, hence implying only one set of Yukawa coefficients. As a result, the quark mass ratios $m_u : m_c : m_t$ should be the same as $m_d : m_s : m_b$, clearly in disagreement with experiments. While this issue may be addressed by introducing a second bidoublet, mixing with vector-like quarks can also achieve the same effect, since the amount of mixing can be made to vary between generations, hence providing an independent means to modify the quark mass ratio $m_d : m_s : m_b$.

We also checked that our model can be made consistent with constraints from flavour physics [52]. For example, we found that unlike in the SM, the Z boson here can contribute tree-level flavour-changing neutral currents (FCNC). This is partic-

ularly noticeable in the coupling to RH down-type quarks, where the flavour non-diagonality comes from the combined effects of mixing between light and vector-like quarks, and between Z and Z'. These FCNCs imply certain constraints on the Yukawa couplings in our model but do not rule the model out.

1.2.3 θ_{13} in A_4 lepton models (Chapter 5)

One curious aspect of the SM is that certain patterns can be observed in the quark and lepton mass spectra, as well as in the Cabibbo-Kobayashi-Maskawa (CKM) [53, 54] and PMNS matrices. Should we simply regard these patterns as ad-hoc, or do they arise from some underlying new physics? For the latter, one class of models can be described as follows:

1. First, one introduces a *family symmetry*, as well as a number of scalar fields called *flavons*. Additional fields may also be introduced as required, e.g. right-handed neutrinos.
2. Next, one assigns group representations to all the fields, and write down the most general Lagrangian consistent with the family symmetry, except with certain constraints on the coefficients so that the flavons can acquire VEVs that are aligned in a certain manner. (These constraints should be rather general and not require any fine-tuning.) Hence, the family symmetry is spontaneously broken either completely or to its subgroup(s).
3. One now writes down an effective theory below this breaking scale with the flavons replaced by their VEVs, i.e. the VEVs enter the masses and Yukawas of the effective theory. At this stage, if additional heavy fields are still present, further steps may be required to reduce it to the SM or νSM

(SM with dimension-five Weinberg operators [55] responsible for Majorana neutrino masses).

With the right choice of family symmetry, fields and representations, the desired patterns in the fermion mass spectra and mixing matrices naturally emerge. Perhaps the most famous example in the quark sector is the Froggatt-Nielsen model [56], based on a $U(1)$ family symmetry. Our focus here will be on lepton models based on a discrete A_4 symmetry, where A_4 is the point group of a regular tetrahedron.

For a while, the PMNS matrix was thought to be consistent with the tri-bimaximal mixing pattern [57]

$$U_{\text{TBM}} = \begin{pmatrix} \sqrt{\frac{2}{3}} & \frac{1}{\sqrt{3}} & 0 \\ -\frac{1}{\sqrt{6}} & \frac{1}{\sqrt{3}} & \frac{1}{\sqrt{2}} \\ \frac{1}{\sqrt{6}} & -\frac{1}{\sqrt{3}} & \frac{1}{\sqrt{2}} \end{pmatrix}. \tag{1.3}$$

Note that this pattern implies $\theta_{13} = 0$ under standard parametrisation. As a result, A_4 models have become popular since they can reproduce such a pattern together with the correct lepton mass spectrum. However, recent measurements by the Daya Bay [58] and RENO [59] experiments have reported a relatively large θ_{13} value at around ~ 0.16, hence throwing the tri-bimaximal mixing pattern into question. While A_4 models and their UV completions now appear to be less motivated, it is still worth asking whether these models can accommodate the measured θ_{13} values.

Chapter 5, based on published work with Y. Grossman [60], examines the size of θ_{13} in a particular UV completion of an A_4 model [61]. The details of the model are as follows:

1. The model, assumed to be valid up to a cutoff scale Λ, begins with a contin-

uous $SO(3)$ family symmetry. This is first spontaneously broken by a flavon T to the A_4 subgroup at a scale $v_T \equiv \langle T \rangle$, hence recovering the A_4 model.

2. Subsequently, the A_4 is spontaneously broken by flavons ϕ, ϕ_5 and ϕ' to the Z_2 subgroup for neutrinos and Z_3 for charged leptons, at a scale $v \equiv \langle \phi \rangle \sim \langle \phi_5 \rangle \sim \langle \phi' \rangle$. (Strictly speaking, A_4 has been completely broken, since neither Z_2 nor Z_3 remain as symmetries of both sectors simultaneously.) This breaking pattern is standard in most A_4 models.

3. The model includes three heavy RH neutrinos, which can be integrated out to generate very small masses for the SM neutrinos via the usual Type I seesaw mechanism. The resulting light neutrino Majorana mass matrix takes the form

$$M_\nu = \begin{pmatrix} a & 0 & 0 \\ 0 & b & c \\ 0 & c & b \end{pmatrix}, \tag{1.4}$$

due to the remaining Z_2 symmetry dictating the form of the RH neutrino mass matrix prior to integrating out. To reproduce from this mass matrix the light neutrino mass hierarchy inferred from neutrino oscillation experiments, one requires $M \ll v \ll v_T \ll \Lambda$, where $M \sim 10^{14}\,\text{GeV}$ is the usual Type I seesaw scale. Since Λ is ultimately limited by the Planck mass M_{Pl}, this implies a relatively squeezed hierarchy of scales.

4. The model also includes three heavy charged leptons, although the SM charged leptons already start off as massive, unlike the neutrinos. The remaining Z_3 symmetry imposes the following form on the light charged-lepton Dirac mass matrix:

$$M_l = \begin{pmatrix} a' & b' & c' \\ a' & b'\omega & c'\omega^2 \\ a' & b'\omega^2 & c'\omega \end{pmatrix}, \tag{1.5}$$

where $\omega \equiv e^{2\pi i/3}$. Note that this does not include any seesaw-like contributions from the heavy charged leptons. The forms Eqs. (1.4) and (1.5) together imply the tri-bimaximal mixing pattern of the PMNS matrix.

We now summarise the main results of Chapter 5. The model description above ignored the seesaw-like contributions to the light charged-lepton mass matrix. However, a careful analysis shows that these contributions are actually important, and in fact the leading contribution is as large as the starting mass matrix. However, it turns out that the leading contribution still preserves the form of the mass matrix given in Eq. (1.5); the form is only modified at the next leading order, a factor of $\mathcal{O}(\frac{v}{v_T})$ smaller. From this, one can show that θ_{13} is expected to be of order $\mathcal{O}(\frac{m_\tau}{m_\mu} \cdot \frac{v}{v_T})$. Given the squeezed hierarchy of scales in the model, a θ_{13} of order $\mathcal{O}(0.1)$ is actually a natural outcome.

A secondary result of Chapter 5 is as follows. Since $\langle T \rangle$ specifies the unbroken A_4 subgroup of $SO(3)$, the VEVs $\langle \phi \rangle$, $\langle \phi_5 \rangle$ and $\langle \phi' \rangle$ have to be aligned in a certain manner relative to $\langle T \rangle$ so that the subgroups Z_2 and Z_3 remain unbroken in the relevant sectors. A common approach to generate a nonzero θ_{13} is simply to allow the VEVs to become misaligned. We verify that the misalignment method also works for the $SO(3) \to A_4$ model discussed here.

1.2.4 Co-decaying dark matter (Chapter 6)

The total mass of a galaxy or galaxy cluster appears to be many times larger than the luminous mass, based on astrophysical observations such as the rotation curves of spiral galaxies [4], and the velocity dispersion of elliptical galaxies [62] and galaxy clusters [63]. The most compelling explanation of the discrepancy so far

is the presence of dark matter (DM). While baryonic DM candidates such as non-luminous gas and dust clouds as well as massive compact halo objects (MACHO) are known to exist, measurements of emission and absorption lines together with micro-lensing observations [64] have indicated that they only make up a small fraction of the missing mass; most of the mass must be non-baryonic. Cosmological observations based on the CMB in conjunctions with galaxy surveys [65, 66] and theoretical considerations from structure formation [67] have shown this also to be the case on the cosmic scale, with the additional requirement that the main contributions cannot come from hot DM candidates such as the SM neutrinos. (A DM candidate is hot if it was still relativistic when the cosmic horizon had grown large enough to encompass an amount of mass comparable to the DM halo of a large galaxy.) This implies the need for a cold DM candidate that lies beyond the SM.

Many classes of DM models have been proposed over the years, including axions and axion-like particles [68], asymmetric DM [69] and freeze-in DM [70], but the most common ones are still those based on thermal freeze-out. These models contain the following elements:

1. The DM is assumed to be produced in large quantities in the early universe, e.g. after reheating from inflaton decay. The same is also assumed for other hidden-sector particles that might be part of the model.

2. There exist reactions that deplete the DM. For instance, weakly-interacting massive particles (WIMP) [71] and their variants [72] usually rely on 2-to-2 annihilation of DM to SM particles, e.g. $AA \to \gamma\gamma$, where A indicates a DM particle. Other models such as secluded [73] and cannibal DM [74] also use 2-to-2 annihilation but to metastable hidden-sector particles that eventually

decay to SM particles, e.g. $AA \to BB$ with $B \to \gamma\gamma$. Self-annihilations such as $AAA \to AA$ have featured in self-interacting DM (SIDM) [75], strongly-interacting massive particles (SIMP) [76], and elastically-decoupling relic (ELDER) [77].

3. Physical conditions exist so as to drive the depletion of the DM. In all the examples cited above, the depletion process keep the DM in chemical equilibrium either with the SM, a hidden sector, or itself, with chemical potential $\mu_A = 0$. As the DM cools to temperature below its rest mass m_A due to Hubble expansion, its number density n_A is now suppressed by a Boltzmann factor. Note that the DM may take on the SM temperature, e.g. in WIMP, secluded DM and SIMP, or it may be thermally decoupled from the SM and hence follow a different temperature, e.g. in cannibal DM, SIDM and ELDER.

4. The depletion eventually terminates, leaving behind the DM as a thermal relic. This is commonly known as freeze-out. Freeze-out is often due to Hubble expansion both diluting and cooling down the DM to the point where the depletion reaction rates are no longer fast enough to keep the DM in the abovementioned chemical equilibrium. (Mathematically, a non-zero chemical potential now builds up so that further cooling does not lead to continued Boltzmann suppression.)

Chapter 6, based on published work [78] with J. A. Dror and E. Kuflik, is motivated by the question of whether it is possible to come up with a different mechanism to drive DM depletion other than the ubiquitous Boltzmann suppression at $\mu_A = 0$. The basic idea is to have the depletion driven by out-of-equilibrium decay that can eventually be switched off. This is achieved with the following setup:

1. The DM candidate A can undergoes 2-to-2 annihilation to a metastable particle B, which then decays to SM particles. We assume mass degeneracy $m_A = m_B$, so their number densities n_A and n_B are equal as long as they remain in chemical equilibrium, i.e. when the 2-to-2 annihilation remains active.

2. We also assume that A and B have been chemically and thermally decoupled from the SM very early on, and that there are no active self-annihilation reactions. (These assumptions distinguish our model from secluded and cannibal DM.) Therefore, Boltzmann suppression of n_A does not occur when the temperature falls below m_A, since the chemical potential μ_A is not required to be zero. In fact, what drives the depletion of A is the out-of-equilibrium decay of B causing n_B and hence n_A to decrease with time. We call this the co-decay mechanism.

3. Eventually, the 2-to-2 annihilation terminates so A and B are no longer in chemical equilibrium. Freeze-out has occurred since n_A no longer tracks n_B which continues to decrease.

Another way to distinguish the Boltzmann suppression and co-decay mechanism is to look at the chemistry. At chemical equilibrium, the net depletion and regeneration rates must be equal. In the usual suppression mechanism, decreasing the temperature alters the balance between the two reaction rates, leading to a new equilibrium density $(n_A)^{\text{eqm}}$ that is suppressed, especially when the temperature falls below m_A. The relation between $(n_A)^{\text{eqm}}$ and time is only indirect, via Hubble expansion causing the temperature to decrease in time. In contrast, in the co-decay mechanism, decreasing the temperature does not directly alters the balance. Rather, what alters the balance is now the slow removal of the reverse

reactants B via out-of-equilibrium decay; hence $(n_A)^{\rm eqm}$ decreases in time. Temperature still plays a role here, albeit a very different one, by affecting the rate of B decay through time dilation.

We perform analytical calculations of the relic abundance, which we then verify with numerical simulations based on the Boltzmann equations. We find that co-decay can be a viable DM freeze-out mechanism, producing the right relic abundance while satisfying constraints from Big Bang nucleosynthesis, the CMB, unitarity of the 2-to-2 annihilation cross-section, as well as the model assumption of the decay being out of equilibrium. The extremely weak coupling between the dark sector and the SM (required for their early decoupling) makes the mechanism hard to probe using direct detection and collider production experiments; however, signatures from indirect detection are enhanced. Finally, we provide a simple but concrete model of a co-decaying DM using gauge bosons from a dark $SU(2)$. The W_D^1 and W_D^2 bosons play the role of the DM candidate A, while the W_D^3, through mixing with the SM Z^0 via a dimension-six operator, plays the role of the metastable partner B.

1.2.5 Hydrogen-antihydrogen oscillations in the interstellar medium (Chapter 7)

Baryon and lepton numbers B and L are often said to be conserved in the SM. However, these conservation laws are accidental, in that they are not imposed on the model, but rather the consequence of including only (super-)renormalisable gauge-invariant operators of dimension four and lower in the Lagrangian[4]. Higher-

[4]Actually, even in this case, B and L conservation are violated by non-perturbative corrections. These corrections may play an important role in the early universe [79], although their present-

dimension operators are inevitable when we derive the SM as the low-energy effective theory of a UV completion, many of which allow processes that violate B and L conservation. (We denote these violations by $\not{B}$ and $\not{L}$ respectively.) Some examples are listed below.

1. Dimension-five Weinberg operators generate Majorana masses for the neutrinos, and also allow $\Delta L = \pm 2$ processes such as neutrinoless double β decay.
2. Dimension-six operators such as $\frac{QQQL}{\Lambda^2}$ and $\frac{u^c u^c d^c e^c}{\Lambda^2}$ [55] allow $\Delta B = \Delta L = \pm 1$ processes, such as proton decay via $p \to e^+ \pi^0$.
3. Dimension-nine operators such as $\frac{QQQQ(d^c d^c)^*}{\Lambda^5}$ and $\frac{u^c d^c d^c u^c d^c d^c}{\Lambda^5}$ [81] allow $\Delta B = \pm 2$ processes, such as neutron-antineutron oscillation $n \leftrightarrow \bar{n}$.
4. Dimension-twelve operators such as $\frac{QQQQQQLL}{\Lambda^8}$ [82] allow $\Delta B = \Delta L = \pm 2$ processes, such as double proton decay via $pp \to e^+ e^+$, and hydrogen-antihydrogen oscillation $\mathrm{H} \leftrightarrow \bar{\mathrm{H}}$.

By using the same scale Λ in the $\not{B}$ operators above, we have implicitly assumed that these operators are generated by the same new physics. We can then compare the probabilities of the corresponding $\not{B}$ processes. Dimensional analysis based on "wavefunction overlap" suggests that the probability of proton decay over a duration t is of order $\left[\frac{\Lambda_{\mathrm{QCD}}^4}{\Lambda^4}\Lambda_{\mathrm{QCD}} \cdot t\right]$. while the probabilities of n-$\bar{n}$ and H-$\bar{\mathrm{H}}$ oscillations are of order $\left[\frac{\Lambda_{\mathrm{QCD}}^5}{\Lambda^5}\Lambda_{\mathrm{QCD}} \cdot \min\{t, \frac{1}{|\Delta_{n\bar{n}}|}\}\right]^2$ and $\left[\frac{\Lambda_{\mathrm{QCD}}^5 (\alpha m_e)^3}{\Lambda^8}\Lambda_{\mathrm{QCD}} \cdot \min\{t, \frac{1}{|\Delta_{\mathrm{H}\bar{\mathrm{H}}}|}\}\right]^2$ respectively. Here, m_e is the electron mass, α the fine-structure constant, and $\Delta_{n\bar{n}}$ and $\Delta_{\mathrm{H}\bar{\mathrm{H}}}$ energy scales related to matter effects (discussed later). We see that the higher the operator dimension a process relies on, the more suppressed the prob-

day effects are unobservably small [80].

ability. Given the already strong experimental constraints on proton decay [83], detecting the other $\not{B}$ processes would seem even less likely.

However, the previous assumption that these operators share the same Λ can certainly be violated. For instance, consider a UV completion like [82] where only processes with even-numbered ΔB and ΔL are allowed. In the low-energy effective theory, one then expects "allowed" operators like $\frac{QQQQ(d^c d^c)^*}{\Lambda^5}$ and $\frac{QQQQQQLL}{\Lambda^8}$ to have Λ of order the scale of this UV completion, whereas "forbidden" operators like $\frac{QQQL}{\Lambda^2}$ now have much higher Λ values that depend on the scale of further UV completion where these ΔB and ΔL selection rules break down. This then leaves open the possibility that the $\not{B}$ oscillations may still be detectable despite the proton decay constraints, provided that the separation between the two Λ scales is large enough.

One way to detect H-$\bar{\text{H}}$ oscillation has been proposed in [84]. Hydrogen exists mostly in atomic form in the HI regions of the interstellar medium (ISM). Should a H atom oscillate into a $\bar{\text{H}}$, the $\bar{\text{H}}$ may then annihilate with another particle to produce γ rays. Therefore, diffuse γ-ray measurements can be used to constrain the oscillation probability after subtracting known astrophysical background.

Chapter 7, based on published work with Y. Grossman and S. Ray [85], re-examines the original bound derived in [84]. The motivations for doing so are as follows:

1. *Matter effects.* In the ISM, H-$\bar{\text{H}}$ oscillations become suppressed due to interactions of the atoms with other particles and each other. In the original analysis, only the annihilation of $\bar{\text{H}}$ with other H atoms was accounted for. However, given the wide variety of processes the atoms can take part in, from elastic scattering to photo-ionisation, it is not clear whether such an

approximation is justified.

2. *Structure of the interstellar medium.* In the original analysis, it was implicitly assumed that most of the H atoms detected along a line of sight by 21 cm line survey come from HI regions with similar properties. However, we now understand that there are actually two HI phases with different physical properties. This affects how the γ-ray data should be interpreted for the purpose of constraining the oscillations.

3. *Availability of cross-section data.* Significant progress has been made in the field of computational atomic physics since the original analysis. In particular, scattering amplitudes and cross-sections of many processes are now available over a wide range of energies. This allows us to reduce the uncertainties in our calculations since we no longer have to rely on order-of-magnitude estimates most of the time.

4. *Improved γ-ray data and background subtraction.* The original analysis was performed using early γ-ray data collected by the Small Astronomy Satellite 2 [86]. With the recent deployment of the *Fermi* Large Area Telescope (LAT) [87], higher quality data is now available. In addition, significant progress have been made in the modelling of diffuse γ-ray backgrounds from cosmic-ray (CR) interaction with matter and inverse Compton scattering of soft interstellar photons, hence allowing for more accurate background subtraction.

While we are ultimately only interested in an order-of-magnitude estimate, we want to reduce the uncertainty in each step as much as is reasonable to limit the cumulative uncertainty. Doing so allow us to discover, for instance, that elastic scattering actually has a greater effect on the oscillations than $\bar{\mathrm{H}}$ annihilation,

contrary to the original assumptions in [84]. At the end, we derive an updated bound that is approximately one order of magnitude weaker than the previous result.

Chapter 2
Probing a slepton Higgs on all frontiers[1]

Chapter abstract

We study several aspects of supersymmetric models with a $U(1)_R$ symmetry where the Higgs doublet is identified with the superpartner of a lepton. We derive new, stronger bounds on the gaugino masses based on current measurements, and also propose ways to probe the model up to scales of $\mathcal{O}(10\,\text{TeV})$ at future e^+e^- colliders. Since the $U(1)_R$ symmetry cannot be exact, we analyse the effects of R-symmetry breaking on neutrino masses and proton decay. In particular, we find that getting the neutrino mixing angles to agree with experiments in a minimal model requires a UV cutoff for the theory at around 10 TeV.

2.1 Introduction

The LHC collaborations have recently discovered the Higgs boson at around 125 GeV [88, 89], but have yet to find any of the particles which should have appeared below the TeV scale as required to solve the hierarchy problem [90]. This suggests that if supersymmetry (SUSY) is present at the TeV scale, it deviates from its most naive implementations. There are many suggestions as to how Nature could be supersymmetric but still avoid the bounds applied by the LHC. In particular, there has been a lot of interest in substituting the R-parity of the Minimal Supersymmetric Standard Model (MSSM) for a continuous R-symmetry,

[1] Based on C. Biggio, J. A. Dror, Y. Grossman and W. H. Ng, *JHEP* **04** (2016) 150, [1602.02162].

($U(1)_R$) [91, 92] (see [93–113] for recent work in this direction).

One interesting feature of imposing a $U(1)_R$ symmetry is that it allows the ordinary down-type Higgs to be in a supermultiplet with one of the charged-lepton doublets,

$$H \equiv (H, \ell_L) \tag{2.1}$$

and still avoid phenomenological bounds. This intriguing possibility has been discussed in several recent papers: see [36, 101, 107] for model building, [114] for stop phenomenology, and [39] for a suggested explanation of the recent $eejj, e\nu jj$ excess [41, 42] as well as further discussion on light squark phenomenology. For the purpose of this work we will focus on the possibility that the Higgs doublet is identified with the selectron doublet, though much of our discussion will be more general. This is motivated in Section 2.2 as it naturally explains the smallness of the electron mass.

While it is more economical to construct SUSY models where the Higgs is identified with a slepton, usually this causes phenomenological difficulties due to violation of lepton number. In particular, the Kähler potential generates electroweak-scale Dirac masses between the partner neutrino (defined as the neutral fermionic component of L_e) and the gauginos. As a result the partner neutrino generically becomes too heavy. This problem can be avoided by introducing a global symmetry to forbid Majorana neutralino masses, and adding additional adjoint chiral superfields as Dirac partners of the gauginos. This ensures a massless physical neutralino that can be identified with the neutrino. However, due to the smallness of neutrino masses, it is important that the symmetry be preserved under electroweak symmetry breaking. This requires that the global symmetry be an R-symmetry such that the neutrino be charged under the $U(1)_R$ but still leave the

Higgs uncharged.

One may wonder why there aren't additional constraints from the many experiments probing lepton flavour number violation. This is because these models generically only have lepton number violation for one flavour (in our case the electron). The stringent limits from lepton number changing processes rely on violation of at least two lepton flavour numbers (most notably $\mu \to e\gamma$, which requires muon and electron number violation).

In this work we explore how Higgs-as-slepton models can be further probed in several different ways. A generic feature of these models is a mixing between the electron doublet and the gauginos, resulting in the physical electron doublet no longer equal to the corresponding gauge eigenstate. This mixing puts bounds on the size of the wino and bino masses. Previous papers have emphasised the corresponding bounds from the high energy frontier through neutral and charged current universality measurements. In this work we explore the limits from low energy measurements of G_F. We find these to be more stringent then the high energy constraints for bounds on the bino masses and competitive with bounds on the wino masses. Furthermore, we look at the discovery potential of the future e^+e^- collider program. Intriguingly, we find that such a machine has the potential to probe this variant of supersymmetry up to $\mathcal{O}(10\,\mathrm{TeV})$.

Another aspect of the model which we will examine is the breaking of R-symmetry through Planck-scale effect, naturally generating a small parameter in the theory. This is responsible for generating neutrino masses which would otherwise be zero, but may also lead to effects such as proton decay.

Experimentally, there has recently been significant development in the neu-

trino sector. The differences in the squares of the neutrino masses and the three neutrino mixing angles have been measured [115]. Having the Higgs be part of a supermultiplet with the lepton has crucial implications in terms of neutrino phenomenology, the consequences of which we will explore. Planck-scale suppression of R-symmetry breaking effects lead to naturally small neutrino masses. Assuming this is the only source of neutrino masses, we find that in order to obtain the large mixing angles measured by neutrino oscillation experiments, the model typically requires a low cutoff scale of at most $\mathcal{O}(10\,\text{TeV})$. In other words, a generic minimal supersymmetric model with the Higgs playing the role of a slepton requires a low ultraviolet (UV) completion scale.

In addition to contributing to neutrino masses, R-symmetry breaking can also lead to proton decay if the gravitino mass is very heavy. Neutrino mass measurements suggests a gravitino mass range between $\mathcal{O}(10\,\text{eV}) - \mathcal{O}(10\,\text{keV})$ assuming generic gravity-mediated R-breaking. With such masses the model could have rapid proton decay which restricts the possible UV completions of the model.

This chapter is structured as follows. We begin by outlining general properties of the Higgs-as-slepton models in Section 2.2. We then proceed to study the constraints on gaugino masses from the lepton-gaugino mixing in Section 2.3. Phenomenological implications on future e^+e^- colliders are covered in Section 2.4. Implications of the lepton mixing angles on these models are discussed in Section 2.5. We move on to bounds on the gravitino mass from proton decay and neutrino mass measurements in Section 2.6. We conclude in Section 2.7 with a summary of our main results.

2.2 The basics of Higgs-as-slepton models

We consider the most minimal version of the Higgs-as-slepton model from a bottom-up perspective, in which the only additional fields added to the Higgs-less Standard Model (SM) and their supersymmetric partners are the Dirac partners of the gauginos. Table 2.1 lists the superfields and their gauge and $U(1)_R$ representations. As mentioned earlier we have chosen the Higgs to be in L_e. In places where we generalise our discussion to other choices of lepton flavour, this will be stated in the text. The R-charges are chosen so that left-handed (LH) and right-handed (RH) quarks and leptons form R-symmetric Dirac pairs, and that the Higgs vacuum expectation value (VEV) does not break R-symmetry.

Note that we keep B and L as free parameters, and thus they are not identified with the usual baryon and lepton numbers. Based on our assignments, the quarks have R-charges B, the muon and tau $-L$, while the electron always carries R-charge -1. Moreover, the normalization of L and B is not determined such that different normalization result in different models with different phenomenology. We learn that B and L are parameters that determine the R-charge of the quarks and the second- and third-generation lepton superfields. No significant change in phenomenology arises from different choices of B, except for $B = 1/3$ or 1 which lead to rapid proton decay and are hence forbidden (see Section 2.6). Therefore, in our discussion we only consider the generic B case. On the other hand, viable models can be built for several choices of L. In particular we will consider the $L = -1$, $L = 0$, $L = 1$ and the generic L case, that is $L \neq -1, 0, 1$. Each of these four choices result in distinct lepton phenomenology and hence can be regarded as a separate model.

For a generic assignment of B and L, the superpotential consistent with the

	$(SU(3)_C, SU(2)_L)_Y$	$U(1)_R$
$H \equiv L_e$	$(1,2)_{-1/2}$	0
E_e^c	$(1,1)_1$	2
$L_{\mu,\tau}$	$(1,2)_{-1/2}$	$1-L$
$E_{\mu,\tau}^c$	$(1,1)_1$	$1+L$
$Q_{1,2,3}$	$(3,2)_{1/6}$	$1+B$
$U_{1,2,3}^c$	$(\bar{3},1)_{-2/3}$	$1-B$
$D_{1,2,3}^c$	$(\bar{3},1)_{1/3}$	$1-B$
$W^{a\alpha}$	$(8,1)_0+(1,3)_0+(1,1)_0$	1
Φ^a	$(8,1)_0+(1,3)_0+(1,1)_0$	0

Table 2.1: Superfields in the minimal low energy model with the Higgs doublet identified with the selectron doublet. The $U(1)_R$ charges are parameterized with two unknown variables L and B, which gives the most general assignment consistent with the requirement of the existence of Yukawas, R-charge conservation after electroweak symmetry breaking, and supersymmetry. The $U(1)_R$ in the table refers to the scalar component of the superfield.

symmetries is

$$\mathcal{W} = \sum_{i,j=1}^{3} y_{d,ij} H Q_i D_j^c + \sum_{i,j\in\{\mu,\tau\}} y_{e,ij} H L_i E_j^c \,. \tag{2.2}$$

For the $B = 1/3$ or $L = 1$ cases there are extra terms, but we do not discuss them here. In the case $L = 1$, the details of which can be found in [107, 114].

The Higgs-as-slepton model faces a number of difficulties and here we discuss two of them. First is the fact that supersymmetry forbids a mass term for the up-type quarks. This problem can be solved by introducing non-renormalizable SUSY-breaking Kähler terms suppressed by a UV cutoff scale, Λ,

$$\int d^4\theta \frac{X^\dagger}{M} \frac{H^\dagger Q U}{\Lambda} \,, \tag{2.3}$$

where M is the R-symmetric mediation scale and X is the spurion whose vacuum expectation value $\langle F_X \rangle$ corresponds to the SUSY breaking scale. Perturbativity

of the couplings requires the cutoff scale to be at most $4\pi\,\mathrm{TeV}$. Thus the model requires a low-scale UV completion. In principle, one can avoid this by introducing an additional pair of Higgs doublets [101, 107], which then allows top masses to be generated by the tree-level superpotential. However, as we will show in Section 2.5, reproducing the correct lepton mixing angles also requires a low cutoff if we assume neutrino masses arise from generic R-breaking. This requirement holds even with the additional Higgs doublets. The second problem is that the superpotential cannot provide a mass term for the fermion component of the $H = L_e$ doublet (related to the left-handed electron field) since $HH = 0$. Again, this can be resolved by generating a mass in an analogous way [116],

$$\int d^4\theta \frac{X^\dagger X}{M^2} \frac{H D^\alpha H D_\alpha E_3}{\Lambda^2}\,, \tag{2.4}$$

where D_α is the superspace derivative. If the electron doublet is the Higgs partner, then this provides a natural explanation for the smallness of the electron mass, hence motivating our original choice.

One of the most important consequences of having the Higgs as a slepton is the mixing between the electroweak gauginos and the Higgs fermionic superpartner. This puts generic constraints on such models. The Kähler potential generates weak scale Dirac mass terms given by

$$\int d^4\theta H^\dagger e^V H \supset -\frac{gv}{\sqrt{2}} e_L \tilde{W}^+ - \frac{gv}{2}\nu_e \tilde{W}^0 + \frac{g'v}{2}\nu_e \tilde{B}^0\,, \tag{2.5}$$

where, g, g' are the $SU(2)_L$ and $U(1)_Y$ coupling constants and $v \simeq 246\,\mathrm{GeV}$ is the vacuum expectation value of the Higgs. The Dirac wino and bino masses, $M_{\tilde{W}}$ and $M_{\tilde{B}}$, are of order of the soft R-symmetric SUSY-breaking scale $M_{\mathrm{soft}} \equiv \langle F_X \rangle / M$. This implies a mixing of order of the ratio of the electroweak scale to the soft R-symmetric scale, which we quantify using the small parameter

$$\epsilon \equiv \frac{gv}{2M_{\tilde{W}}} = \frac{m_W}{M_{\tilde{W}}}, \tag{2.6}$$

where m_W is the mass of the W boson. The above implies that the mass of the gauginos must be high. As discussed in the following, the upper bounds on ϵ are $\mathcal{O}(0.1)$. The mixing can also depend on the size of the non-renormalizable operators arising at the scale Λ. These contributions are model dependent and will be assumed to be negligible. We have also neglected any R-symmetry breaking effects, although we will need to include them when discussing neutrino masses and proton decay later. We also assume that $|M_{\tilde{W}}^2 - M_{\tilde{B}}^2| \gg m_W^2$. While the mixing between the winos and the binos is modified should we relax this assumption, it turns out to have no significant effects on the phenomenology considered in our work. With the above assumptions, and working to $\mathcal{O}(\epsilon^2)$ the mass eigenstates are

$$\begin{aligned}
\chi_{1,L}^- &= \left(1-\epsilon^2\right) e_L^- - \sqrt{2}\epsilon\psi_{\tilde{W}}^-, & \chi_{1,R}^{c,+} &= e_R^{c,+} \\
\chi_{2,L}^- &= \left(1-\frac{1}{2}\epsilon^2\right)\psi_{\tilde{W}}^- + \sqrt{2}\epsilon e_L^-, & \chi_{2,R}^{c,+} &= \tilde{W}^+ \\
\chi_{3,L}^- &= \tilde{W}^-, & \chi_{3,R}^{c,+} &= \tilde{\psi}^+
\end{aligned} \tag{2.7}$$

for the charginos, and

$$\begin{aligned}
\chi_{1,L}^0 &= \left(1-\frac{1}{2}\epsilon^2\left(1+\alpha^2 t_w^2\right)\right)\nu_e - \epsilon\psi_{\tilde{W}} + \epsilon\alpha t_w \psi_{\tilde{B}} & & \\
\chi_{2,L}^0 &= \left(1-\frac{1}{2}\epsilon^2\right)\psi_{\tilde{W}} + \epsilon\nu_e + \epsilon^2\frac{\alpha t_w}{1-\alpha}\psi_{\tilde{B}}, & \chi_{2,R}^{c,0} &= \tilde{W}^0 + \epsilon^2\frac{\alpha^2 t_w}{1-\alpha^2}\tilde{B} \\
\chi_{3,L}^0 &= \left(1-\frac{2}{1}\epsilon^2\alpha^2 t_w^2\right)\psi_{\tilde{B}} - \epsilon\alpha t_w\nu_e - \epsilon^2\frac{\alpha^3 t_w}{1-\alpha^2}\psi_{\tilde{W}} & \chi_{3,R}^{c,0} &= \tilde{B} - \epsilon^2\frac{\alpha^2 t_w}{1-\alpha^2}\tilde{W}^0
\end{aligned} \tag{2.8}$$

for the neutralinos, where t_w denotes the tangent of the Weak mixing angle, and $\alpha \equiv M_{\tilde{W}}/M_{\tilde{B}}$. (For details on the mixing matrices and diagonalisation, see Appendix 2.A.)

2.3 Limits on gaugino-electron doublet mixing

Previous works have shown that the strongest constraints on the model arise from the mixing between the gaugino and the electron doublet [36, 101]. The bounds from neutral current universality have been emphasised (with a mention of the weak charged-current universality bounds in [36]). Charged-current interactions also provide a different set of constraints through non-standard neutrino interactions (NSI) [117–122]. In this section we compute the neutral-current bounds in our general framework and compare the results with additional bounds from NSI. Note that at tree-level neutral current effects can only constrain the wino masses since this arises from mixing of the electrons in the Zee interaction, while charged current measurements are affected by both electron and neutrino mixing in the $We\nu$, yielding bounds on both the wino and bino masses.

We start by computing the electron neutral current. Definitions of the mixing matrices $U_{C,L}$, $U_{C,R}$ and $U_{N,L}$ used here are provided in Appendix 2.A. The interaction is given by

$$\begin{aligned}\Delta\mathcal{L} = \frac{g}{c_w}\Bigg[&\left(c_w^2 - |(U_{C,R})_{11}|^2\right)(\chi_{1,R}^{c,+})^\dagger \bar{\sigma}^\mu Z_\mu \chi_{1,R}^{c,+} \\ &- \left(c_w^2 - \frac{1}{2}|(U_{C,L})_{11}|^2\right)(\chi_{1,L}^-)^\dagger \bar{\sigma}^\mu Z_\mu \chi_{1,L}^-\Bigg].\end{aligned} \tag{2.9}$$

Keeping only terms to $\mathcal{O}(\epsilon^2)$, this gives

$$\Delta\mathcal{L} = \frac{g}{c_w}\left[-s_w^2(\chi_{1,R}^{c,+})^\dagger\bar{\sigma}^\mu\chi_{1,R}^{c,+} - \left(\frac{1}{2}-s_w^2\right)(\chi_{1,L}^-)^\dagger\bar{\sigma}^\mu\chi_{1,L}^-\right]Z_\mu - \frac{g}{c_w}\epsilon^2(\chi_{1,L}^-)^\dagger\bar{\sigma}^\mu Z_\mu\chi_{1,L}^-, \tag{2.10}$$

from which we obtain the axial current coupling of the Z to fermions

$$g_A = g_A^{SM}\left[1+2\epsilon^2\right], \qquad g_A^{SM} = \frac{g}{2c_w}, \tag{2.11}$$

where g_A^{SM} is the SM value of the axial coupling. (Bounds on the vector current are much weaker and hence irrelevant for this discussion.) Experimentally the bounds

on the axial current are [115],

$$\left|\frac{\delta g_A^e}{g_A^e}\right| \approx 1.2 \times 10^{-3} \quad (90\%\ \text{CL})\,. \tag{2.12}$$

This stringent bound applies only to the wino mass. Bounds on the bino mass arise from modifications of the charged current. The left-handed electron charged current are described by

$$\begin{aligned}\Delta\mathcal{L} &= g\left((U_{N,L})^*_{21}(U_{C,L})_{21} + \frac{1}{\sqrt{2}}(U_{N,L})^*_{11}(U_{C,L})_{11}\right) W_\mu(\chi^{c,+}_{1,R})^\dagger \bar{\sigma}^\mu \chi^0_{1,L} \\ &= \frac{g}{\sqrt{2}}\left(1 + \frac{\epsilon^2}{2}\left(1 - \alpha^2 t_w^2\right)\right) W_\mu(\chi^{c,+}_{1,R})^\dagger \bar{\sigma}^\mu \chi^0_{1,L}\,.\end{aligned} \tag{2.13}$$

[36] computed the charged current universality constraints from τ decays. This corresponds to the limit [123],

$$\frac{|\delta g|}{g^{SM}} \lesssim 2.6 \times 10^{-3} \quad (90\%\ \text{CL})\,. \tag{2.14}$$

There are more stringent constraints arising from NSI interactions. The most stringent constraint, in models where the Cabibbo-Kobayashi-Maskawa (CKM) matrix is assumed to be unitary, arise from taking the ratio of G_F measured in two different ways. The first is through beta- and Kaon- decays and the second (and more precise) through muon decay. If the CKM is unitary then these should be equal to each other and the ratio gives the bound [120],

$$\frac{|\delta g|}{g^{SM}} \lesssim 4.0 \times 10^{-4} \quad (90\%\ \text{CL})\,. \tag{2.15}$$

This limit, as well as the one from the neutral current, are presented in Figure 2.1. We see that while neutral current interactions place a stronger constraint on the wino mass than NSI, it does not constrain the bino mass. Meanwhile, the NSI bounds on the bino mass are generally weaker than on the wino mass due to a t_w suppression in the bino mixing with the neutrino. Combining the

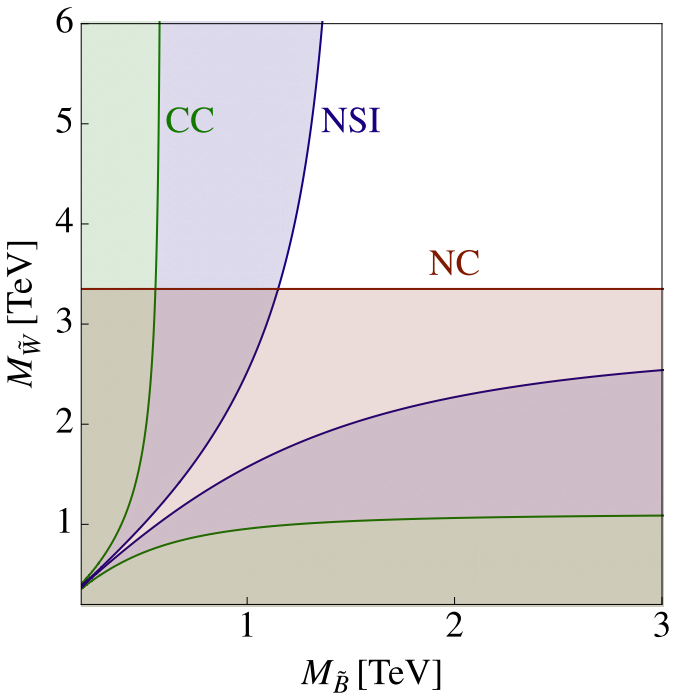

Figure 2.1: Current limits on the bino and wino masses. The regions in blue are excluded by NSI constraints and depend on both the bino and wino mass, while the region in red is ruled out by neutral current constraints. The limits from charged current universality are shown in green.

NSI and neutral current bounds, we can put a constraint on the bino mass of $M_{\tilde{B}} \gtrsim 1.2\,\text{TeV}$. This is more stringent than the existing universality constraint of about 500 GeV [36].

2.4 Discovery potential at an e^+e^- collider

The Higgs-as-slepton model generates deviations of the SM couplings in the electron interactions through modifications of pure SM couplings and from additional interactions with the gauginos. This leads us to expect significant discovery potential at an e^+e^- collider. In this section we consider different $2 \to 2$ processes that will deviate from their SM predictions. In the following we keep terms to

$\mathcal{O}(\epsilon^2)$ and we ignore all non-renormalizable corrections arising at the scale Λ. In particular we consider, $e^+e^- \to W^+W^-, ZZ, hZ$. The relevant Feynman diagrams are displayed in Figure 2.2. Naively one would expect to also have $e^+e^- \to hh$ arising from chargino exchange, however these turn out not to arise at tree level up to $\mathcal{O}(\epsilon^4)$ due to angular momentum conservation suppressing s-wave production. We use the Feynman rules detailed in Appendix 2.A to compute the cross-sections.

To study projections at a future collider we use the condition that the significance, that we take to be $S/\sqrt{B}$, where S is the signal and B is the background, is larger than 1.645 (corresponding to a 90% confidence interval),

$$\frac{\mathcal{L} \times \delta\sigma}{\sqrt{\mathcal{L} \times \sigma^{SM}}} > 1.645\,, \tag{2.16}$$

where $\mathcal{L}$ is the luminosity of the collider and $\delta\sigma \equiv \sigma^{BSM} - \sigma^{SM}$. We expect this to be a reasonable estimate due to the controlled environment offered by a lepton collider, leading to negligible backgrounds.

One subtlety is the cross-section diverges for small t, or equivalently small $|\eta|$, due to a Rutherford singularity. In order to remove sensitivity to this divergence we cut off the phase space integration at $|\eta| = 2$. To avoid this complication in our expressions, we quote the differential $d(\delta\sigma)/dt$ for each process.

2.4.1 $e^+e^- \to W^+W^-$

We begin by computing the effects to $e^+e^- \to W^+W^-$ scattering. The Feynman diagrams which contribute up to $\mathcal{O}(\epsilon^2)$ are shown in Figure 2.2. Note that there are no diagrams with virtual charginos or neutralinos since adding these requires paying the price of additional ϵ's in the vertices. The only modifications to the

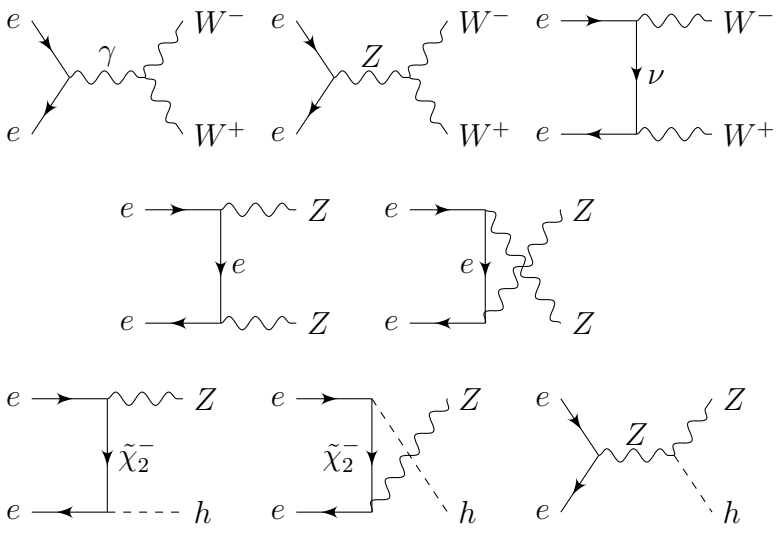

Figure 2.2: Feynman diagrams for the $2 \to 2$ processes that we consider in this work. The top row shows $e^+e^- \to W^+W^-$, the middle row represents $e^+e^- \to ZZ$, and the bottom process is $e^+e^- \to Zh$. We use $\tilde{\chi}_2^-$ to denote the Dirac spinor $\left(\chi_{2,L}^-, (\chi_{2,R}^{c,+})^\dagger\right)$.

SM cross-section are from deviations in the Zee couplings. The effects considered here are a close analogue to deviations considered in $tW \to tW$ scattering at the LHC from anomalous Ztt couplings [124]. The cross-sections are straightforward to compute but the expressions are complicated without making some approximations. For simplicity we only quote the result to lowest order in m_V^2/s ($V = h, Z,$ or W), though in producing the figures we use the full expressions. The result for the signal is

$$\frac{d(\delta\sigma)}{dt} = \frac{1}{4}\frac{\beta}{32\pi s}\left\{\frac{2e^4}{s_w^4}\frac{\left(\frac{1}{2} - s_w^2 - \alpha^2\right)}{\alpha^2}\frac{(-t)}{M_{\tilde{W}}^2}\frac{s+t}{s} + \mathcal{O}\left(\frac{m_V^2}{s}, \frac{s^2}{M_{\tilde{W}}^4}\right)\right\}, \qquad (2.17)$$

where $\beta \equiv \sqrt{1 - 4m_W^2/s}$ is the velocity of either W boson, s_w is the sine of the weak mixing angle, $s \equiv (p_{e^-} + p_{e^+})^2$, $t \equiv (p_{W^-} + p_{W^+})^2$ and $\alpha = m_Z/m_W$.

2.4.2 $e^+e^- \to ZZ$

Next we consider $e^+e^- \to ZZ$ scattering, depicted in Figure 2.2. As for W^+W^-, the chargino-exchange diagrams only arise at higher orders in ϵ. Also in this process the deviation from the SM is in the Zee coupling, but, unlike in the W^+W^- case the total cross-section does not grow with energy but is roughly constant. The difference of the energy scaling between ZZ and W^+W^- production can be traced back to the algebra of $SU(2)$ or equivalently the fact that there doesn't exist a triple gauge coupling ZZZ in the model. The signal is,

$$\frac{d(\delta\sigma)}{dt} = \frac{1}{2}\frac{1}{4}\frac{\beta}{32\pi s}\left\{\frac{2e^4}{s_w^4 c_w^4}\left(1-2s_w^2\right)^2 \frac{m_W^2}{M_{\tilde{W}}^2}\frac{s^2+2st+2t^2}{t(s+t)} + \mathcal{O}\left(\frac{m_V^4}{s^2}, \frac{s^2}{M_{\tilde{W}}^4}\right)\right\}, \tag{2.18}$$

where here $\beta \equiv \sqrt{1-4m_Z^2/s}$ gives the speed of one of the Z bosons.

Note that for $e^+e^- \to ZZ$ the deviation of the coupling is factorizable as the two diagrams (see Figure 2.2) have the same dependence on the anomalous coupling. Thus the new physics contribution is just a rescaling of the SM cross-section.

2.4.3 $e^+e^- \to hZ$

Another interesting channel at a lepton collider is hZ production. The Feynman diagrams are shown in Figure 2.2 with the beyond the SM (BSM) effects entering from chargino exchange as well as modifications to the Zee coupling. Since the $\tilde{\chi}_2 he$ vertex does not have an ϵ suppression, these diagrams are still of $\mathcal{O}(\epsilon^2)$. The signal is,

$$\frac{d(\delta\sigma)}{dt} = \frac{1}{4}\frac{\beta}{32\pi s}\left\{\frac{e^4}{s_w^4 c_w^2}\left(\frac{1}{2}-s_w^2\right)\frac{(-t)}{M_{\tilde{W}}^2}\frac{s+t}{s} + \mathcal{O}\left(\frac{m_V^2}{s^2}, \frac{s^2}{M_{\tilde{W}}^4}\right)\right\}, \tag{2.19}$$

where

$$\beta \equiv \sqrt{1 - m_Z^2/E_Z^2}, \qquad E_Z \equiv \frac{\sqrt{s}}{2}\left(1 + \frac{m_Z^2}{s} - \frac{m_h^2}{s^2}\right) \tag{2.20}$$

such that β denotes the speed of the Z boson. The signal is roughly the same as that of W^+W^- production, however the SM cross-section of hZ is significantly smaller due to the relatively small hZZ vertex. This makes deviations easier to identify, increasing its sensitivity to new physics.

Figure 2.3 compares the reach of the different channels as a function of luminosity for a 1 TeV linear collider. The reach at such a collider is striking. A $300\,\text{fb}^{-1}$ collider can probe wino masses up to $M_{\tilde{W}} \sim 5.4\,\text{TeV}$, $M_{\tilde{W}} \sim 2.3\,\text{TeV}$, and $M_{\tilde{W}} \sim 11.5\,\text{TeV}$ for W^+W^-, ZZ, and hZ respectively. The scale probed by hZ is impressive, exploring physics well beyond the TeV scale. Furthermore, correlated excesses in all these channels would be a smoking-gun for the model. These projections highlight the promising opportunities offered by an e^+e^- collider in testing Higgs-as-slepton models.

Lastly, we note that three body production channels can likely be used to probe the model further. In particular, modifications to hhZ production (important for measuring the Higgs-trilinear coupling) are also affected at $\mathcal{O}(\epsilon^2)$. We leave the study of these channels for future work.

2.5 U_{PMNS} and the need for a TeV-scale cutoff

We next discuss the neutrinos sector in Higgs-as-slepton models. For a generic choices of L, that is, $L \neq 0, 1, -1$, the $U(1)_R$ symmetry forbids neutrino masses. Thus, all neutrino masses are $U(1)_R$-breaking, which can naturally explain the hierarchy between neutrinos and the rest of SM fermions masses. (Exceptions

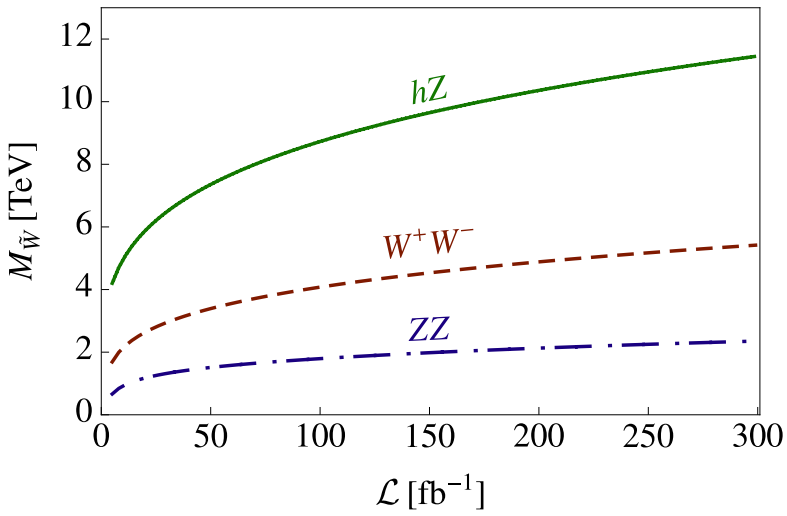

Figure 2.3: The potential reach from $e^+e^- \to VV$ at a future lepton collider as a function of luminosity. The hZ deviations are by far the largest as they scale quickly with energy and have suppressed SM contributions compared to W^+W^-.

occur in the case $L = 0, -1$, which we will address later.) One extra ingredient in the model is that since it singles out one neutrino flavour to be the Higgs superpartner, this can lead to suppression of the mixing between the Higgs-partner neutrino with the other two neutrino flavours, with obvious implications for the Pontecorvo-Maki-Nakagawa-Sakata (PMNS) matrix, $U_{\rm PMNS}$. A large suppression of one or more of the mixing angles would be inconsistent with measured values of the $|\theta_{12}| \approx 0.6$, $|\theta_{23}| \approx 0.7$ and $|\theta_{13}| \approx 0.15$ [115].

In this section, we show that for generic gravity-mediated $U(1)_R$-breaking, consistency with the measured mixing angles requires that the cutoff-scale Λ be less than $\mathcal{O}(10\,\text{TeV})$, so that non-renormalizable contributions to the neutrino mass matrix be of comparable sizes to that from mixing-induced contributions involving gaugino soft masses. This turns out to be the case regardless of the choice of L. It is interesting to note that the upper-bound on the cutoff scale is similar to the one required for generating a large enough top quark mass, despite the two phenomena

being unrelated. While not the focus of this work, we also briefly discuss neutrino mixing in the Higgs-as-slepton model with two additional Higgs doublets (in principle this can replace the UV cutoff needed to produce the top mass). We find that such models also generically require a low energy cutoff, except for particular choices of L.

2.5.1 $L \neq -1, 0, 1$

We establish our analysis framework using the $L \neq -1, 0, 1$ case as an example. We first derive the 3×3 neutrino mass matrix from the full neutralino mass matrix, which we then use to obtain the mixing angles required to diagonalise the neutrino mass matrix. We assume generic gravity mediation and we estimate the sizes of the matrix elements using a spurion analysis, assuming $\mathcal{O}(1)$ coefficients and including non-renormalizable contributions involving the cutoff Λ. Measured values of the mixing angles then translate to bounds on Λ.

To provide a useful picture of the mass scales involved, we refer to Section 2.6, where we find that the gravitino mass should be $m_{3/2} \sim \mathcal{O}(10\,\text{eV} - 100\,\text{eV})$ in order to provide the correct neutrino masses. This is much smaller than the $U(1)_R$-symmetric soft mass scale which, as we discussed above, are of the order of few TeVs.

Neutrino mass matrix

In Sections 2.3 and 2.4, where we studied electroweak precision and collider phenomenology, the main effects came from the mixing between the Higgs-partner neutrinos and the gauginos. Therefore, it was convenient to ignore $U(1)_R$-breaking

masses and work with Dirac mass matrices, even for the neutralinos. However, since we are now interested in the mixing between neutrino flavours, the $U(1)_R$-breaking masses play an important role and so it is more useful to work with a Majorana mass matrix instead.

We begin with the tree-level 7×7 neutralino Majorana mass matrix in the interaction basis $\{\nu_e, \nu_\mu, \nu_\tau, \tilde{B}, \tilde{W}^0, \psi_{\tilde{B}}, \psi^0_{\tilde{W}}\}$. We first diagonalise the matrix only with respect to the $U(1)_R$-symmetric terms, from which we find that three of the eigenvectors $\{\nu'_e, \nu_\mu, \nu_\tau\}$ do not have $U(1)_R$-symmetric masses, where ν'_e is given to order $\mathcal{O}(\epsilon)$ by

$$\nu'_e \simeq \nu_e + \epsilon t_w \alpha \psi_{\tilde{B}} - \epsilon \psi_{\tilde{W}^0}. \tag{2.21}$$

These three eigenvectors can still have $U(1)_R$-breaking masses. The associated 3×3 block of the transformed 7×7 neutralino Majorana mass matrix is (the origin of the terms is derived below)

$$M_\nu \equiv \begin{array}{c} \\ \nu'_e \\ \nu_\mu \\ \nu_\tau \end{array} \begin{array}{c} \begin{array}{ccc} \nu'_e & \nu_\mu & \nu_\tau \end{array} \\ \begin{pmatrix} c_{\psi_{\tilde{W}}} + t_w^2 \alpha^2 c_{\psi_{\tilde{B}}} + \epsilon' c_{ee} & \epsilon' c_{e\mu} & \epsilon' c_{e\tau} \\ \epsilon' c_{\mu e} & \epsilon' c_{\mu\mu} & \epsilon' c_{\mu\tau} \\ \epsilon' c_{\tau e} & \epsilon' c_{\tau\mu} & \epsilon' c_{\tau\tau}, \end{pmatrix} \end{array} \epsilon^2 m_{3/2} \tag{2.22}$$

where

$$\epsilon' \equiv \frac{2M^2_{\tilde{W}}}{g^2 \Lambda^2}. \tag{2.23}$$

ϵ' can be roughly interpreted as the ratio of the soft mass scales to the cutoff scale of the model. Therefore, a small ϵ' implies a high cutoff scale, while an $\mathcal{O}(1)$ ϵ' implies a low cutoff scale only slightly above the sparticle masses.

The overall factor of $\epsilon^2 m_{3/2}$ can be understood from the fact that the neutrino masses break both $U(1)_R$ and electroweak symmetry. We now explain the origin of the various mass terms. The first two terms in $(M_\nu)_{ee}$ arise from the fact that

ν_e' contains $\psi_{\tilde{B}}$ and $\psi^0_{\tilde{W}}$, which in turn are involved in the soft $U(1)_R$-breaking neutralino mass terms

$$\int d^4\theta \frac{X^\dagger}{M_{\rm Pl}} \left(\frac{c_{\psi_{\tilde{B}}}}{2} \Phi_{\tilde{B}} \Phi_{\tilde{B}} + \frac{c_{\psi_{\tilde{W}}}}{2} \Phi_{\tilde{W}} \Phi_{\tilde{W}} \right) \supset m_{3/2} \left(\frac{c_{\psi_{\tilde{B}}}}{2} \psi_{\tilde{B}} \psi_{\tilde{B}} + \frac{c_{\psi_{\tilde{W}}}}{2} \psi^0_{\tilde{W}} \psi^0_{\tilde{W}} \right) , \tag{2.24}$$

where $c_{\psi_{\tilde{B}}}$ and $c_{\psi_{\tilde{W}}}$ are arbitrary $\mathcal{O}(1)$ coefficients since we have assumed generic gravity mediation. As for the other matrix elements, they can be generated by non-renormalizable operators of the form

$$\int d^4\theta \frac{X^\dagger}{M_{\rm Pl}\Lambda^2} \frac{1}{2} c_{ij} \left(L_e^\dagger e^V L_i \right) \left(L_e^\dagger e^V L_j \right) \supset \frac{M_{\tilde{W}}^2}{\Lambda^2} \frac{c_{ij}}{g^2} \epsilon^2 m_{3/2} \nu_i \nu_j \, , \tag{2.25}$$

where $i, j \in \{e, \mu, \tau\}$, and we have again assumed c_{ij} to be $\mathcal{O}(1)$. Note that we have replaced v^2 by $\frac{4M_{\tilde{W}}^2}{g^2}\epsilon^2$ to make the ϵ-dependence manifest.

In principle, one should also take into account loop contributions to M_ν. Generically, we expect the contribution to $(M_\nu)_{ee}$ to be of order $(\epsilon^2 m_{3/2})/(16\pi^2)$, which is a loop factor smaller than the first two tree-level terms and can hence be systematically ignored. For the other matrix elements, the loop contributions cannot be achieved with a single soft $U(1)_R$-breaking insertion (the soft terms cannot supply the required number of units of $U(1)_R$-breaking for these elements), and so require an insertion of a nonrenormalizable operator, in which case they are also a loop factor smaller than the corresponding tree-level terms. Since we will show that agreement with the measured $U_{\rm PMNS}$ requires a low TeV-scale cutoff Λ, these loop contributions are definitely much smaller than the corresponding tree-level non-renormalizable contributions and so it is consistent to ignore the former without affecting the validity of our final results.

Finally, we argue that M_ν should in fact be regarded as the 3×3 neutrino mass matrix. The neutrino mass matrix is obtained by block-diagonalising the transformed 7×7 neutralino mass matrix, this time with respect to the $U(1)_R$-

breaking masses. However, since the four other transformed states have masses $M_{\tilde{W}}$ or $M_{\tilde{B}}$, the remaining "transformation angles" required for block-diagonalisation are at most of $\mathcal{O}(\frac{\epsilon^2 m_{3/2}}{M_{\tilde{W}}})$ or $\mathcal{O}(\frac{\epsilon^2 m_{3/2}}{M_{\tilde{B}}})$. This implies that the basis $\{\nu'_e, \nu_\mu, \nu_\tau\}$ is very close to the actual basis required for block-diagonalisation, and also that the resulting "corrections" to M_ν are at most $\mathcal{O}(\frac{\epsilon^4 m_{3/2}}{M_{\tilde{W}}} m_{3/2})$ or $\mathcal{O}(\frac{\epsilon^4 m_{3/2}}{M_{\tilde{B}}} m_{3/2})$ and hence negligible.

Reproducing U_{PMNS}

To obtain the mixing angles in $U_{\rm PMNS}$, we need to find the transformations that diagonalise the charged-lepton and neutrino mass matrices. We first consider the charged-lepton sector. Unlike the neutrinos, the charged-lepton masses are dominated by $U(1)_R$-symmetric contributions. Therefore, the 3×3 charged-lepton Dirac mass matrix is block-diagonal between the electron and the other lepton flavours to a very good approximation since mass terms of the form $e'_L\mu^c_R$, $e'_L\tau^c_R$, $\mu_L e'^c_R$ and $\tau_L e'^c_R$ are $U(1)_R$-breaking and hence much smaller. Therefore, we are completely justified in choosing the lepton flavour basis to coincide with the charged-lepton mass basis, since the required transformation does not involve the Higgs-partner generation. This means that the PMNS mixing angles are entirely determined by the neutrino sector.

We now consider the neutrinos. We first assume that we can have a high cutoff scale so that $\epsilon' \ll 1$ in which case the neutrino mass matrix takes the form

$$M_\nu \sim \begin{array}{c} \\ \nu'_e \\ \nu_\mu \\ \nu_\tau \end{array} \begin{array}{c} \begin{array}{ccc} \nu'_e & \nu_\mu & \nu_\tau \end{array} \\ \begin{pmatrix} \mathcal{O}(1) & \mathcal{O}(\epsilon') & \mathcal{O}(\epsilon') \\ \mathcal{O}(\epsilon') & \mathcal{O}(\epsilon') & \mathcal{O}(\epsilon') \\ \mathcal{O}(\epsilon') & \mathcal{O}(\epsilon') & \mathcal{O}(\epsilon') \end{pmatrix} \end{array} \epsilon^2 m_{3/2}\,. \tag{2.26}$$

We find that the neutrino mass eigenstate ν_1 (associated most closely with ν'_e) is much heavier than ν_2 and ν_3, and that both mixing angles θ_{12} and θ_{13} are of order ϵ' and hence small. These observations are inconsistent with experimental measurements, implying that we cannot have $\epsilon' \ll 1$. Rather, a $\mathcal{O}(1)$ ϵ' is preferred. In the best-case scenario, allowing for fluctuations in $\mathcal{O}(1)$ coefficients, we place a lower bound of $\epsilon' \gtrsim \mathcal{O}(0.1)$, which in turn implies that

$$\Lambda \lesssim \mathcal{O}\left(\frac{\sqrt{20}}{g} M_{\tilde{W}}\right) . \tag{2.27}$$

For $M_{\tilde{W}} \sim$ TeV the required cutoff scale is $\mathcal{O}(10\,\text{TeV})$. This ensures that the non-renormalizable contributions to M_ν are comparable to the mixing-induced gaugino soft-term contributions to $(M_\nu)_{ee}$ which is required to have large neutrino mixing angles and a mass hierarchy consistent with measurements. Note that it is possible to evade the mass hierarchy issue associated with $\epsilon' \ll 1$ by choosing a different lepton generation for the Higgs (e.g. the choice τ is consistent with normal hierarchy), but the problems associated with the mixing angles remain.

Finally, we recall that in order to generate the top mass in the Higgs-as-slepton model we require $\Lambda \lesssim \mathcal{O}(10\,\text{TeV})$. It is interesting to note that both the top mass and neutrino mixing, that are unrelated physical phenomena, both point towards an $\mathcal{O}(10\,\text{TeV})$ upper bound for the cutoff scale.

2.5.2 $L = 1$

Now we consider the case with $L = 1$ where there are two main differences with respect to the general case discussed above. The first is the fact that in the neutrino sector, the loop contributions to all the M_ν matrix elements can now be generated by a single soft $U(1)_R$-breaking insertion (whereas this is only true for $(M_\nu)_{ee}$ when

$L \neq 1$). Nevertheless, being at least one loop factor smaller than the soft-mass contribution to $(M_\nu)_{ee}$, they are still too small to replace the need for a low cutoff scale Λ.

The second effect is more important; in the charged-lepton sector, the mass terms $e'_L\mu^c_R$, $e'_L\tau^c_R$, $\mu_L e'^c_R$ and $\tau_L e'^c_R$ are no longer $U(1)_R$-breaking, so the charged-lepton Dirac mass matrix isn't diagonal anymore. If we choose the flavour basis to be the charged-lepton mass basis, it is no longer guaranteed that the Higgs be associated with a single flavour, i.e. all the sneutrinos can in principle get VEVs. On the other hand, such a scenario is inconsistent with bounds on lepton-flavour violating processes such as $\mu \to e\gamma$ [115]. For example, if all the sneutrinos get VEVs, the W and Z gauge coupling vertices will then mix the gauginos with all three charged-lepton mass eigenstates such that a W/Z-gaugino loop can induce $\mu \to e\gamma$. Therefore, any successful implementation of the $L = 1$ scenario requires that the sneutrino VEVs be suppressed for two of the generations, which, returning to our original flavour basis, suggests that the Dirac mass matrix should again be approximately block-diagonal. (Note that this also implies that the $L = 1$ model is less favorable than the generic L model due to the need for the sneutrino VEV suppression in the other two generations.)

Therefore, we conclude that these differences do not affect our conclusion of the need for a TeV-scale cutoff. We note that the same conclusion was made in [107] in the context of a Two Higgs Doublet Model (2HDM) extension of the Higgs-as-slepton model. As a result, the authors introduced a right-handed Dirac neutrino as a low-scale UV completion, which is analogous to our idea of a cutoff scale Λ.

The above discussion is only valid for generic gravity mediated $U(1)_R$-breaking. As discussed in [107], anomaly mediation does not generate soft mass terms of the

form $\psi_{\tilde{W}^0}\psi_{\tilde{W}^0}$ and $\psi_{\tilde{B}}\psi_{\tilde{B}}$, so in fact the neutrino mass matrix can be entirely dominated by loop contributions without any constraints on Λ.

2.5.3 $L = 0$

For $L = 0$, before imposing any additional symmetry, the non-renormalizable contributions to $\nu_\mu\nu_\mu$, $\nu_\mu\nu_\tau$ and $\nu_\tau\nu_\tau$ are no longer $U(1)_R$-breaking. As a result, two of the neutrinos become too heavy. Therefore, for such a choice to work, one needs to impose an additional global $U(1)$ lepton number symmetry on L_μ and L_τ [101], assumed to be broken at some flavour scale M_f. At this scale we get an R-conserving but lepton symmetry-violating operator,

$$\int d^4\theta \frac{X^\dagger}{M_f\Lambda^2}\frac{1}{2}c_{ij}\left(L_e^\dagger e^V L_i\right)\left(L_e^\dagger e^V L_j\right) \supset \alpha' \frac{M_{\tilde{W}}^2}{\Lambda^2}\frac{c_{ij}}{g^2}\epsilon^2 m_{3/2}\nu_i\nu_j \quad (i,j \in \{\mu,\tau\}), \tag{2.28}$$

where $\alpha' \equiv M_{\rm Pl}/M_f \geq 1$. Note that we have assumed that the M_f-scale mediators can also mediate SUSY-breaking, due to the involvement of the spurion X. Otherwise, we should either replace one of the Λ by M, or replace M_f by $M_{\rm Pl}$, whichever gives the lower overall suppression. As a result, M_ν now takes the form

$$M_\nu \sim \begin{array}{c} \\ \nu'_e \\ \nu_\mu \\ \nu_\tau \end{array} \begin{array}{c} \begin{array}{ccc} \nu'_e & \nu_\mu & \nu_\tau \end{array} \\ \begin{pmatrix} \mathcal{O}(1) & \mathcal{O}(\epsilon') & \mathcal{O}(\epsilon') \\ \mathcal{O}(\epsilon') & \mathcal{O}(\alpha'\epsilon') & \mathcal{O}(\alpha'\epsilon') \\ \mathcal{O}(\epsilon') & \mathcal{O}(\alpha'\epsilon') & \mathcal{O}(\alpha'\epsilon') \end{pmatrix} \end{array} \epsilon^2 m_{3/2}. \tag{2.29}$$

There are two scenarios that result in the neutrino mixings angles, θ_{12} and θ_{13}, that are very small, which we would like to avoid. The first is if $\epsilon' \ll 1$, and the second if $\alpha'\epsilon' \gg 1$. To avoid both scenarios, we require that $\epsilon' \gtrsim 0.1$ and $\alpha'\epsilon' \lesssim 10$ (or equivalently $\alpha' \lesssim 100$). The first constraint again corresponds to a low TeV-

scale cutoff as was found in the previous cases. The second constraint corresponds to $M_f \gtrsim M_{\rm Pl}/100$ or, in other words, that we need the flavour scale cutoff to be close to the Planck scale so that the $U(1)_R$-symmetric neutrino masses do not become too large. Therefore, the lepton number symmetry should be broken very close to the Planck scale. Yet, we note that this conclusion assumes that M_f-scale mediators can also mediate SUSY-breaking, and is not valid otherwise.

2.5.4 $L = -1$

Next, we consider the $L = -1$ case. While less obvious than the $L = 0$ case, we also have the problem of two of the neutrinos becoming too heavy. This can seen from the fact that ν_e, $\psi_{\tilde{W}^0}$ and $\psi_{\tilde{B}}$ have $U(1)_R$-charges -1, while ν_μ, ν_τ, $\tilde{W}^0$ and $\tilde{B}$ have $U(1)_R$-charges $+1$, so there can be three massive Dirac pairs at the $U(1)_R$-symmetric level, leaving only one massless neutralino. More specifically, one can come up with $U(1)_R$-symmetric mass terms such as

$$\begin{aligned}&\int d^4\theta \frac{X^\dagger}{M}\left(c_{\tilde{B}i}\frac{\Phi_{\tilde{B}}L_e^\dagger e^V L_i}{\Lambda} + c_{\tilde{W}i}\frac{\Phi^a_{\tilde{W}}L_e^\dagger e^V \tau^a L_i}{\Lambda} + c_{ei}\frac{\left(L_e^\dagger e^V L_e\right)\left(L_e^\dagger e^V L_i\right)}{\Lambda^2}\right)\\ &\supset \frac{M_{\rm Pl}}{M}m_{3/2}\left(\frac{\sqrt{2}M_{\tilde{W}}}{g\Lambda}c_{\tilde{B}i}\epsilon\psi_{\tilde{B}}\nu_i + \frac{M_{\tilde{W}}}{\sqrt{2}g\Lambda}c_{\tilde{W}i}\epsilon\psi_{\tilde{W}^0}\nu_i + \frac{M^2_{\tilde{W}}}{g^2\Lambda^2}c_{ei}\epsilon^2\nu_e\nu_i\right),\end{aligned} \tag{2.30}$$

for $i \in \{\mu, \tau\}$, leading to large neutrino masses. Note that $\frac{M_{\rm Pl}}{M}m_{3/2}$ gives the soft $U(1)_R$-symmetric scale.

As in the $L = 0$ case, one way to resolve this issue is to introduce an additional $U(1)$ lepton symmetry on L_μ and L_τ, both of which are broken at the flavour scale M_f. As a result, all instances of M in the above equation should be replaced by M_f. Assuming M_f to be large and hence the above terms to be much smaller than the original $U(1)_R$-symmetric masses, we can then follow the previous pro-

cedure to obtain the neutrino mass matrix. In other words, we first diagonalise the full 7×7 Majorana mass matrix with respect to the original $U(1)_R$-symmetric terms, following which we block-diagonalise with respect to the remaining lepton symmetry-breaking and/or $U(1)_R$-breaking terms. We find that M_ν now takes the form

$$M_\nu \sim \begin{array}{c} \\ \nu'_e \\ \nu_\mu \\ \nu_\tau \end{array} \begin{array}{c} \begin{array}{ccc} \nu'_e & \nu_\mu & \nu_\tau \end{array} \\ \begin{pmatrix} \mathcal{O}(1) & \mathcal{O}(\alpha'\epsilon') & \mathcal{O}(\alpha'\epsilon') \\ \mathcal{O}(\alpha'\epsilon') & \mathcal{O}(\epsilon') & \mathcal{O}(\epsilon') \\ \mathcal{O}(\alpha'\epsilon') & \mathcal{O}('\epsilon') & \mathcal{O}(\epsilon') \end{pmatrix} \end{array} \epsilon^2 m_{3/2}. \tag{2.31}$$

Again, there are two scenarios that lead to small neutrino mixing(s) which we want to avoid. The first is if $\epsilon' \ll 1$, leading to one or two small angles depending on the size of $\alpha'\epsilon'$. The second is if $\alpha'\epsilon' \gg 1$, leading to one small angle. Therefore, just as in the $L = 0$ case, we again see that we require both a low cutoff-scale Λ, and a lepton number-breaking scale M_f close to the Planck scale. Note that the constraints here are slightly weaker since the suppression may now occur only for one mixing angle, which can be identified with the smallest measured angle θ_{13}.

2.5.5 2HDM Higgs-as-slepton model

Finally, we discuss the 2HDM Higgs-as-slepton model (see Appendix 2.B for a summary of the differences), where we will only consider the $L \neq -1, 0, 1$ case for brevity. The 2HDM model may be one possible UV completion of the Higgs-as-sneutrino model [36], completing the model to a much higher scale since the top quark can now gain mass from the up-type Higgs (although the electron mass still has to come from non-renormalizable operators). We now show that the requirement of lepton mixing angles forces also the 2HDM model to have a much

lower UV completion scale than one might expect.

The analysis follows the same procedure as before, although it is now complicated by the fact that there are two additional neutralinos, one associated with the up-type Higgs $\tilde{h}_u^0$, and another with the electroweak doublet required for anomaly cancellation $\tilde{r}_d^0$ (these correspond to the superfields H_u and R_d). Also, there are now additional soft $U(1)_R$-breaking terms that can contribute to the neutrino mass matrix via mixing. For instance, we can now have

$$\int d^4\theta \frac{X^\dagger}{M_{\rm Pl}} c_i L_i H_u \supset c_i m_{3/2} \nu_i \tilde{h}_u^0 \tag{2.32}$$

where $i \in \{e, \mu, \tau\}$. This enters the neutrino mass matrix since ν_e' now also contains a $\tilde{h}_u^0$ component. Finally, being a 2HDM model, there is also a $\tan\beta \equiv v_u/v_d$ dependence (where $v_u(v_d)$ is the vacuum expectation value of $h_u(h_d)$).

We find that the neutrino mass matrix takes the form

$$M_\nu \sim \begin{array}{c} \\ \nu_e' \\ \nu_\mu \\ \nu_\tau \end{array} \begin{array}{c} \begin{array}{ccc} \nu_e' & \nu_\mu & \nu_\tau \end{array} \\ \begin{pmatrix} \mathcal{O}(c_\beta^2) + \mathcal{O}(c_\beta s_\beta) + \mathcal{O}(\epsilon') & \mathcal{O}(c_\beta s_\beta) + \mathcal{O}(\epsilon') & \mathcal{O}(c_\beta s_\beta) + \mathcal{O}(\epsilon') \\ \mathcal{O}(c_\beta s_\beta) + \mathcal{O}(\epsilon') & \mathcal{O}(\epsilon') & \mathcal{O}(\epsilon') \\ \mathcal{O}(c_\beta s_\beta) + \mathcal{O}(\epsilon') & \mathcal{O}(\epsilon') & \mathcal{O}(\epsilon') \end{pmatrix} \end{array} \epsilon^2 m_{3/2} \tag{2.33}$$

where $c_\beta \equiv \cos\beta$ and $s_\beta \equiv \sin\beta$. If we assume that $c_\beta s_\beta \sim \mathcal{O}(1)$ or $c_\beta^2 \sim \mathcal{O}(1)$, then we again find one or two mixing angles with size $\mathcal{O}(\epsilon')$. Therefore, we see that even in the 2HDM model, we still need a low cutoff scale in order to reproduce the PMNS matrix. In general the constraint is slightly weaker than before due to the β dependence. This is a non-trivial result since the 2HDM version can otherwise have a much higher cutoff scale given that the top quark mass can be generated by H_u rather than through nonrenormalizable operators. On the other hand, if $t_\beta \gg 1$, we expect both $c_\beta s_\beta$ and c_β^2 to be small, in which case the constraints on

the cutoff scale can be less stringent depending on the size of t_β. In particular, for large t_β the required cutoff scale is,

$$\Lambda \lesssim \sqrt{\frac{20}{g^2} t_\beta} M_{\tilde{W}} \,, \tag{2.34}$$

raising the cutoff by a factor of $\sqrt{t_\beta}$.

We note that the above conclusion is invalid for the case $L = 0$, since in this specific case the $\mathcal{O}(\epsilon')$ terms in the lower right 2×2 block are then replaced by $\mathcal{O}(\alpha'\epsilon')$. A small ϵ' can be compensated by a large α' to give large mixing angles. In other words, a larger cutoff-scale Λ can be compensated for by a smaller flavour scale M_f.

2.6 Neutrino masses, proton decay and the gravitino mass

The $U(1)_R$ symmetry in Higgs-as-slepton models serves two important roles: to forbid neutrino masses (as long as the gauginos have separate Dirac mass partners $\psi_{\tilde{G}}$, $\psi_{\tilde{W}}$ and $\psi_{\tilde{B}}$) as well as to forbid superpotential and soft terms that might have otherwise led to rapid proton decay. However, since neutrino masses are small but nonzero, we require explicit breaking of the $U(1)_R$ symmetry, possibly through gravity mediation to account for this smallness. In particular, this implies a relation between the neutrino masses and the gravitino mass $m_{3/2} \approx \langle F_X \rangle / M_{\rm Pl}$, the details of which depends on whether the breaking is through generic "Planck-scale" gravity mediation or through anomaly mediation. The $U(1)_R$-breaking may also introduce proton decay channels, which lead to upper bounds on the gravitino mass $m_{3/2}$. It is hence of interest to discuss the bounds on $m_{3/2}$ from the neutrino mass spectrum and from proton decay. In this section we restrict our attention to the case of generic gravity mediation, since the proton decay channels we consider

below do not arise in anomaly mediation despite the $U(1)_R$-breaking.

2.6.1 Bounds from neutrino masses

We have already discussed neutrino masses in Section 2.5 and so we will only briefly review the relevant points. If $L \neq -1, 0$, then all neutrino masses involve $U(1)_R$-breaking and hence scale with the gravitino mass $m_{3/2}$. In particular, for generic gravity mediation, we have shown that the Majorana mass for the Higgs-partner neutrino is given by $\sim \epsilon^2 m_{3/2}$. This arises mainly from the mixing of the neutrino with $\psi_{\tilde{B}}$ and $\psi^0_{\tilde{W}}$ and is generally larger than loop-induced masses. We use this to set the mass scale of the heaviest neutrino, since all other terms in the neutrino mass matrix are expected to be of the same order so as to explain the large mixing angles in U_{PMNS}. Even for the cases $L = 0$ and $L = -1$, while some of the neutrino mass terms are $U(1)_R$-symmetric, we require them to be suppressed by some flavour scale M_f close to the Planck scale so that these mass terms are comparable to the mixing-induced term above.

Mass hierarchy measurements from neutrino oscillation experiments require the heaviest neutrino mass to be at least around 0.1 eV, while cosmology and spectroscopy experiments place an upper bound of around 1 eV [115]. Together, this implies the following bounds on the gravitino mass:

$$\left(\frac{0.1}{\epsilon}\right)^2 10\,\text{eV} \lesssim m_{3/2} \lesssim \left(\frac{0.1}{\epsilon}\right)^2 100\,\text{eV}. \tag{2.35}$$

Note that the bounds are dependent on the wino mass through ϵ. The allowed values of the gravitino mass are shown in Figure 2.4 as a function of the wino mass, with the excluded region shown in blue.

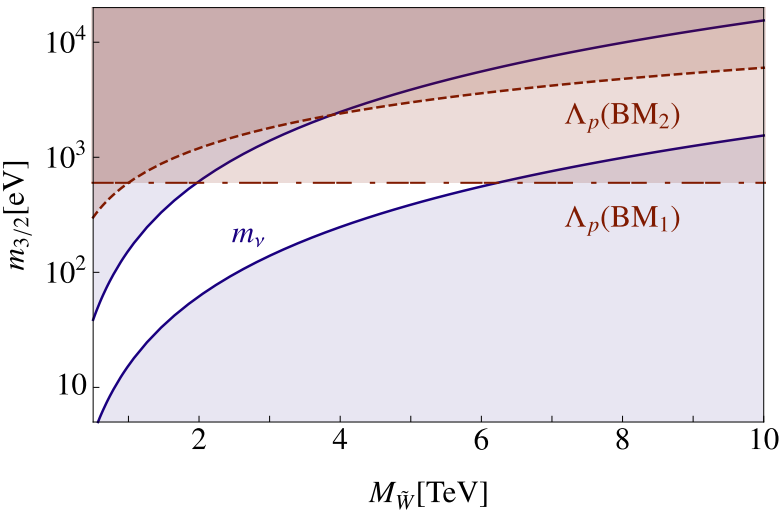

Figure 2.4: The excluded gravitino mass range. The limits in blue correspond to constraints from the neutrino mass scale while the limits in red are from proton lifetime measurements. The constraints from the proton lifetime are dependent on the $m_{\tilde{s}_R}$, $m_{\tilde{g}}$, and we include two benchmark scenarios. BM$_1$ is for $m_{\tilde{s}_R} = M_{\tilde{g}} = 1\,\text{TeV}$ while BM$_2$ is for $m_{\tilde{s}_R} = 1\,\text{TeV}$, $M_{\tilde{g}} = M_{\tilde{W}}$.

2.6.2 Upper bounds from proton decay

After generic gravity-mediated $U(1)_R$-breaking, various operators appear that can give rise to proton decay. For example, we now have $a_{ijk}U^c_{Ri}D^c_{Rj}D^c_{Rk}$ in the superpotential, which comes from

$$\mathcal{L} \supset \int d^4\theta A_{ijk}\frac{X^\dagger}{M_{\text{Pl}}\Lambda}U^c_{Ri}D^c_{Rj}D^c_{Rk}, \tag{2.36}$$

so $a_{ijk} = (m_{3/2}/\Lambda)A_{ijk}$, where A_{ijk} are $\mathcal{O}(1)$ coefficients. In conjunction with $y_{d,ij}L_1Q_{Li}D^c_{Rj} \equiv y_{d,ij}H_dQ_{Li}D^c_{Rj}$ already present in the $U(1)_R$-symmetric superpotential, this gives rise to tree-level proton decay, familiar from the R-parity violating MSSM. Remember that we have already excluded the $B = 1$ scenario, in which $a_{ijk}U^c_{Ri}D^c_{Rj}D^c_{Rk}$ is $U(1)_R$-symmetric and hence a_{ijk} is entirely unsuppressed, leading to rapid proton decay.

Another possibility is the one-loop proton decay channels shown in Figure 2.5,

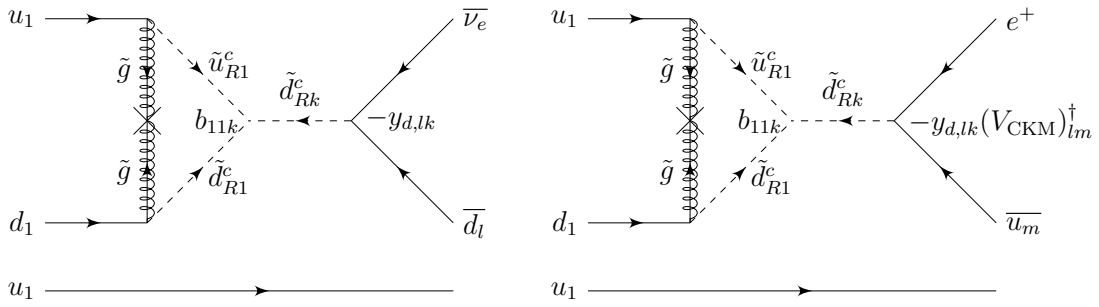

Figure 2.5: One-loop proton decay channels arising from soft trilinear scalar terms $\tilde{u}^c_{Ri}\tilde{d}^c_{Rj}\tilde{d}^c_{Rk}$ and the Majorana gluino mass. All indices here label mass eigenstates. The cross indicates a Majorana gluino mass insertion. There is a similar set of diagrams involving the Majorana mass of the gluino Dirac partner.

which requires soft trilinear terms $b_{ijk}\tilde{u}^c_{Ri}\tilde{d}^c_{Rj}\tilde{d}^c_{Rk}$, as well as the soft Majorana mass $m_{\tilde{g}}$ and $m_{\psi_{\tilde{g}}}$ for the gluinos and their Dirac partners. The latter are always $U(1)_R$-breaking, so we expect that $m_{\tilde{g}} = c_{\tilde{g}} m_{3/2}$ and $m_{\psi_{\tilde{g}}} = c_{\psi_{\tilde{g}}} m_{3/2}$, where $c_{\tilde{g}}$ and $c_{\psi_{\tilde{g}}}$ are $\mathcal{O}(1)$ coefficients. For $B \neq 1/3$, the trilinear terms are also $U(1)_R$-breaking, so we expect that $b_{ijk} = B_{ijk} m_{3/2}$ where B_{ijk} are $\mathcal{O}(1)$ coefficients. For $B = 1/3$ however, the trilinear terms do not break $U(1)_R$ symmetry, so b_{ijk} should instead be of order the $U(1)_R$-symmetric soft mass scale.

We first consider the one-loop proton decay channels since, as we will see later, they are less dependent on the UV completion than the tree-level ones. For convenience, we work in the basis where the flavour eigenstates of $d_{L,i}, d^c_{R,i}$, and $u_{R,i}$ coincide with the mass eigenstates (otherwise we would have additional CKM matrix contributions, which would of course simplify to the same final result), so for instance $y_{d,ij} = \sqrt{2} m_{d,i} \delta_{ij}/v$, where $m_{d,i}$ are the down-type quark masses. We also assume that the quark and squark mass basis are exactly aligned to simplify the index assignments in Figure 2.5. Relaxing this assumption complicates the analysis but is not expected to significantly affect our main results. Antisymmetry of b_{ijk} under exchange of j and k (due to $SU(3)$ contraction) further implies that

$k = 2$ or 3, while kinematic considerations implies $l = 1$ or 2 in the left diagram and $m = 1$ in the right diagram. For an electron-sneutrino Higgs, we find two decay channels: $uud \to u\bar{s}\bar{\nu}$ ($p \to K^+ \bar{\nu}$) is the dominant decay channel, while $uud \to u\bar{u}e^+$ ($p \to \pi^0 e^+$) is subdominant due to CKM suppression, despite having a slight phase space enhancement. (Note that the current bounds on either decay channels are comparable [83, 125].) Since the dominant decay channel is to the neutrino rather than the charged lepton, the subsequent analysis remains valid in the case of a muon- or tau-sneutrino Higgs.

We now focus on the dominant one-loop channel. Integrating out the gluinos and squarks gives us the standard dimension-6 proton decay operator $\bar{d}^c\bar{u}^c q_L l_L/\Lambda_p^2$. For simplicity we assume that the gluinos are somewhat heavier than the squarks (as is typical in R-symmetric models due to the supersoft mechanism [126]) and that $m_{\tilde{g}} \approx m_{\psi_{\tilde{g}}}$. We find that

$$\frac{1}{\Lambda_p^2} \sim \frac{g_s^2}{16\pi^2} \frac{m_{\tilde{g}} b_{112} m_s/v_H}{M_{\tilde{s}_R}^2 M_{\tilde{g}}^2}, \tag{2.37}$$

where g_s is the QCD gauge coupling, m_s the strange quark mass, $M_{\tilde{s}_R}$ the mass of the RH strange squark, and $M_{\tilde{g}}$ Dirac gluino mass. We would like to convert the current lower bound of $\Lambda_p \gtrsim \mathcal{O}(10^{15}\,\mathrm{GeV})$ [125] to an upper bound on $m_{3/2}$. For $B \neq 1/3$, we find that

$$m_{3/2} \lesssim \left(\frac{1}{c_{\tilde{g}} B_{112}}\right)^{1/2} \left(\frac{M_{\tilde{s}_R}}{1\,\mathrm{TeV}}\right) \left(\frac{M_{\tilde{g}}}{1\,\mathrm{TeV}}\right) \times 0.6\,\mathrm{keV}. \tag{2.38}$$

We see that for coefficients of order $\mathcal{O}(1)$ and sparticle masses of order $\mathcal{O}(1\,\mathrm{TeV})$, we require a gravitino mass of less than $\mathcal{O}(1\,\mathrm{keV})$. In Figure 2.4, we compare this to the bounds from neutrino masses for different benchmarks of squark and gluino masses. We see in general that the two bounds still remain compatible.

For $B = 1/3$, we instead have

$$m_{3/2} \lesssim \frac{1}{c_{\tilde{g}}} \left(\frac{1\,\text{TeV}}{b_{112}}\right) \left(\frac{M_{\tilde{s}_R}}{1\,\text{TeV}}\right)^2 \left(\frac{M_{\tilde{g}}}{1\,\text{TeV}}\right)^2 \times 4 \times 10^{-7}\,\text{eV}. \tag{2.39}$$

The bound is much stronger in this case, which is not surprising since $U(1)_R$-breaking now only enters once through the Majorana mass insertion and not the trilinear terms. In fact, this bound clearly conflicts with the bounds from neutrino masses, indicating that $B = 1/3$ is incompatible with generic gravity-mediated $U(1)_R$-breaking.

Now we move on to the the tree-level channel. Integrating out the squarks to obtain the dimension-6 proton decay operator, we find that

$$\frac{1}{\Lambda_p^2} \sim \frac{a_{112} m_s / v_H}{M_{\tilde{s}_R}^2}, \tag{2.40}$$

which translates to a bound of

$$m_{3/2} \lesssim \frac{1}{A_{112}} \left(\frac{M_{\tilde{s}_R}}{1\,\text{TeV}}\right)^2 \left(\frac{\Lambda}{10\,\text{TeV}}\right) \times 3 \times 10^{-8}\,\text{eV}. \tag{2.41}$$

This bound is in conflict with the neutrino mass measurements. This suggests either that the $U(1)_R$-breaking is non-generic, or that we require a non-trivial UV completion such that instead of a suppression by $M_{\text{Pl}}\Lambda$ in the tree-level operator, we have an M_{Pl}^2 suppression. In this case we replace Λ in the above bound by M_{Pl}, from which we get

$$m_{3/2} \lesssim \frac{1}{A_{112}} \left(\frac{M_{\tilde{s}_R}}{1\,\text{TeV}}\right)^2 \times 6\,\text{MeV}. \tag{2.42}$$

which is now consistent with the neutrino constraints and in fact weaker than that from the previous one-loop channel.

To summarise, we have obtained upper bounds on the gravitino mass $m_{3/2}$ from tree-level and one-loop proton decay channels, assuming generic gravity-mediated $U(1)_R$-breaking. Bounds from both channels are consistent with the bounds from

the neutrino mass spectrum, provided that $B \neq 1/3$ and that the tree-level non-renormalizable operator is entirely Planck-scale suppressed. The latter condition implies the need for non-trivial UV completions such that the lighter mass scales M or Λ do not enter in the denominator of the tree-level operator, while the suppression is entirely due to M_{Pl}. Finally, we emphasise that our entire discussion hinges on the assumption of generic gravity mediation. If $U(1)_R$-breaking is non-generic, certain $\mathcal{O}(1)$ coefficients may be suppressed or even forbidden.

2.7 Conclusions

Supersymmetric models with the Higgs as a slepton are interesting alternatives to the MSSM. These models have two distinctive features: an R-symmetry which must be broken by gravity and a mixing of the Higgs superpartner lepton with the electroweakinos. These properties allow us to place general bounds on such models from several different frontiers. In this work, we have studied a variety of such constraints, which we summarise below.

Previous work has pointed out constraints from neutral and charged current universality on the mixing of the electron with the gauginos. These bounds are stringent for the wino, $M_{\tilde{W}} \gtrsim 3.3\,\text{TeV}$, but weaker for the bino, $M_{\tilde{B}} \gtrsim 500\,\text{GeV}$. We revisited these bounds in our framework and compare them to complementary bounds from low energy probes, which are much more stringent for the bino, $M_{\tilde{B}} \gtrsim 1.2\,\text{TeV}$ and competitive for the wino mass, $M_{\tilde{W}} \gtrsim 2.8\,\text{TeV}$. We then moved to study the probing power a future e^+e^- machine. We find large deviations from SM predictions leading to spectacular reach for such a collider. In particular, for an integrated luminosity of $300\,\text{fb}^{-1}$ and a centre of mass energy of 1 TeV, we estimate

the potential to probe winos with masses up to 11.5 TeV in the $e^+e^- \to hZ$ channel.

Higgs-as-slepton models also offer a novel explanation for the smallness of neutrino masses, arising from spontaneous breaking of the $U(1)_R$-symmetry due to gravity. We explore the ability of such models to reproduce the neutrino mass spectrum and the measured mixing angles. Typically, we find that the models must be UV-completed at a low scale of at most $\mathcal{O}(10\,\text{TeV})$ in order to reproduce the large measured mixing angles. Interestingly, this is in agreement with the scale required to give a sufficiently large top mass. For the choices $L = 0$ and -1 (where L parameterizes the R-charge of the non-Higgs-partner leptons), some neutrino mass terms are not R-breaking and hence small neutrino masses require an additional lepton number symmetry, assumed to be broken at a scale M_f. We find that, under certain assumptions, constraints on the mixing angles also force M_f to be close to the Planck scale.

Lastly, R-breaking will also generically lead to tree-level proton decay rates inconsistent with experiment. This puts a restriction on the type of models which can UV complete the model. Furthermore, we study loop contributions to proton decay which will be present regardless of the UV completion. We find that these restrict the viable range for the gravitino mass to within the range $\mathcal{O}(10\,\text{eV}) - \mathcal{O}(1\,\text{keV})$, which is consistent with the predictions from neutrino mass measurements. It may be interesting to study the implications of such a gravitino mass range on observational cosmology, but we will defer this to future work.

The possibility that the Higgs is the superpartner of the electron is an intriguing alternative to standard supersymmetric extensions of the Standard Model. Future tests at the LHC, lepton colliders, low energy experiments, and of the neutrino mixing patterns each provide an avenue to discover this variant of supersymmetry.

2.A Feynman rules

In this appendix, we derive the couplings for Yukawa and gauge interactions in the chargino and neutralino mass basis. The mixing matrices used here are derived prior to introducing any $U(1)_R$-breaking.

2.A.1 Mixing matrices

The chargino and neutralino mass matrices are given by

$$\mathcal{M}_C \equiv \begin{array}{c} \\ e_L^- \\ \psi_{\tilde{W}}^- \\ \tilde{W}^- \end{array} \begin{array}{c} \begin{array}{ccc} e_R^{c,+} & \tilde{W}^+ & \psi_{\tilde{W}}^+ \end{array} \\ \begin{pmatrix} \mathcal{O}(\epsilon_{\rm NR}) & \frac{gv}{\sqrt{2}} & 0 \\ \mathcal{O}(\epsilon_{\rm NR}) & M_{\tilde{W}} & 0 \\ 0 & 0 & M_{\tilde{W}} \end{pmatrix} \end{array}, \qquad \mathcal{M}_N \equiv \begin{array}{c} \\ \nu_{e,L} \\ \psi_{\tilde{W}}^0 \\ \psi_{\tilde{B}} \end{array} \begin{array}{c} \begin{array}{cc} \tilde{W}^0 & \tilde{B} \end{array} \\ \begin{pmatrix} \frac{gv}{2} & -\frac{g'v}{2} \\ M_{\tilde{W}} & \mathcal{O}(\epsilon_{\rm NR}) \\ \mathcal{O}(\epsilon_{\rm NR}) & M_{\tilde{B}} \end{pmatrix} \end{array}, \tag{2.43}$$

where $\mathcal{O}(\epsilon_{\rm NR})$ denotes any non-renormalizable contributions suppressed by the scale Λ. While we usually neglect them in our calculations unless specified, we include them here to distinguish them from terms which are identically zero due to $U(1)_R$ symmetry.

The chargino mass eigenstates are denoted by

$$\begin{aligned} &\begin{pmatrix} \chi_{1,L}^- \\ (\chi_{1,R}^{c,+})^\dagger \end{pmatrix} \text{ or } \begin{pmatrix} e_L^{-\prime} \\ (e_R^{c,+\prime})^\dagger \end{pmatrix} : && \text{mass} \sim \mathcal{O}(\epsilon_{\rm NR}), \\ &\begin{pmatrix} \chi_{2,L}^- \\ (\chi_{2,R}^{c,+})^\dagger \end{pmatrix} : && \text{mass} \approx M_{\tilde{W}}, \\ &\begin{pmatrix} \chi_{3,L}^- \\ (\chi_{3,R}^{c,+})^\dagger \end{pmatrix} : && \text{mass} \approx M_{\tilde{W}}, \end{aligned} \tag{2.44}$$

and the neutralino mass eigenstates by

$$\begin{aligned} \chi^0_{1,L} \text{ or } \nu'_{e,L} &: \quad \text{mass} = 0 \\ \begin{pmatrix} \chi^0_{2,L} \\ (\chi^{c,0}_{2,R})^\dagger \end{pmatrix} &: \quad \text{mass} \approx M_{\tilde{W}}, \\ \begin{pmatrix} \chi^0_{3,L} \\ (\chi^{c,0}_{3,R})^\dagger \end{pmatrix} &: \quad \text{mass} \approx M_{\tilde{B}}, \end{aligned} \tag{2.45}$$

where we have arranged the Weyl fermions into Dirac pairs wherever appropriate.

We denote the unitary transformations between the interaction and mass basis by the matrices $U_{C,L}$, $U_{C,R}$, $U_{N,L}$ and $U_{N,R}$, defined as

$$\begin{aligned} \begin{pmatrix} e^-_L \\ \psi^-_{\tilde{W}} \\ \tilde{W}^- \end{pmatrix} &= U_{C,L} \begin{pmatrix} \chi^-_{1,L} \\ \chi^-_{2,L} \\ \chi^-_{3,L} \end{pmatrix}, \qquad \begin{pmatrix} e^{c,+}_R \\ \tilde{W}^+ \\ \psi^+_{\tilde{W}} \end{pmatrix} = U_{C,R} \begin{pmatrix} \chi^{c,+}_{1,R} \\ \chi^{c,+}_{2,R} \\ \chi^{c,+}_{3,R} \end{pmatrix}, \\ \begin{pmatrix} \nu_{e,L} \\ \psi^0_{\tilde{W}} \\ \psi_{\tilde{B}} \end{pmatrix} &= U_{N,L} \begin{pmatrix} \chi^0_{1,L} \\ \chi^0_{2,L} \\ \chi^0_{3,L} \end{pmatrix}, \qquad \begin{pmatrix} \tilde{W}^0 \\ \tilde{B} \end{pmatrix} = U_{N,R} \begin{pmatrix} \chi^{c,0}_{1,R} \\ \chi^{c,0}_{2,R} \\ \chi^{c,0}_{3,R} \end{pmatrix}. \end{aligned} \tag{2.46}$$

Note that $\chi^{c,0}_{1,R}$ does not correspond to any fields present in the model and has been introduced simply for notational convenience.

Assuming $|M_{\tilde{W}} - M_{\tilde{B}}| > m_W$, we find that

$$
\begin{aligned}
U_{C,L} &= \begin{pmatrix} \mathcal{O}(1) & \mathcal{O}(\epsilon) & 0 \\ \mathcal{O}(\epsilon) & \mathcal{O}(1) & 0 \\ 0 & 0 & 1 \end{pmatrix} \xrightarrow{\mathcal{O}(\epsilon^2),\mathcal{O}(\epsilon^0_{\rm NR})} \begin{pmatrix} 1-\epsilon^2 & \sqrt{2}\epsilon & 0 \\ -\sqrt{2}\epsilon & 1-\epsilon^2 & 0 \\ 0 & 0 & 1 \end{pmatrix}, \\
U_{C,R} &= \begin{pmatrix} \mathcal{O}(1) & \mathcal{O}(\epsilon_{\rm NR}) & 0 \\ \mathcal{O}(\epsilon_{\rm NR}) & \mathcal{O}(1) & 0 \\ 0 & 0 & 1 \end{pmatrix} \xrightarrow{\mathcal{O}(\epsilon^2),\mathcal{O}(\epsilon^0_{\rm NR})} \begin{pmatrix} 1 & 0 & 0 \\ 0 & 1 & 0 \\ 0 & 0 & 1 \end{pmatrix}, \\
U_{N,L} &= \begin{pmatrix} \mathcal{O}(1) & \mathcal{O}(\epsilon) & \mathcal{O}(\epsilon) \\ \mathcal{O}(\epsilon) & \mathcal{O}(1) & \mathcal{O}(\epsilon^2) \\ \mathcal{O}(\epsilon) & \mathcal{O}(\epsilon^2) & \mathcal{O}(1) \end{pmatrix} \xrightarrow{\mathcal{O}(\epsilon^2),\mathcal{O}(\epsilon^0_{\rm NR})} \begin{pmatrix} 1-\epsilon^2\frac{1}{2}\left(1+\alpha^2 t_w^2\right) & \epsilon & -\epsilon\alpha t_w \\ -\epsilon & 1-\frac{1}{2}\epsilon^2 & -\frac{\epsilon^2\alpha^3 t_w}{1-\alpha^2} \\ \epsilon\alpha t_w & \frac{\epsilon^2\alpha t_w}{1-\alpha^2} & 1-\epsilon^2\frac{1}{2}\alpha^2 t_w^2 \end{pmatrix}, \\
U_{N,R} &= \begin{pmatrix} 0 & \mathcal{O}(1) & \mathcal{O}(\epsilon^2) \\ 0 & \mathcal{O}(\epsilon^2) & 1 \end{pmatrix} \xrightarrow{\mathcal{O}(\epsilon^2),\mathcal{O}(\epsilon^0_{\rm NR})} \begin{pmatrix} 0 & 1 & -\frac{\epsilon^2\alpha^2 t_w}{1-\alpha^2} \\ 0 & \frac{\epsilon^2\alpha^2 t_w}{1-\alpha^2} & 1 \end{pmatrix},
\end{aligned}
\tag{2.47}
$$

where $\epsilon \equiv m_W/M_{\tilde{W}} = gv/(2M_{\tilde{W}})$, $\alpha \equiv M_{\tilde{W}}/M_{\tilde{B}}$ and $t_w \equiv \tan\theta_w = g'/g$.

2.A.2 Couplings for Yukawa interactions

The Yukawa interactions between the charginos/neutralinos and the Higgs arise from the Kähler potential of the Higgs/electron supermultiplet. The chargino couplings are given by

$$
\begin{aligned}
\mathcal{L} &\supset -g\frac{h}{\sqrt{2}} e_L^- \tilde{W}^+ \\
&= -\frac{g}{\sqrt{2}} h (U_{C,L})_{1i} (U_{C,R})_{2j} \chi^-_{i,L} \chi^-_{j,L}.
\end{aligned}
\tag{2.48}
$$

To $\mathcal{O}(\epsilon)$ and ignoring $\mathcal{O}(\epsilon_{\rm NR})$, this simplifies to

$$
\mathcal{L} \supset -\frac{g}{\sqrt{2}} h \left(\chi^-_{1,L} \chi^{c,+}_{2,R} + \sqrt{2}\epsilon \chi^-_{2,L} \chi^{c,+}_{2,R} \right). \tag{2.49}
$$

The neutralino couplings are given by

$$\begin{aligned}\mathcal{L} \supset & -g\frac{h}{2}\nu_{e,L}\tilde{W}^0 + g'\frac{h}{2}\nu_{e,L}\tilde{B} \\ & = -g\frac{h}{2}(U_{N,L})_{1i}\left[(U_{N,R})_{1j} - t_w(U_{N,L})_{2j}\right]\chi^0_{i,L}\chi^{c,0}_{j,R}.\end{aligned} \tag{2.50}$$

To $\mathcal{O}(\epsilon)$ and ignoring $\mathcal{O}(\epsilon_{\rm NR})$, this simplifies to

$$\mathcal{L} \supset -g\frac{h}{2}\left(\chi^0_{1,L} + \epsilon\chi^0_{2,L} - t_w\frac{M_{\tilde{W}}}{M_{\tilde{B}}}\epsilon\chi^0_{3,L}\right)\left(\chi^{c,0}_{1,R} - t_w\chi^{c,0}_{2,R}\right). \tag{2.51}$$

2.A.3 Couplings for gauge interactions

We begin with the gauge interactions in the interaction basis:

$$\begin{aligned}\mathcal{L} \supset \;& g\begin{pmatrix}(\tilde{W}^+)^\dagger & (\tilde{W}^0)^\dagger & (\tilde{W}^-)^\dagger\end{pmatrix}\begin{pmatrix}W^0_\mu & -W^+_\mu & 0\\ -W^-_\mu & 0 & +W^+_\mu\\ 0 & +W^-_\mu & -W^0_\mu\end{pmatrix}\bar{\sigma}^\mu\begin{pmatrix}\tilde{W}^+\\ \tilde{W}^0\\ \tilde{W}^-\end{pmatrix} \\ & + g\begin{pmatrix}(\psi^+_{\tilde{W}})^\dagger & (\psi^0_{\tilde{W}})^\dagger & (\psi^-_{\tilde{W}})^\dagger\end{pmatrix}\begin{pmatrix}W^0_\mu & -W^+_\mu & 0\\ -W^-_\mu & 0 & +W^+_\mu\\ 0 & +W^-_\mu & -W^0_\mu\end{pmatrix}\bar{\sigma}^\mu\begin{pmatrix}\psi^+_{\tilde{W}}\\ \psi^0_{\tilde{W}}\\ \psi^-_{\tilde{W}}\end{pmatrix} \\ & + g\begin{pmatrix}(\nu_{e,L})^\dagger & (e^-_L)^\dagger\end{pmatrix}\begin{pmatrix}\frac{W^0_\mu}{2} & \frac{W^+_\mu}{\sqrt{2}}\\ \frac{W^-_\mu}{\sqrt{2}} & -\frac{W^0_\mu}{2}\end{pmatrix}\bar{\sigma}^\mu\begin{pmatrix}\nu_{e,L}\\ e^-_L\end{pmatrix} \\ & - \frac{g'}{2}\begin{pmatrix}(\nu_{e,L})^\dagger & (e^-_L)^\dagger\end{pmatrix}B_\mu\bar{\sigma}^\mu\begin{pmatrix}\nu_{e,L}\\ e^-_L\end{pmatrix} \\ & + g'(e^{c,+}_R)^\dagger B_\mu\bar{\sigma}^\mu e^{c,+}_R.\end{aligned} \tag{2.52}$$

For clarity, we separate this into a few parts before converting to the mass basis.

Charged current interactions

The couplings to W_μ^+ are given by

$$\begin{aligned}\mathcal{L} \supset \; & gW_\mu^+ \Bigg\{ (U_{N,R})^*_{1,i} (\chi^{c,0}_{i,R})^\dagger \bar{\sigma}^\mu \chi^-_{3,L} - (U_{C,R})^*_{2,i} (U_{N,R})_{1j} (\chi^{c,+}_{i,R})^\dagger \bar{\sigma}^\mu \chi^{c,0}_{j,R} \\ & + \left[(U_{N,L})^*_{2i} (U_{C,L})_{2j} + \frac{1}{\sqrt{2}} (U_{N,L})^*_{1i} (U_{C,L})_{1j} \right] (\chi^0_{i,L})^\dagger \bar{\sigma}^\mu \chi^-_{j,L} \\ & - (U_{C,R})^*_{3i} (U_{N,L})_{2j} (\chi^{c,+}_{i,R})^\dagger \bar{\sigma}^\mu \chi^0_{j,L} \Bigg\}. \end{aligned} \tag{2.53}$$

We have used the fact that $\tilde{W}^-$ doesn't mix with e_L^- nor $\psi^-_{\tilde{W}}$ (due to $U(1)_R$ symmetry) to eliminate one of the mixing matrices in the first term. To $\mathcal{O}(\epsilon)$ and ignoring $\mathcal{O}(\epsilon_{\rm NR})$, this simplifies to

$$\begin{aligned}\mathcal{L} \supset \; & gW_\mu^+ \Big[(\chi^{c,0}_{2,R})^\dagger \bar{\sigma}^\mu \chi^-_{3,L} - (\chi^{c,+}_{2,R})^\dagger \bar{\sigma}^\mu \chi^{c,0}_{2,R} + \frac{1}{\sqrt{2}} (\chi^0_{1,L})^\dagger \bar{\sigma}^\mu \chi^-_{1,L} \\ & - \frac{1}{\sqrt{2}} \epsilon (\chi^0_{2,L})^\dagger \bar{\sigma}^\mu \chi^-_{1,L} + (\chi^0_{2,L})^\dagger \bar{\sigma}^\mu \chi^-_{2,L} + \epsilon (\chi^{c,+}_{3,R})^\dagger \bar{\sigma}^\mu \chi^0_{1,L} - (\chi^{c,0}_{3,R})^\dagger \bar{\sigma}^\mu \chi^0_{2,L} \Big]. \end{aligned} \tag{2.54}$$

Note that the $V-A$ violating term $(\chi^{c,+}_{1,R})^\dagger \bar{\sigma}^\mu \chi^0_{1,L}$ does not appear, even when we include higher powers of ϵ as well as $\mathcal{O}(\epsilon_{\rm NR})$. This is not surprising since such a term violates $U(1)_R$ symmetry.

Neutral current interactions

We first consider neutral current interactions with the neutralinos, given by

$$\begin{aligned}\mathcal{L} \supset & \frac{g}{c_w} Z_\mu \frac{1}{2} (\nu_{e,L})^\dagger \bar{\sigma}^\mu \nu_{e,L} \\ = & \frac{g}{c_w} Z_\mu \frac{1}{2} (U_{N,L})^*_{1i} (U_{N,L})_{1j} (\chi^0_{i,L})^\dagger \bar{\sigma}^\mu \chi^0_{j,L}. \end{aligned} \tag{2.55}$$

There are no couplings to the photon as expected. To $\mathcal{O}(\epsilon)$ and ignoring $\mathcal{O}(\epsilon_{\rm NR})$, this simplifies to

$$\mathcal{L} \supset \frac{g}{c_w} Z_\mu \frac{1}{2} \left\{ (\chi^0_{1,L})^\dagger \bar{\sigma}^\mu \chi^0_{1,L} + \left[\epsilon (\chi^0_{1,L})^\dagger \bar{\sigma}^\mu \chi^0_{2,L} - t_w \frac{M_{\tilde{W}}}{M_{\tilde{B}}} \epsilon (\chi^0_{1,L})^\dagger \bar{\sigma}^\mu \chi^0_{3,L} + \text{h.c.} \right] \right\}. \tag{2.56}$$

Now we move on to the charginos. The couplings to the photon are given by

$$\begin{aligned} \mathcal{L} \supset \; & eA_\mu \Big[(e^{c,+}_R)^\dagger \bar{\sigma}^\mu e^{c,+}_R + (\tilde{W}^+)^\dagger \bar{\sigma}^\mu \tilde{W}^+ + (\psi^+_{\tilde{W}})^\dagger \bar{\sigma}^\mu \psi^+_{\tilde{W}} \\ & - (e^-_L)^\dagger \bar{\sigma}^\mu e^-_L - (\psi^-_{\tilde{W}})^\dagger \bar{\sigma}^\mu \psi^-_{\tilde{W}} - (\tilde{W}^-)^\dagger \bar{\sigma}^\mu \tilde{W}^- \Big] \\ = \; & eA_\mu \left[(\chi^{c,+}_{i,R})^\dagger \bar{\sigma}^\mu \chi^{c,+}_{i,R} - (\chi^-_{i,L})^\dagger \bar{\sigma}^\mu \chi^-_{i,L} \right]. \end{aligned} \tag{2.57}$$

The couplings are universal as expected since $U(1)_{\rm EM}$ is unbroken.

The couplings to Z_μ are given by

$$\begin{aligned} \mathcal{L} \supset \; & \frac{g}{c_w} Z_\mu \left[(\tilde{W}^+)^\dagger \bar{\sigma}^\mu \tilde{W}^+ - (\tilde{W}^-)^\dagger \bar{\sigma}^\mu \tilde{W}^- + (\psi^+_{\tilde{W}})^\dagger \bar{\sigma}^\mu \psi^+_{\tilde{W}} - (\psi^-_{\tilde{W}})^\dagger \bar{\sigma}^\mu \psi^-_{\tilde{W}} - \frac{1}{2} (e^-_L)^\dagger \bar{\sigma}^\mu e^-_L \right] \\ & - \frac{g}{c_w} s_w^2 Z_\mu \Big[(e^{c,+}_R)^\dagger \bar{\sigma}^\mu e^{c,+}_R + (\tilde{W}^+)^\dagger \bar{\sigma}^\mu \tilde{W}^+ + (\psi^+_{\tilde{W}})^\dagger \bar{\sigma}^\mu \psi^+_{\tilde{W}} \\ & - (e^-_L)^\dagger \bar{\sigma}^\mu e^-_L - (\psi^-_{\tilde{W}})^\dagger \bar{\sigma}^\mu \psi^-_{\tilde{W}} - (\tilde{W}^-)^\dagger \bar{\sigma}^\mu \tilde{W}^- \Big] \\ = \; & \frac{g}{c_w} Z_\mu \Bigg\{ \left[(U_{C,R})^*_{2i} (U_{C,R})_{2j} + (U_{C,R})^*_{3i} (U_{C,R})_{3j} \right] (\chi^{c,+}_{i,R})^\dagger \bar{\sigma}^\mu \chi^{c,+}_{j,R} \\ & - \left[\frac{1}{2} (U_{C,L})^*_{1i} (U_{C,L})_{1j} + (U_{C,L})^*_{2i} (U_{C,L})_{2i} + (U_{C,L})^*_{3i} (U_{C,L})_{3i} \right] (\chi^-_{i,L})^\dagger \bar{\sigma}^\mu \chi^-_{j,L} \Bigg\} \\ & - \frac{g}{c_w} s_w^2 Z_\mu \left[(\chi^{c,+}_{i,R})^\dagger \bar{\sigma}^\mu \chi^{c,+}_{i,R} - (\chi^-_{i,L})^\dagger \bar{\sigma}^\mu \chi^-_{i,L} \right]. \end{aligned} \tag{2.58}$$

This comprises of a non-universal part related to mixing between different $SU(2)_L$ representations and a universal part related to Q. Using unitarity of $U_{C,L}$ and $U_{C,R}$, this can be written more succinctly as

$$\begin{aligned} \mathcal{L} \supset \; & \frac{g}{c_w} Z_\mu \Big[(1 - s_w^2) (\chi^{c,+}_{i,R})^\dagger \bar{\sigma}^\mu \chi^{c,+}_{i,R} + (-1 + s_w^2) (\chi^-_{i,L})^\dagger \bar{\sigma}^\mu \chi^-_{i,L} \Big] \\ & + \frac{g}{c_w} Z_\mu \Big[- (U_{C,R})^*_{1i} (U_{C,R})_{1j} (\chi^{c,+}_{i,R})^\dagger \bar{\sigma}^\mu \chi^{c,+}_{j,R} + \frac{1}{2} (U_{C,L})^*_{1i} (U_{C,L})_{1j} (\chi^-_{i,L})^\dagger \bar{\sigma}^\mu \chi^-_{i,L} \Big]. \end{aligned} \tag{2.59}$$

	$(SU(3)_C, SU(2)_L)_Y$	$U(1)_R$
$H_d \equiv L_e$	$(1,2)_{-1/2}$	0
E_e^c	$(1,1)_1$	2
$L_{\mu,\tau}$	$(1,2)_{-1/2}$	$1-L$
$E_{\mu,\tau}^c$	$(1,1)_1$	$1+L$
$Q_{1,2,3}$	$(3,2)_{1/6}$	$1+B$
$U_{1,2,3}^c$	$(\bar{3},1)_{-2/3}$	$1-B$
$D_{1,2,3}^c$	$(\bar{3},1)_{1/3}$	$1-B$
$W^{a\alpha}$	$(8,1)_0+(1,3)_0+(1,1)_0$	1
Φ^a	$(8,1)_0+(1,3)_0+(1,1)_0$	0
H_u	$(1,2)_{1/2}$	0
R_d	$(1,2)_{-1/2}$	2

Table 2.2: Superfields and their gauge and $U(1)_R$ representations for the 2HDM version of the Higgs-as-sneutrino model.

To $\mathcal{O}(\epsilon)$ and ignoring $\mathcal{O}(\epsilon_{\rm NR})$, this simplifies to

$$\begin{aligned}\mathcal{L} \supset\ & \frac{g}{c_w} Z_\mu \left[(1-s_w^2)(\chi_{i,R}^{c,+})^\dagger \bar{\sigma}^\mu \chi_{i,R}^{c,+} + (-1+s_w^2)(\chi_{i,L}^-)^\dagger \bar{\sigma}^\mu \chi_{i,L}^-\right] \\ & + \frac{g}{c_w} Z_\mu \left\{ -(\chi_{1,R}^{c,+})^\dagger \bar{\sigma}^\mu \chi_{1,R}^{c,+} + \frac{1}{2}(\chi_{1,L}^-)^\dagger \bar{\sigma}^\mu \chi_{1,L}^- + \left[\sqrt{2}\epsilon (\chi_{1,L}^-)^\dagger \bar{\sigma}^\mu \chi_{2,L}^- + \text{h.c.}\right]\right\}. \end{aligned} \tag{2.60}$$

2.B Two Higgs Doublet Model

Here we briefly review the Higgs-as-slepton model with two additional Higgs doublets, H_u, R_d. The H_u can then be used to provide a mass to the top quark, while R_d is needed for anomaly cancellation. Table 2.2 lists the superfields and their gauge and $U(1)_R$ representations. The most general superpotential consistent

with the symmetries (assuming $B \neq 1/3$ and $L \neq 1$) is

$$\begin{aligned}\mathcal{W} = &\sum_{i,j=1}^{3} y_{d,ij} H_d Q_i D_j^c + \sum_{i,j\in\{\mu,\tau\}} y_{e,ij} H_d L_i E_j^c + \sum_{i,j=1}^{3} y_{u,ij} H_u Q_i U_j^c \\ &+ \mu H_u R_d + \lambda_S H_u \Phi_{\tilde{B}} R_d + \lambda_T H_u \Phi_{\tilde{W}} R_d \,.\end{aligned} \tag{2.61}$$

$\tilde{h}_u$ and $\tilde{r}_d$ are now additional neutralinos and charginos which mix with the gaugino and the Higgs-partner lepton. Unlike in the model with the single Higgs doublet, the top quark mass can arise from an $H_u QU$ term, removing the need for a low UV cutoff.

For the purpose of deriving the neutrino mass matrix in Section 2.5.5, after diagonalising the R-symmetric terms in the 9×9 neutralino mass matrix, we now have

$$\nu_e' \simeq \nu_e + \left(\frac{M_{\tilde{W}}}{M_{\tilde{B}}} t_w\right) c_\beta \epsilon\, \psi_{\tilde{B}} - c_\beta \epsilon\, \psi_{\tilde{W}}^0 + \left(\frac{M_{\tilde{W}}}{\mu}\frac{\lambda_T}{\sqrt{2}g} - \frac{M_{\tilde{W}}^2}{M_{\tilde{B}}\mu}\frac{\sqrt{2}\lambda_S t_w}{g}\right) c_\beta s_\beta \epsilon^2\, \tilde{h}_u^0. \tag{2.62}$$

In contrast to the 1HDM case, ν_e' now contains a $\tilde{h}_u^0$ component, and some of the coefficients depend on c_β and s_β. The $\tilde{h}_u^0$ component induces the $\nu_e'\nu_\mu$ and $\nu_e'\nu_\tau$ terms in the neutrino mass matrix through the R-breaking mass terms $\tilde{h}_u^0\nu_\mu$ and $\tilde{h}_u^0\nu_\tau$.

Chapter 3
Sneutrino Higgs models explain lepton non-universality in CMS excesses[1]

Chapter abstract

Recent searches for first-generation leptoquarks and heavy right-handed W_R bosons have seen excesses in final states with electrons and jets. A bizarre property of these excesses is that they appear to violate flavour universality. With these results in mind, we study the phenomenology of supersymmetric models in which the Higgs arises as the sneutrino in an electron supermultiplet. Since the electron is singled out in this approach, one can naturally account for the lepton flavour structure of the excesses. In this work, we show that in such a framework, one can significantly alleviate the tension between the Standard Model and the data and yet evade current constraints from other searches. Lastly we point out that correlated excesses are expected to be seen in future multilepton searches.

3.1 Introduction

The Standard Model (SM) of particle physics is among the most successful models ever devised, yet it leaves open several puzzles that should be resolved by a more complete description of nature. A well-motivated, broad class of models based on supersymmetry (SUSY) has the potential to resolve one or more of the outstanding puzzles of the SM, including the hierarchy problem, the nature of dark matter, the

[1]Based on J. Berger, J. A. Dror and W. H. Ng, *JHEP* **09** (2015) 156, [1506.08213].

mechanism of baryogenesis, and the running of gauge couplings to a unified value. From a phenomenological point of view, however, there are several issues with models based on SUSY. In particular, the naive implementation of natural R-parity conserving MSSM requires a light spectrum of colour-charged particles to which the experiments at the Large Hadron Collider (LHC) should have sensitivity, yet no hints of SUSY have been seen in the "standard candle" channels with Missing Transverse Energy [90]. Furthermore, a Higgs boson with mass 125 GeV is not generically reconciled with a natural spectrum of superpartners [127]. Both of these tensions hint at the possibility that, if natural SUSY describes our universe, then it may have an alternative structure.

The lack of observation at colliders has lead to the introduction of many variations of supersymmetry such as R-parity violating (RPV) [128–136] and R-symmetric supersymmetry [93–106, 108–113, 137, 138]. Constraints on SUSY, even in the context of RPV models, are already quite stringent [139–141]. These constraints are somewhat less restrictive in models with R-symmetric models due to the requirement of Dirac gauginos [126]. In particular, this prevents same-sign lepton signatures that would be smoking gun indicators of physics Beyond the SM (BSM). An additional intriguing feature of such models is that they allow for the Higgs field to be identified with the superpartner of a left-handed electron[2] [36, 101, 107]. In this unique framework, traditional LLE^c and LQD^c RPV effects are present but necessarily suppressed by the smallness of the Yukawa couplings. However, RPV effects appear due to a mixing between the electron doublet and the gauginos (such mixing has been previously used to put constraints of possible sneutrino VEVs [142]). Since the electron is singled out as the Higgs partner, such models have non-standard lepton flavour structure leading in general to an

[2]In general this can be any lepton, but as we will discuss in Section 3.2, the electron is the most natural choice.

abundance of electrons in the final state. Furthermore as we will show, the requirement of nearly massless neutrinos requires the introduction of an R-symmetry.

The CMS experiment has recently seen hints of potential BSM physics at the $\sim 2.5\sigma$ level in three separate searches that appear to single out the first generation of leptons. Two of these analyses were optimized to look for pair production of leptoquarks. In one case, the leptoquarks decay to an $eejj$ final state, while in the other they decay to an $e\nu jj$ final state [41]. Both showed excesses hinting at a roughly 650 GeV leptoquark, at the 2.4σ and 2.6σ levels respectively. The excesses are not consistent with the only decay modes of the leptoquarks being ej and νj [40, 41]. The third search was optimized for a W_R decaying to an $eejj$ final state and saw a 2.8σ local excess for a resonance near 2.1 TeV [42]. However, the distributions of the excess do not appear to be consistent with those of a W_R [42]. Its important to note that the leptoquark searches did not see an excess in its high leptoquark mass bins. While not emphasised in earlier work, this puts serious limitations on new BSM signals attempting to explain the excess. No excesses were observed in the corresponding channels with muons [42, 43].

Several models have been constructed in order to explain this excess. Many of these models are supersymmetric in nature [143–148] (see [40, 149–159] for non-supersymmetric explanations). The vast majority of them do not attempt to explain the puzzling flavour structure of the observed excesses, but merely choose certain couplings to be larger then others. Standard tools for suppressing flavour-violating processes such as minimal flavour violation (MFV) [160] cannot explain a different coupling for the first and second generations. In MFV, such non-universal terms in the Lagrangian are suppressed by m_μ/m_τ. Furthermore, due to the presence of a heavy resonance, these models often predict an excess in the searches for

higher mass leptoquarks, which has not been observed in the data.

In this chapter, we investigate the possibility that supersymmetric models with the Higgs as a sneutrino could explain the excesses seen by CMS. The lepton flavour structure is naturally obtained within the context of such models. The complex SUSY spectrum yields a rich variety of decay modes, suppressing the number of events seen in individual channels and allowing such models to evade many constraints. Overall, this class of models provides a good fit for the current data, while making several new and testable predictions for the upcoming run of the LHC. The role of the leptoquarks in the model is played by a left-handed first-generation squark with R-parity violating decays, while the heavier $\sim 2\,\text{TeV}$ resonance is explained by gluino-squark production. The masses that give the best fit are an up squark mass of 810 GeV and a gluino mass of 1790 GeV. In addition to accounting for the excesses observed by CMS, this model addresses the lack of an excess when the set of cuts is optimized for higher mass leptoquarks. The model considered in this chapter addresses this potential issue by softening the "leptoquark" spectrum with additional jets, as proposed in [149].

The remainder of this chapter is structured as follows. In Section 2, we review the minimal model with the Higgs as a sneutrino. We determine a set of parameters of this model that provide a good fit to the current CMS data in Section 3. We then conclude discussing current bounds on the model and provide additional predictions.

3.2 Model with Higgs as a slepton

3.2.1 Overview

To illustrate the main ideas behind the Higgs-as-slepton model [36], we begin by attempting to construct a supersymmetric Standard Model that is more minimal than the MSSM. One can identify the SM Higgs doublet H with a slepton doublet $\tilde{L}_a$, since they are both in the same gauge representation $(1,2)_{-1/2}$. The model then requires two fewer doublet chiral superfields than the MSSM. However, a major issue arises from the fact that the Kähler potential generates electroweak-scale Dirac masses between the partner leptons $L_a \equiv (\nu_a, l_a^-)$ and the Winos and Binos:

$$\mathcal{L} \supset -\frac{g v_H}{\sqrt{2}} l_a^- \tilde{W}^+ - \frac{g v_H}{2} \nu_a \tilde{W}^0 + \frac{g' v_H}{2} \nu_a \tilde{B} + \text{h.c.} \tag{3.1}$$

This leads to neutrino masses that are too large.

One way around this difficulty is to first impose a $U(1)_R$ symmetry, with R-charge zero for the slepton doublet $\tilde{L}_a$ and -1 for the partner lepton doublet L_a. The $U(1)_R$ symmetry remains unbroken when $\tilde{L}_a$ acquires a VEV, and can still forbid Majorana masses for all $U(1)_R$-charged neutralinos. By introducing adjoint chiral superfields Φ and SUSY-breaking Dirac gaugino masses, one of the neutralino mass eigenstates becomes massless. This massless neutralino is mainly comprised of ν_a and can be identified with the "physical" neutrino.

We now present the details of the model. Table 3.1 lists all the superfields and their gauge and $U(1)_R$ representations. With the CMS excesses in mind, we have chosen the first-generation leptons to partner the Higgs. This will give rise to experimental signatures specific to the electron, without the need to tweak any

	$SU(3)_C \times SU(2)_L \times U(1)_Y$	$U(1)_R$
$H \equiv L_3$	$(1,2)_{-1/2}$	0
E_3^c	$(1,1)_1$	2
$L_{1,2}$	$(1,2)_{-1/2}$	$1-L$
$E_{1,2}^c$	$(1,1)_1$	$1+L$
$Q_{1,2,3}$	$(3,2)_{1/6}$	$1+B$
$U_{1,2,3}^c$	$(\bar{3},1)_{-2/3}$	$1-B$
$D_{1,2,3}^c$	$(\bar{3},1)_{1/3}$	$1-B$
$W^{a\alpha}$	$(8,1)_0 + (1,3)_0 + (1,1)_0$	1
Φ^a	$(8,1)_0 + (1,3)_0 + (1,1)_0$	0

Table 3.1: Superfields and their gauge and $U(1)_R$ representations in the Higgs-as-slepton model.

lepton couplings. B and L are arbitrary parameters that determine the $U(1)_R$ representations of the quark and the 2nd- and 3rd-generation lepton superfields.

The most general superpotential consistent with the symmetries (assuming $B \neq 1/3$ and $L \neq 1$) is

$$\mathcal{W} = \sum_{i,j=1}^{3} y_{d,ij} H Q_i D_j^c + \sum_{i=1}^{2} y_{e,i} H L_i E_i^c. \tag{3.2}$$

We have chosen to work in the mass basis of the charged leptons. The superpotential does not generate up-type quark masses due to the absence of an up-type Higgs superfield H_u. The same is true for the electron mass, since the required term HHE_3^c is identically zero. Both can be generated by SUSY-breaking Kähler terms of the form [36]

$$\int d^2\theta d^2\bar{\theta} \frac{X^\dagger}{M} \frac{H^\dagger Q_i U_j^c}{\Lambda} \tag{3.3}$$

and

$$\int d^2\theta d^2\bar{\theta} \frac{X^\dagger X}{M^2} \frac{H D^\alpha H D_\alpha E_e^c}{\Lambda^2} \tag{3.4}$$

that are suppressed by a Λ cutoff scale. This also provides a natural explanation for the smallness of the electron mass, hence further motivating our decision to partner the first-generation leptons with the Higgs.

The $U(1)_R$ symmetry forbids mixing between left-handed and right-handed squarks, so the squark phenomenology differs from that of the MSSM [138]. This also simplifies our subsequent analysis of squark production and decay since the squark mass eigenstates are then either left- or right-handed.

We note that the terms in the superpotential can also be interpreted as RPV terms of the form $L_3 Q_i D_j^c$ and $L_3 L_i E_j^c$. Therefore, experimental bounds on RPV coefficients [161] can be applied to the superpotential Yukawas $y_{d,ij}$ and $y_{e,ij}$, which are in turn determined by the SM fermion masses and mixings. We find that these bounds are satisfied by the model for the choices of squark masses to be used in later sections.

While we assume the model described above in this work, our results are largely independent of the detailed mechanism giving the up-type quark and electron masses. Alternative models which introduce additional chiral superfields are also possible [101, 107] and can also produce similar signatures.

3.2.2 Chargino and neutralino mass matrices and mixing

The chargino and neutralino Dirac mass matrices are given by

$$\mathcal{M}_C = \begin{array}{c} \\ \tilde{W}^- \\ \psi^-_{\tilde{W}} \\ e^-_L \end{array} \begin{array}{c} \begin{array}{ccc} \tilde{W}^+ & \psi^+_{\tilde{W}} & e^{c+}_R \end{array} \\ \begin{pmatrix} 0 & M_{\tilde{W}} & 0 \\ M_{\tilde{W}} & 0 & 0 \\ \frac{gv_H}{\sqrt{2}} & 0 & 0 \end{pmatrix} \end{array}, \qquad \mathcal{M}_N = \begin{array}{c} \\ \psi_{\tilde{B}} \\ \psi^0_{\tilde{W}} \\ \nu_e \end{array} \begin{array}{c} \begin{array}{cc} \tilde{B} & \tilde{W}^0 \end{array} \\ \begin{pmatrix} M_{\tilde{B}} & 0 \\ 0 & M_{\tilde{W}} \\ -\frac{g'v_H}{2} & \frac{gv_H}{2} \end{pmatrix} \end{array} \tag{3.5}$$

We have neglected the masses from Λ-suppressed SUSY-breaking terms such as electron masses, since they are much smaller than the present terms and hence not expected to play an important role. To order $\epsilon \equiv gv_H/(2M_{\tilde{W}}) = m_W/M_{\tilde{W}}$, the chargino 4 component mass eigenstates are:

$$\chi^-_1 = \begin{pmatrix} -\sqrt{2}\epsilon\psi^-_{\tilde{W}} + e^-_L \\ e^-_R \end{pmatrix}, \quad \chi^-_2 = \begin{pmatrix} \tilde{W}^- \\ \psi^{+\,c}_{\tilde{W}} \end{pmatrix}, \quad \chi^-_3 = \begin{pmatrix} \psi^-_{\tilde{W}} + \sqrt{2}\epsilon e^-_L \\ \tilde{W}^{+\,c} \end{pmatrix} \tag{3.6}$$

with mass eigenvalues $m_{\chi^-_1} = 0$ and $m_{\chi^-_2} = m_{\chi^-_3} = M_{\tilde{W}}$. The mass eigenstates for the neutralinos are[3] :

$$\chi^0_1 = \begin{pmatrix} \frac{g'}{g}\frac{M_{\tilde{W}}}{M_{\tilde{B}}}\epsilon\psi_{\tilde{B}} - \epsilon\psi^0_{\tilde{W}} + \nu_e \\ 0 \end{pmatrix}, \quad \chi^0_2 = \begin{pmatrix} \psi^0_{\tilde{W}} + \epsilon\nu_e \\ \tilde{W}^{0\,c} \end{pmatrix}, \quad \chi^0_3 = \begin{pmatrix} \psi_{\tilde{B}} - \frac{g'}{g}\frac{M_{\tilde{W}}}{M_{\tilde{B}}}\epsilon\nu_e \\ \tilde{B}^c \end{pmatrix} \tag{3.7}$$

with mass eigenvalues $m_{\chi^0_1} = 0$, $m_{\chi^0_2} = M_{\tilde{W}}$ and $m_{\chi^0_3} = M_{\tilde{B}}$.

χ^-_1 can be identified with the physical electron, and χ^0_1 with the "physical" electron neutrino, before PMNS mixing. We note that the gauge couplings of the

[3]We have assumed here that $\left|M^2_{\tilde{W}} - M^2_{\tilde{B}}\right| \gg m^2_W$. In the converse case where $\left|M^2_{\tilde{W}} - M^2_{\tilde{B}}\right| \ll m^2_W$, the actual heavy neutralino eigenstates are linear superpositions of χ^0_2 and χ^0_3 above, with mixings given by the Weinberg angle θ_W. Nonetheless, this does not affect any of our subsequent results on the partial widths.

physical gauginos and first-generation leptons to $W^{\pm}$ and Z are affected by the $O(\epsilon)$ mixing. One consequence is that the eeZ coupling is modified, hence violating lepton flavour universality. This allows us to place a lower bound of $\sim 2\,\text{TeV}$ on the Dirac chargino mass $M_{\tilde{W}}$ [36]. Another consequence is that the modified gauge couplings mix the physical gauginos and leptons, thus providing a channel for the gauginos to decay completely to SM particles, e.g. $\chi_2^0 \to \chi_1^- W^+$. Should the squarks be lighter than the gauginos, which we assume in the rest of this work, virtual cascades such as $\tilde{d}_L \to d\,\overline{\chi_2^0}^* \to d\,\overline{\chi_1^-}\,W^-$ may also become important decay channels for the first-generation squarks, as we will see below.

3.2.3 First-generation left-handed squark decays

In MSSM with RPV, supersymmetric particles can decay completely to SM particles through channels generated by RPV superpotential and soft SUSY-breaking terms. While this is also true for the Higgs-as-slepton model, there are new decay channels due to the mixing of physical gauginos and leptons by the modified gauge couplings. A typical diagram for the new channel is shown in Figure 3.1. The new channels are especially important for first-generation squarks compared to the standard RPV channels, due to the smallness of the Yukawas in the latter [36]. The approximate partial widths of these channels for first-generation LH squarks are shown in Table 3.2. Figure 3.2 compares the partial widths of the mixing-induced and standard RPV channels for $\tilde{d}_L$ decay, from which we see that the former is dominant except for very large values of $M_{\tilde{W}}$.

Supersymmetric particles (and the Higgs) can also decay into SM particles + the gravitino, which is the lightest supersymmetric particle (LSP) in the model. The decay occurs via goldstino interaction terms fixed by supersymmetry, with

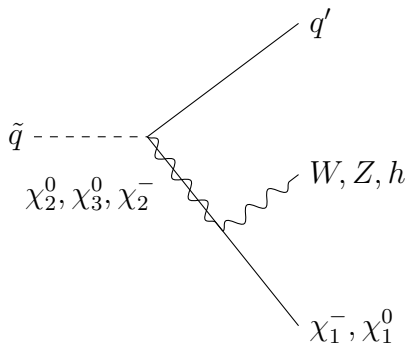

Figure 3.1: Mixing-induced decay channels in which a supersymmetric particle $\tilde{q}_L$ decays completely to SM particles.

Decay channel	Partial width $\Gamma/(\frac{1}{6144\pi^3})$
$\tilde{u}_L \to d\,\overline{\chi_1^-}\,h^0$	$m_{\tilde{u}}^5 g^4/M_{\tilde{W}}^4 \times 1/2$
$\tilde{u}_L \to d\,\overline{\chi_1^-}\,Z$	$m_{\tilde{u}}^5 g^4/M_{\tilde{W}}^4 \times 1/2$
$\tilde{d}_L \to u\,\overline{\chi_1^0}\,W^-$	$m_{\tilde{d}}^5 g^4/M_{\tilde{W}}^4$
$\tilde{u}_L \to u\,\overline{\chi_1^-}\,W^-$	$m_{\tilde{u}}^5 \left[g'^2 Y_Q/M_{\tilde{B}}^2 + g^2/(2M_{\tilde{W}}^2)\right]^2$
$\tilde{d}_L \to d\,\overline{\chi_1^0}\,h^0$	$m_{\tilde{d}}^5 \left[g'^2 Y_Q/M_{\tilde{B}}^2 + g^2/(2M_{\tilde{W}}^2)\right]^2 \times 1/2$
$\tilde{d}_L \to d\,\overline{\chi_1^0}\,Z$	$m_{\tilde{d}}^5 \left[g'^2 Y_Q/M_{\tilde{B}}^2 + g^2/(2M_{\tilde{W}}^2)\right]^2 \times 1/2$
$\tilde{u}_L \to u\,\overline{\chi_1^0}\,h^0$	$m_{\tilde{u}}^5 \left[g'^2 Y_Q/M_{\tilde{B}}^2 - g^2/(2M_{\tilde{W}}^2)\right]^2 \times 1/2$
$\tilde{u}_L \to u\,\overline{\chi_1^0}\,Z$	$m_{\tilde{u}}^5 \left[g'^2 Y_Q/M_{\tilde{B}}^2 - g^2/(2M_{\tilde{W}}^2)\right]^2 \times 1/2$
$\tilde{d}_L \to d\,\overline{\chi_1^-}\,W^-$	$m_{\tilde{d}}^5 \left[g'^2 Y_Q/M_{\tilde{B}}^2 - g^2/(2M_{\tilde{W}}^2)\right]^2$

Table 3.2: Partial widths for the mixing-induced decay channels. Here χ_1^- and χ_1^0 refer to the physical electron and electron neutrino. Y_Q is the hypercharge of the LH quark doublet. The decay channels have been arranged such that the approximate isospin symmetry from the Goldstone boson equivalence theorem is obvious.

partial widths that typically scale as $m_{\rm sp}^5/(m_{3/2}M_{\rm Pl})^2$, where $m_{\rm sp}$ is the sparticle mass, $m_{3/2}$ the gravitino mass and $M_{\rm Pl}$ the Planck scale [36]. However, as long as the gravitino mass is not too small ($m_{3/2} \gg 1\,\text{eV}$), these decays are expected to be sub-dominant and can hence be neglected. For the rest of this work, we assume all first-generation squarks to decay via the mixing-induced decay channels.

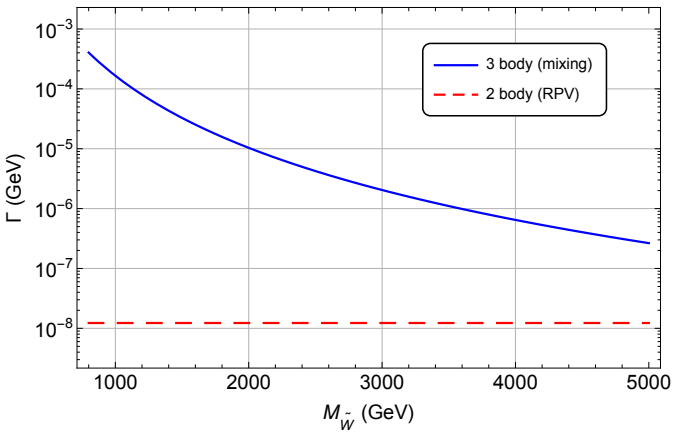

Figure 3.2: Partial widths of $\tilde{d}_L$ for mixing-induced and standard RPV decay channels, assuming $m_{\tilde{d}} = 810\,\text{GeV}$ and $M_{\tilde{B}} = M_{\tilde{W}}$. The mixing-induced channel dominates over the range of $M_{\tilde{W}}$ considered.

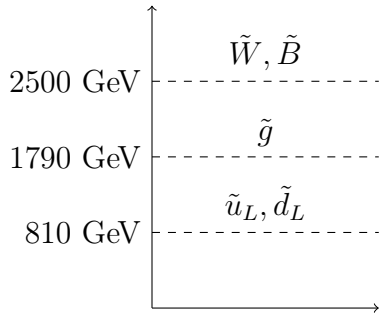

Figure 3.3: The spectrum of our benchmark point. All other fields are decoupled.

3.3 Simulation and Results

In this section, we estimate the contribution of the above model to the CMS leptoquark and W_R searches. The spectrum and production channels of interest are depicted in Figures 3.3 and 3.4.

The model predictions are calculated at tree level using Madgraph [162], Pythia 6.4 [163] for showering and hadronization, and PGS [164] for detector simulation. The model files were created using Feynrules [165]. To estimate the next-to-leading order (NLO effects we scaled the cross-sections by their corresponding K-factors

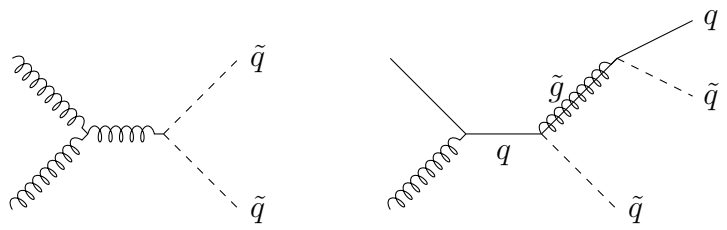

Figure 3.4: Sample production mechanisms for disquark and single gluino production channels. Squarks decay through the 3 body decay shown in Figure 3.1.

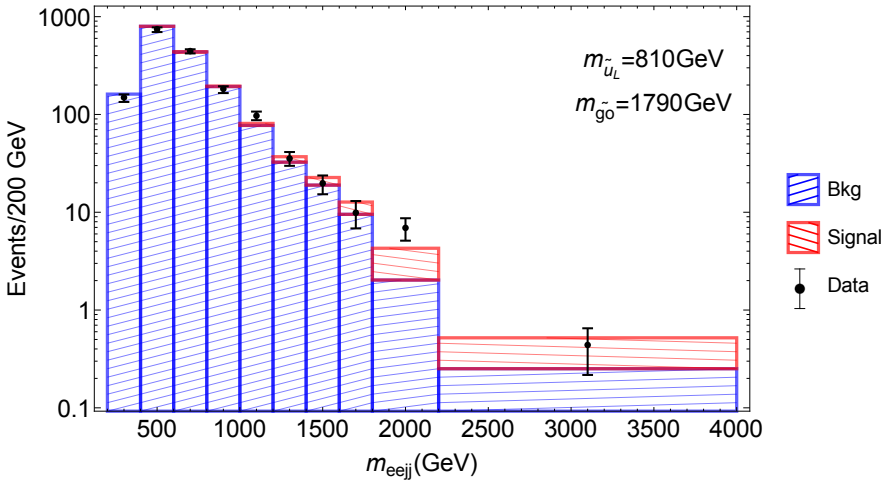

Figure 3.5: The m_{eejj} prediction for our model after applying cuts used in the W_R search. The background and relevant cuts were taken from [42].

calculated using Prospino 2.1 [166]. While Prospino was designed for the MSSM we do not expect significant deviations in the calculations of K-factors.

The W_R search distribution is shown in Figure 3.5. We reproduce the invariant mass distribution of the two leading electrons and two leading jets. We also applied all the relevant cuts detailed by CMS in [42], the most restrictive requiring the invariant mass of the electrons be greater than 200 GeV.

The single gluino production dominates the high mass peak, while the disquark channel contributes broadly to the bins between $1 - 2\,\text{TeV}$. The broad feature is a consequence of a many-body structure of the decay which, and as pointed out

in [149], is useful to evade bounds by the CMS leptoquark search without introducing multiple decay channels. We emphasise that in our model we satisfy both properties of the signal. Firstly, no signal is found in corresponding muon channels as only the electron doublet mixes with the other neutralinos and charginos in this framework. Secondly, the events are dominated by opposite-sign electrons. This is guaranteed by the imposed R symmetry for which an electron and positron have opposite charges.

Next we reproduce the leptoquark (LQ) searches in this framework. In the LQ search a sequence of more stringent cuts are applied, optimized for different mass leptoquarks. In the $eejj$ channel, the main discriminating variables are S_T (the scalar sum of p_T of two leading electrons and jets), m_{ee} (invariant mass of the two electrons), and m_{ej}^{min} (the minimum of the electron-jet invariant mass of the four possible combinations for $eejj$). In the $e\nu jj$ channel, the main discriminating variables are S_T, E_T^{miss}, and m_{ej}. Typically models that predict large m_{eejj} (in order to explain the W_R excess) will also produce large S_T (and m_{ej}^{min} unless they arise from a very light LQ). In general, this leads to expected excess in the heavy LQ mass cut range. Thus it is important to check the predictions of any model attempting to explain the flavour violating anomalies in these high mass bins.

The corresponding cuts for each LQ mass can be found in [41] (see Tables 2 and 3). Here we plot the difference between the data and the SM background as a function of LQ mass cut. The results are shown in Figure 3.6. Each bin is a fraction of the events in the lower LQ mass cut bin and thus the bins are highly correlated. We see moderate agreement of our signal with the observed counts. We are able to explain the excess in the $\sim 650\,\text{GeV}$ region, but see small excess in the higher mass cuts for $eejj$. The excess in the high mass range is a general

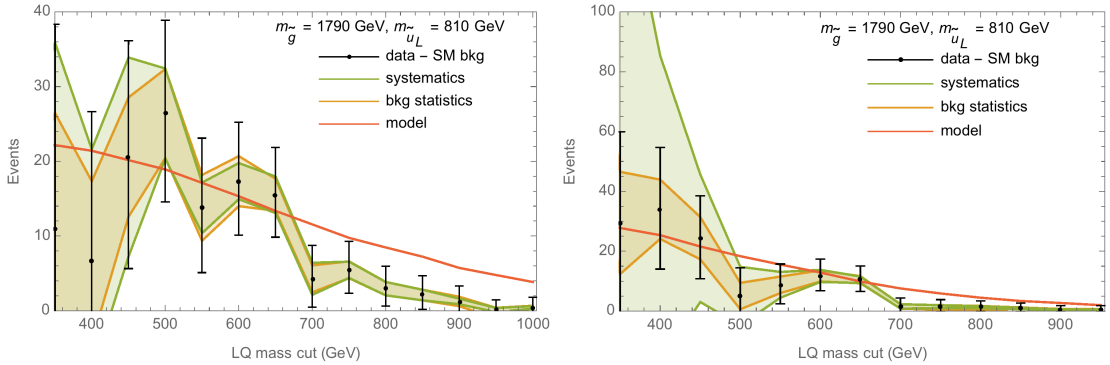

(a) $eejj$ search (b) $e\nu jj$ search

Figure 3.6: Bin-by-bin background-subtracted events for the LQ searches. Each bin count is a subset of the previous bin and hence the bins are highly correlated. The model shows some tension with the data at high LQ mass cuts.

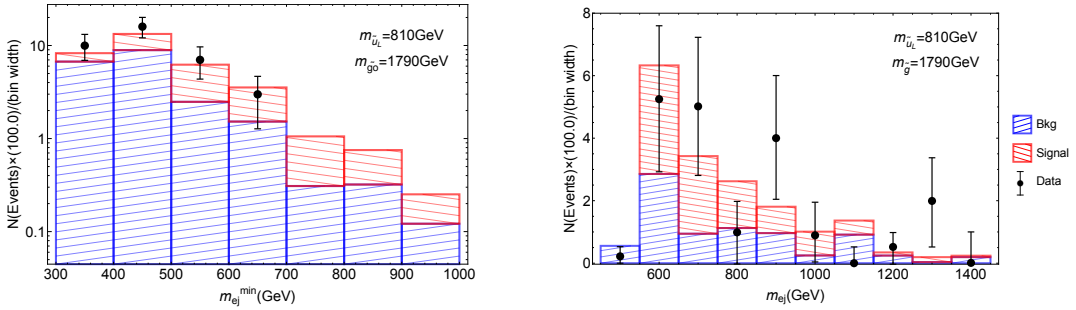

(a) $eejj$ search (figure 5 in [41]) (b) $e\nu jj$ search (figure 8 in [41])

Figure 3.7: The CMS leptoquark search plots.

characteristic of trying to explain both the W_R and LQ searches. Note that the excess is $\mathcal{O}(5)$ events instead of $\mathcal{O}(10)$ which were found in the W_R search. This is a consequence of the large number of jets increasing the effectiveness of the S_T cut.

To further check the kinematic properties of the model we compare our m_{ej}^{min} and m_{ej} distributions at the 650 GeV mass cut point. The results for both searches are shown in Figure 3.7. In both the $eejj$ and $e\nu jj$ channel we see good agreement between the model and experiment. The broad feature of the plots is again a consequence of the many jet signal and is necessary to get the right kinematic

spread in the LQ invariant mass distributions.

This framework has two characteristic features – many electrons in the final state and many jets. Due to their limited background, we expect the most stringent bounds on our model arise from multilepton searches [167, 168]. The model produces more than 2 leptons if each squark decays into an electron and additional leptons arise from vector boson decays. We now roughly estimate the number of expected events in the multilepton searches. The NLO cross section for squark-squark and squark-gluino production at our mass point is 5.7 fb. At $\mathcal{L} \sim 20\,\text{fb}^{-1}$ this corresponds to about 115 events. The probability of both squarks producing electrons (as opposed to neutrinos) is about 1/4. Furthermore, the probability of at least one of the vector bosons decaying leptonically is between 11 and 40% depending on whether there is a WW, WZ, or ZZ is in the final state. This suggests $5 - 10$ events with 3 or more leptons. However, these events don't contain any genuine E_T^{miss} or b-tagged jets, both of which are powerful discrimating variables in such searches. This makes the signal hard to detect, even in a multilepton search. Thus we conclude the model is safe from current multilepton bounds, though we expect sensitivity with more data at higher energies.

3.4 Discussion and Conclusions

In this chapter, we have explored the phenomenology of a class of SUSY models in which the Higgs is a sneutrino. Such models could account for excesses seen in the CMS experiment, while accounting for the observed kinematics and flavour structure in a natural way.

As with most SUSY models, several correlated observables are expected. While

the detailed spectrum and branching fractions are model-dependent, these models have a few generic predictions. Most reliably, there should be correlated excesses in multi-lepton searches. Since the decay of hadronic sparticles necessarily proceeds via electroweakinos, the decays will generally feature leptons, possibly in large numbers and with a preference for electrons. These excesses would come with some missing energy from neutrinos, but decays without neutrinos are certainly possible. The flavour structure of these excesses would again be striking, featuring more electrons than muons or taus. The scales of $\lesssim 1600\,\text{GeV}$ from $\tilde{q}\tilde{q}^*$, $\lesssim 2400\,\text{GeV}$ from $\tilde{q}\tilde{g}$, and $\lesssim 3600\,\text{GeV}$ from $\tilde{g}\tilde{g}$ would also feature in the total invariant (transverse) mass distribution.

The remaining signals are highly dependent on the more weakly coupled or heavier elements of the spectrum. The constraints on sleptons and electroweakinos remain weak after Run 1 of the LHC, but searches for signatures of new electroweak states are a vital part of Run 2 that can only be fully exploited at high luminosity. Such particles with mass $\mathcal{O}(100\,\text{GeV})$ could be in the spectrum and would decay primarily to elecrtoweak bosons, electrons, and neutrinos.

The first run of the LHC has seen a remarkable confirmation of the SM with few searches finding excesses beyond the 2σ level. On the other hand, several searches that have seen excesses indicate similar final states with electrons and jets, as well as large energy scales of $\sim 650\,\text{GeV}$ and $\sim 2\,\text{TeV}$. If such excesses are the first hints of a new state beyond the SM, then Run 2 will bring striking and nearly immediate discoveries, as the sensitivity to physics at $\sim 2\,\text{TeV}$ is vastly superor to that in the first run.

Chapter 4
A 2 TeV W_R, Supersymmetry, and the Higgs Mass[1]

Chapter abstract

A recent ATLAS search for diboson resonances and a CMS search for $eejj$ resonances which both show excesses with significance around 3σ have generated interest in $SU(2)_R$ gauge extensions of the Standard Model with a W' mass around 2 TeV. We investigate the possibility that an $SU(2)_R$ gauge extension of the MSSM compatible with an explanation of the diboson anomaly might give rise to a significant enhancement of the Higgs mass above the MSSM tree level bound $m_{h,\text{tree}} < 90\,\text{TeV}$ due to non-decoupling D-terms. This model contains a vector-like charge $-1/3$ $SU(2)_R$ singlet quark for each generation which mixes significantly with the $SU(2)_R$ doublet quarks, affecting the W_R phenomenology. We find that it is possible to achieve $m_{h,\text{tree}} > 110\,\text{GeV}$, and this requires that the Z' mass is close to 3 TeV.

4.1 Introduction

The recently discovered Higgs boson with mass around 125 GeV creates some tension in the Minimal Supersymmetric Standard Model (MSSM). This is because its quartic interaction comes only from its supersymmetric gauge interactions at tree level, resulting in the well known result that at tree level the Higgs mass is no

[1]Based on J. H. Collins and W. H. Ng, *JHEP* **01** (2016) 159, [1510.08083].

greater than the Z boson mass of 91 GeV.

$$m_{h,\text{tree}}^2 = \frac{1}{4}(g^2 + g'^2)v^2 \cos^2(2\beta) \leq m_Z^2 \tag{4.1}$$

Evading this constraint with minimal matter content requires significant radiative corrections from stop loops, necessitating some combination of a large soft SUSY breaking mass and large A-terms. This in turn incurs a large fine tuning penalty in the Higgs potential due to the quadratic sensitivity of the Higgs soft mass to these parameters. It is possible that this little hierarchy problem is resolved by extending the matter content of the MSSM to allow for new tree level contributions to the Higgs quartic, either from F-terms as in the NMSSM [169, 170], indicating the presence of new chiral superfields, or from new D-term contributions as is possible in gauge extensions of the MSSM [171–173]. The latter possibility predicts the existence of heavy gauge boson resonances that may be observable at the LHC.

With this in mind, it is intriguing that a number of small anomalies with local significance of up to 3.4σ have been reported by the ATLAS and CMS experiments which might speculatively be interpreted as resulting from a new resonance with mass 1.8 – 2 TeV. The most significant excess is in an ATLAS search for resonances decaying in pairs of SM vector bosons (either W or Z) which in turn decay hadronically [49], finding a maximum local significance of 3.4σ and limits weaker than expected for diboson resonances with masses between 1.8 and 2.2 TeV.[2] However, their leptonic and semileptonic searches for diboson resonances which have a similar sensitivity in this mass range saw no deviation from SM expectations [176,177]. A combination of these ATLAS searches finds a maximum significance of 2.5σ, with limits weaker than expected in the mass window 1.9 – 2.1 TeV [178]. A CMS search for hadronically decaying diboson resonances saw a much smaller excess of $1 - 1.5\sigma$ in the mass window 1.8 – 2.0 TeV [179], and their semileptonic search for a lepton-

[2]See also [174, 175] for a detailed discussion of this excess.

ically decaying Z and a hadronically decaying vector boson found a 1.5σ excess in the mass window 1.7 – 1.9 TeV [180]. A CMS search for WH resonances decaying into $l\nu bb$ found a 1.9σ excess in the mass window 1.8 – 2 TeV. In addition, CMS and ATLAS find modest excesses in their dijet mass distributions in the window 1.7 – 1.9 TeV with significance 2.2σ and 1σ respectively [50, 181]. Finally, a CMS search in the $eejj$ final state found a 2.8σ excess consistent with being produced by a resonance in the mass range 1.8 – 2.2 TeV [42].

It has been pointed out that a compelling candidate to explain these anomalies, if they are indeed a first hint of new physics, is a W' from a broken gauge symmetry which couples to right handed (RH) currents [156, 159, 182–191], as in models with Left-Right symmetry (LRS) [47, 48]. Firstly, such a particle is not constrained by the strong limits on l^+l^- or $l\nu$ resonances if it is charged and does not have a significant coupling to LH leptons. Secondly, the $eejj$ excess might be explained by a decay chain via RH neutrinos, $W_R \to e_R\nu_R \to e_R e_R jj$ [192]. The possibility of a new gauge symmetry is exciting in and of itself, but it could have a very special significance in the context of a supersymmetric theory due to the interplay between gauge symmetries and the Higgs mass. The purpose of this chapter is to explore the possibility that these anomalies could be directly related to the Higgs mass. We therefore consider a model with 1.9 TeV W_R with properties necessary to explain the anomalies.

The simplest possibility for electroweak symmetry breaking (EWSB) in these models is that it is generated by the VEVs of a bidoublet under $SU(2)_L \times SU(2)_R$, which contains the H_u, H_d fields of the MSSM with VEVs v_u, v_d. This provides the W_L–W_R mixing that is necessary for the diboson decay signature. As we shall review in more detail in Section 4.2, the D-term contribution to the Higgs mass in

these models is given by [193, 194]

$$m_{h,\text{tree}}^2 \leq \frac{1}{4}\left(g^2 + g_R^2\right) v^2 \cos^2(2\beta)\,, \tag{4.2}$$

where $\tan\beta = v_u/v_d$ as in the MSSM. Large contributions to the Higgs mass therefore require large g_R and large $\tan\beta$. In a minimal model this is not possible to reconcile with the anomalies. This is because the partial width $\Gamma(W' \to WZ)$ is suppressed by a factor $\sin^2(2\beta)/24$ compared to the partial width into dijets. A recent paper [182] fitted the cross sections for the dijet and diboson signatures, and found that

$$\frac{\sigma \times \text{BR}(W' \to WZ)}{\sigma \times \text{BR}(W' \to jj)} = \frac{\sin^2 2\beta}{24} > \frac{2.4\,\text{fb}}{144\,\text{fb}}. \tag{4.3}$$

Satisfying this inequality requires $\tan\beta \simeq 1$. Furthermore, fitting the overall signal cross section requires $g_R/g < 0.8$ in minimal models [156,159,182–191], since $\sigma_{W'} \propto g_R^2$. Fitting the excess with larger $\tan\beta$ and g_R therefore requires a departure from minimality. This might be possible by suppressing the W_R coupling to the RH quark doublets, which would modify the Drell-Yan production cross section and the inequality of Eq. (4.3). In this chapter we achieve this by introducing a vector-like charge $-1/3$ quark for each generation which mixes with the $SU(2)_R$ quark doublets after that gauge symmetry is broken. The right handed down-type quarks of the SM are then admixtures from the $SU(2)_R$ doublets and the singlets, with some mixing angle θ_d. The $W_R u_R d_R$ coupling is then suppressed by a factor of $\cos\theta_d$. Varying this mixing angle allows the freedom to fit the data with a larger value of $\tan\beta$, and since $\sigma_{W'} \propto g_R^2 \cos^2\theta_d$, a smaller $\cos\theta_d$ also allows the excess to be fit with a larger g_R. It is worth noting that while we introduce these new fields for purely phenomenological purposes, they are expected in E6 GUTs [195]. We do not explore the neutrino sector in this chapter, and therefore do not discuss the $eejj$ signature in any detail. The collider phenomenology of the right handed

neutrinos might be modified by light electroweak SUSY states such as Higgsinos as has been discussed in some detail in a recent paper [191].

We describe the model in Section 4.2, where we also review non-decoupling D-terms and the relevant experimental data. The main results of the chapter – the implications for the Higgs mass in our model – are presented in Section 4.3. The couplings associated with the new quark fields are strongly constrained by flavour changing neutral current (FCNC) observables, which we discuss in Section 4.4. Finally, we review the main conclusions of this work in Section 4.5.

4.2 The Model

We work with the gauge group $SU(3)_c \times SU(2)_L \times SU(2)_R \times U(1)_X$, with a symmetry breaking $SU(2)_R \times U(1)_X \to U(1)_Y$ at $\sim 2\,\text{TeV}$. The chiral superfields of the model are summarised in Table 4.1. In general, the RH gauge symmetry might be broken by some combination of doublet and triplet VEVs

$$H_R = \begin{pmatrix} H_R^+ \\ \frac{v_D}{\sqrt{2}} + H_R^0 \end{pmatrix}, \quad \Delta = \begin{pmatrix} \frac{1}{2}\Delta^+ & \Delta^{++} \\ \frac{v_\Delta}{\sqrt{2}} + \Delta^0 & -\frac{1}{2}\Delta^+ \end{pmatrix}, \quad \overline{\Delta} = \begin{pmatrix} \frac{1}{2}\overline{\Delta}^- & \frac{v_{\bar{\Delta}}}{\sqrt{2}} + \overline{\Delta}^0 \\ \overline{\Delta}^{--} & -\frac{1}{2}\overline{\Delta}^- \end{pmatrix}. \tag{4.4}$$

The H_R might be identified with a RH lepton doublet, or else must come with a conjugate superfield with opposite X charge for anomaly cancellation. For simplicity we assume such a field does not acquire a significant VEV, though this would not significantly alter our conclusions. The unbroken hypercharge generator is given by

$$Y = T_R^3 + X, \qquad g'^{-2} = g_R^{-2} + g_X^{-2}. \tag{4.5}$$

	$SU(3)_c$	$SU(2)_L$	$SU(2)_R$	$U(1)_X$
$Q_{Li} = (u_{Li}, d'_{Li})$	$\square$	$\square$	$\mathbf{1}$	$1/6$
$Q^c_{Ri} = (d'^c_{Ri}, u^c_{Ri})$	$\overline{\square}$	$\mathbf{1}$	$\square$	$-1/6$
D'_i	$\square$	$\mathbf{1}$	$\mathbf{1}$	$-1/3$
D'^c_i	$\overline{\square}$	$\mathbf{1}$	$\mathbf{1}$	$1/3$
$L_{Li} = (\nu_{Li}, \ell_{Li})$	$\mathbf{1}$	$\square$	$\mathbf{1}$	$-1/2$
$L_{Ri} = (\ell_{Ri}, \nu_{Ri})$	$\mathbf{1}$	$\mathbf{1}$	$\square$	$1/2$
$\Phi = (H_u, H_d)$	$\mathbf{1}$	$\square$	$\square$	0
$\Delta, \overline{\Delta}$	$\mathbf{1}$	$\mathbf{1}$	$\mathbf{3}$	± 1
H_R	$\mathbf{1}$	$\mathbf{1}$	$\square$	$1/2$

Table 4.1: Chiral superfields.

Writing $v_T^2 = v_\Delta^2 + v_{\bar{\Delta}}^2$, the W' and Z' masses are given by

$$\begin{aligned} m_{W'}^2 &= \frac{1}{4} g_R^2 \left(2v_T^2 + v_D^2\right) \left(1 + \mathcal{O}\left(\frac{v^2}{2v_T^2 + v_D^2}\right)\right), \\ m_{Z'}^2 &= \frac{1}{4} \left(g_R^2 + g_X^2\right) \left(4v_T^2 + v_D^2\right) \left(1 + \mathcal{O}\left(\frac{v^2}{4v_T^2 + v_D^2}\right)\right), \end{aligned} \tag{4.6}$$

with $v = 246\,\text{GeV}$ the EWSB VEV. By analogy with EWSB, the relation between the W' and Z' masses can be parametrized in terms of a new Weinberg angle, $\theta_{w'}$, and ρ' parameter

$$\frac{m_{Z'}^2}{m_{W'}^2} = \frac{\rho'}{c_{w'}^2}, \tag{4.7}$$

with

$$1 \leq \rho' \leq 2, \qquad c_{w'}^2 \equiv \frac{g_R^2}{g_R^2 + g_X^2} = 1 - \frac{s_w^2 g^2}{c_w^2 g_R^2}. \tag{4.8}$$

For pure doublet breaking $\rho' = 1$ as in the SM, while for pure triplet breaking $\rho' = 2$.

If EWSB is achieved with by a bidoublet $\Phi = (H_u, H_d)$ with VEVs $v_u/\sqrt{2}$,

$v_d/\sqrt{2}$ and $v^2 = v_u^2 + v_d^2$ then the W_L–W_R mass matrix is given by

$$M^2_{W,LR} = \frac{1}{4}\begin{pmatrix} g^2v^2 & -2gg_Rv_uv_d^* \\ -2gg_Rv_u^*v_d & g_R^2\left(2v_T^2 + v_D^2 + v^2\right) \end{pmatrix}. \tag{4.9}$$

This matrix is diagonalised with a rotation angle

$$\sin\phi \simeq \frac{g_R}{g}\frac{m_W^2}{m_{W'}^2}\sin 2\beta, \tag{4.10}$$

with $\tan\beta = v_u/v_d$. The decay responsible for the diboson signature, $W' \to WZ$, has a width given by

$$\begin{aligned}\Gamma(W' \to WZ) &\simeq \frac{m_{W'}^5}{192\pi m_W^2 m_Z^2}\frac{g^2}{c_w^2}\sin^2\phi \\ &= \frac{m_{W'}}{192\pi}g_R^2\sin^2 2\beta,\end{aligned} \tag{4.11}$$

which can be calculated from the kinetic terms of the Lagrangian [182, 196]. The diboson signature is therefore maximised for $v_u \simeq v_d$ and hence $\sin 2\beta \simeq 1$.

4.2.1 Non-Decoupling D-terms

In this model, the D-terms in the Higgs sector are given by

$$\begin{aligned}V_D =& \frac{g^2}{8}\left|\Phi^\dagger\sigma_a\Phi\right|^2 + \frac{g_R^2}{8}\left|H_R^\dagger\sigma_a H_R + 2\Delta^\dagger\sigma_a\Delta + 2\overline{\Delta}^\dagger\sigma_a\overline{\Delta} + \Phi\sigma_a\Phi^\dagger\right|^2 \\ &+ \frac{g_X^2}{8}\left|2\Delta^\dagger\Delta - 2\overline{\Delta}^\dagger\overline{\Delta} + H_R^\dagger H_R\right|^2\end{aligned} \tag{4.12}$$

Substituting in the VEVs of Eq. (4.4) and focussing on the terms relevant for the calculation of the potential for the neutral EWSB Higgses, we arrive at

$$\begin{aligned}V_D \supset& \frac{1}{8}\left(g^2 + g_R^2\right)\left(\left|H_u^0\right|^2 - \left|H_d^0\right|^2\right)^2 \\ &+ \frac{g_R^2}{2}\mathrm{Re}\left(2v_\Delta\Delta^0 - 2v_{\overline{\Delta}}\overline{\Delta}^0 + v_D H_R^0\right)\left(\left|H_u^0\right|^2 - \left|H_d^0\right|^2\right).\end{aligned} \tag{4.13}$$

The effective D-term for the MSSM-like Higgs fields is obtained by adding the first term from the equation above with the term obtained by integrating out the linear

combination $\mathrm{Re}(2v_\Delta\Delta^0 - 2v_{\bar{\Delta}}\overline{\Delta}^0 + v_D H_R^0)$. This field is the scalar superpartner of the Goldstone which is eaten by the Z', and in the supersymmetric limit in which this symmetry breaking occurs far above the scale of supersymmetry breaking the mass of this field is the same as that of the Z' and integrating it out returns the classic MSSM result, $V_D = (g^2 + g'^2)(|H_u^0|^2 - |H_d^0|^2)/8$ [171–173].

In the case that $m_{\mathrm{SUSY}} \sim m_{Z'}$ that we will be considering in this chapter, this scalar will gain an additional SUSY breaking contribution to its mass that is important for calculating the effective quartic for the EWSB Higgses. The general result is that the tree level Higgs mass contribution from D-terms is given by

$$m_{h,\mathrm{tree}}^2 = \frac{1}{4}\left(g^2 + \xi g_R^2\right) v^2 \cos^2 2\beta, \qquad \xi = 1 - \frac{g_R^2}{g_R^2 + g_X^2 + \delta}. \tag{4.14}$$

Any model dependence is encoded in the parameter δ, which interpolates between the decoupling limit ($\delta \to 0$) and the non-decoupling limit ($\delta \to \infty$).[3] The relation between δ and the paramers of the scalar potential is generically of the form $\delta \sim m_0^2/v_R^2$, where m_0 is the typical scale of the SUSY breaking parameters in the $SU(2)_R$ Higgs sector. The precise form of this relationship will be model dependent, but larger values of δ will generically correspond to a greater degree of tuning in the $SU(2)_R$ breaking potential. We discuss a simple model of triplet breaking in Appendix 4.B which illustrates the main points. For our numerical work in the next section, we take as benchmark points the values $\delta = \infty$ and $\delta = 2.5$ to describe tuned and untuned scenarios respectively.

As in the MSSM, the D-term contribution to the Higgs mass is maximised for $\cos 2\beta = 1$, while the diboson signature is maximised is for $\sin 2\beta = 1$, Eq. (4.11). This is a key tension in trying to reconcile the diboson signature with large non-decoupling D-terms.

[3] We have implicitly assumed that the decoupling limit exists in this discussion.

4.2.2 Exotic Quarks

The couplings of the quarks to the Higgses are given by the superpotential

$$W \supset y Q_L \Phi Q_R^c + z D' H_R Q_R^c + M D' D'^c \tag{4.15}$$

where y, z, M are matrices in flavour-space. After the breaking of $SU(2)_R$ but before EWSB, a linear combination of $d_R'^c, D'^c$ marries the field D' and obtain a large Dirac mass, $m_D \simeq \sqrt{(z v_D)^2/2 + M^2}$, with the remaining linear combination remaining massless and which can be identified with the RH down-type quarks of the SM, d_R^c. We can write

$$\begin{pmatrix} d_R^c \\ s_R^c \\ b_R^c \end{pmatrix} \simeq \begin{pmatrix} c_d & & \\ & c_d & \\ & & c_b \end{pmatrix} \begin{pmatrix} d_R'^c \\ s_R'^c \\ b_R'^c \end{pmatrix} + \begin{pmatrix} s_d & & \\ & s_d & \\ & & s_b \end{pmatrix} \begin{pmatrix} D'^c \\ S'^c \\ B'^c \end{pmatrix} \tag{4.16}$$

with $c_d = \cos\theta_d, s_d = \sin\theta_d$, and $\tan\theta_d \sim z_{11} v_d/(\sqrt{2} M_{11})$. In the limit $M \to \infty$ we recover the structure of a minimal left-right symmetric model, in which the RH down-type quarks are $SU(2)_R$ partners of the RH up-type quarks and $s_d, s_b \to 0$. In order to evade constraints from FCNCs, we have assumed that the upper left 2×2 block of the rotation matrix is close to the identity matrix and the mixing between the third and first two generations are small. This structure might be enforced by an approximate $U(2) \times U(1)$ flavour symmetry. We will explore the constraints on this flavour structure in more detail in Section 4.4.

Because the up and down type quarks couple to the bidoublet with the same Yukawa matrix y, the expectation from Eqs. (4.15) and (4.16) is that their masses have the relationship

$$\frac{m_u}{m_d} \simeq \frac{m_c}{m_s} \simeq \frac{\tan\beta}{c_d}, \qquad \frac{m_t}{m_b} \simeq \frac{\tan\beta}{c_b}. \tag{4.17}$$

The mass relationships for the light quarks might easily be modified without introducing large FCNCs either as a result of additional loop contributions from the squark sector [197], or from additional small sources of EWSB which couple to the first and second generation quarks via non-renormalizable operators [198]. However, it is difficult to account for the mass ratio for the third generation quarks with small $\tan\beta$ and $c_b = 1$ by altering the EWSB sector without also suppressing the diboson signature. On the other hand, this mass ratio is well accounted for if $c_b \simeq t_\beta m_b/m_t \simeq t_\beta/35$. We will assume this relationship in this chapter. This means that b_R^c is mostly an $SU(2)_R$ singlet and the partial width for $W' \to tb$ is suppressed by a factor c_b^2. On the other hand, due to the potential sensitivity of the light quark masses to other small corrections we do not use these mass ratios to constrain c_d.

As a consequence of this mixing, the production cross section of the W' and its partial width into dijets are modified:

$$\sigma_{W'} \propto c_d^2\, g_R^2, \tag{4.18}$$

$$\Gamma\left(W' \to jj\right) = \frac{m_{W'}}{8\pi} c_d^2\, g_R^2, \tag{4.19}$$

$$\frac{\Gamma\left(W' \to WZ\right)}{\Gamma\left(W' \to jj\right)} = \frac{\sin^2 2\beta}{24\, c_d^2}. \tag{4.20}$$

A smaller c_d allows for a larger diboson branching fraction, providing the freedom to lower $\sin^2 2\beta$, due to Eq. (4.20). It also allows the same W' cross section to be achieved with a larger g_R due to Eq. (4.18). The combination of these factors is what allows for an enhancement of the tree level Higgs mass in Eq. (4.14) compared to the minimal model which corresponds to $c_d = 1$. It is worth bearing in mind that while we are mainly driven by the relation between the experimental excesses and the Higgs mass, the region of parameter space near $c_d \simeq t_\beta\, m_s/m_c \simeq t_\beta/14$ might be particularly interesting for flavour physics.

It is expected that the first and second generation exotic quarks D, S would decay via $D \to Zj$, $D \to Wj$ with significant branching fractions via W'–W and Z'–Z mixing. Only one dedicated LHC search exists for this scenario, a search for $Q \to Wq$ by the ATLAS experiment [199]. They found a broad 2σ excess, and excluded the mass range 320 GeV to 690 GeV for $\mathrm{BR}(Q \to Wq) = 100\%$. There are no exclusions if this branching ratio is less than 40%. On the other hand, there are a variety of searches by both the ATLAS and CMS collaborations for bottom quark partners decaying via $B \to hb$, $B \to Zb$, $B \to Wt$ [200–204]. The strongest bounds were set by CMS, which found upper limits on the mass of the bottom partner ranging between 750 GeV and 900 GeV depending on its branching ratios. Giving the bottom partner a sufficiently large mass to evade these limits requires $v_D \gtrsim 1\,\mathrm{TeV}$ if the theory is weakly coupled. Since we are allowing for a dominantly triplet-breaking scenario with $\rho' \simeq 2$ in our analysis, it needs to be checked that this is compatible with a TeV scale doublet VEV. Indeed, setting $g_R = g$ and $v_D = 1\,\mathrm{TeV}$ results in $\rho' = 1.97$ and $v_T = 4.0\,\mathrm{TeV}$, while for $g_R = 1.4\,g$ we get $\rho' = 1.94$ and $v_T = 2.8\,\mathrm{TeV}$. It is therefore compatible to take $\rho \simeq 2$ while assuming the vector-like quarks are heavy and mix significantly with the doublet quarks.

4.3 Results and Discussion

In this section we explore the parameter space of the model in order to find regions that can explain 2 TeV anomalies and generate a large D-term contribution for the Higgs mass without being excluded by other searches. The main parameters controlling the W' signature in the diboson and dijet channels are g_R, c_d^2, $\tan\beta$. In this section we choose to set $\mathrm{BR}(W' \to \mathrm{SM}) = 100\%$ for simplicity of the analysis.

Experimental Input	**Theoretical Input**	
$m_{W'} = 1.9\,\text{GeV}$	$g_R > g\, s_w/c_w$	
$2.4\,\text{fb} < \sigma_{WZ} < 10.2\,\text{fb}$	$0 < c_d^2 < 1$	Eq. (4.16)
$46\,\text{fb} < \sigma_{jj} < 144\,\text{fb}$	$\tan\beta > 1$	
	$1 \leq \rho' \leq 2$	Eq. (4.7)
	$\delta = \infty, 2.5$	Eq. (4.14)
	$\text{BR}\,(Z' \to \text{SM}) = 100\%, 66\%$	
	$\text{BR}\,(W' \to \text{SM}) = 100\%$	

Table 4.2: Parameter ranges considered in this analysis.

Additional decays are possible into $\ell_R \nu_R$ (which might be responsible for the $eejj$ excess), into exotic quarks and into squarks and other SUSY states. We provide a brief discussion of these effects in Section 4.A and Figure 4.6. Important constraints on the parameter space will come from limits on the mass and couplings of the Z' due to LHC resonance searches and due to electroweak precision constraints. This makes the parameter ρ' relevant to the analysis. Additionally, the Higgs mass depends on the parameter δ which we will take as either 2.5 or ∞. We use the fits to the W' diboson and dijet signatures provided in [182]. The W' and Z' cross sections and branching ratios are calculated using the couplings listed in Appendix 4.A and the NNPDF2.3 PDF set [205]. The parameter ranges considered in this analysis are summarised in Table 4.2.

In the case that the right handed leptons are embedded in $SU(2)_R$ multiplets, the Z' will be strongly constrained by dilepton resonance searches for sufficiently large g_R. ATLAS and CMS have set limits on sequential Z' resonances (which are assumed to have the same couplings to fermions as the SM Z boson) at $\sim 2.8\,\text{TeV}$ [206, 207], and the limit in our model will generically be comparable. Dijet resonance searches are far less constraining for this scenario. There are also

important limits on Z' masses and couplings coming from electroweak precision tests, especially those constraining the oblique parameters, four-Fermi operators involving at least two leptons, and from measurements of the $Zb\bar{b}$ couplings. In order to assess these constraints we use the formalism and results of [208]. That analysis neglects the constraints coming from four-Fermi operators involving right handed quarks as these are generically weaker. However, in the limit of large g_R these might provide important constraints, and so we separately consider the limits on these effective operators derived in [209]. We find that these indirect constraints are always weaker than the ones coming from dilepton resonance searches for the standard lepton embedding.

We also consider the leptophobic case in which the right handed leptons are not charged under $SU(2)_R$. In this scenario the direct constraints coming from dijet and dilepton resonance searches turn out to be comparable and weak. The limits coming from corrections to the oblique parameters then turn out to be the most constraining, which are a consequence of the tree level Z–Z' mixing given by

$$\sin\theta_{ZZ'} \simeq \frac{g_R}{g}\frac{m_Z^2}{m_{Z'}^2} c_w c_{w'}. \tag{4.21}$$

The constraints from four-Fermi operators are weak due to the small coupling of the Z' to leptons, and the corrections to $Z \to b\bar{b}$ are small due to the fact that b_R is mostly an $SU(2)_R$ singlet.

In Figure 4.1 we set $\delta = 2.5$ and $\mathrm{BR}(Z' \to \mathrm{SM}) = 100\%$ and take the RH leptons to be charged under $SU(2)_R$. In the left plot, we scan the c_d^2, $\tan\beta$ plane. In the dark grey region in the top right of the plot, it is not possible to explain the diboson excess without being excluded by dijet resonance searches. This can be

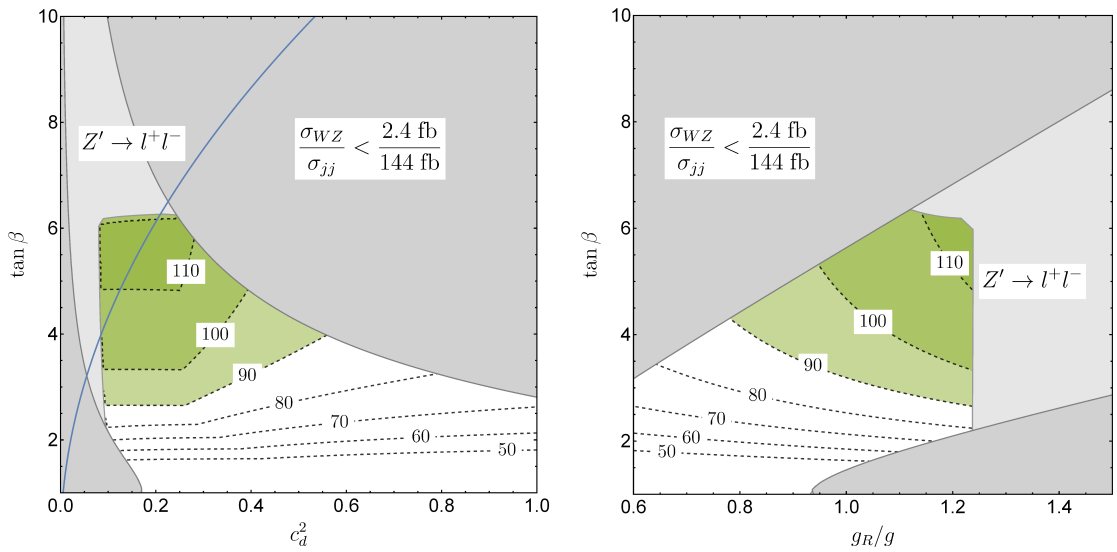

Figure 4.1: Maximum tree level Higgs mass from D-terms consistent with W' data and limits on $Z' \to \ell^+\ell^-$, for $\delta = 2.5$ and $\mathrm{BR}(Z' \to \mathrm{SM}) = 100\%$ with the standard lepton embedding. In each plot we have optimised over all remaining parameters, as explained in the text. Dark grey: Incompatible with the 2 TeV anomalies. Light grey: Excluded by $Z' \to \ell\ell$. Contours: Maximum tree level Higgs mass from D-terms compatible with the above requirements, in GeV. In the region shaded green, it is possible to exceed the MSSM tree level Higgs mass bound of 91 GeV. The blue line is $t_\beta^2/c_d^2 = m_c^2/m_s^2$, near which the charm/strange mass ratio might be explained by the exotic quark mixing.

seen by noting the ratio between these two widths depends only on $\tan\beta$ and c_d^2

$$\frac{\sigma_{WZ}}{\sigma_{jj}} = \frac{\sin^2(2\beta)}{24\, c_d^2}. \tag{4.22}$$

Similarly, the dark grey region in the bottom left of the plot cannot explain the dijet excess without being excluded by the upper limits on the diboson cross section. The remaining region of parameter space is a funnel which can simultaneously explain both excesses. At a generic point in this region, there are a range of values for g_R compatible with the excesses. For small c_d^2, g_R is required to be large to generate a sufficiently large W' cross section due to the relationship $\sigma(W') \propto g_R^2 c_d^2$. On the other hand, large g_R reduces the mass splitting between the Z' and the W' and increases the Z' production cross section, while the dominant production channel for this Z' at the LHC is $u_R\bar{u}_R \to Z'$ which is not suppressed by a small

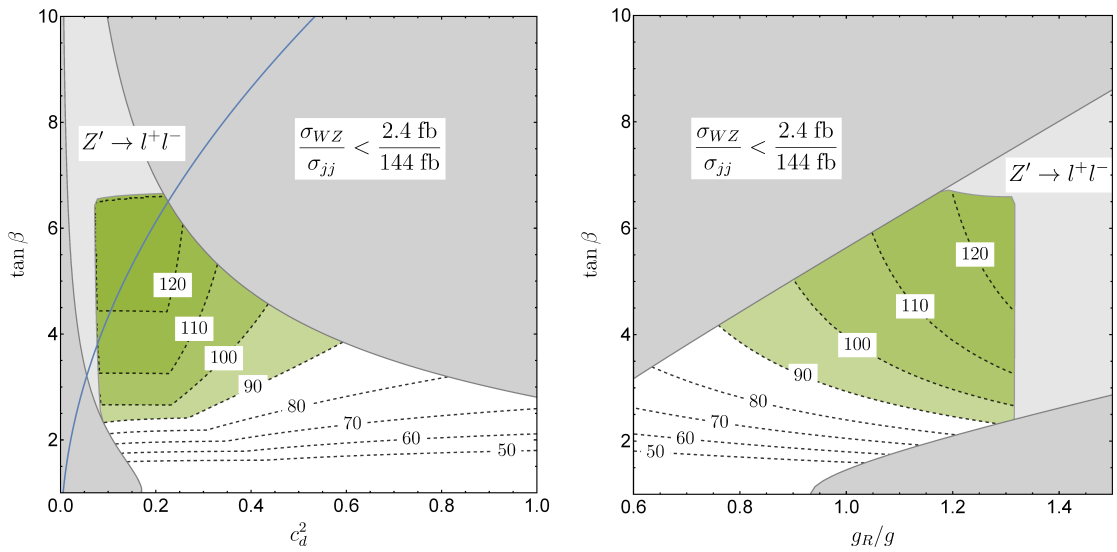

Figure 4.2: Maximum tree level Higgs mass from D-terms consistent with W' data and limits on $Z' \to \ell^+\ell^-$, for $\delta = \infty$ and BR($Z' \to$ SM) = 66% with the standard lepton embedding. In each plot we have optimised over all remaining parameters, as explained in the text. Dark grey: Incompatible with the 2 TeV anomalies. Light grey: Excluded by $Z' \to \ell\ell$. Contours: Maximum tree level Higgs mass from D-terms compatible with the above requirements, in GeV. In the region shaded green, it is possible to exceed the MSSM tree level Higgs mass bound of 91 GeV. The blue line is $t_\beta^2/c_d^2 = m_c^2/m_s^2$, near which the charm/strange mass ratio might be explained by the exotic quark mixing.

mixing angle. The Z' has a significant dilepton branching ratio of 8–18% and so this region of parameter space is constrained by the dilepton resonance searches. In the light grey region in the top left of the plot, it is not possible to evade the Z' limits while explaining the W' excesses.

In the surviving region of parameter space we calculate the maximum value of g_R compatible with the constraints and use this to calculate the maximum D-term contribution to the Higgs mass, which is shown in GeV by the labelled contours. The region of parameter space compatible with $m_{h,\text{tree}}$ larger than the MSSM tree level bound is highlighted in green. The blue contour highlights the part of parameter space in which the charm/strange mass ratio might be explained by the mixing with the exotic quarks. In the right plot we perform a similar scan in the

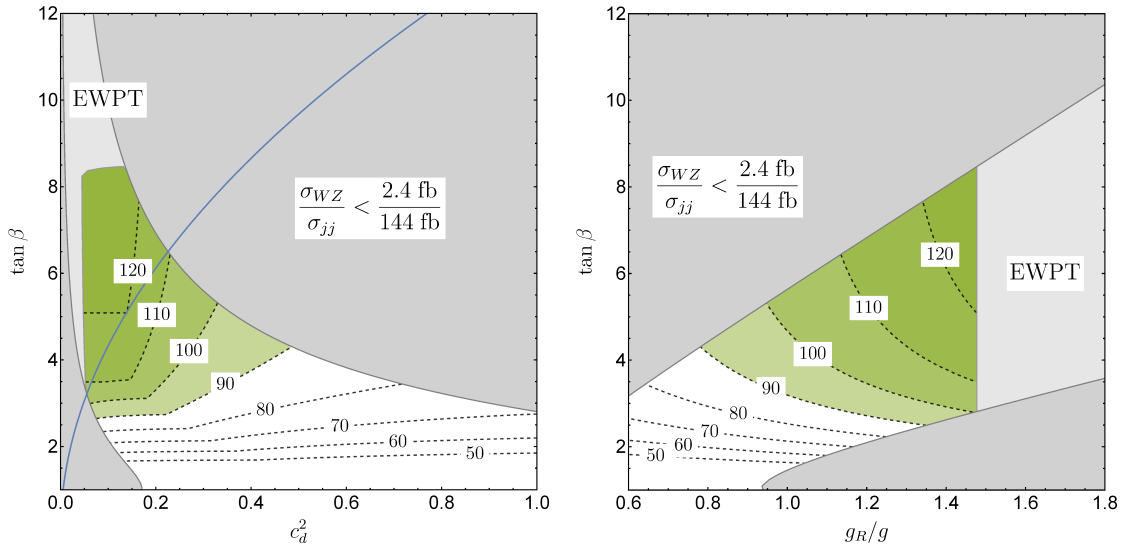

Figure 4.3: Maximum tree level Higgs mass from D-terms in the leptophobic model consistent with W' data and EWPT, for $\delta = 2.5$. In each plot we have optimised over all remaining parameters, as explained in the text. Dark grey: Incompatible with the 2 TeV anomalies. Light grey: Excluded by EWPT. Contours: Maximum tree level Higgs mass from D-terms compatible with the above requirements, in GeV. In the region shaded green, it is possible to exceed the MSSM tree level Higgs mass bound of 91 GeV. The blue line is $t_\beta^2/c_d^2 = m_c^2/m_s^2$, near which the charm/strange mass ratio might be explained by the exotic quark mixing.

g_R, $\tan\beta$ plane, this time optimising over c_d^2. In both plots we have also optimised over ρ' and over the parton luminosities within the 1σ uncertainties calculated from the NNPDF ensemble, assuming that the uncertainties on W' and Z' production are completely correlated. In practise, this means setting $\rho' = 2$ and using the lower prediction for the parton luminosities, except for a narrow band at large $\tan\beta$ where higher estimates are preferred. In Figure 4.2 we perform a similar scan for $\delta = \infty$ and $\text{BR}(Z' \to \text{SM}) = 66\%$. This would be the enhancement in the Z' width if, for example, every SM fermion had a light SUSY partner. In Figure 4.3 we consider a leptophobic scenario with $\delta = 2.5$ and $\text{BR}(Z' \to \text{SM}) = 100\%$. This time the paramer space is constrained by indirect constraints on the Z' in the regions labelled 'EWPT'. In all other respects the procedure is the same as for the previous plots.

We see that there is a region of parameter space with $0.1 \lesssim c_d^2 \lesssim 0.5$, $2.5 \lesssim \tan\beta \lesssim 6$ and $0.8 \lesssim g_R/g \lesssim 1.2$ with a D-term contribution to the Higgs mass at least as large as the MSSM tree level bound consistent with requirement of explaining the 2 TeV and evading Z' limits. Fine tuning considerations are model dependent, but a tree level Higgs mass of 110 GeV is compatible with $\delta = 2.5$ which need not be associated with significant fine tuning. Allowing the Z' to have a significant branching fraction into non SM states allows for a broader region of parameter space to explain the excess, as illustrated in Figure 4.2, though the main impact on the Higgs mass in this scan (which may exceed 120 GeV) comes from taking the decoupling limit $\delta \to \infty$ which would come with a significant fine tuning penalty. Due to the weaker Z' bounds, the leptophobic model allows for the greatest D-term Higgs quartic as larger values of g_R and $\tan\beta$ are permitted. A tree level Higgs mass of 120 GeV is possible in this model with $\delta = 2.5$. Note that the line $c_d^2 = 1$ which corresponds to the model without the exotic quarks cannot accomadate a tree level Higgs mass larger than 70 GeV while explaining the excess.

4.3.1 Implications for the Z' and stops

Due to the constraints on g_R, there is a close relation between the Z' mass and the possible enhancement to the Higgs mass. In the left of Figure 4.4 we plot the maximum possible tree level Higgs mass compatible with all constraints as a function of $m_{Z'}$ in each of the three scenarios described above. For large $m_{Z'}$ the size of g_R is limited by Eq. (4.7) and the requirement $\rho' \leq 2$, and this is the main constraint on the Higgs mass for $m_{Z'} \gtrsim 3$ TeV. Converseley, small $m_{Z'}$ corresponds to larger values of g_R. In this case, the main constraint on the Higgs

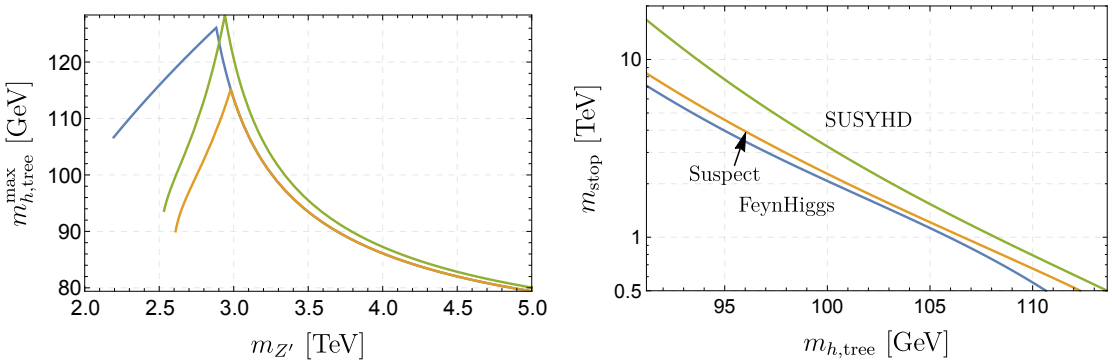

Figure 4.4: Left: Maximum D-term contribution to the tree level Higgs mass for a given value of $m_{Z'}$ in three scenarios. Orange: $\delta = 2.5$, $\text{BR}(Z' \to \text{SM}) = 100\%$. Green: $\delta = \infty$, $\text{BR}(Z' \to \text{SM}) = 66\%$. Blue: Leptophobic, $\delta = 2.5$. Each line stops at small $m_{Z'}$ at the limit from direct searches for dilepton resonances, or electroweak precision constraints in the case of the leptophobic model. Right: Stop mass required to raise the Higgs mass to 125 GeV without left-right stop mixing.

mass are the direct or indirect limits on the Z'. The kinks represent the transition between these scenarios. We see that the requirement $m_{h,\text{tree}} > 100\,\text{GeV}$ can be satisfied only for $2.6\,\text{TeV} \leq m_{Z'} \leq 3.3\,\text{TeV}$, assuming the right handed leptons have $SU(2)_R$ charge. The Higgs mass is maximised for $m_{Z'} \simeq 2.95\,\text{TeV}$. This result is especially interesting in light of the anomalous 2.9 TeV dilepton event observed by the CMS experiment with $65\,\text{pb}^{-1}$ of integrated luminosity [210]. In the case of a leptophobic Z', its mass might be as low as 2.2 TeV while still permitting a large D-term contribution to the Higgs mass.

We now turn to a brief discussion of the radiative corrections to the Higgs mass. In the MSSM, the Higgs mass might be raised to 125 GeV by a large stop mass, but this loop contribution grows more slowly than $\log(m_{\tilde{t}}^2/m_t^2)$, requiring $m_{\tilde{t}} \sim 10\,\text{TeV}$ in the absence of large mixing between the LH and RH stops. This might be reduced to $\sim 2 - 5\,\text{TeV}$ for sufficiently large mixing in the stop sector. A comparison of results using diagrammatic and effective field theory techniques can be found in [211], which compares the codes SUSYHD [211], FeynHiggs [212],

and SuSpect [213]. In our model the requirements on the stop sector will be significantly relaxed due to the increased tree level contribution to the Higgs mass. There will also be additional radiative corrections due to the new (s)quark states in the third generation, but these will not be log enhanced if there is not a large splitting between the exotic quark and squark masses and so are expected to be subdominant compared to the stop contributions. In lieu of a complete calculation of the radiative corrections in this model, we use the following approximation to estimate the relaxed requirements on the stop sector. We consider the MSSM contribution in the limit of no left-right mixing and large $\tan\beta$ and define the function

$$\Delta(m_{\tilde{t}}^2) = m_{h(\mathrm{MSSM})}^2(m_{\tilde{t}}^2) - m_Z^2. \tag{4.23}$$

This function can be taken from the SUSYHD, FeynHiggs, and SuSpect calculations. We then estimate the Higgs mass with the new tree level contributions as:

$$m_h^2(m_{\tilde{t}}^2) = m_{h,\mathrm{tree}}^2 + \Delta(m_{\tilde{t}}^2). \tag{4.24}$$

This approximation neglects additional wavefunction renormalization effects due to the enhanced Higgs quartic, and threshold effects from the exotic states. In Figure 4.4 right we plot the stop mass required to achieve a Higgs mass of 125 GeV using this approximation. We see that stops may be lighter than 1 TeV in this model, alleviating their contribution to the little hierarchy problem of the MSSM.

In the case that the stop mass has been partially decoupled from the question of the Higgs mass, the strongest constraint on fine tuning comes from the present experimental limits on the gluino mass. The main effect of a large gluino mass is to provide large positive radiative corrections to the stop mass at one loop, disfavouring a stop mass much lighter than 1 TeV. The residual tuning is typically worse than $\sim$ (few %) [214]. The non-decoupling D-term contributions to the

Higgs mass are therefore relevant to, but not a panacea for the little hierarchy problem. Nonetheless, the channel $Z' \to \tilde{t}\tilde{t}$ is well motivated and worth further study. For $c_d^2 = 0.2$ and $g_R = g$, the BR for the Z' into a pair of pure $\tilde{t}_R$ states much lighter than $m_{Z'}/2$ is 7%. For $m_{Z'} = 3\,\text{TeV}$, this would correspond to 2 events at $\sqrt{s} = 8\,\text{TeV}$ with $20\,\text{fb}^{-1}$.

4.4 Flavour constraints

There have been numerous studies of flavour constraints on generic LRS models [215–219] and on models with vector-like down-type quarks [220, 221]. However, certain features of our model prevent direct application of the existing constraints, and hence necessitates a separate analysis. First, most constraints on LRS do not consider the effects of large mixings with vector-like quarks in the RH sector, which reduces the coupling of the physical light quarks to the RH gauge bosons. Second, the strongest constraints on most vector-like quark extensions to the SM typically comes from tree-level Z FCNCs involving LH quarks due to violation of the Glashow-Weinberg-Paschos condition [222, 223]. However, this constraint is much weaker in our model since terms of the form $H_d Q_L D'^c$ are now forbidden by the RH gauge symmetry, as a result of which there is an additional Yukawa suppression in the mixing between d'_L and D'. Besides the above constraints, we also have contributions to FCNCs that involve the superpartners, in particular new box diagrams involving gluinos and the exotic squarks. On the other hand, these depend on parameters such as soft squark masses which are not closely related to the phenomenology discussed in the previous sections. There is also the possibility of cancellations between gauge boson and supersymmetric diagrams as suggested in [224].

Since the complete analysis of all flavour constraints on the model is a rather formidable task, we have restricted our attention to mainly tree-level and a small subset of one-loop $|\Delta F| = 2$ FCNC processes that are directly related to the new quarks. We postpone a more complete analysis, including CP violation and other FCNC processes such as $b \to s\gamma$ to future work. We find that the strongest constraints come from tree-level Z' FCNCs involving the RH quarks, which we discuss in this section. Details of the conventions used and constraints from other FCNC diagrams are presented in the appendix.

4.4.1 Tree-level Z' FCNCs

The interaction basis $d_R'^c$ and D'^c can be written in terms of the mass basis as

$$\begin{aligned} d_R'^c &= (c_R U_R^d)^* d_R^c + \text{ terms involving } D^c, \\ D'^c &= (s_R U_R^d)^* d_R^c + \text{ terms involving } D^c. \end{aligned} \tag{4.25}$$

Here, c_R and s_R are matrices that describe the mixing between the $d_R'^c$ and D'^c as discussed in Section 4.2.2, except that we no longer assume c_R to be a diagonal matrix with elements c_d and c_b. U_R^d is the RH unitary transformation that diagonalises the light down-type mass matrix obtained from the pre-diagonalisation with c_R and s_R. For convenience, we also define the RH equivalent of the CKM matrix

$$V_{\text{CKM}}^R \equiv c_R U_d^R. \tag{4.26}$$

Further details of the definitions above can be found in the appendix.

Since $d_R'^c$ and D'^c couple to Z' differently, the Z'-coupling to the mass basis d_R

is non-universal and given by the matrix $\mathcal{C}^{\text{tree}}_{Z-d_L}$, defined as

$$\begin{aligned} \mathcal{L} &\supset Z'^{\mu}\overline{d^c_R}\mathcal{C}^{\text{tree}}_{Z'-d^c_R}\bar{\sigma}_\mu d^c_R, \\ \mathcal{C}^{\text{tree}}_{Z'-d^c_R} &= \frac{g_R}{c_{w'}}\left[\frac{1}{2}V^{R\dagger}_{\text{CKM}}V^{R}_{\text{CKM}} - \frac{1}{3}s^2_{w'}\right]^T. \end{aligned} \tag{4.27}$$

We now consider $|\Delta F| = 2$ processes, in particular $K - \bar{K}$ mixing. While there is a large mass suppression from $m_{Z'}$ in the propagator, if we simply regard c_R as a completely generic matrix of order $\mathcal{O}(c_d)$, the contribution to Δm_K ends up being much larger than the experimental constraints. Instead, we require that

$$\left(\frac{g_R/g}{1.2}\right)\left(\frac{0.9}{c_{w'}}\right)\left(\frac{3\,\text{TeV}}{m_{Z'}}\right)^2\left(\frac{(V^{R\dagger}_{\text{CKM}}V^{R}_{\text{CKM}})_{12}}{0.2}\right)^2 \lesssim 0.001 \tag{4.28}$$

in order to satisfy bounds on Δm_K [52]. (Note that g_R/g and $c_{w'}$ should not be regarded as independent parameters.) In other words, the 12 elements of $V^{R\dagger}_{\text{CKM}}V^{R}_{\text{CKM}}$ should be much smaller than typical values of $\mathcal{O}(c_d^2)$.

To achieve a small $(V^{R\dagger}_{\text{CKM}}V^{R}_{\text{CKM}})_{12}$, one possibility is to consider an analogue of the Glashow-Iliopoulos-Maiani (GIM) mechanism. We recall that $V^{R\dagger}_{\text{CKM}}V^{R}_{\text{CKM}} = (U^d_R)^\dagger c^\dagger_R c_R U^d_R$, and that U^d_R is unitary. Therefore, should $c^\dagger_R c_R$ be proportional to the identity matrix, the same will be true for $V^{R\dagger}_{\text{CKM}}V^{R}_{\text{CKM}}$ so off-diagonal elements become zero. One could impose an approximate $U(3)$ flavour symmetry such that all the couplings are universal, in which case c_R is itself proportional to the identity. However, this is inconsistent with the down-type mass spectrum which requires that the third diagonal element c_b be somewhat smaller than the first two elements c_d. Instead, we impose an approximate $U(2)$ symmetry for the first two generations, and further require that the mixings with the third generation be small. This ensures that c_R remain approximately diagonal, while also suppressing the 31 and 32 elements of U^d_R. The suppression is required since the GIM cancellation is now incomplete.

To quantify the constraints on z and M, we work in a $D' - D'^c$ basis such that M is diagonal. We then parameterise z as $Uz^{\text{diag}}V$, where U and V are arbitrary unitary matrices. For simplicity, we assume the 12 rotation angles in both matrices be of the same order $\mathcal{O}(\theta_{12})$, and the 13 and 23 rotation angles be of order $\mathcal{O}(\theta_3)$. We also define a parameter δ that quantifies the breaking of the universality in the first two generations, i.e. we expect that M_{22}/M_{11} and $(z^{\text{diag}})_{22}/(z^{\text{diag}})_{11}$ are both $1 + \mathcal{O}(\delta)$. In view of the requirements on c_R, we expect a strong constraint on θ_3, and a possibly weaker constraint on θ_{12} that depends on δ.

Figure 4.5 shows regions of θ_{12} and θ_3 for different δ allowed by the tree-level Z' FCNC constraint. For each choice of the three parameters θ_{12}, θ_{13} and δ, 1000 sets of mixing angles, M and z^{diag} are then randomly generated with characteristic sizes specified by the parameters. A parameter choice is "allowed" if at least half of the corresponding 1000 random sets are found to satisfy the Z' constraints. We see from the plot that θ_3 should be at most $\mathcal{O}(0.05\,\text{rad})$ which is comparable to $(V^L_{\text{CKM}})_{13}$ and $(V^L_{\text{CKM}})_{23}$, suggesting an alignment similar to what is already in the SM. Meanwhile, the constraints on θ_{12} are as expected much weaker should the extent of universality breaking be small. For example, a 5% breaking will allow for a alignment angle of more than 1 rad.

4.5 Conclusions

We have explored the possibility that an $SU(2)_R$ gauge extention of the MSSM which is compatible with an explanation of the recent diboson, $eejj$ and dijet resonance excesses in terms of a 1.9 TeV W_R might also give rise to a significant non-decoupling D-term enhancement to the Higgs mass. The inferred diboson

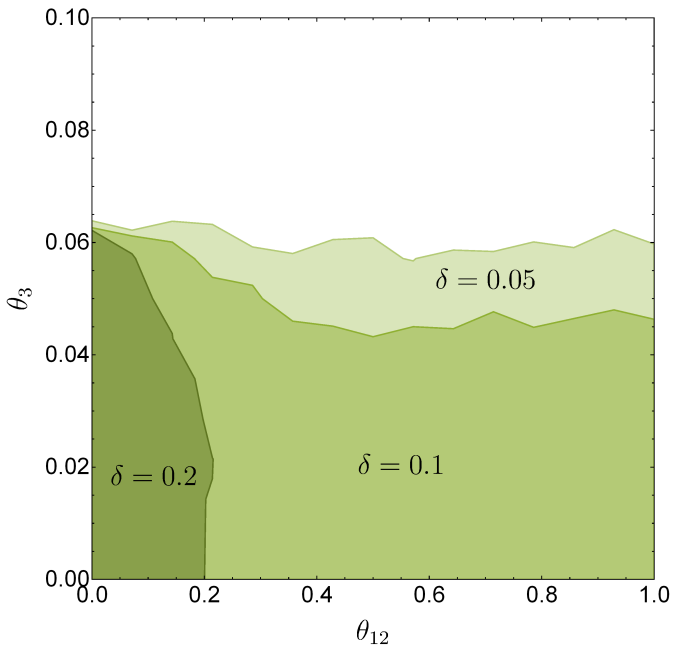

Figure 4.5: Regions in parameter space allowed by the tree-level Z' FCNC constraints. θ_{12} gives the characteristic size of 12 alignment angles, while θ_3 does so for the 13 and 23 angles. δ quantifies the breaking of the universality in the first two generations.

cross section is relatively large compared to the dijet cross section, which requires $\tan\beta \simeq 1$ in minimal models. Furthermore, the total W' cross section implies $g_R < 0.8\, g$ in minimal models. Both of these features are not compatible with large D-terms for the Higgs which requires large $\tan\beta$ and large g_R, and the small value for $\tan\beta$ is also problematic for the top/bottom mass ratio.

We have therefore been lead to an extended model which also includes a charge $-1/3$ vector-like quark for each generation which mixes significantly with the $SU(2)_R$ doublets after that gauge symmetry is broken. We have assumed that the mixing angle is approximately universal for the first two generations, but may be different for the third. For the third generation, this means that m_b/m_t is suppressed by both t_β^{-1} and the cosine of the mixing angle, c_b. More importantly, the mixing angle suppresses the W_R couplings to the SM quarks, enhancing the

diboson to dijet signal cross section ratio by a factor c_d^{-2}, and suppresses the W_R production cross section by a factor c_d^2. This allows the excesses to be fit with larger g_R and $\tan\beta$, compatible with the Higgs mass requirement. An additional key difference compared with previous discussions is the suppression of the branching fraction of the W' into tb which is a consequence of the mechanism we have chosen for achieving the mass ratio m_t/m_b. Without this suppression, the absence of a signature in this channel so far is a leading constraint on g_R.

The additional quark fields raise many questions related to flavour physics, and we have addressed some of these questions in this chapter. We have argued that the strongest constraints on the flavour structure of this new sector will come from FCNCs induced at tree level by the flavour-violating couplings of the Z'. Nonetheless, an approximate universality among the first two generations combined with an alignment of the mixing angles with the third generation comparable in size with that already present in the SM CKM matrix allows us to evade those constraints. Additional contributions to FCNC observables in the quark and lepton sectors are expected to come from the extended Higgs sector and from squark and gaugino loops. Furthermore, we have not yet provided a complete account of the generation of the full flavour structure of the quark sector in the SM. On the other hand, we have found that the region of parameter space which maximises the Higgs mass is also compatible with the naive expectation for the charm/strange mass ratio if this is purely a consequence of $\tan\beta$ and the mixing with the exotic quarks. We leave a complete analysis of the flavour structure of this model to future work. While our analysis places no direct constraints on the masses of the exotic quarks, it is possible that they are sufficiently light to be directly pair-produced and observed at run 2 of the LHC. A natural expectation is that they will decay into $D \to jZ$ with a significant branching fraction via the Z–Z' mixing, which

would provide an opportunity to directly measure their mass from the invariant mass of the j and Z.

The essential result of our analysis is that we have identified a region of parameter space in a model with right handed leptons charged under $SU(2)_R$ with $m_{h,\text{tree}} > 100\,\text{GeV}$ for $0.1 \lesssim c_d^2 \lesssim 0.4$, $3 \lesssim \tan\beta \lesssim 6$, and $1 \lesssim g_R/g \lesssim 1.2$ without imposing an irreducible fine tuning. This region is broadened by relaxing the assumption $\text{BR}\,(Z' \to \text{SM}) = 100\%$ and by taking the extreme decoupling limit for the D-terms. The leptophobic scenario in which the right handed leptons are not embedded in $SU(2)_R$ multiplets is also more weakly constrained and allows for a larger contribution to the Higgs mass.

A key finding of this analysis is that the possible D-term enhancement of the Higgs mass is closely related to the Z' mass. A light Z' is favoured for raising the Higgs mass, as this corresponds to larger g_R. On the other hand the Z' is quite constrained by dilepton resonance searches from LHC run 1 or electroweak precision measurements for $m_{Z'} \lesssim 3\,\text{TeV}$. We find that with the standard lepton embedding, the range $2.6\,\text{TeV} < m_{Z'} < 3.3\,\text{TeV}$ is compatible with $m_{h,\text{tree}} > 100\,\text{GeV}$, while the Higgs mass bound is optimised for $m_{Z'} \simeq 2.95\,\text{TeV}$. This scenario should result in a clear dilepton resonance at run 2 of the LHC. On the other hand, the leptophobic scenario is compatible with large contributions to the Higgs mass and is not excluded for $m_{Z'} > 2.2\,\text{TeV}$. This Z' is more challenging to discover at the LHC. Looking forward we should be paying close attention to any hints of a 2 TeV resonance in the new data from the LHC, but we should bear in mind that the broader and potentially quite significant implications of such a resonance might depend sensitively on the results of searches for related particles like a Z', vector-like quarks and leptons, massive neutrinos, etc.

4.A W' and Z' couplings and partial widths

The partial widths for the W' are taken as

$$\begin{aligned}
\Gamma(W' \to jj) &= \frac{g_R^2 c_d^2}{8\pi} m_{W'}, \\
\Gamma(W' \to tb) &= \frac{g_R^2 c_b^2}{16\pi} m_{W'} \left(1 + \mathcal{O}\left(\frac{m_t^2}{m_{W'}^2}\right)\right), \\
\Gamma(W' \to WZ) &= \frac{g_R^2}{192\pi} m_{W'} \sin^2 2\beta \left(1 + \mathcal{O}\left(\frac{m_W^2}{m_{W'}^2}\right)\right), \\
\Gamma(W' \to Wh) &= \frac{g_R^2}{192\pi} m_{W'} \cos^2(\alpha+\beta) \left(1 + \mathcal{O}\left(\frac{m_W^2}{m_{W'}^2}\right)\right).
\end{aligned} \tag{4.29}$$

We take the decoupling or alignment limit for the Higgs, with $\alpha = \beta + \pi/2$. Calculating the W' production cross section requires the the coupling $\mathcal{L} \supset g_{W' u_R d_R} W^- u_R d_R^c + \text{h.c.}$ which is given by

$$g_{W' u_R d_R} = g_R c_d. \tag{4.30}$$

The Z' couplings to SM fermions, defined by $\mathcal{L} \supset g_{Z' f f'} Z' f f'$, are given in the flavour conserving limit by

$$g_{Z' f \bar{f}} = \frac{g_R}{c_{w'}} \left(c_d^2 T_R^3 - s_{w'}^2 Y\right) \tag{4.31}$$

where c_d is the cosine of the mixing angle of the SM quark into an $SU(2)_R$ state. In particular, the couplings are

$$\begin{aligned}
g_{Z' u_R^c u_R^c} &= \frac{g_R}{c_{w'}} \left(-\frac{1}{2} + \frac{2}{3} s_{w'}^2\right) & g_{Z' u_L u_L} &= -\frac{1}{3} \frac{s_{w'}^2}{c_{w'}} g_R \\
g_{Z' d_R^c d_R^c} &= \frac{g_R}{c_{w'}} \left(\frac{c_d^2}{2} - \frac{1}{3} s_{w'}^2\right) & g_{Z' d_L d_L} &= -\frac{1}{3} \frac{s_{w'}^2}{c_{w'}} g_R \\
g_{Z' \ell_R^c \ell_R^c} &= \frac{g_R}{c_{w'}} \left(\frac{1}{2} - s_{w'}^2\right) & g_{Z' \ell_L \ell_L} &= -\frac{1}{2} \frac{s_{w'}^2}{c_{w'}} g_R \\
g_{Z' \nu_R^c \nu_R^c} &= -\frac{1}{2} \frac{g_R}{c_{w'}} & g_{Z' \nu_L \nu_L} &= -\frac{1}{2} \frac{s_{w'}^2}{c_{w'}} g_R
\end{aligned} \tag{4.32}$$

The partial width to fermions is then given by (up to corrections of order $m_f^2/m_{Z'}^2$)

$$\Gamma(Z' \to f\bar{f}) = \frac{N_c}{24\pi} m_{Z'} g_{Z' f \bar{f}}^2. \tag{4.33}$$

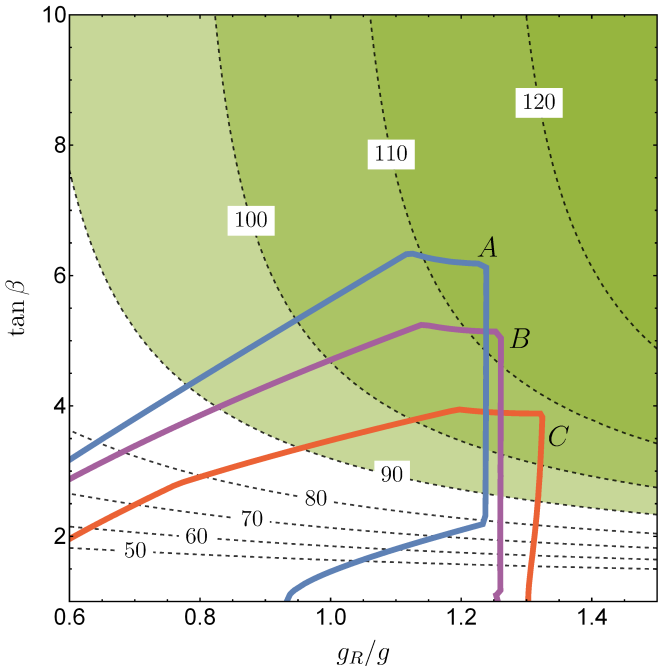

Figure 4.6: Allowed parameter space when considering additional BSM decays for W' and Z'. In each case, the region above and to the right of the coloured line is excluded. Case A: Only decays to SM states. Case B: Include decays of the W' and Z' involving a single light generation of RH neutrino with $m_{\nu_R} \ll m'_W$. Case C: Inlcude decays of the W' and Z' to the first two generations of exotic quark, with $m_D \ll m_{W'}$. In all other respects the plot is generated as described in the caption to Figure 4.1 and the related text in Section 4.3.

The partial widths into SM bosons, again up to corrections suppressed by $m^2_{Z'}$, are given by

$$\begin{aligned} \Gamma(Z' \to WW) &= \frac{g_R^2}{192\pi} m_{Z'} c_{w'} \sin^2 2\beta \\ \Gamma(Z' \to Zh) &= \frac{g_R^2}{192\pi} m_{Z'} c_{w'} \cos^2(\alpha+\beta)\,. \end{aligned} \tag{4.34}$$

The width into WW' is suppressed by $m_W^2/m_W'^2$ compared to those above.

In Figure 4.6 we explore the effect of allowing the W' and Z' to decay into right handed neutrinos or first and second generation vector-like quark. In each case we assume that the new particles are very light, and neglect any kinematic suppression from their masses. There are two main effects at work. Firstly, the additional channels dilute the W' diboson signature, requiring a larger value of

$\sin^2 2\beta$ and a smaller value of $\tan\beta$. Secondly, these channels also dilute the constraining $Z' \to \ell\ell$ signature, allowing for larger values of g_R. The net effect is a small reduction in the allowed size of the tree level Higgs mass from D-terms.

4.B Non-Decoupling D-terms and Fine Tuning

We consider a simple model to illustrate the main features in the relationship between the decoupling parameter δ and the parameters of the $SU(2)_R$ breaking potential. Suppose that $v_D^2 \ll v_T^2$ so that we have a triplet breaking scenario, and the triplet has the superpotential

$$W = \lambda S\left(\Delta\overline{\Delta} - f^2\right), \tag{4.35}$$

where we have introduced a singlet S. We also introduce soft masses

$$V_{\text{soft}} = m_S^2 S^\dagger S + m_\Delta^2 \Delta^\dagger\Delta + m_{\bar{\Delta}}^2 \overline{\Delta}^\dagger\overline{\Delta} + B_\Delta\left(\Delta\overline{\Delta} + \text{h.c.}\right). \tag{4.36}$$

For $m_\Delta^2 = m_{\bar{\Delta}}^2$ and $m_S^2 > 0$, there is a potential minimum with $v_\Delta = v_{\bar{\Delta}}$, $\langle S\rangle = 0$, which satisfies the minimisation condition

$$\frac{1}{2}\lambda^2 v_\Delta^2 = \lambda f^2 - m_\Delta^2 - B_\Delta. \tag{4.37}$$

Integrating out the heavy field now results in

$$V_{D,\text{eff}} \supset \frac{1}{8}\left(g^2 + \xi g_R^2\right)\left(\left|H_u^0\right|^2 - \left|H_d^0\right|^2\right)^2, \qquad \xi = 1 - \frac{g_R^2}{g_R^2 + g_X^2 + \frac{m_\Delta^2}{v_\Delta^2}}. \tag{4.38}$$

This interpolates between the decoupling and non-decoupling limits, $g'^2 \le \xi g_R^2 \le g_R^2$. We see that the non-decoupling limit, $m_\Delta^2/v_\Delta^2 \to \infty$, can only be achieved at the expense of a fine-tuned cancellation between terms on the RHS of Eq. (4.37). A crude fine tuning measure can be defined by $\Delta_{\text{FT}} \equiv 2m_\Delta^2/(\lambda^2 v_\Delta^2)$. For $\lambda^2 \sim 1$,

$m_\Delta^2/v_\Delta^2 \simeq 2.5$ is compatible with $\Delta_{\rm FT} \sim 5$. There will also be a fine tuning associated with the sensitivity of the EWSB Higgs soft masses to m_Δ, but this arises only at two loops [225]

$$\frac{dm_\Phi^2}{d\log\mu} \sim \frac{g_R^4}{16\pi^4} m_\Delta^2 \quad \left(\overline{DR}\right). \tag{4.39}$$

This contribution to the fine tuning of the EWSB Higgs potential is usually subdominant compared to that associated with the RH gauge symmetry scale, and so we will neglect it here.

4.C Flavour constraints: Additional details

In this appendix, we provide more details of the convention used in our flavour analysis, and also present the constraints from other FCNC contributions that we have analysed. Note that these constraints are significantly weaker than that from tree-level Z' presented in the main text.

4.C.1 Down-type quark masses and mixing

Here, we introduce the conventions we have adopted for down-type quark masses and mixing. The full 6×6 down-type quark mass matrix is given by $\mathcal{M}$, where

$$\begin{aligned} \mathcal{L} &\supset -\begin{pmatrix} d_R'^c & D'^c \end{pmatrix} \mathcal{M} \begin{pmatrix} d_L' \\ D' \end{pmatrix} + \text{h.c.}, \\ \mathcal{M} &= \begin{pmatrix} \frac{v_d}{\sqrt{2}} y' & \frac{v_D}{\sqrt{2}} z \\ 0 & M \end{pmatrix}. \end{aligned} \tag{4.40}$$

We have introduced a new Yukawa matrix y' which in general differs from y. This is motivated by the need to modify the tree-level mass matrix as suggested in Section 4.2.2 to obtain the correct light quark mass relations. The origin of such a modification will be discussed later.

We first perform block-diagonalisation of the mass matrix before EWSB, i.e. with $v_d = 0$. No transformation of the LH quarks is required, while the RH quarks transform as

$$\begin{pmatrix} d_R'^c \\ D'^c \end{pmatrix} \equiv \begin{pmatrix} c_R & -\tilde{s}_R \\ s_R & \tilde{c}_R \end{pmatrix}^* \begin{pmatrix} d_R''^c \\ D''^c \end{pmatrix}, \tag{4.41}$$

where $d_R''^c$ and D''^c are intermediate basis. In this basis, the full mass matrix becomes

$$\begin{aligned} \mathcal{M}' &= \begin{pmatrix} 0 & 0 \\ 0 & M_D \end{pmatrix}, \\ M_D &\equiv -\frac{v_D}{\sqrt{2}} \tilde{s}_R^\dagger z + \tilde{c}_R^\dagger M. \end{aligned} \tag{4.42}$$

We reintroduce the EWSB masses, so $\mathcal{M}'$ is no longer block-diagonal

$$\mathcal{M}' = \begin{pmatrix} \frac{v_d}{\sqrt{2}} c_R^\dagger y' & 0 \\ -\frac{v_d}{\sqrt{2}} \tilde{s}_R^\dagger y' & M_D \end{pmatrix}. \tag{4.43}$$

Due to the hierarchy between the EWSB masses and M_D, we can use the see-saw formula for block-diagonalisation. We define $\epsilon \equiv |v_d|/m_D$, where m_D is the characteristic eigenvalue size of M_D. The LH quarks now transform as

$$\begin{aligned} \begin{pmatrix} d_L' \\ D' \end{pmatrix} &\equiv \begin{pmatrix} c_L & -s_L^\dagger \\ s_L & \tilde{c}_L \end{pmatrix} \begin{pmatrix} d_L'' \\ D'' \end{pmatrix} \\ &\approx \begin{pmatrix} 1 - \frac{|v_d|^2}{4} y'^\dagger \tilde{s}_R (M_D M_D^\dagger)^{-1} \tilde{s}_R^\dagger y' & -\frac{v_d^*}{\sqrt{2}} y'^\dagger \tilde{s}_R (M_D^\dagger)^{-1} \\ \frac{v_d}{\sqrt{2}} M_D^{-1} \tilde{s}_R^\dagger y' & 1 - \frac{|v_d|^2}{4} M_D^{-1} \tilde{s}_R^\dagger y' y'^\dagger \tilde{s}_R (M_D^\dagger)^{-1} \end{pmatrix} \begin{pmatrix} d_L'' \\ D'' \end{pmatrix}, \end{aligned} \tag{4.44}$$

with mixing angles of order $\mathcal{O}(\epsilon)$. The RH quarks also transform but with much smaller mixing angles of order $\mathcal{O}(\epsilon^2)$, which we ignore for now. The full 6×6 mass matrix becomes

$$\begin{aligned}\mathcal{M}'' &\approx \begin{pmatrix} M_d & 0 \\ 0 & M_D \end{pmatrix}, \\ M_d &\equiv \frac{v_d}{\sqrt{2}} c_R^\dagger y'.\end{aligned} \tag{4.45}$$

M_d can be thought of as the 3×3 mass matrix for d_L'' and $d_R''^c$, and M_D for D'' and D''^c. We now perform 3×3 unitary transformations U_L^d, $(U_R^d)^*$, U_L^D and $(U_R^D)^*$ on the intermediate basis to diagonalise these mass matrices. Combining all the transformations, we find the following relation between the interaction basis and the mass basis:

$$\begin{aligned}\begin{pmatrix} d_L' \\ D' \end{pmatrix} &= \begin{pmatrix} c_L & -s_L^\dagger \\ s_L & \tilde{c}_L \end{pmatrix} \begin{pmatrix} U_L^d d_L \\ U_L^D D \end{pmatrix}, \\ \begin{pmatrix} d_R'^c \\ D'^c \end{pmatrix} &= \begin{pmatrix} c_R & -\tilde{s}_R \\ s_R & \tilde{c}_R \end{pmatrix}^* \begin{pmatrix} (U_R^d)^* d_R^c \\ (U_R^D)^* D^c \end{pmatrix}.\end{aligned} \tag{4.46}$$

For example, $c_L U_L^d$ can be identified with the usual CKM matrix $V_{\rm CKM}^L$, and $c_R U_R^d$ with the RH analogue $V_{\rm CKM}^R$.

We now discuss the quark mass spectrum. Generic LRS models require that the quarks couple through two sets of Yukawa couplings to the bidoublet Higgs Φ and its conjugate $\tilde{\Phi}$, to generate the correct up- and down-type mass spectrum. In our model however, the coupling to $\tilde{\Phi}$ is forbidden by the holomorphy of the superpotential, so we only have a single set of couplings y. In the up-type mass basis, we expect that $y = \sqrt{2} M_u^{\rm diag}/v_u$, where $M_u^{\rm diag}$ is the diagonalised up-type mass matrix. Meanwhile, due to the mixing between d_R^c and D^c, the down-type mass matrix becomes $c_R^\dagger y v_d/\sqrt{2}$, so a suitable choice of the matrix c_R should in principle reproduce the correct down-type mass matrix. For example, one can

reproduce the correct strange and bottom masses m_s and m_b given c_R of the form

$$c_R \approx \begin{pmatrix} c_d & 0 & 0 \\ 0 & c_d & 0 \\ 0 & 0 & c_b \end{pmatrix}, \tag{4.47}$$

with the appropriate values of c_d and $\tan\beta$ taken from, say, Figure 4.4. We have chosen the first two diagonal elements of c_R to be the same to avoid flavour issues, which we elaborate later. However, the down quark mass m_d always ends up too small, even if we now increase the first diagonal element from c_d to 1. As mentioned in Section 4.2.2, one solution is to introduce nonrenormalisable operators that can contribute to the down-type mass matrix, analogous to the approach used in [198] for up-type quarks. This is equivalent to adding to y a generic matrix of size $\mathcal{O}\left(\sqrt{2}m'_u/v_u\right)$, where we have defined $m'_u \equiv m_c m_d/m_s$. The modified matrix, which we denote as y', remains approximately diagonal and hierarchical:

$$y' \approx \frac{\sqrt{2}}{v_u} \begin{pmatrix} \mathcal{O}(m'_u) & \mathcal{O}(m'_u) & \mathcal{O}(m'_u) \\ \mathcal{O}(m'_u) & m_c & \mathcal{O}(m'_u) \\ \mathcal{O}(m'_u) & \mathcal{O}(m'_u) & m_t \end{pmatrix}. \tag{4.48}$$

We leave the feasibility study of such a modification to future work. We note that it may also be possible to obtain the correct quark mass spectrum through loop effects involving the SUSY-breaking terms [197].

There are various attractive features associated with having y' of the form given in Eq. (4.48). First, as we shall see later, it helps to alleviate some of the FCNC constraints on the model. Second, since U_L^d is the transformation that diagonalises $y'^\dagger c_R c_R^\dagger y'$, and since c_L deviates from identity only by $\mathcal{O}(\epsilon^2)$, the form of y' also ensures that U_L^d and hence $V_{\rm CKM}^L$ is close to identity with only small mixing angles, in agreement with measurements. Finally, we note that the strongest constraint

on CKM unitarity comes from the experimental measurements [226]

$$\Delta_{\rm CKM} \equiv |(V^L_{\rm CKM})_{ud}|^2 + |(V^L_{\rm CKM})_{us}|^2 + |(V^L_{\rm CKM})_{ub}|^2 - 1 = (-1 \pm 6) \times 10^{-4}. \quad (4.49)$$

In the model, $\Delta_{\rm CKM}$ is suppressed both by a factor of $\mathcal{O}(\epsilon^2)$ as well as the small elements of y' and so satisfy the unitarity constraints.

4.C.2 Tree-level FCNCs

Higgses

In generic LRS models, due to the quarks coupling to both Φ and $\tilde{\Phi}$, one linear combination of the neutral Higgs can generate tree-level FCNCs, which in turn constrains its mass to more than 10 TeV. In supersymmetric model, the coupling to $\tilde{\Phi}$ is forbidden due to holomorphy; however, the issue of tree-level Higgs FCNC still lingers in the down-type sector due to the mixing with vector-like quarks. In particular, we consider the quark coupling $\mathcal{C}^{\rm tree}_{hd}$ to the neutral down-type Higgs

$$\begin{aligned}
\mathcal{L} &\supset -\frac{1}{\sqrt{2}} d'^c_R y' d'_L h^0_d + \text{h.c} \\
&= -d^c_R \mathcal{C}^{\rm tree}_{h_d} d_L h^0_d + (\text{terms involving } D \text{ and } D^c) + \text{h.c.}, \\
\mathcal{C}^{\rm tree}_{h_d} &\equiv V^{R\dagger}_{\rm CKM} y' V^L_{\rm CKM} \\
&= \frac{1}{v_d} M^{\rm diag}_d - \frac{v^*_d}{4} M^{\rm diag}_d U^{d\dagger}_L y'^{\dagger} \tilde{s}_R (M_D M^\dagger_D)^{-1} \tilde{s}^\dagger_R y' U^d_L,
\end{aligned} \quad (4.50)$$

where $M^{\rm diag}_d$ is the 3×3 diagonal matrix of down-type quark masses. Besides the overall mass suppression of order $\mathcal{O}(\epsilon^2)$, the off-diagonal terms of $\mathcal{C}^{\rm tree}_{h_d}$ are further suppressed by the fact that $M^{\rm diag}_d$, y' and U^d_L are diagonal and/or hierarchical. As a result, the $|\Delta F| = 2$ FCNC contributions from this coupling turns out to be negligible.

Another source of tree-level FCNC is the down-type quark coupling to the neutral component of the RH Higgs doublet H_R

$$\begin{aligned}
\mathcal{L} &\supset -\frac{1}{\sqrt{2}} d_R'^c z d_L' h_R^0 + \text{h.c} \\
&= -d_R^c \mathcal{C}_{h_R}^{\text{tree}} d_L h_R^0 + (\text{terms involving } D \text{ and } D^c) + \text{h.c.}, \\
\mathcal{C}_{h_R}^{\text{tree}} &\equiv V_{\text{CKM}}^{R\dagger} z s_L U_L^d \\
&= v_d V_{\text{CKM}}^{R\dagger} z (M_D)^{-1} \tilde{s}_R^\dagger y' U_L^d.
\end{aligned} \tag{4.51}$$

There is again a mass suppression of order $\mathcal{O}(\epsilon)$, while y' and U_L^d further suppresses off-diagonal couplings except for $d_R^c b_L$ and $s_R^c b_L$. Therefore, the strongest constraints comes from $B_d - \bar{B}_d$ mixing. Assuming experimental bounds on the operator $(d_R^c b_L)^2$ to be comparable to that of $(d_R^c b_L)(\overline{d_L b_R^c})$, we find that [52]

$$\left(\frac{3\,\text{TeV}}{m_{H_R}}\right)^2 \left(\frac{2\,\text{TeV}}{m_D}\right)^2 \left(\frac{4}{\tan\beta}\right)^2 \left(\frac{(V_{\text{CKM}}^{R\dagger} z (\tilde{M}_D)^{-1} \tilde{s}_R^\dagger)_{13}}{0.4}\right)^2 \lesssim 0.03. \tag{4.52}$$

where we have defined $\tilde{M}_D = M_D/m_D$ so that it is a generic $\mathcal{O}(1)$ matrix. The reference value of 0.4 for $(V_{\text{CKM}}^{R\dagger} z (\tilde{M}_D)^{-1} \tilde{s}_R^\dagger)_{13}$ assumes c_R to be a generic matrix of order $\mathcal{O}(c_d)$, and all other matrices of order $\mathcal{O}(1)$.

The constraint above seems to imply the need for some suppression of the relevant 13 element. However, one finds from numerical simulations with generic z and M that this element is almost always already smaller than what is required above. A brief explanation goes as follows: First, since U_R^d and U_L^d diagonalises M_D, we have $V_{\text{CKM}}^{R\dagger} y' U_L^d = M_d^{\text{diag}}$, which implies that the 12 and 13 elements of $V_{\text{CKM}}^{R\dagger}$ are necessarily small. Second, the $\mathcal{O}(c_d)$ hierarchy between $\frac{v_D}{\sqrt{2}} z$ and M results in the combination $z(\tilde{M}_D)^{-1}\tilde{s}_R^\dagger$ being roughly diagonal. Combining both effects, we find the relevant 13 element to be much smaller than the generic size.

Neutral gauge bosons

We now consider tree-level FCNCs from Z and Z'. We work in the basis before $Z-Z'$ mixing and regard the mixing as a perturbative mass insertion, in which case the couplings to Z and Z' are simply $(g/c_w)(T_L^3 - Q_{\rm EM}s_w^2)$ and $(gs_w/c_w)(T_R^3/t_{w'} - Q_X t_{w'})$ respectively, where $t_{w'} \equiv g_X/g_R$.

Since D' and d'_L have different Z-couplings, the Z-coupling to the mass basis d_L is non-universal and given by the matrix $\mathcal{C}^{\rm tree}_{Z-d_L}$, defined as

$$\begin{aligned} \mathcal{L} &\supset Z^\mu \overline{d_L} \mathcal{C}^{\rm tree}_{Z-d_L} \bar{\sigma}_\mu d_L, \\ \mathcal{C}^{\rm tree}_{Z-d_L} &\equiv \frac{g}{c_w}\left[\frac{1}{3}s_w^2 - \frac{1}{2}V^{L\dagger}_{\rm CKM}V^L_{\rm CKM}\right] \\ &= \frac{g}{c_w}\left[\frac{1}{3}s_w^2 - \frac{1}{2} + \frac{|v_d|^2}{4}U_L^{d\dagger}y'^\dagger \tilde{s}_R (M_D M_D^\dagger)^{-1}\tilde{s}_R^\dagger y' U_L^d\right]. \end{aligned} \tag{4.53}$$

Besides the mass suppression of order $\mathcal{O}(\epsilon^2)$, the off-diagonal terms in $\mathcal{C}^{\rm tree}_{Z-d_L}$ is further suppressed by y' and U_L^d. As a result, their contributions to $|\Delta F| = 2$ processes turns out to be negligible. A similar argument can be made for Z'-couplings to d_L.

We now move on to d_R^c. Since both d'^c_R and D'^c have the same couplings to Z, there is no tree-level FCNC mediated by Z. The FCNC mediated by Z' has already been discussed in the main text.

4.C.3 One-loop FCNCs

Numerous box diagrams in our model can contribute to $|\Delta F| = 2$ processes. Besides those from LRS and vector-like quarks, we also have additional diagrams involving the superpartners. A complete analysis of all such box diagrams and

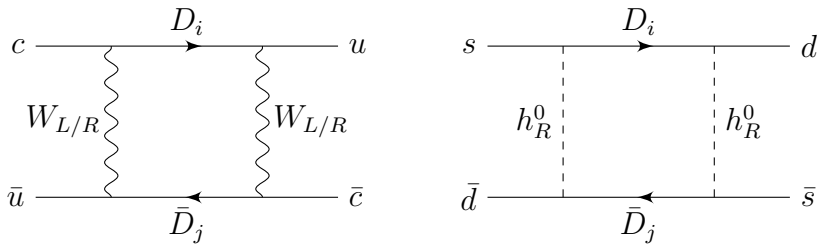

Figure 4.7: Examples of $|\Delta F| = 2$ box diagrams for $D - \bar{D}$ and $K - \bar{K}$ mixings.

interference lies beyond the scope of this work, and we will only consider a small subset of diagrams involving the new quarks as shown in Figure 4.7.

$W_{L/R} - W_{L/R}$ box diagrams for $D - \bar{D}$ mixing

The $W_{L/R}$ gauge couplings of interest are given by

$$\mathcal{L} \supset \frac{g}{\sqrt{2}} W_L^{+\mu} \overline{u_L} (-s_L^\dagger U_L^D) \bar{\sigma}_\mu D - \frac{g_R}{\sqrt{2}} W_R^{+\mu} \overline{D_R^c} (-\tilde{s}_R U_R^D)^T \bar{\sigma}_\mu u_R^c + \text{h.c.} \tag{4.54}$$

Due to the factors of $\mathcal{O}(\epsilon)$ and y' present in s_L, it turns out that the $W_L - W_L$ and $W_L - W_R$ contributions are highly suppressed, so only the $W_R - W_R$ contributions are of interest. The box diagram can in principle be evaluated using the Inami-Lim formula [227]. However, we will make a pessimistic approximation, from which we obtain the effective Hamiltonian

$$\mathcal{H}_{W_R}^{\text{eff}}(|\Delta C| = 2) \approx \frac{g_R^4}{128\pi^2} \frac{m_D^2}{m_{W'}^4} \left(\max_i [(\tilde{s}_R U_R^D)_{ui} (\tilde{s}_R U_R^D)_{ci}^*] \right)^2 (\overline{c_R^c} \bar{\sigma}_\mu u_R^c)^2 + \text{h.c.} \tag{4.55}$$

To satisfy the bounds on Δm_D, we require that

$$\left(\frac{g_R/g}{1.2} \right)^4 \left(\frac{m_D}{2\,\text{TeV}} \right)^2 \left(\max_i [(\tilde{s}_R U_R^D)_{ui} (\tilde{s}_R U_R^D)_{ci}^*] \right)^2 \lesssim 0.01. \tag{4.56}$$

We see that we only require a small suppression of the off-diagonal $\tilde{s}_R U_R^D$ elements since they appear here to the fourth power.

Box diagrams involving H_R

We have chosen to consider box diagrams involving H_R instead of those involving Φ, since we expect constraints from the latter to be weaker due to y' being hierarchical and nearly diagonal. The relevant couplings are given by

$$\mathcal{L} \supset -\frac{1}{\sqrt{2}} d_R^c (V_{\rm CKM}^{R\dagger} z \tilde{c}_L V_L) D h_R^0 + \text{h.c.} \tag{4.57}$$

The formula for the loop integral can be obtained from [228], although we will again make a pessimistic approximations. We then obtain the effective Hamiltonian

$$\mathcal{H}_{H_R}^{\rm eff}(|\Delta S| = 2) \approx \frac{1}{512\pi^2} \frac{1}{m_{h_R}^2} \left(\max_i [(V_{\rm CKM}^R z \tilde{c}_L U_L^D)_{si} (V_{\rm CKM}^R z \tilde{c}_L U_L^D)_{di}^*] \right)^2 (\overline{d_R^c} \bar{\sigma}_\mu s_R^c)^2 + \text{h.c.} \tag{4.58}$$

for $K - \bar{K}$ mixing, from which we require that [52]

$$\left(\frac{3\,\text{TeV}}{m_{h_R}^2} \right)^2 \left(\frac{\max_i [(V_{\rm CKM}^R z \tilde{c}_L U_L^D)_{si} (V_{\rm CKM}^R z \tilde{c}_L U_L^D)_{di}^*]}{0.2} \right)^2 \lesssim 1. \tag{4.59}$$

The reference value of 0.2 is again based on regarding c_R as a generic matrix of order $\mathcal{O}(c_d)$, and all other matrices of order $\mathcal{O}(1)$. We see that the constraint is satisfied without any suppression of the off-diagonal terms. The same holds for box diagrams for $B_{d(s)} - \bar{B}_{d(s)}$ mixing.

Chapter 5
Nonzero θ_{13} in $SO(3) \to A_4$ lepton models[1]

Chapter abstract

The simplest neutrino mass models based on A_4 symmetry predict $\theta_{13} = 0$ at tree level, a value that contradicts recent data. We study models that arise from the spontaneous breaking of an $SO(3)$ symmetry to its A_4 subgroup, and find two ways to get a nonzero θ_{13} at tree level. In the first method extra heavy fields mixed with the charged leptons generate θ_{13} of order the ratio between the A_4-breaking and the $SO(3)$-breaking scales. In the second method the flavon vacuum alignment is modified, such that it generates θ_{13} of order the amount of misalignment.

5.1 Introduction

For a long time, the Pontecorvo-Maki-Nakagawa-Sakata (PMNS) matrix $U_{\rm PMNS}$ [15, 38] was believed to be consistent with the tri-bimaximal mixing matrix [57]:

$$U_{\rm TBM} = \begin{pmatrix} \sqrt{\frac{2}{3}} & \frac{1}{\sqrt{3}} & 0 \\ -\frac{1}{\sqrt{6}} & \frac{1}{\sqrt{3}} & \frac{1}{\sqrt{2}} \\ \frac{1}{\sqrt{6}} & -\frac{1}{\sqrt{3}} & \frac{1}{\sqrt{2}} \end{pmatrix}. \tag{5.1}$$

The pattern exhibited by the tri-bimaximal mixing matrix seemed to suggest some underlying symmetry in the lepton sector, thus motivating the development of lepton models based on discrete flavour symmetries. One class of models was based

[1] Based on Y. Grossman and W. H. Ng, *Phys. Rev.* **D91** (2015) 073005, [1404.1413].

Parameter	Best fit	1σ range	3σ range
$\sin^2(\theta_{12})$ (NH, IH)	0.307	$0.291 - 0.325$	$0.259 - 0.359$
$\sin^2(\theta_{13})$ (NH)	0.0243	$0.0216 - 0.0266$	$0.0169 - 0.0313$
$\sin^2(\theta_{13})$ (IH)	0.0242	$0.0219 - 0.0267$	$0.0171 - 0.0315$
$\sin^2(\theta_{23})$ (NH)	0.386	$0.365 - 0.410$	$0.331 - 0.637$
$\sin^2(\theta_{23})$ (IH)	0.392	$0.370 - 0.431$	$0.335 - 0.663$
δ (NH)	1.08π	$0.77\pi - 1.36\pi$	–
δ (IH)	1.09π	$0.83\pi - 1.47\pi$	–

Table 5.1: Current experimental status of the mixing angles in $U_{\rm PMNS}$ [286]. NH and IH stands for normal and inverted hierarchy respectively.

on the discrete group A_4 [229–273] (see [274–277] for reviews). The most basic implementation of these A_4 models comprise the Standard Model (SM) leptons and Higgs, right-handed singlet neutrinos, as well as two scalar flavons ϕ and ϕ'. These fields are assigned into representations of A_4, where the flavons, in particular, are three-dimensional representations. The Lagrangian is invariant under A_4, but this symmetry is spontaneously broken when the flavons acquire VEVs, thus generating mass terms for the leptons. To reproduce the tri-bimaximal mixing at tree level, the lepton mass matrices have to take specific forms, which imply specific alignments $\langle\phi\rangle = (v, v, v)$ and $\langle\phi'\rangle = (v', 0, 0)$ for the flavon VEVs. Such alignments may be explained by various UV completions based on supersymmetry or extra dimensions [278–285].

The recent discoveries of finite θ_{13} by the Daya Bay [58] and RENO [59] experiments have thrown the tri-bimaximal mixing pattern into question. The current experimental status of the elements of $U_{\rm PMNS}$ is shown in Table 5.1. The best fit value of $|\sin(\theta_{13})|$ for both hierarchies is approximately 0.16, and is different from zero in a statistical significant way.

Various ideas have been proposed to modify these models so as to reproduce a nonzero θ_{13}. One way is to consider higher dimension operators, which introduce correction terms to the mass matrices of relative size given by v/Λ and v'/Λ (where Λ is the cutoff) [276,285,287]. Another avenue is to extend the A_4 model to include more flavons that contribute to the lepton mass matrices [288–296]. Yet another method is to introduce perturbations in the flavon sector that modify their vacuum alignments and hence the form of the lepton mass matrices [297–299]. Radiative corrections as a way to generate finite θ_{13} have been considered in [300–303].

In this chapter, we focus on a specific class of models [61, 304, 305] that can be regarded as UV completions of certain A_4 models. These models are invariant under a continuous symmetry group, for example $SO(3)$, of which A_4 is a subgroup. This symmetry is spontaneously broken to A_4 by some flavons that acquire a specific pattern of VEVs, generating the A_4 model as an effective low energy theory. Now that it has become clear that θ_{13} is finite, such models need to be modified to account for this fact.

We study the model of [61] and found two ways to modify it to give nonzero θ_{13}. One approach, specific to these class of models, is based on the fact that $SO(3)$ based models already require additional charged leptons. While the mixing between these additional leptons and the SM leptons is very small, it is enough to modify the pattern of the light charged lepton mass matrix, which breaks the tri-bimaximal mixing pattern. An interesting result is that the size of θ_{13} scales like the ratio of A_4-breaking to $SO(3)$-breaking scales. A second approach, similar to some of the general methods mentioned above, is to allow the flavon alignments to become arbitrary and therefore it can be adjusted to reproduce the experimental $U_{\rm PMNS}$.

This chapter is organised as follows. In Section 5.2 we provide an overview of the specific $SO(3) \to A_4$ model of [61]. In Section 5.3 we demonstrate that mixing of the charged leptons with heavy fields give rise to a nonzero tree-level θ_{13}. In Section 5.4 we consider the second approach of directly modifying the flavon vacuum alignments, to show that it can be used to give rise to a nonzero θ_{13}. We summarise our results in Section 5.5.

5.2 Review of the $SO(3) \to A_4$ model

5.2.1 Field content

We review an example of a lepton model involving a larger continuous flavour symmetry that is spontaneously broken to the A_4 subgroup [61]. The symmetries of this model are the electroweak gauge symmetry $SU(2)_L \times U(1)_Y$ as well as a global $SO(3)_F \times Z_2$. The fields and their representations are summarised in Table 5.2.

For the lepton sector, the three Standard Model left-handed $SU(2)_L$ doublets ψ_l form a **3** under $SO(3)_F$. Among the three Standard Model charged right-handed $SU(2)_L$ singlets, ψ_e is a **1**, while the other two have been subsumed into a **5** denoted by ψ_m. In doing so, we have now three extra charged right-handed $SU(2)_L$ singlets from ψ_m, to which we give large Dirac masses by introducing three new charged left-handed $SU(2)_L$ singlets ψ_f that form a **3**. Finally we have three right-handed neutrinos ψ_n which form a **3**.

In the scalar sector, we have the Standard Model Higgs, H, which is a singlet

Field	$SU(2)_L$	$U(1)_Y$	$SO(3)_F$	Z_2
ψ_l	**2**	$-\frac{1}{2}$	**3**	$-$
ψ_f	**1**	-1	**3**	$-$
ψ_e	**1**	-1	**1**	$+$
ψ_m	**1**	-1	**5**	$+$
ψ_n	**1**	0	**3**	$-$
H	**2**	$\frac{1}{2}$	**1**	$+$
ϕ	**1**	0	**3**	$-$
ϕ'	**1**	0	**3**	$+$
ϕ_5	**1**	0	**5**	$-$
T	**1**	0	**7**	$-$

Table 5.2: Matter fields and the representations they transform as under the gauge symmetry $SU(2)_L \times U(1)_Y$ and global symmetry $SO(3)_F \times Z_2$. The fields have been divided into left-handed leptons, right-handed leptons and scalars.

of the flavour group, and four flavons ϕ, ϕ', ϕ_5, and T which form **3**, **3**, **5** and **7** respectively. The flavon T is responsible for the $SO(3)_F \to A_4$ breaking, and is required to be at least a **7** since that is the smallest representation of $SO(3)$ that can have an A_4-invariant VEV. While ϕ and ϕ' can be identified with the flavons in the minimal A_4 model, the extra flavon ϕ_5 is required here to prevent the muon and tau from becoming degenerate. This is since the right-handed muon and tau are a part of the same $SO(3)_F$ multiplet and share the same Yukawa coupling with ϕ, and thus we need an extra flavon in an $SO(3)_F$ representation different from that of ϕ to lift this degeneracy.

5.2.2 Lagrangian

We now consider all possible mass and interaction terms in the Lagrangian consistent with the symmetries of the model. In particular, we identify one set involving charged leptons:

$$\begin{aligned}\mathcal{L}_e = &- y_e \overline{\psi_l^a} \frac{H}{\Lambda} \phi^a \psi_e - y_m \overline{\psi_l^a} \frac{H}{\Lambda} \phi^b \psi_m^{ab} - y_m^T \overline{\psi_l^a} \frac{H}{\Lambda} T^{abc} \psi_m^{bc} - y_m^5 \epsilon^{abc} \overline{\psi_l^a} \frac{H}{\Lambda} \phi_5^{bd} \psi_m^{cd} \\ &- y_e' \overline{\psi_f^a} \phi^a \psi_e - y_m' \overline{\psi_f^a} \phi^b \psi_m^{ab} - y_m^{T\prime} \overline{\psi_f^a} T^{abc} \psi_m^{bc} - y_m^{5\prime} \epsilon^{abc} \overline{\psi_f^a} \phi_5^{bd} \psi_m^{cd},\end{aligned} \tag{5.2}$$

and another set involving neutrinos:

$$\mathcal{L}_\nu = -M \overline{\psi_n^{ca}} \psi_n^a - \frac{x_\nu}{\Lambda} \overline{\psi_n^{ca}} \psi_n^b \phi'^c T^{abc} - y_\nu \overline{\psi_l^a} H \psi_n^a, \tag{5.3}$$

where a, b, and c are $SO(3)_F$ indices running from 1 to 3, and Λ is the cutoff scale of the model. The Z_2 global symmetry prevents ϕ' from coupling to the charged lepton sector, and ϕ and ϕ_5 to the neutrino sector. This sectorisation of flavons is also required in the minimal A_4 model to ensure the correct form of the lepton mass matrices. The dimension-five operators are required to give nonzero masses to the light charged leptons that are extremely small compared to the energy scale of the flavons, as well as to break the degeneracy of the light neutrinos.

There is a third set of terms involving only the scalars, the most general form of which we will not consider here. Rather, we focus on just the renormalizable self-interaction potential of the flavon T:

$$V(T) = -\frac{\mu^2}{2} T^{abc} T^{abc} + \frac{\lambda}{4} (T^{abc} T^{abc})^2 + c T^{abc} T^{bcd} T^{def} T^{efa}. \tag{5.4}$$

It is shown in [61] that conditions on λ and c exist such that $V(T)$ has an A_4 invariant global minimum, which breaks $SO(3)_F$ into its A_4 subgroup. We then end up with an effective non-minimal A_4 model, with three more pairs of left-handed and right-handed charged leptons and one more flavon, ϕ_5.

5.2.3 Lepton mass matrices and $U_{\mathbf{PMNS}}$

We assume that the flavons ϕ, ϕ_5 and ϕ' acquire VEVs with the following alignments:

$$\langle\phi\rangle = \begin{pmatrix} v \\ v \\ v \end{pmatrix}, \qquad \langle\phi_5\rangle = \begin{pmatrix} 0 & v_5 & v_5 \\ v_5 & 0 & v_5 \\ v_5 & v_5 & 0 \end{pmatrix}, \qquad \langle\phi'\rangle = \begin{pmatrix} v' \\ 0 \\ 0 \end{pmatrix}. \tag{5.5}$$

We consider the case where the VEV of T satisfies $v_T \gg v, v', v_5$, in accordance to the picture of $SO(3)_F$ broken to A_4. After electroweak symmetry breaking, the Higgs boson H acquires a VEV $v_H = 246/\sqrt{2}\,\text{GeV}$, and we obtain two 6×6 mass matrices: the charged lepton one, $M_l^{6\times6}$, and the neutrino Majorana mass matrix, $M_\nu^{6\times6}$.

In [61], the mixing between the charged leptons and the new states were considered to be very small and thus negligible. In that case the mass matrix for the three light charged leptons, M_l, is simply given by the upper-left 3×3 block of $M_l^{6\times6}$:

$$M_l = \begin{pmatrix} \frac{y_e v_H v}{\Lambda} & \frac{y_m v_H v}{\Lambda} + \frac{y_m^5 v_H v_5}{\Lambda}(\omega^2 - \omega) & \frac{y_m v_H v}{\Lambda} + \frac{y_m^5 v_H v_5}{\Lambda}(\omega - \omega^2) \\ \frac{y_e v_H v}{\Lambda} & [\frac{y_m v_H v}{\Lambda} + \frac{y_m^5 v_H v_5}{\Lambda}(\omega^2 - \omega)]\omega & [\frac{y_m v_H v}{\Lambda} + \frac{y_m^5 v_H v_5}{\Lambda}(\omega - \omega^2)]\omega^2 \\ \frac{y_e v_H v}{\Lambda} & [\frac{y_m v_H v}{\Lambda} + \frac{y_m^5 v_H v_5}{\Lambda}(\omega^2 - \omega)]\omega^2 & [\frac{y_m v_H v}{\Lambda} + \frac{y_m^5 v_H v_5}{\Lambda}(\omega - \omega^2)]\omega \end{pmatrix}, \tag{5.6}$$

where $\omega = e^{2\pi i/3}$. The charged lepton masses can be obtained by diagonalising $M_l(M_l)^\dagger$ and taking the square root, and we obtain

$$m_e = \left|\sqrt{3}\frac{y_e v_H v}{\Lambda}\right|, \qquad m_\mu, m_\tau = \left|\sqrt{3}\frac{y_m v_H v}{\Lambda} \pm 3i\frac{y_m^5 v_H v_5}{\Lambda}\right|. \tag{5.7}$$

The unitary transformation required for this diagonalisation

$$U_l = \frac{1}{\sqrt{3}} \begin{pmatrix} 1 & 1 & 1 \\ 1 & \omega & \omega^2 \\ 1 & \omega^2 & \omega \end{pmatrix}. \tag{5.8}$$

It is important to note that Eq. (5.8) is a result of M_l taking the form

$$M_{\text{aligned}} = \begin{pmatrix} a & b & c \\ a & b\,\omega & c\,\omega^2 \\ a & b\,\omega^2 & c\,\omega \end{pmatrix}, \tag{5.9}$$

where a, b and c are constants.

For the neutrino sector, the 6×6 Majorana mass matrix $M_\nu^{6\times 6}$ can be block-diagonalised, and the resulting upper-left 3×3 block is identified with the mass matrix M_ν of the three light neutrinos

$$M_\nu = \begin{pmatrix} -\frac{y_\nu^2 v_H^2}{M} & 0 & 0 \\ 0 & -\frac{y_\nu^2 M v_H^2 \Lambda^2}{M^2\Lambda^2 - x_\nu^2 v'^2 v_T^2} & \frac{y_\nu^2 x_\nu v_H^2 v' v_T \Lambda}{M^2\Lambda^2 - x_\nu^2 v'^2 v_T^2} \\ 0 & \frac{y_\nu^2 x_\nu v_H^2 v' v_T \Lambda}{M^2\Lambda^2 - x_\nu^2 v'^2 v_T^2} & -\frac{y_\nu^2 M v_H^2 \Lambda^2}{M^2\Lambda^2 - x_\nu^2 v'^2 v_T^2} \end{pmatrix}. \tag{5.10}$$

Note that this is the see-saw mechanism, as M_ν becomes very small if the dimensionful parameters in the denominators are much larger than v_H. The light neutrino masses can be obtained by diagonalising M_ν

$$m_1 = \left| \frac{y_\nu^2 v_H^2}{M} \right|, \qquad m_2, m_3 = \left| \frac{y_\nu^2 v_H^2 \Lambda}{M\Lambda \pm x_\nu v' v_T} \right|. \tag{5.11}$$

The unitary transformation required for this diagonalisation is:

$$U_\nu = i \begin{pmatrix} 1 & 0 & 0 \\ 0 & \frac{1}{\sqrt{2}} & \frac{1}{\sqrt{2}} \\ 0 & \frac{1}{\sqrt{2}} & -\frac{1}{\sqrt{2}} \end{pmatrix}. \tag{5.12}$$

The PMNS matrix is then given by:

$$U_{\text{PMNS}} = U_l (U_\nu)^\dagger = \begin{pmatrix} -i\frac{1}{\sqrt{3}} & -i\sqrt{\frac{2}{3}} & 0 \\ -i\frac{1}{\sqrt{3}} & i\frac{1}{\sqrt{6}} & \frac{1}{\sqrt{2}} \\ -i\frac{1}{\sqrt{3}} & i\frac{1}{\sqrt{6}} & -\frac{1}{\sqrt{2}} \end{pmatrix}, \tag{5.13}$$

which can be brought into the form $U_{\rm TBM}$ by swapping the labels of ν_1 and ν_2, and redefining the phases of ν_1, ν_2 and τ. Note that the tri-bimaximal mixing pattern obtained above depends on U_l taking the form in Eq. (5.8). Any deviation of M_l from $M_{\rm aligned}$ would result in deviation of $U_{\rm PMNS}$ from $U_{\rm TBM}$. We will exploit this fact in the next section in order to generate a finite θ_{13}. We also note that Eq. (5.13) actually omits certain nonunitary matrix factors which we show in Appendix 5.A to be negligible.

Before concluding this section, it is useful to obtain a rough picture of the energy scales for the various dimensionful parameters and VEVs. Most of the information turns out to come from the neutrino sector. Based on experimental bounds for the light neutrino masses and their splittings, Eq. (5.11) implies that $M \ll v'$. This gives rise to the following picture:

$$v_H \sim 100\,\text{GeV} \ll M \ll v \sim v_5 \sim v' \ll v_T \ll \Lambda. \tag{5.14}$$

If we also assume that $x_\nu \sim y_\nu \sim O(1)$, Eq. (5.11) also implies that $M \geq 10^{14}\,\text{GeV}$. Since we introduce a number of scales within the interval between $10^{14}\,\text{GeV}$ and Λ (limited by the Planck scale), the scales may not be well-separated and corrections that are proportional to ratios of scales may become important.

5.3 Effects of mixing in the charged lepton sector

5.3.1 Obtaining the light charged lepton mass-squared matrix

As we have seen in the previous section, the tri-bimaximal mixing pattern in this model relies on the unitary matrix U_l that diagonalises $M_l(M_l)^\dagger$ taking the form in Eq. (5.8). This in turn relies on the light charged lepton mass matrix M_l taking the form M_{aligned} in Eq. (5.9). In some region of the parameter space these assumptions are not very good, and as a result there are corrections that lead to a nonzero θ_{13}.

To obtain the exact form of $M_l(M_l)^\dagger$ in the general case, we start with the full 6×6 mass matrix $M_l^{6\times 6}$ obtained from the Lagrangian in Eq. (5.2). For simplicity, we express $M_l^{6\times 6}$ in terms of 3×3 matrices A, B, C and D:

$$M_l^{6\times 6} \equiv \begin{pmatrix} \frac{v_H}{\Lambda}A & \frac{v_H}{\Lambda}B \\ C & D \end{pmatrix}. \tag{5.15}$$

where

$$A = \begin{pmatrix} y_e v & [y_m v + y_m^5 v_5(\omega^2-\omega)] & [y_m v + y_m^5 v_5(\omega-\omega^2)] \\ y_e v & [y_m v + y_m^5 v_5(\omega^2-\omega)]\,\omega & [y_m v + y_m^5 v_5(\omega-\omega^2)]\,\omega^2 \\ y_e v & [y_m v + y_m^5 v_5(\omega^2-\omega)]\,\omega^2 & [y_m v + y_m^5 v_5(\omega-\omega^2)]\,\omega \end{pmatrix}, \tag{5.16}$$

$$B = \begin{pmatrix} y_m v + 2y_m^T v_T & y_m v + y_m^5 v_5 & -y_m^5 v_5 \\ y_m v & 2y_m^T v_T & y_m v \\ y_m v + y_m^5 v_5 + y_m^T v_T & y_m v - y_m^5 v_5 & y_m^T v_T \end{pmatrix}, \tag{5.17}$$

$$C = \begin{pmatrix} y'_e v & [y'_m v + y_m^{5\prime} v_5(\omega^2-\omega)] & [y'_m v + y_m^{5\prime} v_5(\omega-\omega^2)] \\ y'_e v & [y'_m v + y_m^{5\prime} v_5(\omega^2-\omega)]\,\omega & [y'_m v + y_m^{5\prime} v_5(\omega-\omega^2)]\,\omega^2 \\ y'_e v & [y'_m v + y_m^{5\prime} v_5(\omega^2-\omega)]\,\omega^2 & [y'_m v + y_m^{5\prime} v_5(\omega-\omega^2)]\,\omega \end{pmatrix}, \tag{5.18}$$

$$D = \begin{pmatrix} y'_m v + 2y^{T\prime}_m v_T & y'_m v + y^{5\prime}_m v_5 & -y^{5\prime}_m v_5 \\ y'_m v & 2y^{T\prime}_m v_T & y'_m v \\ y'_m v + y^{5\prime}_m v_5 + y^{T\prime}_m v_T & y'_m v - y^{5\prime}_m v_5 & y^{T\prime}_m v_T \end{pmatrix}. \tag{5.19}$$

For our discussion it is important to note that A and C are both of the form M_{aligned}. The eigenvalues of A and C are of order v while that of B and D are of order v_T. We further define

$$E \equiv B - \frac{y^T_m}{y^{T\prime}_m} D, \tag{5.20}$$

such that the eigenvalues of E are of order v. We then block-diagonalise $M_l^{6\times 6}(M_l^{6\times 6})^\dagger$ and obtain $M_l(M_l)^\dagger$ from the upper-left 3×3 block:

$$M_l(M_l)^\dagger = \frac{v_H^2}{\Lambda^2}\left[AA^\dagger + BB^\dagger - (AC^\dagger + BD^\dagger)(CC^\dagger + DD^\dagger)^{-1}(CA^\dagger + DB^\dagger)\right]. \tag{5.21}$$

We see when assuming M_l to be given by Eq. (5.6) that we have kept only the leading term that is proportional to $AA^\dagger$.

In order to see the effect of the other terms we assume that all the Yukawa couplings are of the same order and that $v \sim v_5 \ll v_T$, and we expand in the small parameter

$$\epsilon = O(v/v_T) \sim O(v'/v_T). \tag{5.22}$$

To the lowest nontrivial order we obtain

$$M_l = \frac{v_H}{\Lambda}\left(A - BD^{-1}C\right) = \frac{v_H}{\Lambda}\left(A - \frac{y^T_m}{y^{T\prime}_m}C - ED^{-1}C\right). \tag{5.23}$$

Since both A and C are of the form M_{aligned}, so is any linear superposition of them, and thus the first correction term proportional to C does not give a nonzero θ_{13}. Since ED^{-1} is not proportional to the identity matrix, the second correction term, which is of order ϵ, is what generate deviations of M_l from M_{aligned}. This in turn suggests that the size of θ_{13} is also of order ϵ. In other words, θ_{13} reflects the ratio of the A_4-breaking to $SO(3)_F$-breaking scales.

5.3.2 Amplification from nearly degenerate mass eigenvalues

While we have shown above that $\theta_{13} \propto \epsilon$, there is actually a numerical factor that enhances the size of θ_{13}. This enhancement factor is associated with the fact that the charged lepton masses exhibit a hierarchy. The very basic reason for this is the well-known result that a mixing angle approaches $\pi/4$ as the two relevant diagonal terms become degenerate relative to off-diagonal perturbations. We have implicitly assumed in our previous analysis that the difference between mass eigenvalues are of order the tau mass scale. In reality, the electron and muon are almost degenerate relative to the tau mass, suggesting an enhancement in the mixing angle.

To illustrate this enhancement we consider

$$\begin{aligned} U_l M_l (M_l)^\dagger (U_l)^\dagger &= \frac{v_H^2}{\Lambda^2} U_l \left(A - \frac{y_m^T}{y_m^{T\prime}} C \right) \left(A - \frac{y_m^T}{y_m^{T\prime}} C \right)^\dagger (U_l)^\dagger + \Delta \\ &= \begin{pmatrix} m_a^2 & 0 & 0 \\ 0 & m_b^2 & 0 \\ 0 & 0 & m_c^2 \end{pmatrix} + \begin{pmatrix} \Delta_{11} & \Delta_{21}^* & \Delta_{31}^* \\ \Delta_{21} & \Delta_{22} & \Delta_{32}^* \\ \Delta_{31} & \Delta_{32} & \Delta_{33} \end{pmatrix}, \end{aligned} \tag{5.24}$$

where U_l is the specific unitary matrix in Eq. (5.8) and

$$\Delta \equiv \frac{v_H^2}{\Lambda^2} U_l \left[\left(A - \frac{y_m^T}{y_m^{T\prime}} C \right) C^\dagger (D^\dagger)^{-1} E^\dagger + E D^{-1} C \left(A - \frac{y_m^T}{y_m^{T\prime}} C \right)^\dagger \right] U_l^\dagger, \tag{5.25}$$

parametrizes the higher order correction terms in Eq. (5.23). The original eigenvector $\frac{1}{\sqrt{3}}(1,1,1)$ has been transformed to $(1,0,0)$ by the basis change generated by U_l. The eigenvalues m_a, m_b and m_c need to be approximately the charged lepton masses. The matrix elements Δ_{ij} are typically of order $\sim O(m_\tau^2 \cdot \epsilon)$, with the exception of $\Delta_{21} \sim O(m_\mu m_\tau \cdot \epsilon)$, which as we will see below is important to get the correct size of enhancement.

We assume that ϵ is small enough so that $\Delta_{ij} \ll m_\mu^2$. The correction term Δ causes the zeroth order eigenvectors to mix by an amount of order Δ_{21}/m_μ^2 and Δ_{31}/m_τ^2. While $\Delta_{31}/m_\tau^2 \sim \epsilon$, notice that $\Delta_{21}/m_\mu^2 \sim O(m_\tau \epsilon/m_\mu)$. Hence the mixing is enhanced compared to the naive expectation ϵ by $O(m_\tau/m_\mu)$, and we conclude that

$$\theta_{13} \sim O\left(\frac{m_\tau}{m_\mu}\,\epsilon\right). \tag{5.26}$$

We now move on to explain why $\Delta_{21} \sim O(m_\mu m_\tau \epsilon)$. From Eq. (5.25), we have $\Delta = FG + G^\dagger F^\dagger$, where $F \equiv \frac{v_H}{\Lambda} U_l \left(A - \frac{y_m^T}{y_m^{T\prime}} C\right)$ and $G \equiv \frac{v_H}{\Lambda} C^\dagger (D^\dagger)^{-1} E^\dagger U_l^\dagger$. Here, U_l takes the form in Eq. (5.8). An important observation is that

$$F = \begin{pmatrix} F_{11} & 0 & 0 \\ 0 & 0 & F_{23} \\ 0 & F_{32} & 0 \end{pmatrix} \tag{5.27}$$

where

$$\begin{aligned} F_{11} &= \frac{v_H}{\Lambda}\left(y_e - \frac{y_m^T}{y_m^{T\prime}} y_e'\right) v, \\ F_{23} &= \sqrt{3}\frac{v_H}{\Lambda}\left(y_m - \frac{y_m^T}{y_m^{T\prime}} y_m'\right) v + 3i\frac{v_H}{\Lambda}\left(y_m^5 - \frac{y_m^T}{y_m^{T\prime}} y_m^{5\prime}\right) v_5, \\ F_{32} &= \sqrt{3}\frac{v_H}{\Lambda}\left(y_m - \frac{y_m^T}{y_m^{T\prime}} y_m'\right) v - 3i\frac{v_H}{\Lambda}\left(y_m^5 - \frac{y_m^T}{y_m^{T\prime}} y_m^{5\prime}\right) v_5. \end{aligned} \tag{5.28}$$

We note from Eq. (5.37) that $|F_{11}| \sim m_e$, $|F_{23}| \sim m_\mu$ and $|F_{32}| \sim m_\tau$. Meanwhile, explicit evaluation of G shows that $G_{ij} \sim O(m_\tau \epsilon)$. Therefore, we have:

$$\Delta_{21} = F_{23} G_{31} + G_{12}^* F_{11}^* \sim O(m_\mu m_\tau \epsilon). \tag{5.29}$$

In other words, the specific form of F has caused Δ_{21} to be $O(m_\mu m_\tau \cdot \epsilon)$ rather than $O(m_\tau^2 \cdot \epsilon)$. This restrict the enhancement effect of θ_{13} to just $O(\frac{m_\tau}{m_\mu})$ as opposed to $O(\frac{m_\tau^2}{m_\mu^2})$.

5.3.3 Numerical simulation

To verify the above estimates, we compute the exact tree-level $U_{\rm PMNS}$ for a large number of randomly generated parameter sets. Details for their generation are provided in Appendix 5.B. Two collections $\mathcal{C}_1$ and $\mathcal{C}_2$ of parameter sets have been generated. In collection $\mathcal{C}_1$, all the Yukawas are completely unconstrained $O(1)$ numbers. Figure 5.1(a) shows the value of $\sin(\theta_{13})$ against $\sup\{v/v_T, v_5/v_T\}$, which in general agrees with the expectation that $\theta_{13} \sim O(\epsilon)$. We also find that all three light charged lepton masses are $O(m_\tau)$ for almost the entire collection, clearly in disagreement with the physical masses. This suggests that the region of parameter space that reproduce the correct mass spectrum has a very small measure.

In collection $\mathcal{C}_2$, constraints are first applied to two of the Yukawas to increase the chance of reproducing the correct mass spectra. Of all the parameter sets generated with these constraints, only those with $10^{-3} < m_\mu^2/m_\tau^2 < 10^{-2}$ are then added to the collection. Figure 5.1(b) shows the value of $\sin(\theta_{13})$ against $\sup\{v/v_T, v_5/v_T\}$ for this collection. While still in general agreement with $\theta_{13} \sim O(\epsilon)$, we observe that the proportionality constant here is roughly ten times that of the first collection. This increase is due to amplification from nearly degenerate mass eigenvalues, as we discussed above.

5.4 Modifying the flavon vacuum alignment

In this section, we demonstrate that changing the alignments of the flavon VEVs can give rise to a nonzero θ_{13}. We assume that the corrections discussed in the previous section are not important and thus $M_l(M_l)^\dagger \propto AA^\dagger$. A no longer takes

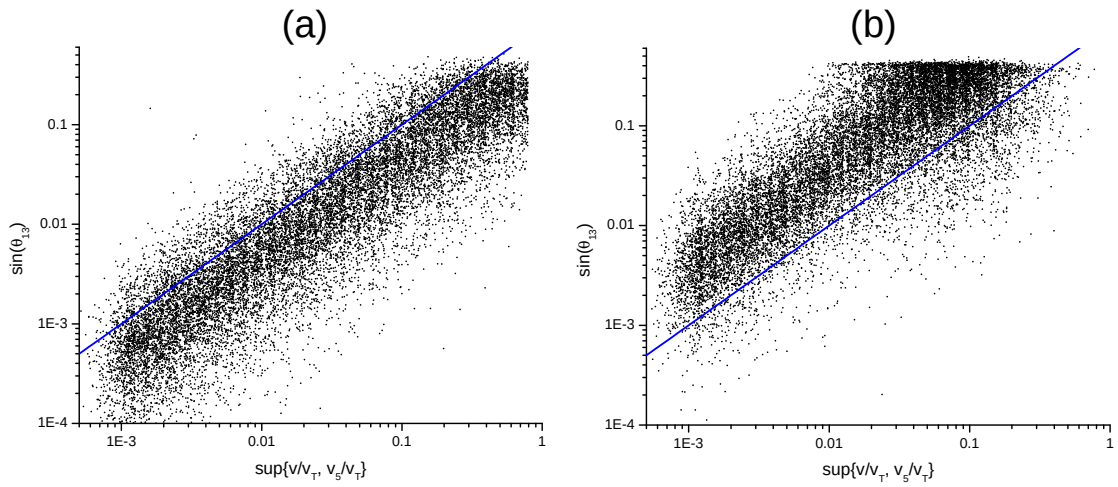

Figure 5.1: Graphs of $\sin(\theta_{13})$ against $\sup\{v/v_T, v_5/v_T\}$ for two collections (a) $\mathcal{C}_1$ and (b) $\mathcal{C}_2$ of random parameter sets. Both graphs demonstrate the expected linear proportionality. Collection $\mathcal{C}_2$ has charged lepton mass spectra closer to the actual hierarchy than $\mathcal{C}_1$, as a result of which θ_{13} has been enhanced by roughly $O(m_\tau/m_\mu)$ as predicted. For reference, the blue lines correspond to the equation $\sin(\theta_{13}) = \sup\{v/v_T, v_5/v_T\}$.

the form in Eq. (5.16). In particular it is not of the form M_{aligned} and therefore a nonzero θ_{13} can then be generated.

As a simple illustration, let us vary only the alignment of $\langle\phi\rangle$:

$$\langle\phi\rangle = \sqrt{3}v \begin{pmatrix} \sin(a)\cos(b) \\ \sin(a)\sin(b) \\ \cos(a) \end{pmatrix}. \tag{5.30}$$

We recover the original alignment with $a = \arcsin\left(\sqrt{2/3}\right)$ and $b = \frac{\pi}{4}$. With this new alignment, where $s_x \equiv \sin x$ and $c_x \equiv \cos x$, we obtain

$$A = \sqrt{3} \begin{pmatrix} y_e v s_a c_b & y_m v s_a c_b + \frac{y_m^5 v_5}{\sqrt{3}}(\omega^2 - \omega) & y_m v s_a c_b + \frac{y_m^5 v_5}{\sqrt{3}}(\omega - \omega^2) \\ y_e v s_a s_b & y_m v s_a s_b \omega + \frac{y_m^5 v_5}{\sqrt{3}}(1 - \omega^2) & y_m v s_a s_b \omega^2 + \frac{y_m^5 v_5}{\sqrt{3}}(1 - \omega) \\ y_e v c_a & y_m v c_a \omega^2 + \frac{y_m^5 v_5}{\sqrt{3}}(\omega - 1) & y_m v c_a \omega + \frac{y_m^5 v_5}{\sqrt{3}}(\omega^2 - 1) \end{pmatrix} \tag{5.31}$$

At first glance, we might expect the size of θ_{13} to be given by the misalignment angle of $\langle\phi\rangle$. However, the effect of having two much smaller eigenvalues again

Parameters					
Energy scales (GeV)		Yukawas		Alignment angles	
v_H	$246/\sqrt{2}$	y_e	0.000987876	a	0.3168π
v_5	9×10^{15}	y_m	0.933304	b	0.200722π
v	7×10^{16}	y_m^5	$-3.84556i$		
Λ	3×10^{19}				
Results					
Mass spectrum (GeV)		$\lvert U_{\text{PMNS}}\rvert = \begin{pmatrix} 0.805 & 0.574 & 0.150 \\ 0.387 & 0.670 & 0.633 \\ 0.450 & 0.470 & 0.759 \end{pmatrix}$			
m_e	5.11×10^{-4}				
m_μ	0.1057				
m_τ	1.7778				

Table 5.3: Example of a set of parameters that reproduces the correct charged lepton mass spectrum, as well as a U_{PMNS} within 2σ of experimental values. The precision quoted here for the parameters is required to reproduce the correct values of m_e and m_μ.

comes into play, and θ_{13} can be amplified by a factor of $O(m_\tau^2/m_\mu^2)$. Another useful observation is that

$$\text{Tr}\left[M_l(M_l)^\dagger\right] = m_e^2 + m_\nu^2 + m_\tau^2 = 3\frac{v_H^2 v^2}{\Lambda^2}(|y_e|^2 + 2|y_m|^2) + 18\frac{v_H^2 v_5^2}{\Lambda^2}|y_m^5|^2, \quad (5.32)$$

is independent of the alignment. This fact, together with a somewhat small set of parameters in the limit we have assumed, make a parameter scan in this case feasible. Table 5.3 shows an example of a parameter set found from such a scan, with the correct light charged lepton mass spectrum, as well as a U_{PMNS} that falls within 2σ of experimental values.

Finally, we note that in general it is also possible to have scenarios where the alignments of all the flavons are allowed to vary, or even scenarios where we have both effects of changing vacuum alignments as well as correction terms from mixing coming into play in θ_{13}. We have chosen to work in the scenario where mixing can

be neglected simply to highlight the effects of changing vacuum alignments.

5.5 Discussion and conclusion.

Having discussed the two approaches of obtaining a nonzero θ_{13}, there remains various issues that we did not touch on and are worth further investigations. First, we have not addressed any shortcomings of the model originally mentioned in [61]. This includes the issue of Goldstone bosons when the global $SO(3)_F$ symmetry is broken, and the issue of anomalies should we gauge the $SO(3)_F$ symmetry to eat up these Goldstone bosons. Second, our analysis so far is only at the classical level. We have yet to consider running of the various parameters down to the electroweak scale, nor loop corrections to the various observables [300–303,306–314]. Last, large cancellations between the matrix elements of $M_l(M_l)^\dagger$ are required in order to give the the correct charged lepton mass spectrum. This is essentially the usual charged lepton mass hierarchy problem, but now in a more complicated guise since it is no longer clear which part of the parameter space such a working region lies in, making it hard to come up with a UV explanation for this fine-tuning.

To conclude, the $SO(3)_F \to A_4$ model of [61] is a UV completion of an effective A_4 model with the purpose of reproducing the tri-bimaximal mixing pattern in U_{PMNS}. However, as we have shown, the model actually predicts a nonzero θ_{13} with the size of θ_{13} determined by the ratio of the A_4 breaking scale to the $SO(3)_F$ breaking scale. Avoiding too large a ratio generates a θ_{13} within the observed range. When the ratio is very small, we have shown that there is one more possibility to generate a nonzero $\sin(\theta_{13})$ by modifying the alignment of the flavon VEVs. We thus conclude that this model can be modified to accommodate the measured θ_{13}.

5.A Nonunitary factors in U_{PMNS}

In this appendix, we discuss the origin of nonunitary factors mentioned in Section 5.2 and why they turn out to be negligible. The charged current weak interaction acts between the left-handed SM charged leptons and neutrinos, both of which are linear combinations of light and heavy mass eigenstates. U_{PMNS} characterizes the interaction between only the light mass eigenstates. More explicitly, let us define $U_l^{6\times6,\text{full}}$ and $U_\nu^{6\times6,\text{full}}$ to be the 6×6 unitary matrices required to diagonalise $M_l^{6\times6}(M_l^{6\times6})^\dagger$ and $M_\nu^{6\times6}$, i.e. that $U_l^{6\times6,\text{full}} M_l^{6\times6}(M_l^{6\times6})^\dagger(U_l^{6\times6,\text{full}})^\dagger$ and $U_\nu^{6\times6,\text{full}} M_\nu^{6\times6}(U_\nu^{6\times6,\text{full}})^T$ are fully diagonal. U_{PMNS} is then given by

$$U_{\text{PMNS}} = U_l^{\text{full}}(U_\nu^{\text{full}})^\dagger, \tag{5.33}$$

where U_l^{full} and U_ν^{full} are the upper-left 3×3 blocks of $U_l^{6\times6,\text{full}}$ and $U_\nu^{6\times6,\text{full}}$ and are in general nonunitary matrices. Hence we also do not expect U_{PMNS} to be unitary.

It is perhaps more illustrative to regard the diagonalisation as a two-step process, which we demonstrate here with the neutrino sector. One can first block-diagonalise $M_\nu^{6\times6}$ using a 6×6 unitary matrix $U_\nu^{6\times6,\text{bd}}$:

$$U_\nu^{6\times6,\text{bd}} M_\nu^{6\times6}(U_\nu^{6\times6,\text{bd}})^T = \begin{pmatrix} M_\nu & 0 \\ 0 & M_{\nu'} \end{pmatrix}. \tag{5.34}$$

M_ν and $M_{\nu'}$ are the 3×3 Majorana mass matrices for the light and heavy neutrinos. Let U_ν be the 3×3 unitary matrix required to diagonalise M_ν, and U_ν^{bd} be the (generally nonunitary) upper-left 3×3 block of $U_\nu^{6\times6,\text{bd}}$. We then find that $U_\nu^{\text{full}} = U_\nu U_\nu^{\text{bd}}$. In other words, U_ν^{full} can be decomposed into a unitary factor associated with the diagonalisation of M_ν, and a non-unitary factor associated with the block-diagonalisation of $M_\nu^{6\times6}$. We can apply the same two-step process to the charged lepton sector, first block-diagonalising $M_l^{6\times6}(M_l^{6\times6})^\dagger$ and then diagonalising the

resultant 3×3 light charged lepton mass-squared matrix $M_l(M_l)^\dagger$. We find a similar factorization $U_l^{\text{full}} = U_l U_l^{\text{bd}}$. U_{PMNS} is then given by

$$U_{\text{PMNS}} = U_l U_l^{\text{bd}} (U_\nu^{\text{bd}})^\dagger (U_\nu)^\dagger. \tag{5.35}$$

This expression differs from Eq. (5.13) by the nonunitary factor $U_l^{\text{bd}}(U_\nu^{\text{bd}})^\dagger$ from the block-diagonalisation process. However, we can show that U_l^{bd} and U_ν^{bd} deviate from the identity matrix by terms of order $O(\frac{v_H^2}{\Lambda^2})$ and $O(\frac{v_H^2}{M^2})$ respectively, which based on the energy scales in Eq. (5.14) are exceedingly small deviations. Hence, their effects on U_{PMNS} are negligible and U_{PMNS} can be considered to be unitary.

5.B Generation of random parameter sets

In this appendix, we discuss the generation of the two collections of random parameter sets used in Figure 5.1(a) and 5.1(b). The VEV v_T is generated as a log flat random variable between $10^{16} - 10^{19}\,\text{GeV}$, while v and v_5 are random variables uniformly distributed between $10^{15} - 10^{16}\,\text{GeV}$. For the Yukawas, we define random variables R_i and Θ_i uniformly distributed between $0.4 - 4$ and $0 - 2\pi$ respectively, so $R_i^{\Theta_i}$ is a random complex variable with magnitude of $O(1)$. In the first collection $\mathcal{C}_1$ ($\sim 20,000$ sets), all the eight Yukawas in the model are generated using $R_i^{\Theta_i}$.

However, as we have noted, the very small measure of the regions of parameter space that generates the correct mass spectra meant that most of the mass spectra in $\mathcal{C}_1$ deviate substantially from the physical spectrum, with only $\sim 1\%$ of the $\frac{m_\mu^2}{m_\tau^2}$ lying within $10^{-3} - 10^{-2}$. In order to increase the likelihood of the random parameter sets falling into the desired regions, two constraints on the Yukawas

have been introduced for the second collection $\mathcal{C}_2$:

$$\begin{aligned} y'_e &= \frac{y_m^{T\prime}}{y_m^T} y_e - \frac{R_1^{\Theta_1}}{1000}, \\ y_m^5 &= \frac{y_m^T}{y_m^{T\prime}} y_m^{5\prime} + \frac{i}{\sqrt{3}} \frac{v}{v_5} \left(y_m - \frac{y_m^T}{y_m^{T\prime}} y'_m \right) - \frac{i}{\sqrt{3}} \frac{R_2^{\Theta_2}}{20} \end{aligned} \tag{5.36}$$

In other words, the values of y'_e and y_m^5 are determined by the other Yukawas up to random fluctuations of size $O(\frac{1}{1000})$ and $O(\frac{1}{20})$ respectively. These constraints were motivated by the fact that the eigenvalues of $\frac{v_H^2}{\Lambda^2} \left(A - \frac{y_m^T}{y_m^{T\prime}} C \right) \left(A - \frac{y_m^T}{y_m^{T\prime}} C \right)^\dagger$ are given by

$$\begin{aligned} m_a^2 &= \left| \sqrt{3} \frac{v_H}{\Lambda} \left(y_e - \frac{y_m^T}{y_m^{T\prime}} y'_e \right) v \right|^2, \\ m_b^2, m_c^2 &= \left| \sqrt{3} \frac{v_H}{\Lambda} \left(y_m - \frac{y_m^T}{y_m^{T\prime}} y'_m \right) v \pm 3i \frac{v_H}{\Lambda} \left(y_m^5 - \frac{y_m^T}{y_m^{T\prime}} y_m^{5\prime} \right) v_5 \right|^2. \end{aligned} \tag{5.37}$$

With these constraints, the likelihood of m_μ^2/m_τ^2 to be within $10^{-3} - 10^{-2}$ is $\sim 35\%$.

$50,000$ sets of random parameters based on the above constraints were generated. Out of these parameter sets, those with y'_e and y_m^5 generated from the constraints that are not $O(1)$ are rejected, together with those with m_μ^2/m_τ^2 outside $10^{-3} - 10^{-2}$. This leaves $\sim 17,000$ parameter sets that form $\mathcal{C}_2$.

We note that this method of imposing constraints to generate parameter sets is not ideal, for it excludes regions of parameter space with the correct mass eigenvalues that do not satisfy the constraints, should such regions exist. A better way is to generate a much larger initial number of unconstrained parameter sets from which the second collection can then be extracted from, although this is also computationally much more intensive.

Chapter 6
Co-Decaying Dark Matter[1]

Chapter abstract

We propose a new mechanism for thermal dark matter freezeout, termed *Co-Decaying Dark Matter*. Multi-component dark sectors with degenerate particles and out-of-equilibrium decays can co-decay to obtain the observed relic density. The dark matter density is exponentially depleted through the decay of nearly degenerate particles, rather than from Boltzmann suppression. The relic abundance is set by the dark matter annihilation cross-section, which is predicted to be boosted, and the decay rate of the dark sector particles. The mechanism is viable in a broad range of dark matter parameter space, with a robust prediction of an enhanced indirect detection signal. Finally, we present a simple model that realizes co-decaying dark matter.

6.1 Introduction

The nature of dark matter (DM) is one of the most important open questions in physics. The possibility that dark matter is a thermal relic with mass around the weak scale is intriguing, but has been under significant experimental pressure from direct detection [316–318] and at the LHC [319]. This motivates the study of models which are not constrained by these searches, but can still be discovered by

[1]Based on J. A. Dror, E. Kuflik and W. H. Ng, *Phys. Rev. Lett.* **117** (2016) 211801, [1607.03110]. During the preparation of this work we became aware of [315] which considers a similar scenario.

indirect detection, where limits are weaker and have made rapid progress in recent years [320].

Mechanisms for thermal dark matter freezeout usually rely on the DM remaining in chemical and thermal equilibrium with the Standard Model (SM) bath while non-relativistic, which leads to depletion of DM through Boltzmann suppression. In this work we consider the possibility that part of the dark sector decays out of equilibrium with the SM. This delays the exponential suppression of the DM density well beyond the point where the DM candidate becomes non-relativistic.

The mechanism, which we refer to as *Co-Decaying Dark Matter*, has the following properties:

1. The dark sector has decoupled from the SM before it becomes non-relativistic.
2. The lightest dark sector particle decays into the SM out of equilibrium.
3. The dark sector contains additional particles that are (approximately) degenerate with the decaying particle, and remain in chemical and thermal equilibrium with it until freezeout. One or more of these particles are DM candidates.

Co-decaying DM will be a generic feature of large dark sectors in which the lightest state decays. To illustrate the idea, we will focus on the simplified case of two degenerate dark sector particles: A will be the DM candidate, and B will be the decaying state, with sizable annihilations $AA \to BB$.

After the dark sector decouples from the SM bath, the A and B comoving entropy density is conserved, and their number density does not exponentially deplete when they become non-relativistic (in contrast to the Weakly Interacting

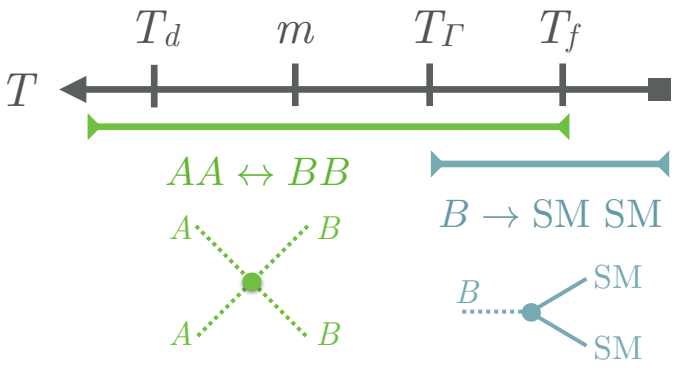

Figure 6.1: Co-decay dark matter timeline. At T_d the SM and dark sector decouple; at T_Γ the decay of B's begin to deplete the dark sector density; and at T_f the $AA \leftrightarrow BB$ process freezes out, resulting in a relic abundance for the A particles.

Massive Particle (WIMP)). Instead, the exponential suppression is delayed until the B's begin decaying:

$$n_A \sim n_B \propto e^{-\Gamma_B t} \simeq e^{-\frac{1}{2}\Gamma_B/H}\,, \tag{6.1}$$

where $n_{A,B}$ is the number density, Γ_B is the decay rate of the B particle, and H is the Hubble parameter. The A population tracks the B population until the $AA \to BB$ process cannot keep up with the expansion of the universe. At this point the A population freezes out and the B's continue to decay. The relic density of A is then set by both the annihilation rate, $\langle\sigma v\rangle$, as well as the B decay rate, Γ_B. A schematic illustration of the timeline for co-decaying DM is shown in Figure 6.1.

The delay in the starting point of exponential suppression from the temperature in which DM becomes non-relativistic to the temperature at which B-decay begins, causes freezeout to occur at later times than the WIMP. The DM relic density has less time to redshift to today, and therefore, must have a smaller density at freezeout. In order to match the observed DM relic abundance a larger annihilation cross-section is required. This leads to a boosted indirect detection signal relative to WIMP models.

Previous work on multi-component dark sectors where interactions within the dark sector are necessary to get the correct dark matter relic abundance is extensive. Some examples including co-annihilating [72, 321], Secluded [73], SIMP [76,322], Cannibalising [74,75,77,315,323,324] and Forbidden [72,325] DM. Additionally, models of particle decays affecting the relic abundance have been considered in [70, 315, 326–334]. The freezeout mechanism of co-decaying DM is unique, with differing phenomenology. Furthermore, we emphasise that while we are mainly interested in the implications on dark matter, the dynamics studied here have a broad impact and can take place for any thermal relic.

In this chapter we study the co-decaying DM mechanism. We present an intuitive estimate of the relic density and check the results numerically using the Boltzmann equations. The constraints and signals of co-decaying DM are described, with a significant enhancement in the indirect detection signature. We conclude by presenting an explicit model realizing the phenomena.

6.2 Freezeout and Relic Abundance

The DM relic abundance can be solved in the standard sudden freezeout approximation, when $AA \to BB$ annihilations effectively stop:

$$n_{A,f}\langle\sigma v\rangle_f = H_f \implies \Omega_A = \frac{s_0}{\rho_c}\frac{\sqrt{g_{\star,m}}}{\sqrt{g_{\star,f}}}\frac{mH_m}{s_m}\frac{x_f}{\langle\sigma v\rangle_f}. \tag{6.2}$$

Here m is the DM mass, $x_i = m/T_i$, s is the entropy density of the SM bath, and the subscripts m and f denote quantities at temperatures $T = m$ and freezeout, respectively[2]. Note that Eq. (6.2) is identical to the standard WIMP scenario.

[2]Throughout this section we will neglect the differences in effective entropy degrees of freedom $g_{\star s}$ and effective energy degrees of freedom $g_\star$.

However, for co-decaying DM, we will see that $x_f \gg 1$, leading to a boosted annihilation cross section relative to the standard WIMP case, where $x_f \simeq 20$.

We now compute the SM and dark sector temperatures at freezeout. To this end, we study the temperature evolution of the dark sector through the three stages depicted in Figure 6.1: from the time of decoupling of the dark sector from the SM (T_d), to the onset of the B decay (T_Γ), and until freezeout of the $AA \to BB$ annihilations (T_f). We use the d, Γ, and f subscripts throughout to denote quantities evaluated at these stages, respectively, and primes to denote dark sector (total $A + B$) quantities.

At high temperatures, A and B decouple from the SM plasma when relativistic. The entropy densities in each sector are separately conserved until the decay of B begins, and therefore

$$s'_\Gamma = \frac{s'_d}{s_d} s_\Gamma \equiv \xi s_\Gamma \,, \tag{6.3}$$

The dark sector number density at the onset of decay, roughly when $\Gamma_B \simeq H_\Gamma$, is given by the second law of thermodynamics for non-relativistic particles:

$$n'_\Gamma = \frac{T'_\Gamma}{m - \mu'_\Gamma + \frac{5}{2} T'_\Gamma} \xi s_\Gamma \,, \tag{6.4}$$

where μ' is the chemical potential of A and B.

While the $AA \leftrightarrow BB$ process is fast, the A density matches the B density. Taking the number of degrees of freedom in A and B to be equal (which we will assume throughout the chapter for simplicity), the total dark sector density at the time of $AA \leftrightarrow BB$ freezeout is

$$n'_f a_f^3 = n'_\Gamma a_\Gamma^3 e^{-\frac{1}{2}\Gamma_B (t_f - t_\Gamma)} \simeq \frac{\xi s_\Gamma a_\Gamma^3}{x'_\Gamma - \frac{\mu'}{T'_\Gamma} + \frac{5}{2}} e^{-\frac{1}{4}\frac{\Gamma_B}{H_f}} \,. \tag{6.5}$$

where a is the cosmic scale factor. The A abundance is hence depleted through the decay of B particles. Using Eq. (6.2) with Eq. (6.5), the temperature at freezeout

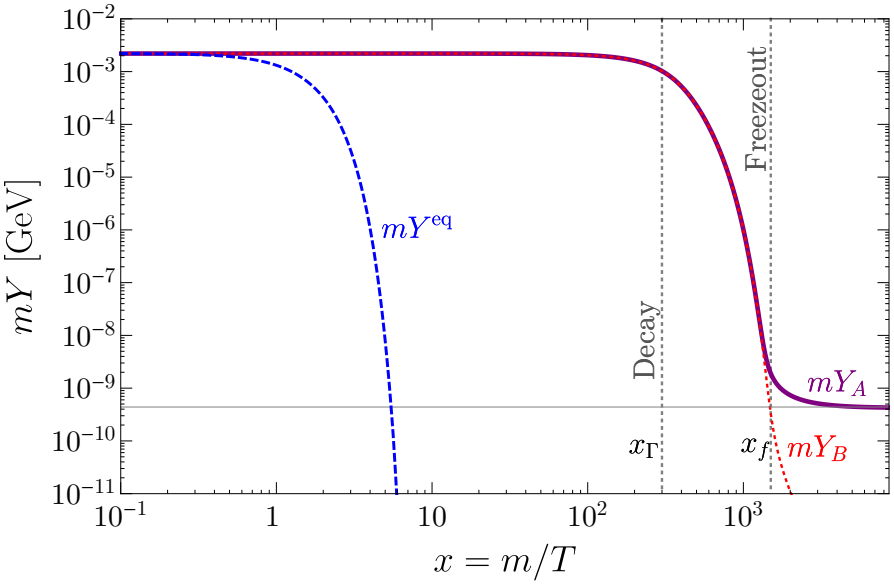

Figure 6.2: Yields ($Y \equiv n/s$) as a function of SM temperature without cannibalism for a benchmark point $g_A = g_B = 1$, $m = 1\,\text{GeV}$, $\sigma = 1 \times 10^{-30}\,\text{cm}^2$, $\Gamma_B = 6 \times 10^{-23}\,\text{GeV}$. The (**purple**/solid) and (**red**/dotted) lines show the yield for A and B particles, respectively. For comparison, the (**blue**/dashed) line shows the yield assuming the DM was in chemical and thermal equilibrium. For this choice of parameters $x_\Gamma \simeq 300$, while freezeout occurs at $x_f \simeq 1500$. The dark temperature at freezeout is $x'_f \simeq 5 \times 10^6$.

is given by

$$x_f \simeq \frac{2}{\sqrt{\Gamma_B/H_m}} \log^{1/2} \frac{\frac{2}{\sqrt{\pi}} \frac{s_m}{H_m} \xi\sigma}{x_f \sqrt{x'_f} x'_\Gamma (1 - \frac{\mu'_\Gamma}{m} + \frac{5}{2x'_\Gamma})}\,, \tag{6.6}$$

where $n_{A,f} = \frac{1}{2} n'_f$ and for brevity we have dropped ratios of $g_\star$. Here we have taken

$$\langle \sigma v \rangle = \frac{4}{\sqrt{\pi}} \frac{\sigma}{\sqrt{x'}} \tag{6.7}$$

for $x' \gg 1$ and s-wave scattering, where σ is the $2 \to 2$ cross-section at threshold. (For reference, note that the observed relic density for a WIMP would require $\sigma \simeq 10^{-36}\,\text{cm}^2$.) Since Γ_B/H_m may be as small as 10^{-18} (see Figure 6.3), x_f may be as large as 10^8.

The chemical potential and dark temperature will depend on whether number

changing processes are active in the A, B system, e.g., $3 \to 2$ processes. Without number changing processes, the comoving entropy and number densities are separately conserved in the dark sector between decoupling and decay ($s'_\Gamma/s_\Gamma = s'_d/s_d$ and $n'_\Gamma/s_\Gamma = n'_d/s_d$). This decreases the dark temperature relative to the SM temperature, while inducing a chemical potential:

$$x'_\Gamma \simeq \frac{1}{3.7}\left(\frac{g_{\star,d}}{g_{\star,\Gamma}}\right)^{\frac{2}{3}} x_\Gamma^2, \qquad \frac{\mu'_\Gamma}{m} \simeq 1 - \frac{3}{2x'_\Gamma} \quad \text{(w/o cannib)}, \tag{6.8}$$

In contrast, if number changing processes are active, cannibalisation can occur [75]. The SM temperature decreases exponentially relative to the dark sector, while the chemical potential is held fixed ($\mu' = 0$). Using conservation of comoving entropy in the hidden sector, one finds

$$x'_\Gamma \simeq \log \frac{x_\Gamma^3}{3.\,\xi\, x_\Gamma'^{1/2} g_{\star,\Gamma}}, \qquad \frac{\mu'_\Gamma}{m} = 0 \quad \text{(w cannib)}. \tag{6.9}$$

In both cases, the dark temperature at freezeout is redshifted from the temperature at decay,

$$x'_f \simeq x'_\Gamma \left(\frac{a_f}{a_\Gamma}\right)^2 \sim x'_\Gamma \left(\frac{x_f}{x_\Gamma}\right)^2. \tag{6.10}$$

Note that the dark matter will have a large energy density before it decays, and may come to dominate the energy density of the universe. When the DM decays, it will release a significant amount of entropy and reheat the SM bath. However, since the reheating occurs before DM freezeout, the entropy dump does not dilute the DM relic abundance. The most important effects are a delay in the start of the decay and a modification to the final relationship in Eq. (6.10). These effects are taken into account in the numerical solutions to the Boltzmann equations and in computing the viable parameter space.

Combining Eqs. (6.2) and (6.6) to (6.10), the relic abundance in the absence

of cannibalisation and when cannibalisation is active throughout is:

$$\frac{\Omega_A}{\Omega_{\rm DM}} \simeq \left(\frac{10^{-36}}{\sigma/{\rm cm}^2}\right) \times \begin{cases} \left(\frac{m}{\rm GeV}\right)\left(\frac{10^{-18}}{\Gamma_B/m}\right) & \text{(w/o cannib)}, \\ \left(\frac{m}{\rm GeV}\right)^{\frac{1}{2}}\left(\frac{10^{-17}}{\Gamma_B/m}\right)^{\frac{1}{2}} & \text{(w cannib)}. \end{cases} \tag{6.11}$$

where we have taken, $g_{\star,\,d} = 106.75$, and $\Omega_{\rm DM} = 0.27$ [66]. Here and throughout we will take the entropy density ratio at decoupling, defined in Eq. (6.3), to be $\xi = (g_A + g_B)/g_{\star,\,d} \simeq 0.02$.

Generically in any given model, one expects number changing self-interactions to be present, which leads to some amount of cannibalisation. Additionally, in much of parameter space cannibalisation can shut off before decays begin. Therefore, a realistic scenario will likely be between the two limiting cases in Eq. (6.11).

6.3 Boltzmann equations

We now present a numerical study of co-decaying dark matter. To track the number densities of A and B as well as the dark temperature T', 3 different equations are required:

$$\begin{aligned} &\dot{n}_A + 3Hn_A = -\langle\sigma v\rangle(n_A^2 - n_B^2), \\ &\dot{n}_{A+B} + 3Hn_{A+B} = -\left(\langle\Gamma_B\rangle_{T'} n_B - \langle\Gamma_B\rangle_T n_T^{\rm eq}\right), \\ &\dot{\rho}_{A+B} + 3H(\rho_{A+B} + P_{A+B}) = -m\Gamma_B\left(n_B - n_T^{\rm eq}\right), \end{aligned} \tag{6.12}$$

where $\langle\Gamma_B\rangle_{T(T')}/\Gamma_B = m\langle E_B^{-1}\rangle_{T(T')}$ is the thermally averaged inverse boost factor over the DM (SM) phase-space distributions. Time derivatives can be related to derivatives of the SM temperature T using the Friedman equation and second law

of thermodynamics,

$$H^2 \equiv \left(\frac{\dot{a}}{a}\right)^2 = \frac{8\pi G}{3}(\rho + \rho'),$$
$$a\frac{d}{da}(s\,a^3) = \frac{1}{T}\frac{d(\rho\,a^4)}{da} = \frac{m\Gamma_B}{HT}\left(n_B - n_T^{\rm eq}\right)a^3, \tag{6.13}$$

where G is the gravitational constant.

If number-changing processes in the dark sector are present, such as $3 \to 2$ processes, then there are additional terms in the number density equations of the form

$$-\left\langle \sigma v^2 \right\rangle_{ijk\to lm}\left(n_i n_j n_k - n_l n_m n^{\rm eq}\right), \tag{6.14}$$

where n_i can be n_A or n_B.

The Boltzmann equations, Eq. (6.12), are straightforward to solve numerically, and the results for a benchmark point are given in Figure 6.2. As shown, the dark sector does not follow the equilibrium distribution; instead it undergoes exponential decay at a later time. When the dark matter becomes non-relativistic ($x \simeq 1$), the co-moving number density remains constant, until decay begins ($x \simeq x_\Gamma$). The A density matches the B density until freezeout ($x \simeq x_f$) , where the DM candidate A decouples, while B continues to decay. For smaller Γ_B, the co-moving number density remains constant for longer and the decays will begin later. Depending on the size of Γ_B, the cross section needed to decouple at the correct time, and match the observed relic abundance, can be orders of magnitude larger than those of the WIMP scenario. The solutions to the Boltzmann equations match well the analytic estimates given by Eq. (6.11).

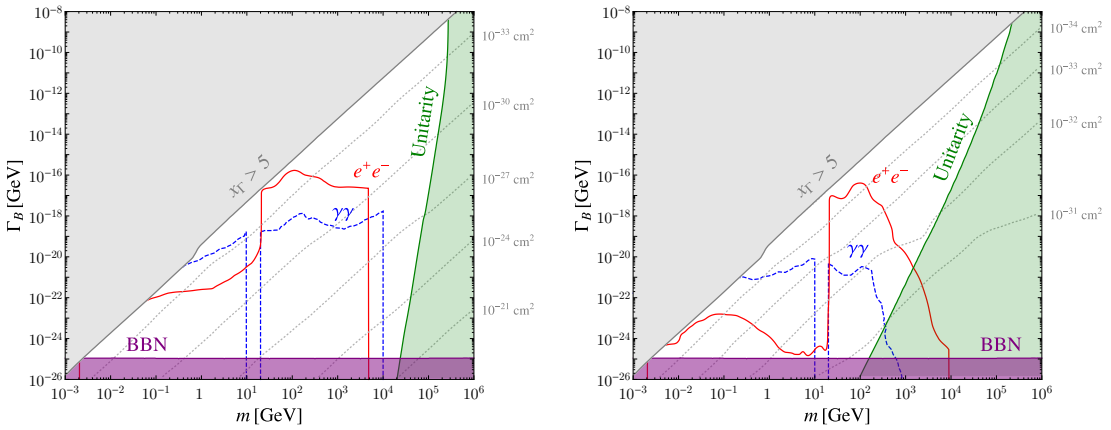

Figure 6.3: The viable parameter space for co-decaying dark matter assuming no cannibalisation (**Left**), and a cannibalising dark sector (**Right**). The central white region shows the range of validity of the model. The different regions show constraints from N_{eff} (**purple**); DM decays out of equilibrium (**gray**); unitarity constraints (**green**); and indirect detection assuming decays into e^+e^- (**red**/solid) or $\gamma\gamma$ (**blue**/dashed), excluding the region below the curve. The gap in the $\gamma\gamma$ limit between $10 - 20\,\text{GeV}$ is due to thresholds used in the two recasts. The **light gray** dotted lines represent contours of constant σ with values indicated on the right.

6.4 Signatures and constraints

We now discuss the signatures and constraints of co-decaying dark matter , whose parameter space is characterized by m, Γ_B, and σ. The viable parameter space is summarised in Figure 6.3, where the dotted gray lines represent contours of constant σ. As expected by the rough estimate in Eq. (6.11), the cross section contours are much more widely spaced without cannibalisation than with.

First, the co-decay setup requires B to decay out of equilibrium; otherwise the dark matter candidate will be Boltzmann suppressed when it becomes non-relativistic, effectively reducing to the WIMP scenario. This corresponds to $x_\Gamma \gtrsim 1$, though requiring that the DM does not re-thermalize with the SM imposes $x_\Gamma \gtrsim 5$. This is depicted by the gray shaded area in Figure 6.3.

Next we consider constraints on $N_{\rm eff}$ [335, 336]. This gives the rough condition that the DM decays before big bang nucleosynthesis (BBN), $\Gamma_B \gtrsim H_{m_e}$. This is depicted by the shaded purple regions in Figure 6.3.

Unitarity places constraints on the size of the thermally averaged cross section. The requirement of unitarity is given for s-wave scattering by [337],

$$\langle \sigma v \rangle_f \leq \frac{4\pi \langle v^{-1} \rangle_f}{m^2} \quad \Longrightarrow \quad \sigma \lesssim \frac{\pi\sqrt{2}}{m^2} x'_f, \tag{6.15}$$

where $\langle v^{-1} \rangle_f \simeq \sqrt{2x'_f/\pi}$ is the thermally averaged inverse velocity. The severity of the bound is dependent on whether or not the dark sector is cannibalising. Without cannibalisation, fixing the relic density corresponds to $\sigma \propto 1/\Gamma_B$ and $x'_f \propto 1/\Gamma_B$, and thus the unitarity bound is roughly Γ_B-independent. On the other hand, with cannibalisation, $\sigma \propto 1/\sqrt{\Gamma_B}$ and x'_f is only log-dependent on Γ_B, and the unitarity bound reads:

$$\frac{m}{100\,\text{TeV}} \lesssim \begin{cases} 1 & \text{(w/o cannib)}, \\ 100 \left(\frac{\Gamma_B}{\text{GeV}}\right)^{1/6} & \text{(w cannib)}\,. \end{cases} \tag{6.16}$$

These relations are modified for small Γ by matter-domination effects. The resulting unitarity bounds are shown in the green shaded regions in Figure 6.3.

Since co-decaying DM is decoupled from the SM, it is difficult to discover using direct detection or direct production. The signature from indirect detection is, however, enhanced with respect to WIMP candidates due to the large thermally averaged cross section. This makes indirect detection a powerful tool to probe co-decaying DM.

We map the current constraints from telescope and satellite data on the (m, Γ_B) parameter space, using the analyses of Refs. [338, 339]. The constraint on our four-body final state from two-body final states analysed in [338, 339] are obtained by

rescaling the mass and cross-section limits appropriately. For illustration, we plot the full constraints from B decays into only e^+e^- (red, solid) or into only $\gamma\gamma$ (blue, dashed) in Figure 6.3, excluding the region below the curves.

Lastly we note that co-decaying dark matter is not constrained by the Cosmic Microwave Background, since the thermally averaged cross-sections is always velocity suppressed.

The combined allowed parameter space is shown in Figure 6.3, without cannibalisation (left-panel) and with cannibalisation (right-panel). We learn that co-decaying dark matter can occur over a broad range of DM masses, spanning an MeV up to hundreds of TeV, and decay rates spanning many orders of magnitude.

6.5 Mass splitting

Thus far, we focused on degenerate dark sector particles, which can result from an underlying symmetry. However, a realistic model may include symmetry-breaking effects, which can lift the degeneracy. It is then important to understand the effect of mass-splittings on the co-decaying DM framework. We leave a detailed study of the phenomenology of co-decays with mass splittings to future work and highlight the expected features here.

If $m_A > m_B$, the co-decay mechanism remains conceptually unchanged. However, for mass splitting $\mathcal{O}(\%)$ or more, the parameter space to produce the observed relic abundance can differ significantly. To understand this, consider s-wave annihilation, which can proceed as zero temperature in the presence of mass-splittings.

Comparing the annihilation rates at large x', we have

$$\langle \sigma v \rangle_{m_A > m_B} \simeq \frac{\sqrt{\pi x'}}{2} \langle \sigma v \rangle_{m_A = m_B} \tag{6.17}$$

for fixed matrix-element. Since freezeout occurs for $x' \gg 1$, obtaining the observed relic abundance requires σ smaller than in the degenerate case.

If $m_A < m_B$, then annihilations proceed off the exponential tail of A's velocity distribution, $\langle \sigma v \rangle_{AA \to BB} \propto e^{-2\Delta x'}$,, where $\Delta \equiv (m_B - m_A)/m_A$. This exponential suppression of the cross-section significantly alters the parameters required to produce the correct relic density.

6.6 Model

Having described the general framework, we now present a simple model where co-decay can drive dark matter freezeout. Consider a dark $\mathrm{SU}(2)_D$ gauge theory with coupling g_D, and a dark Higgs doublet Φ_D,

$$\mathcal{L} \supset D^\mu \Phi_D^\dagger D_\mu \Phi_D - \frac{1}{4} F_D^{a,\mu\nu} F^a_{D,\mu\nu} - \lambda_D \left(\Phi_D^\dagger \Phi_D - \frac{v_D^2}{2} \right)^2 , \tag{6.18}$$

The dark Higgs' VEV, $v_D/\sqrt{2}$, spontaneously breaks $\mathrm{SU}(2)_D$. All three dark gauge bosons acquire masses $m_D = \frac{1}{2} g_D v_D$, while the dark Higgs boson, h_D, gains a mass $m_{h_D} = \sqrt{2\lambda_D} v_D$. The stability and degeneracy of the gauge bosons are ensured by an unbroken SU(2) custodial symmetry. We take $m_{h_D} \gg m_D$, which decouples the dark Higgs.

We introduce a dimension-six operator, which explicitly breaks the custodial symmetry down to U(1),

$$\mathcal{L} \supset \frac{(\Phi_D^\dagger D^\mu \Phi_D)(\Phi^\dagger D_\mu \Phi)}{\Lambda^2} , \tag{6.19}$$

where Φ is the SM Higgs doublet. This can be generated by integrating out heavy fermions charged under both $\mathrm{SU}(2)_D$ and the SM gauge symmetry, $\mathrm{SU}(2)_L$. This operator mixes the gauge boson $Z_D \equiv W_D^3$ and the Z boson, decaying Z_D to the SM. The remaining gauge bosons $W_D^\pm \equiv (W_D^1 \mp i W_D^2)/\sqrt{2}$ are stable since they are the lightest particles charged under the unbroken U(1) custodial symmetry.

The $W_D^\pm$ are stable and play the role of A, while the nearly-degenerate Z_D plays the role of B. For $m_D \sim$ GeV and $\Lambda \sim 10$'s TeV, negligible mass differences between $W_D^\pm$ and Z_D are generated, and corrections to electroweak precision observables are small. Number-changing processes, e.g., $Z_D Z_D Z_D \to W_D^+ W_D^-$, are large and cannibalisation effects must be taken into account.

This model can be mapped onto the constraints of the previous sections using

$$\sigma = \frac{688}{3}\frac{\alpha_D^2}{m_D^2}, \qquad \Gamma_{Z_D} = \frac{1}{48\pi^2\alpha_D^2}\frac{m_D^5}{\Lambda^4}|g|^2, \tag{6.20}$$

where $|g|^2 \equiv \sum_i |g_i|^2 \left(|g_V^i|^2 + |g_A^i|^2\right)$, g_V (g_A) is the vector (axial) coupling of the fermion i to the Z-boson.

Lastly, we comment on further model building directions. To build a viable model one needs a approximate symmetry to achieve degeracy between the lightest dark states, but whose breaking induces a decay into the SM. In this section we considered the possibility that a remnant of a broken SU(2) gauge symmetry protects the masses, however interesting alternatives include flavour symmetries or supersymmetry, both of which could play a role in a larger framework. Depending on the type of symmetry used to ensure the degenaracy, this may or may not induce significant cannibalisation.

Chapter 7
Re-visiting the bounds on hydrogen-antihydrogen oscillations from diffuse γ-ray surveys[1]

Chapter abstract

Surveys of diffuse γ-ray in the interstellar medium (ISM) can be used to probe hydrogen-antihydrogen oscillations, by detecting the γ-ray emission from antihydrogen annihilation. A bound on the oscillation parameter δ was originally derived by Feinberg, Goldhaber and Steigman (1978). In this chapter, we re-visit the original derivation by performing a more detailed analysis that (1) incorporates suppression effects from additional elastic and inelastic processes, (2) treats the ISM as a multi-phase medium, and (3) utilises more recent γ-ray data from the *Fermi* Large Area Telescope. We find that suppression from elastic scattering plays a more important role than previously thought, while the multi-phase nature of the ISM affects how the γ-ray data should be utilised. We derive a more accurate bound on the oscillation period that is about an order of magnitude weaker than the older bound.

7.1 Introduction

At the classical level, baryon (B) and lepton (L) numbers are conserved quantities in the Standard Model (SM). One of Sakharov's condition [17] for a dynamical explanation of the baryon asymmetry in the universe requires that B conservation

[1]Based on Y. Grossman, W. H. Ng and S. Ray, *Phys. Rev.* **D98** (2018) 035020, [1806.08233].

be violated. Mechanisms like electroweak baryogenesis [79] or leptogenesis [340] achieve this through sphaleron processes that makes use of $B + L$ violation in the SM at the quantum level, while mechanisms like baryogenesis in the Grand Unified Theories (GUT) [341] introduce processes that directly violate B at the classical level. However, proton decay imposes strong constraints on models that directly allow $\Delta B = \Delta L = 1$ processes. One intriguing possibility is to consider models [342, 343] where proton decay is forbidden/suppressed, but yet allow processes with $\Delta B = 2$ or $\Delta B = \Delta L = 2$ to occur. In these cases, processes such as neutron-antineutron oscillations [344], $pp \to e^+e^+$ annihilations [345] or hydrogen-antihydrogen (H-$\bar{\text{H}}$) oscillation may become more important probes of B violation. In this chapter we concentrate on H-$\bar{\text{H}}$ oscillation.

One way to detect H-$\bar{\text{H}}$ oscillations is through γ-rays from the annihilation of $\bar{\text{H}}$ with other particles in its vicinity (henceforth called "oscillation-induced γ-rays"). A good place to look for this is the interstellar medium (ISM), first because of the immense amount of atomic hydrogen present, and second because the low density allow a larger oscillation amplitude and hence a larger proportion of $\bar{\text{H}}$ to exist than in terrestrial sources. These γ-rays then show up in diffuse γ-ray surveys on top of other γ-ray emitting processes, such as cosmic ray (CR) interaction with matter. This idea is not new and a bound on the oscillation was first derived in [84]. The goal of the present chapter is to revisit the bounds, for the following reasons.

1. In the original derivation, the amplitude of oscillation was assumed to be limited by H-$\bar{\text{H}}$ annihilation. However, we do not know *a priori* how this compares to the effects of other processes such as elastic scattering.
2. We now have a better understanding of the phases of the ISM, γ-ray production within the ISM, as well as updated γ-ray survey results from the *Fermi*

Large Area Telescope (LAT).

3. Finally, many steps are involved in deriving the experimental bounds on the oscillations. While we are only interested in an order-of-magnitude estimate, we want to reduce the uncertainty in each step as much as possible to avoid having the cumulative errors become too large. Therefore, besides improving on the oscillation and ISM model, we also want to utilise updated parameter values from literature rather than just rely on crude estimates.

This chapter is structured as follows. In Section 7.2, we present a model that describes H-$\bar{\text{H}}$ oscillations in a medium, and use the model to derive a formula for the oscillation-induced γ-ray emissivity. In Section 7.3, we use this formula, together with available data for various elastic and inelastic processes, to calculate the emissivities of the relevant phases of the ISM. It then allows us in Section 7.4 to obtain a bound on the oscillation parameter δ based on the *Fermi* LAT data presented in [346]. We conclude in Section 7.5 with a comparison of our bound with that from other $\Delta B = \Delta L = \pm 2$ processes. To keep the text focused, most technical details have been placed in the appendices.

7.2 Model of H-$\bar{\text{H}}$ oscillation

To infer the oscillation-induced γ-ray emissivity, we need to know the probability of an H atom in the ISM becoming a $\bar{\text{H}}$. This in turn can be derived from a single-atom model of H-$\bar{\text{H}}$ oscillation. The vacuum formalism is very straightforward; however the main issue here is to account for interactions with the environment. Some of the effects are well-understood: for example, forward scattering gives rise to coherent matter effects known from neutrino oscillations, while inelastic processes

such as $\bar{\mathrm{H}}$ annihilation cause the state to leave the Hilbert space of interest and hence their effects are analogous to decays in meson oscillations. Both of these effects can be taken care of by modifications to the effective Hamiltonian.

Less well-recognised are effects that require going beyond the effective Hamiltonian, and require a density matrix formalism. First, say H and $\bar{\mathrm{H}}$ have different elastic scattering amplitudes off the same target, i.e. $f(\theta) \neq \bar{f}(\theta)$, where θ is the angle of scattering. Then non-forward scattering cause the identity of the atom (H or $\bar{\mathrm{H}}$) to become entangled with its momentum and hence a two-level pure state formalism does not work if we want to incorporate elastic scattering beyond just forward scattering. Also, since the scattering environment is usually random, even a pure state formalism incorporating both identity and momentum degrees of freedom is insufficient. Second, chemical reactions such as recombination generate new "unoscillated" H atoms to replenish those lost to inelastic processes. Since these reactions should be treated as classical source terms, again a density matrix formalism is required. The model we adopt is similar to the original Feinberg-Weinberg model [347] that was also used in [84]. We then extend it to take into account more general sources of suppression. We also highlight the differences between our work and that of [84].

7.2.1 Model description

We regard H and $\bar{\mathrm{H}}$ as basis states of a two-level system (Hilbert space $\mathcal{H}_A$). In principle, there are other degrees of freedom such as momentum, atomic level and spin (Hilbert space $\mathcal{H}_B$), but since we are only interested in finding the probability of being $\bar{\mathrm{H}}$, we trace them out in the full density matrix $\rho_{\mathrm{full}}(t)$ to obtain a reduced 2×2 density matrix $\rho(t)$. The quantum kinetic equation of $\rho(t)$ will then depend on

the moments of the other degrees of freedom, e.g. $\mathrm{Tr}_B[p^2\rho_{\rm full}(t)]$, and is hence not closed. To close this equation, we replace, say, the example above by $\langle p^2(t)\rangle\rho(t)$, and assume that $\langle p^2(t)\rangle$ is just given by the present-day value (since we are only interested in a quasi-steady solution). Also, since most of the atoms in the ISM phases of interest are in the $1S$ state, any average involving atomic level and spin is equivalent to a $1S$ hyperfine average.

Elastic scattering

First, we take into account elastic scattering of the atom with other particles (targets). Let i denote the target species. Then $\rho(t)$ satisfies the kinetic equation [347]

$$\partial_t\rho(t) = -i[H\rho(t) - \rho(t)H^\dagger] + \sum_i \left[n_i v_i \int d\Omega F_i(\theta)\rho F_i^\dagger(\theta)\right], \qquad (7.1)$$

where

$$H \equiv \begin{pmatrix} E - \sum_i \left[\frac{2\pi n_i v_i}{p_i} f_{i,p_i}(0)\right] & \frac{\delta}{2} \\ \frac{\delta^*}{2} & E - \sum_i \left[\frac{2\pi n_i v_i}{p_i} \bar{f}_{i,p_i}(0)\right] \end{pmatrix}, \quad F_i(\theta) \equiv \begin{pmatrix} f_{i,p_i}(\theta) & 0 \\ 0 & \bar{f}_{i,p_i}(\theta) \end{pmatrix}, \qquad (7.2)$$

and the symbols used here are defined as follows:

- E: the mean energy of an atom in vacuum (equal for H and $\bar{\rm H}$ by CPT) in the ISM rest frame,
- n_i: the number density of species i,
- v_i: the r.m.s. speed of approach between atom and a species i particle,
- p_i: the r.m.s. momentum in centre-of-mass frame of the atom and a species i particle,

- $f_{i,p_i}(\theta)$ ($\bar{f}_{i,p_i}(\theta)$): scattering amplitude of H ($\bar{\text{H}}$) off a species i particle with momentum p_i in centre-of-mass frame, and
- $\frac{\delta}{2}$: off-diagonal matrix element generated by $\Delta B = \Delta L = \pm 2$ operators.

The assumptions involved are presented in Appendix 7.A.1. We just explain a few features of Eq. (7.1) here. The first term describes the usual time-evolution with an effective non-Hermitian Hamiltonian H, comprising the energy E of the atom in vacuum, the oscillation term δ, and coherent forward scattering $f_{i,p_i}(0)$ and $\bar{f}_{i,p_i}(0)$, summed over all target species i. Differences in $f_{i,p_i}(0)$ and $\bar{f}_{i,p_i}(0)$ can suppress the oscillations, just like coherent matter effects in neutrino oscillations. The optical theorem ensures that even for elastic scattering $f_{i,p_i}(0)$ and $\bar{f}_{i,p_i}(0)$ are complex quantities, with the imaginary parts related to the total scattering rate. As a result, time evolution under the first term alone cause the total probability represented by $\text{Tr}(\rho)$ to decrease. This decrease is analogous to the effects of the "out" collision term in Boltzmann transport equation. Probability conservation is restored by the second term, analogous to the "in" collision term.

Inelastic and production processes

To complete the picture, we want to include inelastic processes as well. We argue in Appendix 7.A.2 that among all the inelastic processes, only those where the H/$\bar{\text{H}}$ atom "disappears" are potentially important. This includes ionisation, chemical reactions as well as $\bar{\text{H}}$ annihilation. Since these processes take the state out of the Hilbert space $\mathcal{H}_A$, they can be represented by imaginary contributions $i\omega_I/2$ and $i\bar{\omega}_I/2$ to the diagonal elements of H, where ω_I ($\bar{\omega}_I$) denotes the total rate of these processes per H ($\bar{\text{H}}$) atom.

However, just as $H/\bar{H}$ atoms can "disappear", they can also "reappear" through production process such as recombination and H_2 dissociation. These processes correspond to source terms for the ρ_{11} matrix element, which we introduce as $\omega_P \rho_{11}$ in Eq. (7.4). ω_P can be interpreted as the rate of H production per unit volume, normalised by the number density of H. Furthermore, if we assume that the ISM is in a quasi-steady state (approximate ionisation balance, chemical equilibrium, etc.), then this source term can be approximated as $\omega_P \simeq \omega_I$ up to a small difference of order the quasi-steady rate of change. In principle, we can also include a source term for ρ_{22}, e.g. from re-combination of CR positrons and antiprotons to form $\bar{H}$. However, based on measurements of the CR antiproton flux [348], this contribution is expected to be negligible compared to $\bar{H}$ production from oscillations at the upper bound of $|\delta|$.

The time-evolution equation is then given by

$$\partial_t \rho = -i[H\rho - \rho H^\dagger] + \sum_i \left[n_i v_i \int d\Omega F_i(\theta) \rho F_i^\dagger(\theta) \right] + \begin{pmatrix} \omega_P \rho_{11} & 0 \\ 0 & 0 \end{pmatrix} \tag{7.3}$$

with a modified effective Hamiltonian

$$H \equiv \begin{pmatrix} E - \sum_i \left[\frac{2\pi n_i v_i}{p_i} f_{i,p_i}(0) \right] - \frac{i}{2}\omega_I & \frac{\delta}{2} \\ \frac{\delta^*}{2} & E - \sum_i \left[\frac{2\pi n_i v_i}{p_i} \bar{f}_{i,p_i}(0) \right] - \frac{i}{2}\bar{\omega}_I \end{pmatrix}. \tag{7.4}$$

Reformulating the model

It is instructive to rewrite $\rho(t)$ as a column vector $\rho(t) \equiv (\rho_{11}, \rho_{12}, \rho_{21}, \rho_{22})^T$ [84]. The time evolution equation then becomes

$$\partial_t \rho(t) = M\rho, \tag{7.5}$$

where

$$M \equiv \begin{pmatrix} \omega_P - \omega_I & i\frac{\delta^*}{2} & -i\frac{\delta}{2} & 0 \\ i\frac{\delta}{2} & \epsilon' & 0 & -i\frac{\delta}{2} \\ -i\frac{\delta^*}{2} & 0 & \epsilon'^* & i\frac{\delta^*}{2} \\ 0 & -i\frac{\delta^*}{2} & i\frac{\delta}{2} & -\bar{\omega}_I \end{pmatrix}, \tag{7.6}$$

$$\epsilon' \equiv i\sum_i n_i v_i \left[\Delta_i + \int d\Omega \mathrm{Im}(\bar{f}^*_{i,p_i} f_{i,p_i})\right] - \left[\frac{\omega_I + \bar{\omega}_I}{2} + \sum_i \frac{n_i v_i}{2} \int d\Omega |f_{i,p_i} - \bar{f}_{i,p_i}|^2\right], \tag{7.7}$$

$$\Delta_i \equiv \frac{2\pi}{p_i} \mathrm{Re}[f_{i,p_i}(0) - \bar{f}_{i,p_i}(0)]. \tag{7.8}$$

Some observations:

- If $f_{i,p_i} = \bar{f}_{i,p_i}$, then all instances of f_{i,p_i} and $\bar{f}_{i,p_i}$ vanish from M. In other words, elastic scattering does not suppress oscillations unless it can differentiate between H and $\bar{\mathrm{H}}$ amplitude-wise. This means, for example, that we can ignore elastic scattering with photons.
- If $\omega_I = \bar{\omega}_I$, then their combined contributions to M is just proportional to the identity, so they only lead to an overall decay factor. Therefore, inelastic processes also do not suppress oscillations unless they can differentiate between H and $\bar{\mathrm{H}}$ rate-wise.
- Oscillations are also suppressed by the source term $\omega_P \rho_{11}$, although the physical mechanism is somewhat indirect. Here new H atoms that have yet to oscillate are being added to the system. This suppression is why despite our previous comment, we still need to consider inelastic processes such as photo-ionisation that have the same rate for H and $\bar{\mathrm{H}}$, since ω_I informs us about ω_P in the quasi-steady state.

Note that our formalism here is similar to the one used in [84] (see Eq. (2.4) there). However, they did not include a source term ω_P, and they also assumed that the only important process is H-$\bar{\text{H}}$ annihilation. As a result, they have $\bar{\omega}_I \gg \omega_I$ (since it is much easier for a $\bar{\text{H}}$ to find a H to annihilate with, than vice versa) and $|\epsilon'| \simeq \bar{\omega}_I/2$. In contrast, we do not make the same assumptions but instead consider a wide range of elastic and inelastic processes.

7.2.2 Formula for γ-ray emissivity

We want to use our model to derive a formula for the γ-ray emissivity. To do so, we need to find the solution to Eq. (7.5) that best describes a H/$\bar{\text{H}}$ atom in the ISM, from which we can then obtain the $\bar{\text{H}}$ number density and hence the emissivity.

Most of the parameters in M depend on the number densities of atomic hydrogen and other species in the ISM, so Eq. (7.5) is actually much harder to solve than it seems. However, since we are only interested in the quasi-steady solution, it is actually self-consistent to assume these parameters as constants, at least for timescales short compared to the quasi-steady rate of change. Even though the quasi-steady solution based on this assumption may become inaccurate at longer times, it does not matter since we are using *present-day* parameter values. In other words, the reference starting time is actually the present, so we read off the present-day $\bar{\text{H}}$ probability ρ_{22} from the solution at $t = 0$.

With this assumption, among the four eigenvectors of M, three have eigenvalues with negative real parts of order $|\epsilon'|$ or $\bar{\omega}_I$, while the fourth is given by

$$\lambda = \omega_P - \omega_I + \mathcal{O}(\epsilon^2|\epsilon'|, \epsilon^2|\bar{\omega}_I|) \tag{7.9}$$

where $\epsilon \equiv \text{Max}\left\{\left|\frac{\delta}{\epsilon'}\right|, \left|\frac{\delta}{\bar{\omega}_I}\right|\right\}$ is a small parameter. The first three solutions cor-

respond to transients that decay rapidly (although the actual decay rate may be somewhat different since these solutions are not consistent with the assumption about the parameters being constant), while the fourth solution does indeed change at the quasi-steady rate $|\omega_P - \omega_I|$ and is thus the one we want. The corresponding eigenvector is given by

$$v = \begin{pmatrix} 1 + \mathcal{O}(\epsilon^2) \\ -\frac{i\delta}{2(\epsilon' + \omega_I - \omega_P)} + \mathcal{O}(\epsilon^3) \\ \left[-\frac{i\delta}{2(\epsilon' + \omega_I - \omega_P)} + \mathcal{O}(\epsilon^3)\right]^* \\ -\left|\frac{\delta}{\epsilon' + \omega_I - \omega_P}\right|^2 \frac{\mathrm{Re}(\epsilon' + \omega_I - \omega_P)}{2(\bar{\omega}_I - \omega_I + \omega_P)} + \mathcal{O}(\epsilon^4) \end{pmatrix}. \tag{7.10}$$

We observe that of the four components, $v_1 \simeq 1$, $v_2 = v_3^* \sim \mathcal{O}(\epsilon)$, and $v_4 \sim \mathcal{O}(\epsilon^2)$.

Since $\frac{v_1}{v_1+v_4}$ and $\frac{v_4}{v_1+v_4}$ correspond to the probability of being H and $\bar{\mathrm{H}}$, we can estimate the rate of $\bar{\mathrm{H}}$ annihilation per unit volume as

$$\frac{v_4}{v_1} n_{\mathrm{H}} n_i \langle \sigma_i v_i \rangle \simeq -\left|\frac{\delta}{\epsilon'}\right|^2 \frac{\mathrm{Re}(\epsilon')}{2\bar{\omega}_I} \bar{\omega}_{\mathrm{ann}} \tag{7.11}$$

where $\bar{\omega}_{\mathrm{ann}}$ is the annihilation rate per $\bar{\mathrm{H}}$ (we allow it to differ from $\bar{\omega}_I$ in case there are other more important $\bar{\mathrm{H}}$ "disappearance" processes), and we have dropped the much smaller quasi-steady rate $|\omega_P - \omega_I|$ relative to $\bar{\omega}_I$ and ϵ'. This is a positive quantity since $\mathrm{Re}(\epsilon') < 0$. Note that ω_P has disappeared completely (it is not present in ϵ') since its main role is to cancel ω_I at certain places to give a much smaller quasi-steady rate that can then be neglected.

For comparison with γ-ray data later, it is useful to convert the previous rate per unit volume into an oscillation-induced emissivity per H atom, which gives

$$\epsilon_\gamma = -\frac{g_\gamma}{4\pi} \left|\frac{\delta}{\epsilon'}\right|^2 \frac{\mathrm{Re}(\epsilon')}{2\bar{\omega}_I} \bar{\omega}_{\mathrm{ann}} \,\mathrm{photons\,sr^{-1}}, \tag{7.12}$$

where g_γ is the average number of γ-ray photons emitted in the annihilation. We discuss its value below for specific situations.

7.3 Calculating the emissivities

In the previous section, we derived a formula for the oscillation-induced γ-ray emissivity per H atom, Eq. (7.12). To make further progress, we need numerical values of the parameters in this formula, except for the unknown $|\delta|$ that we want to constrain. We begin this section by identifying phases of the ISM that are expected to be the dominant sources of these γ-rays. Using available data for a wide variety of elastic and inelastic processes, we then calculate the parameter values and hence the emissivity for each phase. We adopt the standard astronomical notation of HI and HII for atomic and ionised hydrogen.

7.3.1 Phases of the ISM

The *Fermi* LAT data presented in Abdo *et al.* [346] focuses on γ-ray emission from HI and is hence of particular relevance to our work. We want to consider the same sector of the ISM, bounded by Galactic longitude $200^\circ < l < 260^\circ$, and latitude $22^\circ < |b| < 60^\circ$. Even within this sector, the ISM is not homogeneous and has a number of phases, each with a different HI density and presenting a different environment for H-$\bar{\text{H}}$ oscillations.

In Appendix 7.B, we describe these phases and explain why we expect most of the oscillation-induced γ-rays to come from three of them, namely the cold neutral medium (CNM), warm neutral medium (WNM) and warm ionised medium (WIM). Here we present a short description of these three phases, as well as the nominal values we assume for their physical properties [349–352]. T here represents the phase temperature, and x the ionisation fraction.

- CNM: Comprises clumps of cold HI clouds.

  $n_{\rm H} \simeq 50\,{\rm cm}^{-3}$, $T \simeq 80\,{\rm K}$, $x = 0.001$.

- WNM: Intercloud region containing warm diffuse HI.

  $n_{\rm H} \simeq 0.5\,{\rm cm}^{-3}$, $T \simeq 8000\,{\rm K}$, $x = 0.05$.

- WIM: Intercloud region containing warm diffuse HII.

  $n_{\rm H^+} \simeq 0.3\,{\rm cm}^{-3}$, $T \simeq 8000\,{\rm K}$, $x = 0.9$.

The uncertainties in these nominal values, in particular the ionisation fraction, is a significant source of error in our analysis. Henceforth, most values that we present should only be interpreted as *order-of-magnitude estimates*.

7.3.2 Emissivities of the CNM, WNM and WIM

We now want to determine the oscillation-induced emissivities of the three phases. To do so, we first need the values of ϵ', $\bar{\omega}_I$ and $\bar{\omega}_{\rm ann}$ used in the emissivity formula Eq. (7.12). The values we present below incorporate a wide range of elastic targets as well as inelastic processes, using available data on scattering phase shifts, cross-sections and reaction rate constants [353–365] (more details can be found in Appendix 7.C):

- CNM:

  $\epsilon' \simeq (-1 \pm i) \times 10^{-7}\,{\rm s}^{-1}$, mostly from elastic scattering with H.

  $\bar{\omega}_I \simeq \bar{\omega}_{\rm ann} \simeq 6 \times 10^{-8}\,{\rm s}^{-1}$, mostly from H-$\bar{\rm H}$ annihilation.

- WNM:

  $\epsilon' \simeq (-5 \pm 5i) \times 10^{-9}\,{\rm s}^{-1}$, mostly from elastic scattering with H.

  $\bar{\omega}_I \simeq \bar{\omega}_{\rm ann} \simeq 8 \times 10^{-10}\,{\rm s}^{-1}$, mostly from H-$\bar{\rm H}$ annihilation.

- WIM:

  $\epsilon' \simeq (-2-i) \times 10^{-8}\,\mathrm{s}^{-1}$, mostly from elastic scattering with e^-.

  $\bar{\omega}_I \simeq \bar{\omega}_{\mathrm{ann}} \simeq 7 \times 10^{-10}\,\mathrm{s}^{-1}$, mostly from H^+-$\bar{\mathrm{H}}$ annihilation.

Our estimate for ϵ' are a few orders of magnitude larger than in [84], where it was assumed that $2|\epsilon'| \simeq \bar{\omega}_I \simeq 10^{-10}\,\mathrm{s}^{-1}$. This discrepancy is mainly due to contributions from elastic scattering that they have neglected. Hence, their assumption that H-$\bar{\mathrm{H}}$ oscillations are mainly suppressed by $\bar{\mathrm{H}}$ annihilation is not justified.

With these values, we can finally obtain the following oscillation-induced γ-ray emissivities per H atom.

- CNM: $\epsilon_\gamma \simeq 2 g_\gamma |\delta|^2 \times 10^5\,\mathrm{s\,srad}^{-1}$.
- WNM: $\epsilon_\gamma \simeq 4 g_\gamma |\delta|^2 \times 10^6\,\mathrm{s\,srad}^{-1}$.
- WIM: $\epsilon_\gamma \simeq g_\gamma |\delta|^2 \times 10^6\,\mathrm{s\,srad}^{-1}$.

Since the γ-ray data in [346] starts at 100 MeV, using the experimental and simulation results in [366], we estimate the average number of photons from $\bar{\mathrm{H}}$ annihilation above this threshold to be $g_\gamma \simeq 2.7$.

7.4 Deriving bound on $|\delta|$ using *Fermi* LAT data

In this section, we explain how we derive a bound on the oscillation parameter $|\delta|$ using *Fermi* LAT data. The main idea is to compare the results of γ ray measurements with predictions from astrophysical models. The difference between them can then be used to constrain additional oscillation-induced emissivity and hence $|\delta|$.

More specifically, one can perform a linear regression of the observed γ ray intensity against the HI column density. The slope corresponds to the emissivity per H atom, and the offset (intercept) a spatially homogeneous source of emissivity. The observed slope can be compared with independent astrophysical predictions to constrain $|\delta|$, and this was indeed what was done in [84]. However, we argue that the oscillation-induced emissivity should really show up in the offset rather than the slope, which lacks an independent prediction. Therefore, the whole measured offset is used to constrain $|\delta|$. We explain these points in more details below.

7.4.1 Review of relevant γ-ray data

In this section we review the analysis and results in [346]. One of their goals was to determine the HI γ-ray emissivity, and compare it with predictions based on CR interaction with matter. The authors used *Fermi* LAT γ-ray data from the sector we previously described, in the energy range $100\,\mathrm{MeV} - 9.05\,\mathrm{GeV}$. This sector is known to be free of large molecular clouds. In this region, HII column-density is relatively smooth and is in the range $(1-2)\times 10^{20}\,\mathrm{cm}^{-2}$, while HI distribution is more clumpy with a column density in the range $(1-18)\times 10^{20}\,\mathrm{cm}^{-2}$.

Known background such as point sources and inverse Compton scattering of soft photons with CR electrons were subtracted, leaving only data that are expected to come from CR interaction with matter as well as an isotropic extragalactic diffuse background. By comparing the post-subtraction γ-ray intensity map (Figure 1 of [346]) with a HI column density map derived from 21 cm radio surveys (Figure 3 of [346]), the authors found a linear relationship between the γ-ray intensity I_γ and the HI column density $N(\mathrm{HI})$ for each energy bin, which we index by i (Figure 4

of [346])

$$I_{\gamma,i} \approx S_i \cdot N(\text{HI}) + O_i \tag{7.13}$$

where the slope S_i represents the HI emissivity per atom, and the offset O_i the contributions from residual particles and the extragalactic background. The authors found good agreement between the slope-derived HI emissivity and the predictions based on CR interaction with matter. Summing the results in Table 1 of [346] over the bins in the energy range $100 - 1130\,\text{MeV}$ (relevant for $\bar{\text{H}}$ annihilation), we find that the HI emissivity given by the combined slopes is

$$S = 1.5 \times 10^{-26}\,\text{photons}\,\text{s}^{-1}\,\text{sr}^{-1}\ \text{per H atom}, \tag{7.14}$$

and the combined offset is

$$O = 1.4 \times 10^{-5}\,\text{photons}\,\text{cm}^{-2}\,\text{s}^{-1}\,\text{sr}^{-1}. \tag{7.15}$$

7.4.2 Bounds on $|\delta|$

Let us now consider what happens if there are extra oscillation-induced γ-rays on top of the known sources. Distribution-wise, both the WIM and WNM have relatively low volume densities and large volume filling factors, so their contributions to the HI column density should be relatively uniform over the column density map. In contrast, the CNM is clumpy with much higher density and smaller filling factor, so the small regions in the map with high column densities probably correspond to lines of sight which pass through the CNM. In other words, lines of sight with more H from the CNM provide the high leverage points that determine the slope in the linear regression of emissivity against column density. On the other hand, as we have seen, the extra emissivity per H atom varies among the three phases of ISM, with the WNM and WIM values being one order of magnitude

higher than the CNM. Together, this suggests that the extra γ-ray intensity is more likely to show up in Figure 4 of [346] as a contribution to the offset rather than the slope.

We perform a simple calculation to show that this is indeed the case. The WNM and WIM are assumed to be layers parallel to the galactic disk. Therefore, their contributions to the HI column density are constant, except for a $\frac{1}{\sin|b|}$ latitudinal variation since a more "glancing" line of sight travels a longer distance through the layer. Using Eq. (7.22) and (7.23) and the nominal ionisation fraction, this corresponds to a contribution of $\frac{1.7}{\sin|b|} \times 10^{20}\,\mathrm{cm}^{-2}$ from the WNM and $\frac{0.08}{\sin|b|} \times 10^{20}\,\mathrm{cm}^{-2}$ from the WIM. On top of that, the CNM is assumed to add a random contribution that ranges from 0 to $\frac{10}{\sin|b|} \times 10^{20}\,\mathrm{cm}^{-2}$. For each line of sight within the latitudinal range of interest, we calculate the total HI column density and oscillation-induced γ-ray intensity, repeated many times over different random CNM contributions. Figure 7.1 shows a plot of intensity against column density, with the horizontal errorbars indicating the bin intervals, and the vertical errorbars the intensity range of the corresponding bins. The plot is mostly horizontal, indicating that the extra intensity is indeed more likely to show up in the offset, with a contribution of roughly

$$O_{\mathrm{osc.}} \simeq 4|\delta|^2 \times 10^{27}\,\mathrm{photons\,cm^{-2}\,s^{-1}\,sr^{-1}}. \tag{7.16}$$

To obtain a bound on $|\delta|$, we identify this extra offset with the entire experimental offset value, which we found earlier to be around $1.4 \times 10^{-5}\,\mathrm{photons\,cm^{-2}\,s^{-1}\,sr^{-1}}$. In principle, we could have performed further background subtraction from this experimental value before making the identification. Possible background includes CR interaction with smoothly-distributed residual particles such as HII, incomplete earlier subtraction of inverse Compton scattering

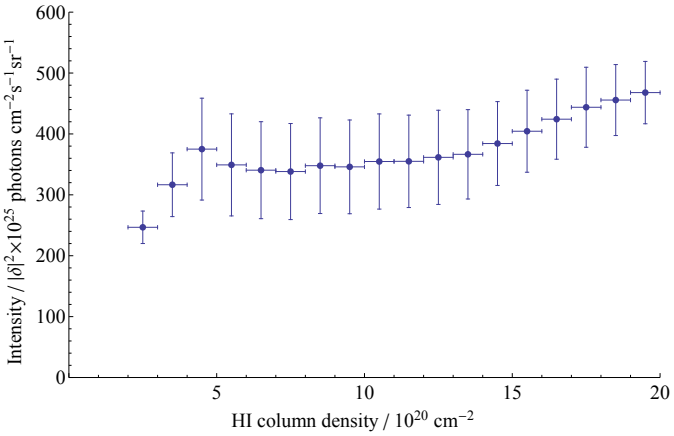

Figure 7.1: Results of a simple calculation showing how the oscillation-induced γ-ray intensity varies with the HI column density.

due to model uncertainties, as well as extragalactic sources. However, these contributions are either not well-quantified, or turn out to be small compared to the experimental value, so the subtraction is unlikely to have made a big difference. Comparing O and $O_{\text{osc.}}$ from Eqs. (7.15) and (7.16), we find that

$$|\delta| \lesssim 6 \times 10^{-17}\,\text{s}^{-1}. \tag{7.17}$$

This is about one order of magnitude weaker than the bound derived in [84]. In other words, the earlier bound may have been too stringent. We also note that [84] used the slope (from older γ-ray data [86]) instead of the offset to derive the bound, so it did not account for the most likely scenario in which the CNM is mainly responsible for the variation in HI column density from which the slope is derived, whereas the WNM dominates the extra oscillation-induced intensity.

7.5 Discussion and conclusions

The bounds we have derived on $|\delta|$ can be translated to a bound on four-fermion contact operators involving protons and electrons. For instance, [84] considered

the operator

$$\mathcal{O}_1 = \frac{1}{\Lambda^2}[\bar{p}^c\gamma_\mu(1+\gamma_5)e][\bar{p}^c\gamma^\mu(1+\gamma_5)e] + \text{h.c.}, \tag{7.18}$$

and found that δ is related to Λ via

$$\delta = \frac{16}{\Lambda^2\pi a^3}, \tag{7.19}$$

where a is the Bohr radius.

On the other hand, *ppee* operators can also be constrained by other processes such as $pp \to ee$. For instance, results from Super-Kamiokande can be used to set an upper bound on the proton annihilation rate in oxygen nuclei. For a benchmark operator

$$\mathcal{O}_2 = \frac{1}{\Lambda^2}(i\bar{p}^c\gamma_5 p)(i\bar{e}^c\gamma_5 e) + \text{h.c.}, \tag{7.20}$$

this translates to a bound of $\Lambda > 7 \times 10^{14}\,\text{GeV}$ [345]. If we now assume that the same cutoff scale can be used in Eq. (7.19) to estimate a bound on $|\delta|$, we find that

$$|\delta| \lesssim 10^{-21}\,\text{s}^{-1}, \tag{7.21}$$

which is actually four orders of magnitude more stringent than the bound that we have obtained from γ-ray observations.

It is unlikely that choosing a different region for γ-ray observations can give an improved bound on $|\delta|$ that is just as competitive, so it is worth speculating whether a terrestrial laboratory-based oscillation experiment might do better. For instance, if a falling H atom oscillates partially into an $\bar{\text{H}}$, the experiment can attempt to detect γ-rays from annihilation when this atom comes into contact with a solid surface. Compared to measurements based on the ISM, the advantages are that annihilation no longer relies on chance encounters with other atoms, and that the γ-rays background can potentially be controlled. If there are N H atoms each

with a characteristic flight time t before reaching a solid surface, then the absence of γ-rays indicate a crude bound of $(|\delta|t)^2 \lesssim \frac{1}{N}$. Unfortunately, even obtaining a bound close to that from the ISM is unlikely to be feasible. For instance, a bound of $|\delta| \lesssim 10^{-16}\,\mathrm{s}^{-1}$, assuming a flight time of $t = 1\,\mathrm{s}$, will require about $10^8\,\mathrm{mol}$ of atomic hydrogen, a very large number. In addition, there are practical concerns about how rarefied the H atoms should be so that they do not start to interact, and the cryogenics required so that thermal motion does not substantially reduce the flight time.

To conclude, we have updated the bounds on H-$\bar{\mathrm{H}}$ oscillations based on oscillation-induced γ-ray emission in the ISM. Suppression from elastic collisions turn out to be more significant than assumed in previous work, and using a multi-phase ISM model as well as updated parameter values and γ-ray data, we show that the upper bound on $|\delta|$ is about $6 \times 10^{-17}\,\mathrm{s}^{-1}$, one order of magnitude weaker than previously thought.

7.A More details about the H-$\bar{\mathrm{H}}$ oscillation model

7.A.1 Elastic scattering

The model we used in this work was originally derived in [347] somewhat heuristically based on the notion of a classical sum over different "histories", where in each infinitesimal time interval δt, the atom may undergo either elastic scattering or quantum time evolution. We have been able to re-derive the model on a more rigourous basis as follows.

The atom is originally described by a density matrix in the product space $\mathcal{H}_A \otimes \mathcal{H}_B$, where $\mathcal{H}_A$ is associated with the atom's identity, and $\mathcal{H}_B$ with momentum degrees of freedom (for simplicity we neglect atomic level and spin; including them simply increases the number of Wigner functions). We then extend the impurity-scattering formalism described in [367] to derive quantum kinetic equations for the 2×2 Wigner functions. By making a number of assumptions before and after integrating over momentum space (equivalent to tracing out $\mathcal{H}_B$), we finally obtain the same kinetic equation for the reduced 2×2 density matrix $\rho(t)$ as [347].

We now examine the various assumptions made in this derivation.

- The derivation of the Wigner function kinetic equations assumed that the mean free path be much larger than the de Broglie wavelength, and that quantum degeneracy as well as two-body correlation between atom and target can be ignored. These are probably reasonable assumptions for an atom in the ISM.
- In further reducing these kinetic equations to the one for $\rho(t)$, two further assumptions are made. First, we take the classical limit of the scattering terms, which requires that memory effects be neglected, again a reasonable assumption given that the momentum relaxation time of an atom is much shorter than our timescale of interest (the quasi-steady rate of change). Second, as mentioned in Section 7.2.1, in order to close the kinetic equation for $\rho(t)$, we assume that moments in momentum and other degrees of freedom can be replaced by products of $\rho(t)$ with the relevant expectation values. While some errors are introduced in doing so, they are not expected to be very significant.
- The impurity-scattering formalism assumes that the targets are immobile,

certainly not true for real targets in the ISM. Nonetheless, this can be addressed by replacing v and p, not by the r.m.s. values in the lab frame, but rather the r.m.s. values evaluated in the two-particle centre-of-mass frame comprising the atom and a target particle (hence this also involves averaging over the target velocity distribution). Only E should still be the lab frame value.

- Finally, the impurity-scattering formalism assumes that the atom and target are distinguishable particles. This is clearly violated if we consider scattering with other H atoms. Both $f(\theta)$ and $f(\pi-\theta)$ will then contribute to the same H-H scattering process, and one must also be careful not to double-count the phase space. This is probably the biggest source of error (possibly up to a factor of 2) in the model, at least for the CNM and WNM. However, there is not much point in trying to derive a more accurate treatment due to the lack of accurate scattering data.

7.A.2 Inelastic processes

In Section 7.2.1, we only considered inelastic processes where the H/$\bar{\text{H}}$ atom "disappears", e.g. H_2 formation or $\bar{\text{H}}$ annihilation. These processes cause the state to leave the Hilbert space $\mathcal{H}_A$ and can hence be represented by imaginary diagonal contributions to the effective Hamiltonian. However, there are other processes where the atom does not disappear but are nonetheless inelastic. We now explain why they can be neglected.

First, we consider processes like $\text{H}/\bar{\text{H}}(1S) + X \rightarrow \text{H}/\bar{\text{H}}(1S) + Y$, where the H/$\bar{\text{H}}$ atom remains in the $1S$ state but the target is collisionally ex-

cited/ionised/dissociated. As far as the $\mathrm{H}/\bar{\mathrm{H}}$ atom is concerned, these processes are not very different from elastic scattering, and so enters the model in a similar manner (except without a forward scattering contribution). However, we expect them to be less important than elastic scattering off the same target X since the rates are usually Boltzmann-suppressed in comparison, even in the warm phases.

Next, we consider collisional and photo-excitations of $\mathrm{H}/\bar{\mathrm{H}}$ to $n \geq 2$ atomic states. These processes (together with collisional and radiative decays) are responsible for maintaining the quasi-steady distribution of atomic levels. However, if the transition amplitudes for H and $\bar{\mathrm{H}}$ are different, then one also needs to examine how they might directly affect the oscillations. Collisional excitations can again be neglected since they are Boltzmann-suppressed compared to elastic scattering. For photo-excitations, the electric dipole transition amplitudes for H and $\bar{\mathrm{H}}$ do indeed differ by a sign; however, there is hardly any time for the $\mathcal{H}_A$ part of the state to evolve (except by an overall phase) before the atom undergoes radiative decay that undoes the sign change. Therefore, the net direct effects are also unimportant.

The arguments above do not apply to $1S$ hyperfine transitions. In particular, collisional excitations to the higher-energy hyperfine state are not Boltzmann-suppressed. However, since these processes involve electron spin flips, they are either magnetic in nature and hence have smaller cross-sections, or rely on electron exchange (e.g. when the target is e^- or other H atoms) and hence already included in conventional elastic scattering data. Photo-excitations can also occur via dipole transition to nP states followed by decays to the higher $1S$ hyperfine state, but as explained above the net direct effects are unimportant due to sign cancellation.

7.B Phases of the ISM

The ISM comprises a number of phases that accounts for most of its mass and volume. Parameter values are taken from [349–352].

- Neutral atomic gases: There are two phases that contain predominantly HI. The CNM comprises HI clouds typically of size $\mathcal{O}(10)\,\mathrm{pc}$, number density $20-50\,\mathrm{cm}^{-3}$, temperature $50-100\,\mathrm{K}$ and volume filling factor $\mathcal{O}(0.01)$. The WNM comprises diffuse intercloud HI, typically with a lower number density $0.2-0.6\,\mathrm{cm}^{-3}$, and higher temperature $5000-10000\,\mathrm{K}$ and filling factor $0.3-0.4$. Locally, a simple model for the vertical HI distribution (filling factor incorporated) is given by

$$n_{\mathrm{H}}(z)/\mathrm{cm}^{-3} = 0.40e^{-\left(\frac{z}{127\,\mathrm{pc}}\right)^2} + 0.10e^{-\left(\frac{z}{318\,\mathrm{pc}}\right)^2} + 0.063e^{-\frac{|z|}{403\,\mathrm{pc}}}, \tag{7.22}$$

  where the first term corresponds to the CNM, and the second and third terms the WNM.

- Warm ionised gases: Radiation from O and B stars cause almost-complete ionisation of nearby clouds, so most of the hydrogen are in the ionised form HII. These HII regions, typically of size $\mathcal{O}(1)\,\mathrm{pc}$, are generally very dense and hot, with number densities up to $\mathcal{O}(10^5)\,\mathrm{cm}^{-3}$, temperatures $8000-10000\,\mathrm{K}$, and negligibly small filling factors. Besides these dense regions, there also exists a diffuse warm ionised phase called the WIM. This phase has comparable temperature, but much lower number density $\sim 0.1-0.5\,\mathrm{cm}^{-3}$, and much higher filling factor $0.05-0.25$. A simple "two-disk" model for the vertical HII distribution is given by

$$n_e(z)/\mathrm{cm}^{-3} = 0.015e^{-\frac{|z|}{70\,\mathrm{pc}}} + 0.025e^{-\frac{|z|}{900\,\mathrm{pc}}}, \tag{7.23}$$

where the first term represents the collection of localised HII regions as a "thin-disk", and the second term the WIM as a "thick disk".

- Coronal gases: Besides the WIM, there is another diffuse ionised phase referred to as coronal gases, because the temperature and ionisation state are believed to be similar to that of the solar corona. This phase is much hotter and rarefied, with temperature $\mathcal{O}(10^5 - 10^6)\,\mathrm{K}$, number density $0.003 - 0.007\,\mathrm{cm}^{-3}$, and filling factor $0.2 - 0.5$. The vertical profile depends on the measurements used (e.g. choice of spectral lines) but usually fits a large scale height of 3 kpc (assuming exponential distribution) or above.
- Molecular clouds: These comprise gravitationally-bound clouds, typically of size $\mathcal{O}(10)\,\mathrm{pc}$ with H_2 as the dominant species. They are typically very cold and dense, with temperature $10 - 20\,\mathrm{K}$, number density up to $\mathcal{O}(10^6)\,\mathrm{cm}^{-3}$, and negligible filling factor. Vertically, they tend to be concentrated near the galactic disk, with a Gaussian scale height around $70 - 80\,\mathrm{pc}$.

While the main constituents in these phases are H, H_2, H^+ and e^-, also present are other gaseous elements and dust.

- Other gaseous elements: From photospheric and meteoritic measurements, the cosmic composition in terms of number density are as follows: He 10%, C 0.03%, O 0.05%, and all other species individually each below 0.01% (combined $\sim 0.03\%$). There is also evidence that a significant fraction of these elements might have been locked up in dust and hence depleted in the gaseous form.
- Dust: Dust grains are generally well-mixed with the gases in the ISM, with a dust-to-gas mass ratio believed to be around $\mathcal{O}(0.01)$. The dust grains are

primarily composed of heavier elements like C, N, O, Mg, Si and Fe, with a typical specific density of $3\,\mathrm{g\,cm^{-3}}$. A popular model for the grain-size distribution (based on the extinction curve) is the Mathis-Rumpl-Nordsieck model. In the model, the dust grains are assumed to graphite and silicates, and the distribution given by

$$n_i(a)da = A_i n_{\mathrm{H}} a^{-3.5} da, \tag{7.24}$$

where a is the grain size, and A_i is 7.8×10^{-26} and $6.9 \times 10^{-26}\,\mathrm{cm}^{2.5}$ for silicates and graphite respectively. This relation holds over the range $50\,\text{Å} < a < 2500\,\text{Å}$. Besides large dust grains, it is also believed that there exists a population of large polycyclic aromatic hydrocarbon molecules, with an relative abundance of $\mathcal{O}(10^{-5})\%$.

Having described the phases of the ISM, we now argue that we only need to consider oscillation-induced γ-ray contributions from the CNM, WNM and WIM. For instance, consider the dense molecular clouds. Looking at Eq. (7.12), since most contributions to ϵ', $\bar{\omega}_I$ and $\bar{\omega}_{\mathrm{ann}}$ scale roughly with the gas density, this means that the emissivity per H atom is much smaller than in the more rarefied phases. While the gas column density may be very high along lines of sight passing through the clouds, only a tiny fraction of the gas is HI, so this is unlikely to compensate for the lower emissivity per H atom. In addition, [346] specifically mentions that large molecular clouds are known to be absent in the sector of interest. Similar types of arguments can also be made for the dense HII regions and the coronal gases to explain why they can be neglected.

7.C Parameter values

We present here a summary of the contributions from both elastic and inelastic processes to the parameters ϵ', $\bar{\omega}_I$ and $\bar{\omega}_{\rm ann}$. Properties of the three phases are assumed to follow the nominal values given in Section 7.3.1.

7.C.1 Elastic scattering

From Eq. (7.7), recall that the contribution of elastic scattering to ϵ' from target species i is given by

$$\Delta\epsilon' = n_i v_i \left\{ -\int d\Omega \frac{|f_{i,p_i} - \bar{f}_{i,p_i}|^2}{2} + i \left[\frac{2\pi \mathrm{Re}[f_{i,p_i}(0) - \bar{f}_{i,p_i}(0)]}{p_i} + \int d\Omega \mathrm{Im}(\bar{f}^*_{i,p_i} f_{i,p_i}) \right] \right\}. \tag{7.25}$$

We now calculate this contribution for different target species.

e^- as targets

It is useful to begin with elastic (H/$\bar{\rm H}$)-e^- scattering for the WNM and WIM (we neglect the CNM due to its extremely low ionisation fraction). First, amplitude data are available for both H and $\bar{\rm H}$. Second, e^- may potentially be the dominant target species, since the much lower reduced mass (around $m_{\rm e}$) implies a higher speed of approach v and smaller centre-of-mass momentum p, hence boosting $\Delta\epsilon'$.

For H-e^- partial wave phase shifts, we use [353, 354, 360], while for $\bar{\rm H}$-e^- phase shifts, we use [355, 357, 359, 362]. At the warm phase temperature (about 1 eV), we

find that

$$\begin{aligned}
\tfrac{1}{4}\int d\Omega \tfrac{|f_s-\bar{f}|^2}{2} + \tfrac{3}{4}\int d\Omega \tfrac{|f_t-\bar{f}|^2}{2} &\simeq 13\,\text{Å}^2, \\
\tfrac{1}{4}\tfrac{2\pi\text{Re}[f_s(0)-\bar{f}(0)]}{p} + \tfrac{3}{4}\tfrac{2\pi\text{Re}[f_t(0)-\bar{f}(0)]}{p} &\simeq -11\,\text{Å}^2, \\
\tfrac{1}{4}\int d\Omega \text{Im}(f_s\bar{f}) + \tfrac{3}{4}\int d\Omega \text{Im}(f_t\bar{f}) &\simeq 3.8\,\text{Å}^2,
\end{aligned} \tag{7.26}$$

where f_s and f_t and are the electronic singlet and triplet H-e$^-$ amplitudes. To check that the first value makes sense, we note that the elastic H-e$^-$ singlet and triplet cross-sections ($39\,\text{Å}^2$ and $15\,\text{Å}^2$) are much larger than the $\bar{\text{H}}$-e$^-$ cross-section ($1.6\,\text{Å}^2$). This suggests that $f_s, f_t \gg \bar{f}$, in which case the first value should be approximately half the spin-averaged H-e$^-$ cross-section. This gives a reasonably close value of $11\,\text{Å}^2$.

For an r.m.s. speed of approach $v = \sqrt{\frac{3kT}{m_e}} \simeq 6 \times 10^7\,\text{cm}\,\text{s}^{-1}$, we obtain

- WNM: $\Delta\epsilon' \simeq (-2-i) \times 10^{-9}\,\text{s}^{-1}$.
- WIM: $\Delta\epsilon' \simeq (-2-i) \times 10^{-8}\,\text{s}^{-1}$.

H^+ as targets

Next, we consider elastic (H/$\bar{\text{H}}$)-H^+ scattering, again for the WNM and WIM. Here, a number of issues arise. First, a much larger number of partial waves are required to accurately reconstruct the scattering amplitudes, since the centre-of-mass momentum p is now much higher. For H-H^+ scattering, while phase shifts for nearly 200 partial waves are available [368], we found that they are nonetheless insufficient for the forward scattering amplitude[2]. Second, we have not been able to find scattering data for H^+-$\bar{\text{H}}$ scattering. Therefore, unlike the previous case, here an accurate calculation is not possible. The approach we adopt is as follows.

[2]Recall that for partial wave amplitudes a_l, $f(0)$ involves a summation of $(2l+1)a_l$ as opposed to $(2l+1)|a_l|^2$ for the total cross-section, hence implying a slower convergence.

[361] claims that the elastic H-$\bar{\text{p}}$ (charge-conjugate of $\bar{\text{H}}$-H^+) cross-section is comparable to the re-arrangement cross-section ($11\,\text{Å}^2$ from [356]). Should this indeed be the case, this implies that the elastic $\bar{\text{H}}$-H^+ cross-section is much smaller than that of H-H^+ ($160\,\text{Å}^2$ from [363] after nuclear-spin averaging). If we then assume that $\bar{f} \ll f$, we can drop $\bar{f}$ in the expression for $\Delta\epsilon'$, giving

$$\Delta\epsilon' \simeq nv \left\{ -\int d\Omega \tfrac{|f|^2}{2} + i\tfrac{2\pi \text{Re}[f(0)]}{p} \right\}, \tag{7.27}$$

so only H-H^+ data is required. The first term requires the nuclear-spin averaged cross-section, and the second term the averaged forward scattering amplitude.

Instead of the phase shifts from [368], we mostly rely on the averaged differential and total cross-sections from [363], since the latter is more recent and includes a larger number of partial waves (more than 500). To extract the averaged $\text{Re}[f(0)]$, we first note that the nuclear singlet and triplet amplitudes are given by $f_{s,t}(\theta) = f_d(\theta) \pm f_e(\pi - \theta)$, where f_d and f_e are the "direct" and "charge exchange" amplitudes had the nuclei been distinguishable [363]. At energies $\gtrsim 1\,\text{eV}$, both $f_d(\theta)$ and $f_e(\theta)$ become so forward-distributed that $f_s(0) \simeq f_t(0) \simeq f_d(0)$, while the overlap between $f_d(\theta)$ and $f_e(\pi - \theta)$ become so small that the singlet and triplet total cross-sections become identical. We then use the optical theorem to estimate $\text{Im}[f_d(0)]$ from the spin-averaged cross-section, which in turn can be used to estimate $|\text{Re}[f_d(0)]|$ from the spin-averaged differential cross-section at $\theta \simeq 0$. We only use the phase shifts from [368] to fix the sign of $\text{Re}[f_d(0)]$ and to check the validity of the assumptions above. We find that

$$\int d\Omega \tfrac{|f|^2}{2} \simeq 81\,\text{Å}^2,$$
$$\tfrac{2\pi \text{Re}[f(0)]}{p} \simeq 74\,\text{Å}^2,$$

from which we obtain

- WNM: $\Delta\epsilon' \simeq (-4+4i)\times 10^{-10}\,\mathrm{s}^{-1}$.
- WIM: $\Delta\epsilon' \simeq (-5+4i)\times 10^{-9}\,\mathrm{s}^{-1}$.

These $\Delta\epsilon'$ values are smaller than that of (H/$\bar{\mathrm{H}}$)-e$^-$ scattering, mostly due to the much smaller speed of approach v.

H as targets

Finally, we consider elastic (H/$\bar{\mathrm{H}}$)-H scattering for the CNM and WNM (we neglect the WIM due to its high ionisation fraction). We have not been able to find amplitude-level data, and even differential cross-section data is only limited to the WNM. Therefore, we will only perform a crude estimate of $\Delta\epsilon'$ using total cross-section data. We use [363] and [365] for H-H and [364] for H-$\bar{\mathrm{H}}$ cross-sections. Actually [364] only covers up to 0.27 eV, a few times lower than the WNM temperature. However, since the cross-section appears relatively constant near 0.27 eV, the cross-section should not differ significantly between 0.27 eV and 1 eV.

For H-H scattering, the CNM electronic singlet and triplet cross-sections are around $130\,\text{Å}^2$ and $60\,\text{Å}^2$, and the WNM spin-averaged cross-section $50\,\text{Å}^2$. For H-$\bar{\mathrm{H}}$ scattering, the CNM cross-section is $90\,\text{Å}^2$, and the WNM $60\,\text{Å}^2$. Based on these cross-sections, we now assume that $-\mathrm{Re}(\Delta\epsilon') \simeq |\mathrm{Im}(\Delta\epsilon')| \simeq nv(100\,\text{Å}^2)$ for the CNM, and $nv(50\,\text{Å}^2)$ for the WNM. We then obtain

- CNM: $\Delta\epsilon' \simeq (-1\pm i)\times 10^{-7}\,\mathrm{s}^{-1}$.
- WNM: $\Delta\epsilon' \simeq (-5\pm 5i)\times 10^{-9}\,\mathrm{s}^{-1}$.

Other targets

While other neutral targets such as He and H_2 may offer slightly larger cross-sections than H, nonetheless their much lower abundances mean that their contributions to ϵ' can be ignored. The same can be said for other charged targets compared to H^+ or e^-.

7.C.2 Inelastic processes

For inelastic processes, we consider $\bar{H}$ annihilation, ionisation of $H/\bar{H}$, as well as chemical reactions involving H. Keep in mind that ω_I only enters Eq. (7.12) as $\omega_I + \bar{\omega}_I$, so even the dominant contribution to ω_I can be ignored if it turns out to be much smaller than $\bar{\omega}_I$.

$\bar{H}$ annihilation with H

We use the semi-classical calculations of the rearrangement cross-section from [358]. Note that while there are fully-quantum calculations of the annihilation cross-section that include both rearrangement and annihilation-in-flight [369–372], they only include the s-wave component and hence give values that are much smaller. We now discuss each phase in turn.

- CNM: The cross-section is $\sigma \simeq 60\,\text{Å}^2$, corresponding to a rate coefficient of $\langle\sigma v\rangle \simeq 10^{-9}\,\text{cm}^3\,\text{s}^{-1}$. The contribution to $\bar{\omega}_I$ is given by $n_\text{H}\langle\sigma v\rangle \simeq 6 \times 10^{-8}\,\text{s}^{-1}$.
- WNM: The cross-section is $\sigma \simeq 8\,\text{Å}^2$, corresponding to a rate coefficient

of $\langle\sigma v\rangle \simeq 2 \times 10^{-9}\,\mathrm{cm^3\,s^{-1}}$. The contribution to $\bar{\omega}_I$ is given by $n_{\mathrm{H}}\langle\sigma v\rangle \simeq 8 \times 10^{-10}\,\mathrm{s^{-1}}$.

We ignore this for the WIM due to the high ionisation fraction.

$\bar{\mathrm{H}}$ annihilation with H^+

We again use semi-classical calculations from [356], since more updated cross-sections are either again for s-waves [369], or do not fully cover our energy range of interest [373, 374]. (In any case, we note that discrepancies between [356] and [373, 374] where they do overlap are rather small.)

We ignore this for the CNM due to the extremely low ionisation fraction. For the WNM and WIM, we find a cross-section of $\sigma = 10\,\mathrm{\AA}^2$, corresponding to a rate coefficient of $\langle\sigma v\rangle \simeq 2 \times 10^{-9}\,\mathrm{cm^3\,s^{-1}}$. Hence we obtain the following results.

- WNM: The contribution to $\bar{\omega}_I$ is $n_{\mathrm{H}^+}\langle\sigma v\rangle \simeq 6 \times 10^{-11}\,\mathrm{s^{-1}}$.
- WIM: The contribution to $\bar{\omega}_I$ is $n_{\mathrm{H}^+}\langle\sigma v\rangle \simeq 7 \times 10^{-10}\,\mathrm{s^{-1}}$.

Other $\bar{\mathrm{H}}$ annihilation processes

One might expect $\mathrm{e^-}$-$\bar{\mathrm{H}}$ annihilation to be important (especially in the WIM) since the relative speed v is much higher. However, the annihilation cross-section turns out to be much smaller, due to the 6.8 eV energy threshold for re-arrangement, and that direct annihilation-in-flight in this case involves the electromagnetic interaction as opposed to the strong interaction [372].

Finally, annihilation of $\bar{\mathrm{H}}$ with any other neutral or charged species is expected to be less important than with H or H^+, due to their much lower abundances.

Ionisation

Ionisation in the HI phases proceeds mainly via CR ionisation, at a rate per atom of order $10^{-16}\ rms^{-1}$ [351, 352]. For the WIM, photo-ionisation plays the more important role [351]. A reasonable ionisation rate per atom in the WIM is $\mathcal{O}(10^{-13} - 10^{-12})\,\mathrm{s}^{-1}$, consistent with the degree of ionisation given typical recombination rates, as well as estimates of the ionisation parameter based on spectral measurements. Nonetheless, we see that in all three phases, the ionisation rates are much smaller than the contributions to $\bar{\omega}_I$ from $\bar{\mathrm{H}}$ annihilation.

Chemical reactions

Many chemical reactions involve H and may contribute to ω_I. However, all the rates are much smaller than $\bar{\omega}_I$, either because they involve species with very low abundances, or that they have very small rate coefficients. We discuss a number of examples here. The rate coefficients are taken from [351].

- Neutral reaction $\mathrm{H} + \mathrm{CH} \rightarrow \mathrm{C} + \mathrm{H}_2$ has a rate coefficient $k = 1.2 \times 10^{-9} \left(\frac{T}{300\,\mathrm{K}}\right)^{0.5} e^{-\frac{2200\,\mathrm{K}}{T}}$. Even in the warm phases where the exponential suppression (from the activation barrier) becomes insignificant, the rate per H atom remains small due to the low abundance of CH.
- H_2 formation through $\mathrm{H} + \mathrm{H}^- \rightarrow \mathrm{H}_2 + \mathrm{e}^-$ has a high rate coefficient $k = 1.3 \times 10^{-9}\,\mathrm{cm}^3\,\mathrm{s}^{-1}$, but the H^- abundance is very low.

- Radiative association $\mathrm{H} + \mathrm{e^-} \rightarrow \mathrm{H^-} + \gamma$ has a very low rate coefficient $k = 10^{-18} \frac{T}{1\,\mathrm{K}}\,\mathrm{cm^3\,s^{-1}}$.
- Radiative association $\mathrm{H} + \mathrm{H} \rightarrow \mathrm{H_2} + \gamma$ has a very low rate coefficient $k \lesssim 10^{-23}\,\mathrm{cm^3\,s^{-1}}$.
- Accretion of H on dust grain surface (an important catalytic reaction for $\mathrm{H_2}$ formation) occurs at a very low rate of roughly $10^{-17} \left(\frac{T}{10\,\mathrm{K}}\right)^{0.5} n_\mathrm{H}\,\mathrm{s^{-1}}$ per atom. (The n_H dependence comes from the assumption of a constant dust-to-gas mass ratio.)

Bibliography

[1] I. J. Lovette and J. W. Fitzpatrick, eds., *Handbook of Bird Biology*. Cornell Lab of Ornithology, 3nd ed., 2016.

[2] S. Weinberg, *Newtonianism, reductionism and the art of congressional testimony*, *Nature* **330** (1987) 433–437.

[3] P. W. Anderson, *More Is Different*, *Science* **177** (1972) 393–396.

[4] V. C. Rubin, N. Thonnard and W. K. Ford, Jr., *Rotational properties of 21 Sc galaxies with a large range of luminosities and radii, from NGC 4605 (R = 4 kpc) to UGC 2885 (R = 122 kpc)*, *Astrophys. J.* **238** (1980) 471.

[5] R. Davis, Jr., D. S. Harmer and K. C. Hoffman, *Search for neutrinos from the sun*, *Phys. Rev. Lett.* **20** (1968) 1205–1209.

[6] Super-Kamiokande collaboration, Y. Fukuda et al., *Evidence for oscillation of atmospheric neutrinos*, *Phys. Rev. Lett.* **81** (1998) 1562–1567, [hep-ex/9807003].

[7] SNO collaboration, Q. R. Ahmad et al., *Measurement of the rate of $\nu_e + d \to p + p + e^-$ interactions produced by ^8B solar neutrinos at the Sudbury Neutrino Observatory*, *Phys. Rev. Lett.* **87** (2001) 071301, [nucl-ex/0106015].

[8] Muon g-2 collaboration, G. W. Bennett et al., *Final report of the muon E821 anomalous magnetic moment measurement at BNL*, *Phys. Rev.* **D73** (2006) 072003, [hep-ex/0602035].

[9] R. Pohl et al., *The size of the proton*, *Nature* **466** (2010) 213–216.

[10] A. A. Penzias and R. W. Wilson, *A measurement of excess antenna temperature at* 4080 *Mc/s*, *Astrophys. J.* **142** (1965) 419–421.

[11] R. H. Dicke, P. J. E. Peebles, P. G. Roll and D. T. Wilkinson, *Cosmic black-body radiation*, *Astrophys. J.* **142** (1965) 414–419.

[12] COBE collaboration, G. F. Smoot et al., *Structure in the COBE differential microwave radiometer first year maps*, *Astrophys. J.* **396** (1992) L1–L5.

[13] L. Canetti, M. Drewes and M. Shaposhnikov, *Matter and antimatter in the universe*, *New J. Phys.* **14** (2012) 095012, [1204.4186].

[14] B. Pontecorvo, *Mesonium and anti-mesonium*, *Sov. Phys. JETP* **6** (1957) 429.

[15] B. Pontecorvo, *Inverse beta processes and nonconservation of lepton charge*, *Sov. Phys. JETP* **7** (1958) 172–173.

[16] G. Bertone, D. Hooper and J. Silk, *Particle dark matter: Evidence, candidates and constraints*, *Phys. Rept.* **405** (2005) 279–390, [hep-ph/0404175].

[17] A. D. Sakharov, *Violation of CP invariance, C asymmetry, and baryon asymmetry of the universe*, *Pisma Zh. Eksp. Teor. Fiz.* **5** (1967) 32–35.

[18] A. A. Starobinsky, *A new type of isotropic cosmological models without singularity*, *Phys. Lett.* **91B** (1980) 99–102.

[19] A. H. Guth, *The inflationary universe: A possible solution to the horizon and flatness problems*, *Phys. Rev.* **D23** (1981) 347–356.

[20] A. D. Linde, *A new inflationary universe scenario: A possible solution of the horizon, flatness, homogeneity, isotropy and primordial monopole problems*, *Phys. Lett.* **108B** (1982) 389–393.

[21] A. Albrecht and P. J. Steinhardt, *Cosmology for grand unified theories with radiatively induced symmetry breaking*, *Phys. Rev. Lett.* **48** (1982) 1220–1223.

[22] J. C. Maxwell, *A dynamical theory of the electromagnetic field*, *Phil. Trans. Roy. Soc. Lond.* **155** (1865) 459–512.

[23] K. G. Wilson, *The renormalization group and strong interactions*, *Phys. Rev.* **D3** (1971) 1818.

[24] G. 't Hooft, *Naturalness, chiral symmetry, and spontaneous chiral symmetry breaking*, *NATO Sci. Ser. B* **59** (1980) 135–157.

[25] H.-Y. Cheng, *The strong CP problem revisited*, *Phys. Rept.* **158** (1988) 1.

[26] S. Weinberg, *The cosmological constant problem*, *Rev. Mod. Phys.* **61** (1989) 1–23.

[27] T. Berners-Lee and M. Fischetti, *Weaving the Web: The Original Design and Ultimate Destiny of the World Wide Web by its Inventor*. HarperInformation, 2000.

[28] J. M. Maldacena, *The large N limit of superconformal field theories and supergravity*, *Int. J. Theor. Phys.* **38** (1999) 1113–1133, [hep-th/9711200].

[29] M. B. Green, J. H. Schwarz and E. Witten, *Superstring Theory. Vol. 1: Introduction*. Cambridge Monographs on Mathematical Physics. Cambridge University Press, 1988.

[30] M. B. Green, J. H. Schwarz and E. Witten, *Superstring Theory. Vol. 2: Loop Amplitudes, Anomalies and Phenomenology*. Cambridge Monographs on Mathematical Physics. Cambridge University Press, 1988.

[31] M. B. Green and J. H. Schwarz, *Anomaly cancellation in supersymmetric $D = 10$ gauge theory and superstring theory*, *Phys. Lett.* **149B** (1984) 117–122.

[32] P. Kovtun, D. T. Son and A. O. Starinets, *Viscosity in strongly interacting quantum field theories from black hole physics*, *Phys. Rev. Lett.* **94** (2005) 111601, [hep-th/0405231].

[33] S. Sachdev, *What can gauge-gravity duality teach us about condensed matter physics?*, *Ann. Rev. Condensed Matter Phys.* **3** (2012) 9–33, [1108.1197].

[34] G. 't Hooft et al., *A theory of everything?*, *Nature* **433** (2005) 257–259.

[35] S. P. Martin, *A supersymmetry primer*, hep-ph/9709356.

[36] F. Riva, C. Biggio and A. Pomarol, *Is the 125 GeV Higgs the superpartner of a neutrino?*, *JHEP* **02** (2013) 081, [1211.4526].

[37] C. Biggio, J. A. Dror, Y. Grossman and W. H. Ng, *Probing a slepton Higgs on all frontiers*, *JHEP* **04** (2016) 150, [1602.02162].

[38] Z. Maki, M. Nakagawa and S. Sakata, *Remarks on the unified model of elementary particles*, *Prog. Theor. Phys.* **28** (1962) 870–880.

[39] J. Berger, J. A. Dror and W. H. Ng, *Sneutrino Higgs models explain lepton non-universality in eejj, evjj excesses*, *JHEP* **09** (2015) 156, [1506.08213].

[40] Y. Bai and J. Berger, *Coloron-assisted leptoquarks at the LHC*, *Phys. Lett.* **B746** (2015) 32–36, [1407.4466].

[41] CMS collaboration, *Search for pair-production of first generation scalar leptoquarks in pp collisions at* $\sqrt{s} = 8$ *TeV*, CMS-PAS-EXO-12-041.

[42] CMS collaboration, V. Khachatryan et al., *Search for heavy neutrinos and W bosons with right-handed couplings in proton-proton collisions at* $\sqrt{s} = 8$ *TeV*, *Eur. Phys. J.* **C74** (2014) 3149, [1407.3683].

[43] CMS collaboration, *Search for pair production of second-generation scalar leptoquarks in pp collisions at* $\sqrt{s} = 8$ *TeV with the CMS detector*, CMS-PAS-EXO-12-042.

[44] H. Georgi and S. L. Glashow, *Unity of all elementary particle forces*, *Phys. Rev. Lett.* **32** (1974) 438–441.

[45] H. Georgi, *The state of the art – Gauge theories*, *AIP Conf. Proc.* **23** (1975) 575–582.

[46] H. Fritzsch and P. Minkowski, *Unified interactions of leptons and hadrons*, *Annals Phys.* **93** (1975) 193–266.

[47] J. C. Pati and A. Salam, *Lepton number as the fourth color*, *Phys. Rev.* **D10** (1974) 275–289.

[48] R. N. Mohapatra and J. C. Pati, *Left-right gauge symmetry and an isoconjugate model of CP violation*, *Phys. Rev.* **D11** (1975) 566–571.

[49] ATLAS collaboration, G. Aad et al., *Search for high-mass diboson resonances with boson-tagged jets in proton-proton collisions at* $\sqrt{s} = 8$ *TeV with the ATLAS detector*, *JHEP* **12** (2015) 055, [1506.00962].

[50] CMS collaboration, V. Khachatryan et al., *Search for resonances and quantum black holes using dijet mass spectra in proton-proton collisions at* $\sqrt{s} = 8$ *TeV*, *Phys. Rev.* **D91** (2015) 052009, [1501.04198].

[51] J. H. Collins and W. H. Ng, *A 2 TeV* W_R *, supersymmetry, and the Higgs mass*, *JHEP* **01** (2016) 159, [1510.08083].

[52] G. Isidori, Y. Nir and G. Perez, *Flavor physics constraints for physics beyond the Standard Model*, *Ann. Rev. Nucl. Part. Sci.* **60** (2010) 355, [1002.0900].

[53] N. Cabibbo, *Unitary symmetry and leptonic decays*, *Phys. Rev. Lett.* **10** (1963) 531–533.

[54] M. Kobayashi and T. Maskawa, *CP violation in the renormalizable theory of weak interaction*, *Prog. Theor. Phys.* **49** (1973) 652–657.

[55] S. Weinberg, *Baryon and lepton nonconserving processes*, *Phys. Rev. Lett.* **43** (1979) 1566–1570.

[56] C. D. Froggatt and H. B. Nielsen, *Hierarchy of quark masses, Cabibbo angles and CP violation*, *Nucl. Phys.* **B147** (1979) 277–298.

[57] P. F. Harrison, D. H. Perkins and W. G. Scott, *Tri-bimaximal mixing and the neutrino oscillation data*, *Phys. Lett.* **B530** (2002) 167, [hep-ph/0202074].

[58] Daya Bay collaboration, F. P. An et al., *Observation of electron-antineutrino disappearance at Daya Bay*, *Phys. Rev. Lett.* **108** (2012) 171803, [1203.1669].

[59] RENO collaboration, J. K. Ahn et al., *Observation of reactor electron antineutrino disappearance in the RENO experiment*, *Phys. Rev. Lett.* **108** (2012) 191802, [1204.0626].

[60] Y. Grossman and W. H. Ng, *Nonzero θ_{13} in $SO(3) \to A_4$ lepton models*, *Phys. Rev.* **D91** (2015) 073005, [1404.1413].

[61] J. Berger and Y. Grossman, *Model of leptons from $SO(3) \to A_4$*, *JHEP* **02** (2010) 071, [0910.4392].

[62] S. M. Faber and R. E. Jackson, *Velocity dispersions and mass to light ratios for elliptical galaxies*, *Astrophys. J.* **204** (1976) 668.

[63] F. Zwicky, *Die rotverschiebung von extragalaktischen nebeln*, *Helv. Phys. Acta* **6** (1933) 110–127.

[64] EROS-2 collaboration, P. Tisserand et al., *Limits on the MACHO content*

of the galactic halo from the EROS-2 survey of the Magellanic Clouds, *Astron. Astrophys.* **469** (2007) 387–404, [astro-ph/0607207].

[65] WMAP collaboration, E. Komatsu et al., *Seven-year Wilkinson Microwave Anisotropy Probe (WMAP) observations: Cosmological interpretation*, *Astrophys. J. Suppl.* **192** (2011) 18, [1001.4538].

[66] Planck collaboration, P. A. R. Ade et al., *Planck 2015 results. XIII. Cosmological parameters*, *Astron. Astrophys.* **594** (2016) A13, [1502.01589].

[67] E. W. Kolb and M. S. Turner, *The Early Universe*, vol. 69 of *Frontiers in Physics*. Addison-Wesley, 1990.

[68] J. E. Kim, *Light pseudoscalars, particle physics and cosmology*, *Phys. Rept.* **150** (1987) 1–177.

[69] D. E. Kaplan, M. A. Luty and K. M. Zurek, *Asymmetric dark matter*, *Phys. Rev.* **D79** (2009) 115016, [0901.4117].

[70] L. J. Hall, K. Jedamzik, J. March-Russell and S. M. West, *Freeze-in production of FIMP dark matter*, *JHEP* **03** (2010) 080, [0911.1120].

[71] G. Jungman, M. Kamionkowski and K. Griest, *Supersymmetric dark matter*, *Phys. Rept.* **267** (1996) 195–373, [hep-ph/9506380].

[72] K. Griest and D. Seckel, *Three exceptions in the calculation of relic abundances*, *Phys. Rev.* **D43** (1991) 3191–3203.

[73] M. Pospelov, A. Ritz and M. B. Voloshin, *Secluded WIMP dark matter*, *Phys. Lett.* **B662** (2008) 53–61, [0711.4866].

[74] D. Pappadopulo, J. T. Ruderman and G. Trevisan, *Dark matter freeze-out in a nonrelativistic sector*, *Phys. Rev.* **D94** (2016) 035005, [1602.04219].

[75] E. D. Carlson, M. E. Machacek and L. J. Hall, *Self-interacting dark matter*, *Astrophys. J.* **398** (1992) 43–52.

[76] Y. Hochberg, E. Kuflik, T. Volansky and J. G. Wacker, *Mechanism for thermal relic dark matter of strongly interacting massive particles*, *Phys. Rev. Lett.* **113** (2014) 171301, [1402.5143].

[77] E. Kuflik, M. Perelstein, N. R.-L. Lorier and Y.-D. Tsai, *Elastically decoupling dark matter*, *Phys. Rev. Lett.* **116** (2016) 221302, [1512.04545].

[78] J. A. Dror, E. Kuflik and W. H. Ng, *Codecaying dark matter*, *Phys. Rev. Lett.* **117** (2016) 211801, [1607.03110].

[79] V. A. Kuzmin, V. A. Rubakov and M. E. Shaposhnikov, *On the anomalous electroweak baryon number nonconservation in the early universe*, *Phys. Lett.* **155B** (1985) 36.

[80] G. 't Hooft, *Symmetry breaking through Bell-Jackiw anomalies*, *Phys. Rev. Lett.* **37** (1976) 8–11.

[81] T.-K. Kuo and S. T. Love, *Neutron oscillations and the existence of massive neutral leptons*, *Phys. Rev. Lett.* **45** (1980) 93.

[82] R. N. Mohapatra and G. Senjanovic, *Spontaneous breaking of global $B - L$ symmetry and matter-antimatter oscillations in grand unified theories*, *Phys. Rev.* **D27** (1983) 254.

[83] Super-Kamiokande collaboration, H. Nishino et al., *Search for proton decay via $p \to e^+\pi^0$ and $p \to \mu^+\pi^0$ in a large water Cherenkov detector*, *Phys. Rev. Lett.* **102** (2009) 141801, [0903.0676].

[84] G. Feinberg, M. Goldhaber and G. Steigman, *Multiplicative baryon number conservation and the oscillation of hydrogen into anti-hydrogen*, *Phys. Rev.* **D18** (1978) 1602.

[85] Y. Grossman, W. H. Ng and S. Ray, *Revisiting the bounds on hydrogen-antihydrogen oscillations from diffuse γ-ray surveys*, *Phys. Rev.* **D98** (2018) 035020, [1806.08233].

[86] C. E. Fichtel, G. A. Simpson and D. J. Thompson, *Diffuse gamma radiation*, *Astrophys. J.* **222** (1978) 833.

[87] Fermi-LAT collaboration, W. B. Atwood et al., *The Large Area Telescope on the Fermi Gamma-ray Space Telescope mission*, *Astrophys. J.* **697** (2009) 1071–1102, [0902.1089].

[88] ATLAS collaboration, G. Aad et al., *Observation of a new particle in the search for the Standard Model Higgs boson with the ATLAS detector at the LHC*, *Phys. Lett.* **B716** (2012) 1–29, [1207.7214].

[89] CMS collaboration, S. Chatrchyan et al., *Observation of a new boson at a mass of 125 GeV with the CMS experiment at the LHC*, *Phys. Lett.* **B716** (2012) 30–61, [1207.7235].

[90] N. Craig, *The State of Supersymmetry after Run I of the LHC*, in *Beyond the Standard Model after the First Run of the LHC, Arcetri, Florence, Italy, May 20-July 12, 2013*, 2013, 1309.0528.

[91] L. J. Hall and L. Randall, *$U(1)_R$ symmetric supersymmetry*, *Nucl. Phys.* **B352** (1991) 289–308.

[92] L. Randall and N. Rius, *The Minimal $U(1)_R$-symmetric model revisited*, *Phys. Lett.* **B286** (1992) 299–306.

[93] G. D. Kribs, E. Poppitz and N. Weiner, *Flavor in supersymmetry with an extended R-symmetry*, *Phys. Rev.* **D78** (2008) 055010, [0712.2039].

[94] S. D. L. Amigo, A. E. Blechman, P. J. Fox and E. Poppitz, *R-symmetric gauge mediation*, *JHEP* **01** (2009) 018, [0809.1112].

[95] K. Benakli and M. D. Goodsell, *Dirac Gauginos in general gauge mediation*, *Nucl. Phys.* **B816** (2009) 185–203, [0811.4409].

[96] R. Fok and G. D. Kribs, *μ to e in R-symmetric supersymmetry*, *Phys. Rev.* **D82** (2010) 035010, [1004.0556].

[97] K. Benakli, M. D. Goodsell and A.-K. Maier, *Generating μ and $B\mu$ in models with Dirac gauginos*, *Nucl. Phys.* **B851** (2011) 445–461, [1104.2695].

[98] K. Benakli, *Dirac gauginos: A user manual*, *Fortsch. Phys.* **59** (2011) 1079–1082, [1106.1649].

[99] R. Davies and M. McCullough, *Small neutrino masses due to R-symmetry breaking for a small cosmological constant*, *Phys. Rev.* **D86** (2012) 025014, [1111.2361].

[100] S. J. De Lope Amigo, *R-symmetry, gauge mediation and decaying dark matter*, Ph.D. thesis, Toronto U., 2011.

[101] C. Frugiuele and T. Gregoire, *Making the sneutrino a Higgs with a $U(1)_R$ lepton number*, *Phys. Rev.* **D85** (2012) 015016, [1107.4634].

[102] M. Heikinheimo, M. Kellerstein and V. Sanz, *How many supersymmetries?*, *JHEP* **04** (2012) 043, [1111.4322].

[103] J. Kalinowski, *Higgs bosons of R-symmetric supersymmetric theories*, *PoS* **EPS-HEP2011** (2011) 265.

[104] J. Kalinowski, *R-symmetric supersymmetric Higgs bosons at the LHC*, *Acta Phys. Polon.* **B42** (2011) 1419–1426.

[105] P. Kumar and E. Ponton, *Electroweak baryogenesis and dark matter with an approximate R-symmetry*, *JHEP* **11** (2011) 037, [1107.1719].

[106] K. Benakli, M. D. Goodsell and F. Staub, *Dirac gauginos and the 125 GeV Higgs*, *JHEP* **06** (2013) 073, [1211.0552].

[107] E. Bertuzzo and C. Frugiuele, *Fitting neutrino physics with a $U(1)_R$ lepton number*, *JHEP* **05** (2012) 100, [1203.5340].

[108] R. Fok, G. D. Kribs, A. Martin and Y. Tsai, *Electroweak baryogenesis in R-symmetric supersymmetry*, *Phys. Rev.* **D87** (2013) 055018, [1208.2784].

[109] Y. Morita, H. Nakano and T. Shimomura, *Neutrino mass and proton decay in a $U(1)_R$ symmetric model*, *PTEP* **2013** (2013) 053B02, [1212.4304].

[110] S. Chakraborty and S. Roy, *Higgs boson mass, neutrino masses and mixing and keV dark matter in an $U(1)_R$-lepton number model*, *JHEP* **01** (2014) 101, [1309.6538].

[111] C. Csaki, J. Goodman, R. Pavesi and Y. Shirman, *The m_D-b_M problem of Dirac gauginos and its solutions*, *Phys. Rev.* **D89** (2014) 055005, [1310.4504].

[112] G. D. Kribs and N. Raj, *Mixed gauginos sending mixed messages to the LHC*, *Phys. Rev.* **D89** (2014) 055011, [1307.7197].

[113] P. Dießner, J. Kalinowski, W. Kotlarski and D. Stöckinger, *Higgs boson mass and electroweak observables in the MRSSM*, *JHEP* **12** (2014) 124, [1410.4791].

[114] S. Chakraborty, A. Datta, K. Huitu, S. Roy and H. Waltari, *Light top squarks in $U(1)_R$-lepton number model with a right handed neutrino and the LHC*, *Phys. Rev.* **D93** (2016) 075005, [1508.01875].

[115] Particle Data Group collaboration, K. A. Olive et al., *Review of Particle Physics*, *Chin. Phys.* **C38** (2014) 090001.

[116] A. K. Grant and Z. Kakushadze, *Higgs as a slepton*, *Phys. Lett.* **B465** (1999) 108–112, [hep-ph/9906556].

[117] S. Davidson, C. Pena-Garay, N. Rius and A. Santamaria, *Present and future bounds on nonstandard neutrino interactions*, *JHEP* **03** (2003) 011, [hep-ph/0302093].

[118] J. Barranco, O. G. Miranda, C. A. Moura and J. W. F. Valle, *Constraining non-standard neutrino-electron interactions*, *Phys. Rev.* **D77** (2008) 093014, [0711.0698].

[119] A. Bolanos, O. G. Miranda, A. Palazzo, M. A. Tortola and J. W. F. Valle, *Probing non-standard neutrino-electron interactions with solar and reactor neutrinos*, *Phys. Rev.* **D79** (2009) 113012, [0812.4417].

[120] C. Biggio, M. Blennow and E. Fernandez-Martinez, *General bounds on non-standard neutrino interactions*, *JHEP* **08** (2009) 090, [0907.0097].

[121] Super-Kamiokande collaboration, G. Mitsuka et al., *Study of non-standard neutrino interactions with atmospheric neutrino data in Super-Kamiokande I and II*, *Phys. Rev.* **D84** (2011) 113008, [1109.1889].

[122] T. Ohlsson, *Status of non-standard neutrino interactions*, *Rept. Prog. Phys.* **76** (2013) 044201, [1209.2710].

[123] W. Loinaz, N. Okamura, S. Rayyan, T. Takeuchi and L. C. R. Wijewardhana, *The NuTeV anomaly, lepton universality, and nonuniversal neutrino gauge couplings*, *Phys. Rev.* **D70** (2004) 113004, [hep-ph/0403306].

[124] J. A. Dror, M. Farina, E. Salvioni and J. Serra, *Strong tW scattering at the LHC*, *JHEP* **01** (2016) 071, [1511.03674].

[125] Super-Kamiokande collaboration, K. Abe et al., *Search for proton decay via $p \to \nu K^+$ using 260 kiloton·year data of Super-Kamiokande*, *Phys. Rev.* **D90** (2014) 072005, [1408.1195].

[126] P. J. Fox, A. E. Nelson and N. Weiner, *Dirac gaugino masses and supersoft supersymmetry breaking*, *JHEP* **08** (2002) 035, [hep-ph/0206096].

[127] L. J. Hall, D. Pinner and J. T. Ruderman, *A natural SUSY Higgs near 126 GeV*, *JHEP* **04** (2012) 131, [1112.2703].

[128] E. Nikolidakis and C. Smith, *Minimal flavor violation, seesaw, and R-parity*, *Phys. Rev.* **D77** (2008) 015021, [0710.3129].

[129] C. Csaki, Y. Grossman and B. Heidenreich, *MFV SUSY: A natural theory for R-parity violation*, *Phys. Rev.* **D85** (2012) 095009, [1111.1239].

[130] B. Bhattacherjee, J. L. Evans, M. Ibe, S. Matsumoto and T. T. Yanagida, *Natural supersymmetry's last hope: R-parity violation via UDD operators*, *Phys. Rev.* **D87** (2013) 115002, [1301.2336].

[131] C. Csaki, E. Kuflik and T. Volansky, *Dynamical R-parity violation*, *Phys. Rev. Lett.* **112** (2014) 131801, [1309.5957].

[132] C. Csaki and B. Heidenreich, *A complete model for R-parity violation*, *Phys. Rev.* **D88** (2013) 055023, [1302.0004].

[133] L. Di Luzio, M. Nardecchia and A. Romanino, *Framework for baryonic R-parity violation in grand unified theories*, *Phys. Rev.* **D88** (2013) 115008, [1305.7034].

[134] R. Franceschini and R. N. Mohapatra, *New patterns of natural R-parity violation with supersymmetric gauged flavor*, *JHEP* **04** (2013) 098, [1301.3637].

[135] G. Krnjaic and Y. Tsai, *Soft RPV through the baryon portal*, *JHEP* **03** (2014) 104, [1304.7004].

[136] A. Monteux, *Natural, R-parity violating supersymmetry and horizontal flavor symmetries*, *Phys. Rev.* **D88** (2013) 045029, [1305.2921].

[137] J. Kalinowski, *Phenomenology of R-symmetric supersymmetry*, *Acta Phys. Polon.* **B42** (2011) 2425–2432.

[138] C. Frugiuele, T. Gregoire, P. Kumar and E. Ponton, *'L=R' – $U(1)_R$ lepton number at the LHC*, *JHEP* **05** (2013) 012, [1210.5257].

[139] M. Asano, K. Rolbiecki and K. Sakurai, *Can R-parity violation hide vanilla supersymmetry at the LHC?*, *JHEP* **01** (2013) 128, [1209.5778].

[140] Z. Han, A. Katz, M. Son and B. Tweedie, *Boosting searches for natural supersymmetry with R-parity violation via gluino cascades*, *Phys. Rev.* **D87** (2013) 075003, [1211.4025].

[141] J. Berger, M. Perelstein, M. Saelim and P. Tanedo, *The same-sign dilepton signature of RPV/MFV SUSY*, *JHEP* **04** (2013) 077, [1302.2146].

[142] D. E. Brahm, L. J. Hall and S. D. H. Hsu, *Ruling out large sneutrino VEVs*, *Phys. Rev.* **D42** (1990) 1860–1862.

[143] B. Allanach, S. Biswas, S. Mondal and M. Mitra, *Explaining a CMS $eejj$ excess with R-parity violating supersymmetry and implications for neutrinoless double beta decay*, *Phys. Rev.* **D91** (2015) 011702, [1408.5439].

[144] B. C. Allanach, S. Biswas, S. Mondal and M. Mitra, *Resonant slepton production yields CMS $eejj$ and $ep\not{T}jj$ excesses*, *Phys. Rev.* **D91** (2015) 015011, [1410.5947].

[145] S. Biswas, D. Chowdhury, S. Han and S. J. Lee, *Explaining the lepton non-universality at the LHCb and CMS within a unified framework*, *JHEP* **02** (2015) 142, [1409.0882].

[146] E. J. Chun, S. Jung, H. M. Lee and S. C. Park, *Stop and sbottom LSP with R-parity violation*, *Phys. Rev.* **D90** (2014) 115023, [1408.4508].

[147] M. Dhuria, C. Hati, R. Rangarajan and U. Sarkar, *Explaining the CMS $eejj$ and $ep\not{T}jj$ excess and leptogenesis in superstring inspired E_6 models*, *Phys. Rev.* **D91** (2015) 055010, [1501.04815].

[148] B. A. Ovrut, A. Purves and S. Spinner, *The minimal SUSY $B - L$ model: From the unification scale to the LHC*, *JHEP* **06** (2015) 182, [1503.01473].

[149] B. A. Dobrescu and A. Martin, *Interpretations of anomalous LHC events with electrons and jets*, *Phys. Rev.* **D91** (2015) 035019, [1408.1082].

[150] M. Heikinheimo, M. Raidal and C. Spethmann, *Testing right-handed currents at the LHC*, *Eur. Phys. J.* **C74** (2014) 3107, [1407.6908].

[151] F. S. Queiroz, K. Sinha and A. Strumia, *Leptoquarks, dark matter, and anomalous LHC events*, *Phys. Rev.* **D91** (2015) 035006, [1409.6301].

[152] B. Allanach, A. Alves, F. S. Queiroz, K. Sinha and A. Strumia, *Interpreting the CMS $l^+l^-jj\not{E}_T$ excess with a leptoquark model*, *Phys. Rev.* **D92** (2015) 055023, [1501.03494].

[153] M. Dhuria, C. Hati, R. Rangarajan and U. Sarkar, *Falsifying leptogenesis for a TeV scale $W_R^\pm$ at the LHC*, *Phys. Rev.* **D92** (2015) 031701, [1503.07198].

[154] M. Dhuria, C. Hati, R. Rangarajan and U. Sarkar, *The $eejj$ excess signal at the LHC and constraints on leptogenesis*, *JCAP* **1509** (2015) 035, [1502.01695].

[155] B. A. Dobrescu, *Leptophobic boson signals with leptons, jets and missing energy*, 1506.04435.

[156] B. A. Dobrescu and Z. Liu, *W' Boson near 2 TeV: Predictions for Run 2 of the LHC*, *Phys. Rev. Lett.* **115** (2015) 211802, [1506.06736].

[157] C. Englert, P. Harris, M. Spannowsky and M. Takeuchi, *Unitarity-controlled resonances after the Higgs boson discovery*, *Phys. Rev.* **D92** (2015) 013003, [1503.07459].

[158] J. L. Evans and N. Nagata, *Signatures of leptoquarks at the LHC and right-handed neutrinos*, *Phys. Rev.* **D92** (2015) 015022, [1505.00513].

[159] J. Gluza and T. Jeliński, *Heavy neutrinos and the $pp \to lljj$ CMS data*, *Phys. Lett.* **B748** (2015) 125–131, [1504.05568].

[160] G. D'Ambrosio, G. F. Giudice, G. Isidori and A. Strumia, *Minimal flavor violation: An effective field theory approach*, *Nucl. Phys.* **B645** (2002) 155–187, [hep-ph/0207036].

[161] R. Barbier et al., *R-parity violating supersymmetry*, *Phys. Rept.* **420** (2005) 1–202, [hep-ph/0406039].

[162] J. Alwall, M. Herquet, F. Maltoni, O. Mattelaer and T. Stelzer, *MadGraph 5: Going beyond*, *JHEP* **06** (2011) 128, [1106.0522].

[163] T. Sjostrand, S. Mrenna and P. Z. Skands, *PYTHIA 6.4 physics and manual*, *JHEP* **05** (2006) 026, [hep-ph/0603175].

[164] J. Conway, *PGS 4*, http://conway.physics.ucdavis.edu/research/software/pgs/pgs4-general.htm.

[165] A. Alloul, N. D. Christensen, C. Degrande, C. Duhr and B. Fuks, *FeynRules 2.0 – A complete toolbox for tree-level phenomenology*, *Comput. Phys. Commun.* **185** (2014) 2250–2300, [1310.1921].

[166] W. Beenakker, R. Hopker and M. Spira, *PROSPINO: A program for the production of supersymmetric particles in next-to-leading order QCD*, hep-ph/9611232.

[167] CMS collaboration, *Search for supersymmetry in pp collisions at $\sqrt{s} = 8$ TeV in events with three leptons and at least one b-tagged jet*, CMS-PAS-SUS-13-008.

[168] ATLAS collaboration, G. Aad et al., *Search for supersymmetry at $\sqrt{s} = 8$ TeV in final states with jets and two same-sign leptons or three leptons with the ATLAS detector*, *JHEP* **06** (2014) 035, [1404.2500].

[169] M. Drees, *Supersymmetric models with extended Higgs sector*, *Int. J. Mod. Phys.* **A4** (1989) 3635.

[170] J. R. Ellis, J. F. Gunion, H. E. Haber, L. Roszkowski and F. Zwirner, *Higgs bosons in a nonminimal supersymmetric model*, *Phys. Rev.* **D39** (1989) 844.

[171] P. Batra, A. Delgado, D. E. Kaplan and T. M. P. Tait, *The Higgs mass bound in gauge extensions of the minimal supersymmetric Standard Model*, *JHEP* **02** (2004) 043, [hep-ph/0309149].

[172] A. Maloney, A. Pierce and J. G. Wacker, *D-terms, unification, and the Higgs mass*, *JHEP* **06** (2006) 034, [hep-ph/0409127].

[173] E. Bertuzzo and C. Frugiuele, *Natural SM-like 126 GeV Higgs boson via nondecoupling D terms*, *Phys. Rev.* **D93** (2016) 035019, [1412.2765].

[174] B. C. Allanach, B. Gripaios and D. Sutherland, *Anatomy of the ATLAS diboson anomaly*, *Phys. Rev.* **D92** (2015) 055003, [1507.01638].

[175] S. Fichet and G. von Gersdorff, *Effective theory for neutral resonances and a statistical dissection of the ATLAS diboson excess*, *JHEP* **12** (2015) 089, [1508.04814].

[176] ATLAS collaboration, G. Aad et al., *Search for resonant diboson production in the $llq\bar{q}$ final state in pp collisions at $\sqrt{s} = 8$ TeV with the ATLAS detector*, *Eur. Phys. J.* **C75** (2015) 69, [1409.6190].

[177] ATLAS collaboration, G. Aad et al., *Search for production of WW/WZ resonances decaying to a lepton, neutrino and jets in pp collisions at $\sqrt{s} = 8$ TeV with the ATLAS detector*, *Eur. Phys. J.* **C75** (2015) 209, [1503.04677].

[178] ATLAS collaboration, *Search for WW, WZ, and ZZ resonances in pp collisions at $\sqrt{s} = 8$ TeV with the ATLAS detector*, ATLAS-CONF-2015-045.

[179] CMS collaboration, V. Khachatryan et al., *Search for massive resonances in dijet systems containing jets tagged as W or Z boson decays in pp collisions at $\sqrt{s} = 8$ TeV*, *JHEP* **08** (2014) 173, [1405.1994].

[180] CMS collaboration, V. Khachatryan et al., *Search for massive resonances decaying into pairs of boosted bosons in semi-leptonic final states at $\sqrt{s} = 8$ TeV*, *JHEP* **08** (2014) 174, [1405.3447].

[181] ATLAS collaboration, G. Aad et al., *Search for new phenomena in the dijet mass distribution using pp collision data at $\sqrt{s} = 8$ TeV with the ATLAS detector*, *Phys. Rev.* **D91** (2015) 052007, [1407.1376].

[182] J. Brehmer, J. Hewett, J. Kopp, T. Rizzo and J. Tattersall, *Symmetry restored in dibosons at the LHC?*, *JHEP* **10** (2015) 182, [1507.00013].

[183] Q.-H. Cao, B. Yan and D.-M. Zhang, *Simple non-Abelian extensions of the Standard Model gauge group and the diboson excesses at the LHC*, *Phys. Rev.* **D92** (2015) 095025, [1507.00268].

[184] K. Cheung, W.-Y. Keung, P.-Y. Tseng and T.-C. Yuan, *Interpretations of the ATLAS diboson anomaly*, *Phys. Lett.* **B751** (2015) 188–194, [1506.06064].

[185] P. Coloma, B. A. Dobrescu and J. Lopez-Pavon, *Right-handed neutrinos and the 2 TeV W' boson*, *Phys. Rev.* **D92** (2015) 115023, [1508.04129].

[186] F. F. Deppisch, L. Graf, S. Kulkarni, S. Patra, W. Rodejohann, N. Sahu et al., *Reconciling the 2 TeV excesses at the LHC in a linear seesaw left-right model*, *Phys. Rev.* **D93** (2016) 013011, [1508.05940].

[187] P. S. Bhupal Dev and R. N. Mohapatra, *Unified explanation of the eejj, diboson and dijet resonances at the LHC*, *Phys. Rev. Lett.* **115** (2015) 181803, [1508.02277].

[188] B. A. Dobrescu and Z. Liu, *Heavy Higgs bosons and the 2 TeV W' boson*, *JHEP* **10** (2015) 118, [1507.01923].

[189] Y. Gao, T. Ghosh, K. Sinha and J.-H. Yu, *$SU(2) \times SU(2) \times U(1)$ interpretations of the diboson and Wh excesses*, *Phys. Rev.* **D92** (2015) 055030, [1506.07511].

[190] J. Hisano, N. Nagata and Y. Omura, *Interpretations of the ATLAS diboson resonances*, *Phys. Rev.* **D92** (2015) 055001, [1506.03931].

[191] M. E. Krauss and W. Porod, *Is the CMS eejj excess a hint for light supersymmetry?*, *Phys. Rev.* **D92** (2015) 055019, [1507.04349].

[192] W.-Y. Keung and G. Senjanovic, *Majorana neutrinos and the production of the right-handed charged gauge boson*, *Phys. Rev. Lett.* **50** (1983) 1427.

[193] Y. Zhang, H. An, X.-d. Ji and R. N. Mohapatra, *Light Higgs mass bound in SUSY left-right models*, *Phys. Rev.* **D78** (2008) 011302, [0804.0268].

[194] K. S. Babu and A. Patra, *Higgs boson spectra in supersymmetric left-right models*, *Phys. Rev.* **D93** (2016) 055030, [1412.8714].

[195] J. L. Hewett and T. G. Rizzo, *Low-energy phenomenology of superstring inspired $E(6)$ models*, *Phys. Rept.* **183** (1989) 193.

[196] N. G. Deshpande, J. A. Grifols and A. Mendez, *Signatures of right-handed gauge bosons through their decays into W and Z bosons in high-energy pp collisions*, *Phys. Lett.* **B208** (1988) 141.

[197] K. S. Babu, B. Dutta and R. N. Mohapatra, *Partial Yukawa unification and a supersymmetric origin of flavor mixing*, *Phys. Rev.* **D60** (1999) 095004, [hep-ph/9812421].

[198] D. Guadagnoli and R. N. Mohapatra, *TeV scale left right symmetry and flavor changing neutral Higgs effects*, *Phys. Lett.* **B694** (2011) 386–392, [1008.1074].

[199] ATLAS collaboration, G. Aad et al., *Search for pair production of a new heavy quark that decays into a W boson and a light quark in pp collisions at $\sqrt{s} = 8$ TeV with the ATLAS detector*, *Phys. Rev.* **D92** (2015) 112007, [1509.04261].

[200] ATLAS collaboration, G. Aad et al., *Search for pair and single production of new heavy quarks that decay to a Z boson and a third-generation quark in pp collisions at $\sqrt{s} = 8$ TeV with the ATLAS detector*, *JHEP* **11** (2014) 104, [1409.5500].

[201] ATLAS collaboration, G. Aad et al., *Analysis of events with b-jets and a pair of leptons of the same charge in pp collisions at $\sqrt{s} = 8$ TeV with the ATLAS detector*, *JHEP* **10** (2015) 150, [1504.04605].

[202] ATLAS collaboration, G. Aad et al., *Search for production of vector-like quark pairs and of four top quarks in the lepton-plus-jets final state in pp collisions at $\sqrt{s} = 8$ TeV with the ATLAS detector*, *JHEP* **08** (2015) 105, [1505.04306].

[203] ATLAS collaboration, G. Aad et al., *Search for vector-like B quarks in events with one isolated lepton, missing transverse momentum and jets at $\sqrt{s} = 8$ TeV with the ATLAS detector*, *Phys. Rev.* **D91** (2015) 112011, [1503.05425].

[204] CMS collaboration, V. Khachatryan et al., *Search for pair-produced vectorlike B quarks in proton-proton collisions at $\sqrt{s} = 8$ TeV*, *Phys. Rev.* **D93** (2016) 112009, [1507.07129].

[205] R. D. Ball et al., *Parton distributions with LHC data*, *Nucl. Phys.* **B867** (2013) 244–289, [1207.1303].

[206] ATLAS collaboration, G. Aad et al., *Search for high-mass dilepton resonances in pp collisions at $\sqrt{s} = 8$ TeV with the ATLAS detector*, *Phys. Rev.* **D90** (2014) 052005, [1405.4123].

[207] CMS collaboration, V. Khachatryan et al., *Search for physics beyond the Standard Model in dilepton mass spectra in proton-proton collisions at $\sqrt{s} = 8$ TeV*, *JHEP* **04** (2015) 025, [1412.6302].

[208] G. Cacciapaglia, C. Csaki, G. Marandella and A. Strumia, *The minimal set of electroweak precision parameters*, *Phys. Rev.* **D74** (2006) 033011, [hep-ph/0604111].

[209] M. Carpentier and S. Davidson, *Constraints on two-lepton, two quark operators*, *Eur. Phys. J.* **C70** (2010) 1071–1090, [1008.0280].

[210] CMS collaboration, *Event display of a candidate electron-positron pair with an invariant mass of 2.9 TeV*, CMS-DP-2015-039.

[211] J. Pardo Vega and G. Villadoro, *SusyHD: Higgs mass determination in supersymmetry*, *JHEP* **07** (2015) 159, [1504.05200].

[212] S. Heinemeyer, W. Hollik and G. Weiglein, *FeynHiggs: A program for the calculation of the masses of the neutral CP even Higgs bosons in the MSSM*, *Comput. Phys. Commun.* **124** (2000) 76–89, [hep-ph/9812320].

[213] A. Djouadi, J.-L. Kneur and G. Moultaka, *SuSpect: A Fortran code for the supersymmetric and Higgs particle spectrum in the MSSM*, *Comput. Phys. Commun.* **176** (2007) 426–455, [hep-ph/0211331].

[214] A. Arvanitaki, M. Baryakhtar, X. Huang, K. van Tilburg and G. Villadoro, *The last vestiges of naturalness*, *JHEP* **03** (2014) 022, [1309.3568].

[215] G. Ecker and W. Grimus, *CP violation and left-right symmetry*, *Nucl. Phys.* **B258** (1985) 328–360.

[216] N. G. Deshpande, J. F. Gunion, B. Kayser and F. I. Olness, *Left-right symmetric electroweak models with triplet Higgs*, *Phys. Rev.* **D44** (1991) 837–858.

[217] H. Nishiura, E. Takasugi and M. Tanaka, *Light W_R and the spontaneous CP violation. II*, *Prog. Theor. Phys.* **85** (1991) 343–354.

[218] Y. Zhang, H. An, X. Ji and R. N. Mohapatra, *General CP violation in minimal left-right symmetric model and constraints on the right-handed scale*, *Nucl. Phys.* **B802** (2008) 247–279, [0712.4218].

[219] A. Maiezza, M. Nemevsek, F. Nesti and G. Senjanovic, *Left-right symmetry at LHC*, *Phys. Rev.* **D82** (2010) 055022, [1005.5160].

[220] J. D. Bjorken, S. Pakvasa and S. F. Tuan, *Yet another extension of the Standard Model: Oases in the desert?*, *Phys. Rev.* **D66** (2002) 053008, [hep-ph/0206116].

[221] E. Golowich, J. Hewett, S. Pakvasa and A. A. Petrov, *Implications of D^0-$\bar{D}^0$ mixing for new physics*, *Phys. Rev.* **D76** (2007) 095009, [0705.3650].

[222] S. L. Glashow and S. Weinberg, *Natural conservation laws for neutral currents*, *Phys. Rev.* **D15** (1977) 1958.

[223] E. A. Paschos, *Diagonal neutral currents*, *Phys. Rev.* **D15** (1977) 1966.

[224] Y. Zhang, H. An and X.-d. Ji, *Constraining the right-handed scale through kaon mixing in the supesymmetric left-right model*, *Phys. Rev.* **D78** (2008) 035006, [0710.1454].

[225] S. P. Martin and M. T. Vaughn, *Two loop renormalization group equations for soft supersymmetry breaking couplings*, *Phys. Rev.* **D50** (1994) 2282, [hep-ph/9311340].

[226] M. Gonzalez-Alonso, *New physics bounds from CKM-unitarity*, in *Proceedings, 45th Rencontres de Moriond on Electroweak Interactions and Unified Theories: La Thuile, Italy, March 6-13, 2010*, pp. 509–512, 2010, 1101.4679.

[227] T. Inami and C. S. Lim, *Effects of superheavy quarks and leptons in low-energy weak processes $K_L \to \mu\bar{\mu}$, $K^+ \to \pi^+\nu\bar{\nu}$ and $K^0 \leftrightarrow \bar{K}^0$*, *Prog. Theor. Phys.* **65** (1981) 297.

[228] V. D. Barger, J. L. Hewett and R. J. N. Phillips, *New constraints on the charged Higgs sector in two-Higgs-doublet models*, *Phys. Rev.* **D41** (1990) 3421–3441.

[229] E. Ma and G. Rajasekaran, *Softly broken A_4 symmetry for nearly degenerate neutrino masses*, *Phys. Rev.* **D64** (2001) 113012, [hep-ph/0106291].

[230] E. Ma, *Quark mass matrices in the A_4 model*, *Mod. Phys. Lett.* **A17** (2002) 627–630, [hep-ph/0203238].

[231] K. S. Babu, E. Ma and J. W. F. Valle, *Underlying A_4 symmetry for the neutrino mass matrix and the quark mixing matrix*, *Phys. Lett.* **B552** (2003) 207–213, [hep-ph/0206292].

[232] M. Hirsch, J. C. Romao, S. Skadhauge, J. W. F. Valle and A. Villanova del

Moral, *Phenomenological tests of supersymmetric A_4 family symmetry model of neutrino mass*, *Phys. Rev.* **D69** (2004) 093006, [hep-ph/0312265].

[233] M. Hirsch, J. C. Romao, S. Skadhauge, J. W. F. Valle and A. Villanova del Moral, *Degenerate neutrinos from a supersymmetric A_4 model*, hep-ph/0312244.

[234] E. Ma, *Non-Abelian discrete family symmetries of leptons and quarks*, in *Summer Institute 2004 (SI 2004) Fuji-Yoshida, Japan, August 12-19, 2004*, 2004, hep-ph/0409075.

[235] E. Ma, *Non-Abelian discrete symmetries and neutrino masses: Two examples*, *New J. Phys.* **6** (2004) 104, [hep-ph/0405152].

[236] E. Ma, *A_4 symmetry and neutrinos with very different masses*, *Phys. Rev.* **D70** (2004) 031901, [hep-ph/0404199].

[237] K. S. Babu and X.-G. He, *Model of geometric neutrino mixing*, hep-ph/0507217.

[238] S.-L. Chen, M. Frigerio and E. Ma, *Hybrid seesaw neutrino masses with A_4 family symmetry*, *Nucl. Phys.* **B724** (2005) 423–431, [hep-ph/0504181].

[239] M. Hirsch, A. Villanova del Moral, J. W. F. Valle and E. Ma, *Predicting neutrinoless double beta decay*, *Phys. Rev.* **D72** (2005) 091301, [hep-ph/0507148].

[240] E. Ma, *Tetrahedral family symmetry and the neutrino mixing matrix*, *Mod. Phys. Lett.* **A20** (2005) 2601–2606, [hep-ph/0508099].

[241] E. Ma, *Aspects of the tetrahedral neutrino mass matrix*, *Phys. Rev.* **D72** (2005) 037301, [hep-ph/0505209].

[242] A. Zee, *Obtaining the neutrino mixing matrix with the tetrahedral group*, *Phys. Lett.* **B630** (2005) 58–67, [hep-ph/0508278].

[243] B. Adhikary, B. Brahmachari, A. Ghosal, E. Ma and M. K. Parida, *A_4 symmetry and prediction of U_{e3} in a modified Altarelli-Feruglio model*, *Phys. Lett.* **B638** (2006) 345–349, [hep-ph/0603059].

[244] X.-G. He, Y.-Y. Keum and R. R. Volkas, *A_4 flavor symmetry breaking*

scheme for understanding quark and neutrino mixing angles, *JHEP* **04** (2006) 039, [hep-ph/0601001].

[245] S. F. King and M. Malinsky, *A_4 family symmetry and quark-lepton unification*, *Phys. Lett.* **B645** (2007) 351–357, [hep-ph/0610250].

[246] L. Lavoura and H. Kuhbock, *Predictions of an A_4 model with a five-paramete neutrino mass matrix*, *Mod. Phys. Lett.* **A22** (2007) 181–189, [hep-ph/0610050].

[247] M. Hirsch, A. S. Joshipura, S. Kaneko and J. W. F. Valle, *Predictive flavour symmetries of the neutrino mass matrix*, *Phys. Rev. Lett.* **99** (2007) 151802, [hep-ph/0703046].

[248] S. Morisi, M. Picariello and E. Torrente-Lujan, *Model for fermion masses and lepton mixing in $SO(10) \times A_4$*, *Phys. Rev.* **D75** (2007) 075015, [hep-ph/0702034].

[249] F. Yin, *Neutrino mixing matrix in the 3-3-1 model with heavy leptons and A_4 symmetry*, *Phys. Rev.* **D75** (2007) 073010, [0704.3827].

[250] B. Adhikary and A. Ghosal, *Nonzero U_{e3}, CP violation and leptogenesis in a see-saw type softly broken A_4 symmetric model*, *Phys. Rev.* **D78** (2008) 073007, [0803.3582].

[251] G. Altarelli, F. Feruglio and C. Hagedorn, *A SUSY $SU(5)$ grand unified model of tri-bimaximal mixing from A_4*, *JHEP* **03** (2008) 052, [0802.0090].

[252] F. Bazzocchi, M. Frigerio and S. Morisi, *Fermion masses and mixing in models with $SO(10) \times A_4$ symmetry*, *Phys. Rev.* **D78** (2008) 116018, [0809.3573].

[253] B. Brahmachari, S. Choubey and M. Mitra, *The A_4 flavor symmetry and neutrino phenomenology*, *Phys. Rev.* **D77** (2008) 073008, [0801.3554].

[254] F. Feruglio, C. Hagedorn, Y. Lin and L. Merlo, *Lepton flavour violation in models with A_4 flavour symmetry*, *Nucl. Phys.* **B809** (2009) 218–243, [0807.3160].

[255] W. Grimus and L. Lavoura, *Tri-bimaximal lepton mixing from symmetry only*, *JHEP* **04** (2009) 013, [0811.4766].

[256] M. Hirsch, S. Morisi and J. W. F. Valle, *Tri-bimaximal neutrino mixing and neutrinoless double beta decay*, *Phys. Rev.* **D78** (2008) 093007, [0804.1521].

[257] M. Honda and M. Tanimoto, *Deviation from tri-bimaximal neutrino mixing in A_4 flavor symmetry*, *Prog. Theor. Phys.* **119** (2008) 583–598, [0801.0181].

[258] Y. Lin, *A predictive A_4 model, charged lepton hierarchy and tri-bimaximal sum rule*, *Nucl. Phys.* **B813** (2009) 91–105, [0804.2867].

[259] G. C. Branco, R. Gonzalez Felipe, M. N. Rebelo and H. Serodio, *Resonant leptogenesis and tri-bimaximal leptonic mixing with A_4 symmetry*, *Phys. Rev.* **D79** (2009) 093008, [0904.3076].

[260] M.-C. Chen and S. F. King, *A_4 see-saw models and form dominance*, *JHEP* **06** (2009) 072, [0903.0125].

[261] P. Ciafaloni, M. Picariello, E. Torrente-Lujan and A. Urbano, *Neutrino masses and tri-bimaximal mixing in minimal renormalizable SUSY $SU(5)$ grand unified model with A_4 flavor symmetry*, *Phys. Rev.* **D79** (2009) 116010, [0901.2236].

[262] Y. Lin, *A dynamical approach to link low energy phases with leptogenesis*, *Phys. Rev.* **D80** (2009) 076011, [0903.0831].

[263] S. Morisi, *Tri-bimaximal lepton mixing with $A_4 \ltimes (Z_2)^3$*, *Phys. Rev.* **D79** (2009) 033008, [0901.1080].

[264] T. Araki, J. Mei and Z.-z. Xing, *Intrinsic deviation from the tri-bimaximal neutrino mixing in a class of A_4 flavor models*, *Phys. Lett.* **B695** (2011) 165–168, [1010.3065].

[265] D. Meloni, S. Morisi and E. Peinado, *Neutrino phenomenology and stable dark matter with A_4*, *Phys. Lett.* **B697** (2011) 339–342, [1011.1371].

[266] A. Adulpravitchai and R. Takahashi, *A_4 flavor models in split seesaw mechanism*, *JHEP* **09** (2011) 127, [1107.3829].

[267] G.-J. Ding and D. Meloni, *A model for tri-bimaximal mixing from a completely broken A_4*, *Nucl. Phys.* **B855** (2012) 21–45, [1108.2733].

[268] Y. BenTov, X.-G. He and A. Zee, *An $A_4 \times Z_4$ model for neutrino mixing*, *JHEP* **12** (2012) 093, [1208.1062].

[269] M. Holthausen, M. Lindner and M. A. Schmidt, *Lepton flavor at the electroweak scale: A complete A_4 model*, *Phys. Rev.* **D87** (2013) 033006, [1211.5143].

[270] R. González Felipe, H. Serôdio and J. P. Silva, *Models with three Higgs doublets in the triplet representations of A_4 or S_4*, *Phys. Rev.* **D87** (2013) 055010, [1302.0861].

[271] R. Gonzalez Felipe, H. Serodio and J. P. Silva, *Neutrino masses and mixing in A_4 models with three Higgs doublets*, *Phys. Rev.* **D88** (2013) 015015, [1304.3468].

[272] P. M. Ferreira, L. Lavoura and P. O. Ludl, *A new A_4 model for lepton mixing*, *Phys. Lett.* **B726** (2013) 767–772, [1306.1500].

[273] S. Morisi, D. V. Forero, J. C. Romão and J. W. F. Valle, *Neutrino mixing with revamped A_4 flavor symmetry*, *Phys. Rev.* **D88** (2013) 016003, [1305.6774].

[274] G. Altarelli, *Theoretical models of neutrino mixing: Recent developments*, in *Proceedings, 13th International Workshop on Neutrino Telescopes: Venice, Italy, March 10-13, 2009*, pp. 377–396, 2009, 0905.2350.

[275] G. Altarelli and F. Feruglio, *Discrete flavor symmetries and models of neutrino mixing*, *Rev. Mod. Phys.* **82** (2010) 2701–2729, [1002.0211].

[276] G. Altarelli, F. Feruglio, L. Merlo and E. Stamou, *Discrete flavour groups, θ_{13} and lepton flavour violation*, *JHEP* **08** (2012) 021, [1205.4670].

[277] G. Altarelli, F. Feruglio and L. Merlo, *Tri-bimaximal neutrino mixing and discrete flavour symmetries*, *Fortsch. Phys.* **61** (2013) 507–534, [1205.5133].

[278] G. Altarelli and F. Feruglio, *Tri-bimaximal neutrino mixing from discrete symmetry in extra dimensions*, *Nucl. Phys.* **B720** (2005) 64–88, [hep-ph/0504165].

[279] G. Altarelli and F. Feruglio, *Tri-bimaximal neutrino mixing, A_4 and the modular symmetry*, *Nucl. Phys.* **B741** (2006) 215–235, [hep-ph/0512103].

[280] E. Ma, *Tribimaximal neutrino mixing from a supersymmetric model with A_4 family symmetry*, *Phys. Rev.* **D73** (2006) 057304, [hep-ph/0511133].

[281] E. Ma, *Supersymmetric $A_4 \times Z_3$ and A_4 realizations of neutrino tribimaximal mixing without and with corrections*, *Mod. Phys. Lett.* **A22** (2007) 101–106, [hep-ph/0610342].

[282] F. Bazzocchi, S. Kaneko and S. Morisi, *A SUSY A_4 model for fermion masses and mixings*, *JHEP* **03** (2008) 063, [0707.3032].

[283] C. Csaki, C. Delaunay, C. Grojean and Y. Grossman, *A model of lepton masses from a warped extra dimension*, *JHEP* **10** (2008) 055, [0806.0356].

[284] P. H. Frampton and S. Matsuzaki, *Renormalizable A_4 model for lepton sector*, 0806.4592.

[285] G. Altarelli and D. Meloni, *A simplest A_4 model for tri-bimaximal neutrino mixing*, *J. Phys.* **G36** (2009) 085005, [0905.0620].

[286] G. L. Fogli, E. Lisi, A. Marrone, D. Montanino, A. Palazzo and A. M. Rotunno, *Global analysis of neutrino masses, mixings and phases: Entering the era of leptonic CP violation searches*, *Phys. Rev.* **D86** (2012) 013012, [1205.5254].

[287] Y. Lin, *Tri-bimaximal neutrino mixing from A_4 and $\theta_{13} \sim \theta_C$*, *Nucl. Phys.* **B824** (2010) 95–110, [0905.3534].

[288] S. Antusch, S. F. King, C. Luhn and M. Spinrath, *Trimaximal mixing with predicted θ_{13} from a new type of constrained sequential dominance*, *Nucl. Phys.* **B856** (2012) 328–341, [1108.4278].

[289] S. F. King and C. Luhn, *A_4 models of tri-bimaximal-reactor mixing*, *JHEP* **03** (2012) 036, [1112.1959].

[290] S. F. King and C. Luhn, *Trimaximal neutrino mixing from vacuum alignment in A_4 and S_4 models*, *JHEP* **09** (2011) 042, [1107.5332].

[291] E. Ma and D. Wegman, *Nonzero θ_{13} for neutrino mixing in the context of A_4 symmetry*, *Phys. Rev. Lett.* **107** (2011) 061803, [1106.4269].

[292] Y. Shimizu, M. Tanimoto and A. Watanabe, *Breaking tri-bimaximal mixing and large θ_{13}*, *Prog. Theor. Phys.* **126** (2011) 81–90, [1105.2929].

[293] Y. H. Ahn, S. Baek and P. Gondolo, *Simple renormalizable flavor symmetry for neutrino oscillations*, *Phys. Rev.* **D86** (2012) 053004, [1207.1229].

[294] M.-C. Chen, J. Huang, J.-M. O'Bryan, A. M. Wijangco and F. Yu, *Compatibility of θ_{13} and the Type I seesaw model with A_4 symmetry*, *JHEP* **02** (2013) 021, [1210.6982].

[295] H. Ishimori and E. Ma, *New simple A_4 neutrino model for nonzero θ_{13} and large δ_{CP}*, *Phys. Rev.* **D86** (2012) 045030, [1205.0075].

[296] E. Ma, A. Natale and A. Rashed, *Scotogenic A_4 neutrino model for nonzero θ_{13} and large δ_{CP}*, *Int. J. Mod. Phys.* **A27** (2012) 1250134, [1206.1570].

[297] J. Barry and W. Rodejohann, *Deviations from tri-bimaximal mixing due to the vacuum expectation value misalignment in A_4 models*, *Phys. Rev.* **D81** (2010) 093002, [1003.2385].

[298] S. F. King, *Vacuum misalignment corrections to tri-bimaximal mixing and form dominance*, *JHEP* **01** (2011) 115, [1011.6167].

[299] G. C. Branco, R. Gonzalez Felipe, F. R. Joaquim and H. Serodio, *Spontaneous leptonic CP violation and nonzero θ_{13}*, *Phys. Rev.* **D86** (2012) 076008, [1203.2646].

[300] S. Antusch, J. Kersten, M. Lindner and M. Ratz, *Running neutrino masses, mixings and CP phases: Analytical results and phenomenological consequences*, *Nucl. Phys.* **B674** (2003) 401–433, [hep-ph/0305273].

[301] A. Dighe, S. Goswami and W. Rodejohann, *Corrections to tri-bimaximal neutrino mixing: Renormalization and Planck scale effects*, *Phys. Rev.* **D75** (2007) 073023, [hep-ph/0612328].

[302] A. Dighe, S. Goswami and P. Roy, *Radiatively broken symmetries of nonhierarchical neutrinos*, *Phys. Rev.* **D76** (2007) 096005, [0704.3735].

[303] M. Borah, B. Sharma and M. K. Das, *Radiative generation of non-zero θ_{13} in MSSM with broken A_4 flavor symmetry*, *Nucl. Phys.* **B885** (2014) 76–96, [1304.0164].

[304] A. Adulpravitchai, A. Blum and M. Lindner, *Non-Abelian discrete groups from the breaking of continuous flavor symmetries*, *JHEP* **09** (2009) 018, [0907.2332].

[305] C. Luhn, *Spontaneous breaking of $SU(3)$ to finite family symmetries: A pedestrian's approach*, *JHEP* **03** (2011) 108, [1101.2417].

[306] K. S. Babu, C. N. Leung and J. T. Pantaleone, *Renormalization of the neutrino mass operator*, *Phys. Lett.* **B319** (1993) 191–198, [hep-ph/9309223].

[307] P. H. Chankowski and Z. Pluciennik, *Renormalization group equations for seesaw neutrino masses*, *Phys. Lett.* **B316** (1993) 312–317, [hep-ph/9306333].

[308] P. H. Chankowski, W. Krolikowski and S. Pokorski, *Fixed points in the evolution of neutrino mixings*, *Phys. Lett.* **B473** (2000) 109–117, [hep-ph/9910231].

[309] S. F. King and N. N. Singh, *Renormalization group analysis of single right-handed neutrino dominance*, *Nucl. Phys.* **B591** (2000) 3–25, [hep-ph/0006229].

[310] S. Antusch, M. Drees, J. Kersten, M. Lindner and M. Ratz, *Neutrino mass operator renormalization revisited*, *Phys. Lett.* **B519** (2001) 238–242, [hep-ph/0108005].

[311] S. Antusch, M. Drees, J. Kersten, M. Lindner and M. Ratz, *Neutrino mass operator renormalization in two-Higgs-doublet models and the MSSM*, *Phys. Lett.* **B525** (2002) 130–134, [hep-ph/0110366].

[312] S. Antusch and M. Ratz, *Supergraph techniques and two loop beta functions for renormalizable and nonrenormalizable operators*, *JHEP* **07** (2002) 059, [hep-ph/0203027].

[313] S. Antusch, J. Kersten, M. Lindner and M. Ratz, *Neutrino mass matrix running for nondegenerate seesaw scales*, *Phys. Lett.* **B538** (2002) 87–95, [hep-ph/0203233].

[314] S. Antusch, J. Kersten, M. Lindner, M. Ratz and M. A. Schmidt, *Running neutrino mass parameters in see-saw scenarios*, *JHEP* **03** (2005) 024, [hep-ph/0501272].

[315] M. Farina, D. Pappadopulo, J. T. Ruderman and G. Trevisan, *Phases of cannibal dark matter*, *JHEP* **12** (2016) 039, [1607.03108].

[316] P. Cushman et al., *Working group report: WIMP dark matter direct detection*, in *Proceedings, 2013 Community Summer Study on the Future of U.S. Particle Physics: Snowmass on the Mississippi (CSS2013): Minneapolis, MN, USA, July 29-August 6, 2013*, 2013, 1310.8327.

[317] LUX collaboration, D. S. Akerib et al., *Improved limits on scattering of weakly interacting massive particles from reanalysis of 2013 LUX data*, *Phys. Rev. Lett.* **116** (2016) 161301, [1512.03506].

[318] XENON collaboration, E. Aprile et al., *Physics reach of the XENON1T dark matter experiment*, *JCAP* **1604** (2016) 027, [1512.07501].

[319] A. Askew, S. Chauhan, B. Penning, W. Shepherd and M. Tripathi, *Searching for dark matter at hadron colliders*, *Int. J. Mod. Phys.* **A29** (2014) 1430041, [1406.5662].

[320] J. Buckley et al., *Working group report: WIMP dark matter indirect detection*, in *Proceedings, 2013 Community Summer Study on the Future of U.S. Particle Physics: Snowmass on the Mississippi (CSS2013): Minneapolis, MN, USA, July 29-August 6, 2013*, 2013, 1310.7040.

[321] M. J. Baker et al., *The coannihilation codex*, *JHEP* **12** (2015) 120, [1510.03434].

[322] Y. Hochberg, E. Kuflik, H. Murayama, T. Volansky and J. G. Wacker, *Model for thermal relic dark matter of strongly interacting massive particles*, *Phys. Rev. Lett.* **115** (2015) 021301, [1411.3727].

[323] N. Bernal, X. Chu, C. Garcia-Cely, T. Hambye and B. Zaldivar, *Production regimes for self-interacting dark matter*, *JCAP* **1603** (2016) 018, [1510.08063].

[324] N. Bernal and X. Chu, *Z_2 SIMP dark matter*, *JCAP* **1601** (2016) 006, [1510.08527].

[325] R. T. D'Agnolo and J. T. Ruderman, *Light dark matter from forbidden channels*, *Phys. Rev. Lett.* **115** (2015) 061301, [1505.07107].

[326] T. Moroi and L. Randall, *Wino cold dark matter from anomaly mediated SUSY breaking*, *Nucl. Phys.* **B570** (2000) 455–472, [hep-ph/9906527].

[327] J. L. Feng, A. Rajaraman and F. Takayama, *Superweakly interacting massive particles*, *Phys. Rev. Lett.* **91** (2003) 011302, [hep-ph/0302215].

[328] M. Kaplinghat, *Dark matter from early decays*, *Phys. Rev.* **D72** (2005) 063510, [astro-ph/0507300].

[329] B. S. Acharya, G. Kane, S. Watson and P. Kumar, *A non-thermal WIMP miracle*, *Phys. Rev.* **D80** (2009) 083529, [0908.2430].

[330] D. E. Morrissey, D. Poland and K. M. Zurek, *Abelian hidden sectors at a GeV*, *JHEP* **07** (2009) 050, [0904.2567].

[331] T. Cohen, D. J. Phalen, A. Pierce and K. M. Zurek, *Asymmetric dark matter from a GeV hidden sector*, *Phys. Rev.* **D82** (2010) 056001, [1005.1655].

[332] P. Bandyopadhyay, E. J. Chun and J.-C. Park, *Right-handed sneutrino dark matter in $U(1)'$ seesaw models and its signatures at the LHC*, *JHEP* **06** (2011) 129, [1105.1652].

[333] M. Farina, *Asymmetric twin dark matter*, *JCAP* **1511** (2015) 017, [1506.03520].

[334] A. Berlin, D. Hooper and G. Krnjaic, *PeV-scale dark matter as a thermal relic of a decoupled sector*, *Phys. Lett.* **B760** (2016) 106–111, [1602.08490].

[335] C. Boehm, M. J. Dolan and C. McCabe, *A lower bound on the mass of cold thermal dark matter from Planck*, *JCAP* **1308** (2013) 041, [1303.6270].

[336] E. Di Valentino, S. Gariazzo, M. Gerbino, E. Giusarma and O. Mena, *Dark radiation and inflationary freedom after Planck 2015*, *Phys. Rev.* **D93** (2016) 083523, [1601.07557].

[337] K. Griest and M. Kamionkowski, *Unitarity limits on the mass and radius of dark matter particles*, *Phys. Rev. Lett.* **64** (1990) 615.

[338] R. Essig, E. Kuflik, S. D. McDermott, T. Volansky and K. M. Zurek, *Constraining light dark matter with diffuse X-ray and gamma-ray observations*, *JHEP* **11** (2013) 193, [1309.4091].

[339] G. Elor, N. L. Rodd, T. R. Slatyer and W. Xue, *Model-independent indirect*

detection constraints on hidden sector dark matter, *JCAP* **1606** (2016) 024, [1511.08787].

[340] M. Fukugita and T. Yanagida, *Baryogenesis without grand unification*, *Phys. Lett.* **B174** (1986) 45–47.

[341] D. V. Nanopoulos and S. Weinberg, *Mechanisms for cosmological baryon production*, *Phys. Rev.* **D20** (1979) 2484.

[342] R. N. Mohapatra and G. Senjanovic, *Hydrogen - anti-hydrogen oscillations and spontaneously broken global $B - L$ symmetry*, *Phys. Rev. Lett.* **49** (1982) 7.

[343] P. Fileviez Perez and M. B. Wise, *Low energy supersymmetry with baryon and lepton number gauged*, *Phys. Rev.* **D84** (2011) 055015, [1105.3190].

[344] D. G. Phillips, II et al., *Neutron-antineutron oscillations: Theoretical status and experimental prospects*, *Phys. Rept.* **612** (2016) 1–45, [1410.1100].

[345] J. Bramante, J. Kumar and J. Learned, *Proton annihilation at hadron colliders and Kamioka: High-energy versus high-luminosity*, *Phys. Rev.* **D91** (2015) 035012, [1412.2140].

[346] Fermi-LAT collaboration, A. A. Abdo et al., *Fermi LAT observation of diffuse gamma-rays produced through interactions between local interstellar matter and high energy cosmic rays*, *Astrophys. J.* **703** (2009) 1249–1256, [0908.1171].

[347] G. Feinberg and S. Weinberg, *Conversion of muonium into antimuonium*, *Phys. Rev.* **123** (1961) 1439–1443.

[348] AMS collaboration, M. Aguilar et al., *Antiproton flux, antiproton-to-proton flux ratio, and properties of elementary particle fluxes in primary cosmic rays measured with the Alpha Magnetic Spectrometer on the International Space Station*, *Phys. Rev. Lett.* **117** (2016) 091103.

[349] K. M. Ferriere, *The interstellar environment of our galaxy*, *Rev. Mod. Phys.* **73** (2001) 1031–1066, [astro-ph/0106359].

[350] D. P. Cox, *The three-phase interstellar medium revisited*, *Annu. Rev. Astron. Astrophys.* **43** (2005) 337–385.

[351] A. G. G. M. Tielens, *The Physics and Chemistry of the Interstellar Medium*. Cambridge University Press, 2005.

[352] B. T. Draine, *Physics of the Interstellar and Intergalactic Medium*. Princeton Series in Astrophysics. Princeton University Press, 2010.

[353] C. Schwartz, *Electron scattering from hydrogen*, *Phys. Rev.* **124** (1961) 1468.

[354] R. L. Armstead, *Electron-hydrogen scattering calculation*, *Phys. Rev.* **171** (1968) 91–93.

[355] A. K. Bhatia, A. Temkin, R. J. Drachman and H. Eiserike, *Generalized hylleraas calculation of positron-hydrogen scattering*, *Phys. Rev. A* **3** (1971) 1328.

[356] D. L. Morgan and V. W. Hughes, *Atom-antiatom interactions*, *Phys. Rev.* **A7** (1973) 1811–1825.

[357] A. K. Bhatia, A. Temkin and H. Eiserike, *Rigorous precision p-wave positron-hydrogen scattering calculation*, *Phys. Rev. A* **9** (1974) 219.

[358] W. Kolos, D. L. Morgan Jr., D. M. Schrader and L. Wolniewicz, *Hydrogen-antihydrogen interactions*, *Phys. Rev. A* **11** (1975) 1792.

[359] D. Register and R. T. Poe, *Algebraic variational method – a quantitative assessment in $e^{\pm}$-h scattering*, *Phys. Lett. A* **51** (1975) 431–433.

[360] W. C. Fon, P. G. Burke and A. E. Kingston, *Elastic scattering of electrons by atomic hydrogen*, *J. Phys. B* **11** (1978) 521.

[361] D. L. Morgan, *Atomic processes in antiproton-matter interactions*, *Hyperfine Interactions* **44** (1989) 399–411.

[362] J. Mitroy, *Close coupling calculations of positron-hydrogen scattering at low energies*, *J. Phys. B* **26** (1993) 4861.

[363] P. S. Krstic and D. R. Schultz, *Elastic and Related Transport Cross Sections for Collisions among Isotopomers of $H^+ + H$, $H^+ + H_2$, $H^+ + He$, $H + H$, and $H + H_2$*, vol. 8 of *Atomic and Plasma-material Interaction Data for Fusion*. International Atomic Energy Agency, 1999.

[364] P. K. Sinha, P. Chaudhuri and A. S. Ghosh, *Total elastic cross section for $\bar{h}$- h scattering at thermal energies*, *Phys. Rev. A* **69** (2004) 014701.

[365] S. Chakraborty, A. Sen and A. S. Ghosh, *Cold hydrogen-hydrogen scattering using cca model*, *Eur. Phys. J. D* **45** (2007) 261–266.

[366] G. Backenstoss et al., *Proton - anti-proton annihilations at rest into $\pi^0\omega$, $\pi^0\eta$, $\pi^0\gamma$, $\pi^0\pi^0$, and $\pi^0\eta'$*, *Nucl. Phys.* **B228** (1983) 424–438.

[367] J. Rammer, *Quantum Transport Theory*, vol. 99 of *Frontiers in Physics*. Westview Press, 2004.

[368] G. Hunter and M. Kuriyan, *Scattering of protons by hydrogen atoms at low energies: Phase shifts and differential cross sections*, *Atomic Data and Nuclear Data Tables* **25** (1980) 287–310.

[369] A. Y. Voronin and J. Carbonell, *Antiproton-hydrogen annihilation at subkelvin temperatures*, *Phys. Rev. A* **57** (1998) 4335.

[370] S. Jonsell, A. Saenz, P. Froelich, B. Zygelman and A. Dalgarno, *Stability of hydrogen-antihydrogen mixtures at low energies*, *Phys. Rev. A* **64** (2001) 052712.

[371] E. A. G. Armour and C. W. Chamberlain, *Calculation of cross sections for very low-energy hydrogen–antihydrogen scattering using the kohn variational method*, *J. Phys. B* **35** (2002) L489.

[372] E. A. G. Armour, Y. Liu and A. Vigier, *Inclusion of the strong interaction in low-energy hydrogen–antihydrogen scattering using a complex potential*, *J. Phys. B* **38** (2005) L47.

[373] K. Sakimoto, *Protonium formation in slow collisions of antiprotons with hydrogen atoms*, *J. Phys. B* **34** (2001) 1769.

[374] K. Sakimoto, *Full quantum-mechanical study of protonium formation in slow collisions of antiprotons with hydrogen atoms*, *Phys. Rev. A* **65** (2001) 012706.